NREL/TP-425-7636 • UC Category 1500 • DE96007953

Effects of Uncertainty in SAPRC90 Rate Constants and Selected Product Yields on Reactivity Adjustment Factors for Alternative Fuel Vehicle Emissions

M.S. Bergin, A.G. Russell, Y.J. Yang, J.B. Milford, F. Kirchner, and W.R. Stockwell

Technical Monitor: Brent Bailey

National Renewable Energy Laboratory
1617 Cole Boulevard
Golden, Colorado 80401-3393
A national laboratory of the U.S. Department of Energy
Managed by Midwest Research Institute
for the U.S. Department of Energy
under Contract No. DE-AC36-83CH10093

Prepared under Subcontract No. XAU-3-12228-02

July 1996

NOTICE

Available to DOE and DOE contractors from:
Office of Scientific and Technical Information (OSTI)
P.O. Box 62
Oak Ridge, TN 37831
Prices available by calling (423) 576-8401

Available to the public from:
National Technical Information Service (NTIS)
U.S. Department of Commerce
5285 Port Royal Road
Springfield, VA 22161
(703) 487-4650

Printed on paper containing at least 50% wastepaper, including 10% postconsumer waste

FINAL REPORT

Effects of Uncertainty in SAPRC90 Rate Constants and Selected Product Yields on Reactivity Adjustment Factors for Alternative Fuel Vehicle Emissions

An Integrated Approach Using Formal Sensitivity and Uncertainty Analysis and Three-Dimensional Air Quality Modeling

July 1996

Prepared by:

Michelle S. Bergin[1] and Armistead G. Russell[2]
Department of Mechanical Engineering
Carnegie Mellon University
Pittsburgh, PA 15213

Yueh-Jiun Yang[2]
Department of Civil and Environmental Engineering
University of Connecticut
Storrs, CT 06269

Jana B. Milford
Department of Mechanical Engineering
University of Colorado
Boulder, CO 80309-0427

and
Frank Kirchner and William R. Stockwell
Fraunhofer Institute for Atmospheric Environmental Research (IFU)
Kreuzeckbahnstr. 19
82467 Garmisch-Partenkirchen
Germany

This report was prepared for the National Renewable Energy Laboratory (NREL) of the Department of Energy (DOE) under contract number XAU-3-13013-1. The views expressed in the report are those of the authors and do not necessarily represent the views of NREL or DOE.

---

[1]Current address: National Renewable Energy Laboratory, Center for Transportation Technologies and Systems, 1617 Cole Blvd., Golden, CO 80401.

[2]Current address: School of Civil and Environmenal Engineering, Georgia Institute of Technology, Atlanta, GA 30332-0355.

Acknowledgments

This report was prepared for the National Renewable Energy Laboratory (NREL) of the Department of Energy (DOE) under Contract No. XAU-3-13013-01. Views expressed in the report are those of the authors and do not necessarily represent the views of the NREL or DOE. Our work benefited greatly from the help of Dr. William P.L. Carter, the computer expertise and assistance of Erik Riedel, and the assistance of Madharuma Das. We would also like to thank the report reviewers for their comments and suggestions.

Table of Contents

7. APPENDIXES

Appendix A

Urban Ozone Control and Atmospheric Reactivity of Organic Gases

Appendix B

Uncertain Product Yields and Associated Constraints

Appendix C

C1. Species Name Key

C2. SAPRC90 Mechanism

Appendix D

CIT Model Results Used to Calculate Chapter 4 Figures

Appendix E

A Brief Comparison of CIT Modeling of RAF Effects Using Two Different Chemical Mechanisms

1. INTRODUCTION

1.1 Overview

Tropospheric ozone is formed in the atmosphere by a series of reactions involving volatile organic compounds (VOCs) and nitrogen oxides (NO_X). While NO_X emissions are primarily composed of only two compounds, nitrogen oxide (NO) and nitrogen dioxide (NO_2), there are hundreds of different VOCs being emitted. In general, VOCs promote ozone formation, however, the rate and extent of ozone produced by the individual VOCs varies considerably. For example, it is widely acknowledged that formaldehyde (HCHO) is a very reactive VOC, and produces ozone rapidly and efficiently under most conditions. On the other hand, VOCs such as methane, ethane, propane, and methanol do not react as quickly, and are likely to form less urban ozone than a comparable mass of HCHO.

This difference in ozone-forming potential is one of the bases for considering the use of alternative fuels. The five fuels examined in this study are compressed natural gas (CNG), which is primarily methane and ethane; liquefied petroleum gas (LPG), which is primarily propane; M85, a mixture of 85% methanol and 15% CA Phase 2 gasoline; E85, a mixture of 85% ethanol and 15% CA Phase 2 gasoline; and CA Phase 2 reformulated gasoline (RFG). All five appear to have lower overall reactivities than conventional gasoline. Alternative fuels and RFG are considered important elements in the effort to reduce levels of ozone in the lower atmosphere to meet the National Ambient Air Quality Standards. One question, however, is how to account for the differences in the emissions impacts from the various fuels. In 1990, the California Air Resources Board (CARB) adopted new motor vehicle emissions regulations that attempted to adjust for differences in ozone-forming tendencies among different fuel/vehicle combinations (CARB, 1990).

According to CARB (1992), adjustment of allowable mass emissions rates by "reactivity credits" that account for air quality impacts appears to be "the only way to assure fair and equitable treatment for both manufacturers of motor vehicles and for producers of gasoline and all cleaner burning fuels." However, the task of assessing the air quality benefits of RFG and various alternative fuels is relatively difficult compared to evaluations of control measures that have

typically been undertaken for regulatory purposes. Control measures have usually been evaluated solely in terms of changes in total mass emissions of VOCs. Assessing the effects of changes in the composition of VOC emissions requires more refined emissions estimates and a more detailed understanding of chemical mechanisms than have been needed in the past. Moreover, uncertainties in the analysis of air quality impacts may take on greater significance.

California's Low-Emission Vehicles and Clean Fuels (LEV/CF) regulations (adopted in September 1990) impose increasingly stringent exhaust emissions limits for nonmethane organic gases (NMOG), NO_x, carbon monoxide, and HCHO. For new vehicles, fleet average exhaust nonmethane hydrocarbon (NMHC) emissions limits of 0.25 g mi^{-1} were scheduled to be imposed for 1993, with progressive tightening leading to an NMOG limit of 0.062 g mi^{-1} for 2003. A key innovation in the LEV/CF program is the application of a *Reactivity Adjustment Factor* (RAF) to the mass emissions rates for vehicles operated on fuels other than conventional gasoline, to account for changes in emissions composition that would likely lead to reduced ozone formation.

RAFs being applied in California are calculated from the measured composition of exhaust emissions associated with a particular fuel/vehicle combination, with the emissions fraction of each compound weighted by a model-estimated "incremental reactivity" that indicates the sensitivity of ozone to that compound. The significance of the RAFs is potentially great, as the relative credit or penalty applied to a particular fuel/vehicle combination could prove to be a critical factor in the costs of complying with the regulations. As an indication of the magnitude of the adjustments at issue, CARB has adopted an RAF of 0.41 for M85-fueled vehicles (based on the mass of the emissions) relative to conventional gasoline (CARB, 1992). Thus, an M85-fueled vehicle can emit almost 2.5 times (1/0.41) as much VOC mass per mile as a gasoline-fueled vehicle. The adjustments for other alternative fuels (e.g., CNG) are potentially larger.

The calculation and use of RAFs, or VOC reactivity adjustments in general, has been controversial. Pertinent arguments against using reactivity adjustments include the inadequacy of the technique used to quantify the reactivity of the individual VOCs, the uncertainty in our knowledge of the atmospheric chemistry, and the environmental variability of VOC reactivity.

A recent article (Russell et al., 1995, included as Appendix A) addresses all three issues and considers economic factors. This study addresses the first two of these issues using a variety of modeling techniques, including both box and three-dimensional modeling. Similar techniques were used in a study supported by the Auto/Oil Air Quality Improvement Research Program (AQIRP) (Yang et al., 1994). The current study is a continuation of that work. Primary extensions include quantification of the impact of product speciation uncertainties (as well as reaction-rate parameters) in the chemical mechanisms, and more explicit treatment of the uncertainties in the RAFs of alternative fuels and RFG. Familiarity with the previous study would be useful to fully benefit from this report.

To help resolve the controversy about how much confidence to place in RAFs, this study has quantified the uncertainty in RAFs that results from uncertainties in the rate and product yield parameters of the SAPRC (Statewide Air Pollution Research Center) chemical mechanism (Carter, 1990a), which was used in the RAF calculations. To obtain first-order estimates of uncertainties in SAPRC outputs, sensitivity coefficients (Dunker, 1984) calculated in box model simulations were combined with rate and product yield parameter uncertainty estimates developed for the SAPRC mechanism. Parameters identified as influential (based on the first-order analysis) were then treated as random variables in Monte Carlo simulations to calculate overall uncertainties in incremental reactivities for selected components of vehicle emissions. Data from the Auto/Oil AQIRP (Burns et al., 1991), CARB (1992, 1994), and the National Renewable Energy Laboratory (NREL, 1994) were used to estimate emissions compositions and associated uncertainties, which were then combined with the incremental reactivity results to estimate overall uncertainties in RAFs.

Complementing the box model uncertainty calculations, an extended version of the CIT (California Institute of Technology/Carnegie Institute of Technology) (Harley et al., 1992) airshed model was applied to a multiday episode for the South Coast Air Basin. This model was recently updated to include the SAPRC90 mechanism, which was also used in the box modeling conducted here and for the maximum incremental reactivity (MIR) assessment by Carter (1994). Using the same mechanism allows more direct comparison between the single-cell model, which was exercised for a 10-hour period, and the multiday simulations, which were performed with

the three-dimensional grid model.

1.2 CARB LEV Regulations and Reactivity Adjustment Factors

The California vehicle emission standards are historically the most stringent in the nation, reflecting the severity of the ozone problems in that state. More recently other regions, such as the northeastern United States, have shown indications that similar emissions reductions from motor vehicles will be an important part of their air quality improvement strategy. Some states have even proposed the adoption of regulations similar to those of California. This increases the importance of the concepts adopted in California's standards, one of which is reactivity adjustment. For this reason, we review the California LEV exhaust emissions standards, as was done in Yang et al. (1994).

The California LEV exhaust emissions standards for passenger cars, certified at 50,000 miles, are shown in Table 1-1. The NMOG emissions limits shown in the table apply directly to vehicles fueled on conventional gasoline. For vehicles fueled with RFG or alternative fuels such as M85 or CNG, compliance with the emissions limits is based on weighting the mass emissions rate by a RAF, defined as:

$$RAF = \frac{\sum_{i=1}^{N} F_{Ai}\, IR_i}{\sum_{i=1}^{N} F_{Bi}\, IR_i} \qquad (1.1)$$

where F_{A_i} = mass fraction of compound i in exhaust from test fuel;

F_{B_i} = mass fraction of compound i in exhaust from base fuel; and

IR_i = maximum incremental reactivity of compound i per unit mass.

Equation (1.1) is straightforward, once the IR_i, F_{A_i}, and F_{B_i} have been estimated. However, in addition to questions that have arisen regarding incremental reactivities, the approach to determining emissions mass fraction compositions is at issue. For example, the dependence of vehicle emissions composition on temperature, driving mode, and vehicle age may not be the same for one fuel as another, and it is not clear how best to account for these differences in

estimating the average composition of exhaust emissions.

Table 1-1. Low-Emission Vehicle Exhaust Emission Standards for Passenger Cars at 50,000 Miles (CARB, 1992)

Vehicle Category	NMOG[a] g/mile	NO_x g/mile	CO g/mile	HCHO[b] g/mile
1993	0.250	0.4	3.4	0.015[b]
TLEV	0.125	0.4	3.4	0.015
LEV	0.075	0.2	3.4	0.015
ULEV	0.040	0.2	1.7	0.008
ZEV[c]	0.000	0.0	0.0	0.000

[a] NMHC for 1993, NMOG with reactivity adjustment for other vehicle categories
[b] Methanol-fueled vehicles only
[c] Does not include power generation emissions

To assign the incremental reactivity values needed in Equation (1.1), CARB adopted the MIR scale. The MIR scale is described below, following a more general discussion of the reactivity of organic compounds.

Individual organic compounds differ in the degree to which they contribute to photochemical pollution. This was recognized in early studies of smog formation. Accordingly, numerous attempts have been made to develop reactivity scales to quantify these differences. As discussed by Carter (1990b), early approaches based on irradiation of individual organic compounds with NO_x in smog chambers were flawed because of smog chamber artifacts, and also because the chemical behavior of an isolated compound is not the same as its behavior in the presence of a complex mixture of compounds. A second approach that has been suggested is to scale reactivities according to the rate at which compounds react with the hydroxyl radical (HO, the predominant atmospheric oxidant of organics). However, the HO-reaction rate is only one of several critical factors that influence the contribution of an organic compound to photochemical air pollution. Most recently, computer modeling studies have been used to estimate the change in product concentrations (usually ozone) that would result from changing emissions or the

initial concentration of a particular pollutant (Bufalini and Dodge, 1983; Dodge, 1984; Carter and Atkinson, 1989; Carter, 1994). Important limitations of these studies are that the resulting reactivity estimates hold only for the conditions simulated, and that the models used were extremely simplified representations of atmospheric processes.

The approach that CARB has adopted to estimate reactivities for individual organic compounds is to look at how ozone concentrations change when computer simulations are repeated with small changes made in the initial concentration and/or the simulated emissions rate of the compound under investigation (CARB, 1990). The SAPRC chemical mechanism developed by Carter (1990a) is a core element of the exercise, as this mechanism is capable of explicitly treating the chemistry of more than 150 organic compounds, comprising most of the mass of motor vehicle emissions. Carter and Atkinson (1989) give the following definition for the incremental reactivity of organic compound j (IR_j):

$$IR_j = \lim_{\Delta HC_j \to 0} \left[\frac{R(HC_j + \Delta HC_j) - R(HC_j)}{\Delta HC_j} \right] = \frac{\partial R}{\partial HC_j} \qquad (1.2)$$

where

$R(HC_j)$ = the maximum value of ($[O_3]$ - [NO]) calculated in a base case simulation

$R(HC_j + \Delta HC_j)$ = the maximum value of ($[O_3]$ - [NO]) calculated in a second simulation in which ΔHC_j, a small amount of organic compound j (in units of mass of carbon), has been added.

As discussed by Carter and Atkinson (1989), incremental reactivity (IR) values can be viewed as the product of two components: $IR_j = KR_j\ MR_j$, where KR, the kinetic reactivity, represents the amount of the compound that reacts during the simulation; and MR, the mechanistic reactivity, represents the amount of ozone formed per fraction reacted.

Modeling studies undertaken to develop reactivity estimates have typically used single-day simulations and single-cell model formulations, which treat chemical reactions in detail but make simplifying assumptions about transport and mixing. The box model on which CARB relies uses Carter's mechanism with time-varying photolysis conditions and temperatures that

control the chemical reaction rates. The box model formulation assumes instantaneous mixing of time-varying emissions throughout a single cell with a variable mixing height. Except through the specification of initial conditions, the model does not account for carryover of pollutants from one day to the next. In developing a generalized reactivity scale, CARB has argued that more sophisticated treatment of transport and mixing is not warranted, because establishing representative chemical conditions and adequately describing chemical reactions are more critical considerations (CARB, 1992). This issue is addressed in Russell et al. (1995) (included as Appendix A).

As evidence of the adequacy of its approach, CARB (1992) cited McNair et al. (1992), who applied the CIT airshed model to calculate incremental reactivities under conditions in the South Coast Air Basin for a 3-day period during the 1987 Southern California Air Quality Study. As used for that study, the CIT airshed model employed three-dimensional spatial resolution and transport, and incorporated the LCC (Lurmann, Carter, and Coyner, 1987) chemical mechanism. Agreement between the airshed model-derived incremental reactivities and those calculated with CARB's box model approach were within about 15%. One issue of using a box model is that it does not fully account for initial composition changes that could occur from changes in VOC emissions. As a test of the overall RAF approach, McNair et al. (1992, 1994) also compared the effect of emissions from a conventional gasoline fleet with those of fleets of alternative fuel vehicles, assuming emissions rates that would lead to equivalent reactivity by using RAF adjustment. They concluded that the original RAF approach underestimated the impact of M85 emissions, relative to conventional gasoline. Based in part on the airshed modeling results, CARB adopted an RAF value for M85 that was about 10% higher than would have been assigned on the basis of the box model calculations.

1.3 Uncertainties in Incremental Reactivities and the SAPRC Mechanism

RAF uncertainties include those associated with emissions composition and with the IRs of the compounds in the emissions. Uncertainties in emissions composition begin with measurement uncertainties in emissions test results. Moreover, major uncertainties result from differences between laboratory and in-use conditions, including driving patterns; distributions of vehicle age, models, and upkeep; the composition of test fuels versus those distributed in a given

market; and environmental factors such as temperature. Statistical analysis of vehicle test results can provide estimates of uncertainties associated with vehicle-to-vehicle variability and limitations on the reproducibility of measurements. At present, however, uncertainties associated with systematic measurement errors and laboratory versus in-use discrepancies are estimated subjectively. Developing such subjective uncertainty estimates was beyond the scope of this study. As a first step toward exploring the influence on RAFs of uncertainties in emissions composition, this study considers only the portion of the uncertainty that can be estimated statistically from laboratory tests of vehicle emissions.

Uncertainties associated with incremental reactivities of the compounds in the emissions arise from various possibilities — that simulation conditions used to derive MIRs may not adequately represent atmospheric conditions leading to smog formation, that the treatment of transport and mixing may be oversimplified, and that pollutant carryover in multiday episodes may affect MIRs. These three issues are addressed in this study by comparing the results of box model calculations for idealized simulation conditions to airshed model calculations for a historical pollution episode. Also, there are additional uncertainties associated with the chemical mechanism used to calculate MIRs.

Uncertainties in chemical mechanisms are associated with errors in measured rate parameters and selected product yields. Moreover, parameters of many reactions employed in chemical mechanisms have never been directly measured. Some reactions are included in a mechanism because, for example, they are analogous to known reactions and thermodynamically possible, even though their rate constants or product yields have not been measured. The rate constant for reaction with the HO radical is well known for many organic compounds, but the product yields and subsequent secondary chemistry are not. Additional uncertainties are introduced in the process of eliminating or combining reactions or chemical species to "condense" chemical mechanisms for inclusion in photochemical models. Again, representing only a first step toward a comprehensive analysis, this study uses formal methods of uncertainty propagation to examine the consequences of uncertainties in the rate constants used in the SAPRC mechanism.

The SAPRC mechanism (Carter, 1990a) is the latest in a line of mechanisms based on studies by

Atkinson et al. (1982) and Lurmann et al. (1986). This mechanism has been evaluated by comparison to the results of more than 550 smog chamber simulations. According to Carter (1990a), the inorganic chemistry is similar to that of other older mechanisms, such as the CB-IV (Carbon Bond, version IV) mechanism (Gery et al., 1989). An important feature of the SAPRC mechanism is that it includes assignments of kinetic and mechanistic parameter values for more than 150 organic compounds. With the SAPRC mechanism, the user has the option of including the initial reaction of many compounds explicitly, or using generalized initial reactions for alkanes, aromatics, and alkenes. The values of the parameters of these reactions depend on the specific compounds represented in the initial conditions or the emissions of a given simulation.

Although the primary reactions of a large number of organic compounds are explicitly represented, the organic chemistry in the SAPRC mechanism is nevertheless highly condensed, compared to the total set of reactions that occur in the atmosphere. The organic products of photooxidation of the emitted organics are represented by 19 species, including HCHO, acetaldehyde, higher aldehydes, acetone, higher ketones, and four peroxyacetyl nitrate (PAN) analogs. Organic peroxy radicals are represented by six "operators" that account for the effects of all peroxy radical reactions on NO, NO_2, and HO_2, and on both organic nitrate and peroxide formation. A total organic peroxy radical operator is used to account for the rates of reaction of peroxy radicals with other peroxy radicals and acyl peroxy radicals. Four types of acyl peroxy radicals are analogously supplemented with a total acyl peroxy radical.

Carter (1990a) provided insight into organic atmospheric chemistry by classifying the individual organic compounds included in the SAPRC mechanism according to the strength of the empirical or theoretical support for their representations. Of almost 150 compounds listed, five (n-butane, ethylene, HCHO, methanol, and ethanol) were included in a group of compounds for which he considered the chemistry to be well established. According to Carter, these are compounds for which "we believe we understand at least the most important of the fundamental processes by which the VOC promotes ozone formation, and whose mechanisms have been tested at least to some extent using environmental chamber data." At the other extreme are nearly 100 compounds, primarily of higher molecular weight, "whose mechanisms are uncertain and for which no adequate chamber data are available. Mechanisms for these compounds have

been estimated based on analogy or extrapolation from mechanisms developed for other compounds."

More recently, as a first step toward providing uncertainty estimates for the MIR values he calculated for CARB, Carter made subjective judgments of uncertainties in the mechanistic reactivity component of the MIRs for selected classes of organics (CARB, 1992). Table 1-2 reproduces those assessments. According to CARB (1992), the estimates represent Carter's judgment based on published uncertainties in key parameters, sensitivity calculations, differences between results calculated with the SAPRC versus CB-IV mechanisms, and an assumed lower bound of 20%.

Finally, in addition to the uncertainties in the mechanism that result from inadequacies in the underlying experimental data base or from the need to condense the mechanism from a fully explicit description of the relevant chemistry, another issue in establishing an appropriate degree of confidence in the SAPRC mechanism is the recognized need to update some critical parameters. A review of the SAPRC mechanism by Gery (1991) highlighted absorption cross sections for HCHO photolysis and rate constants associated with acetyl peroxy radical and PAN (peroxyacetyl nitrate) chemistry as obsolete elements of the SAPRC mechanism. In these cases, experimental results published since the mechanism was developed have led to significant revisions in the accepted parameter values. Although the need for these updates was identified prior to finalization of MIR calculations for CARB, they were not made because 1991 regulatory timetable precluded thorough evaluation of the revised mechanism. However, it is expected that MIR factors will be updated periodically.

1.4 Study Objectives

As mentioned previously, this study is an extension of a recent project conducted for the Auto/Oil AQIRP. That study concentrated primarily on the effects of rate parameter uncertainties on the quantification of VOC reactivity. However, it is widely viewed that there is also significant uncertainty in the product yields of the current chemical mechanisms used for following atmospheric pollutant evolution. A first part of this study was to assess the uncertainties in the chemical reaction product yields. This information is then used to quantify

the uncertainties in the VOC reactivities and fuel RAFs. Included in this analysis is the impact of variation in the fuel emissions speciation. To accomplish this objective, sensitivity and uncertainty analyses were performed for VOC-reactivity estimates. These calculations were performed with a single-cell model that incorporated the SAPRC chemical mechanism and incorporating both the uncertainty in the rate parameters and in product speciation. In addition to estimates of uncertainties in MIRs and RAFs for selected fuels, the analysis identified the chemical mechanism parameters in the SAPRC90 mechanism that contribute the most uncertainty.

Table 1-2. Mechanistic Reactivity Uncertainty Estimates for MIR Conditions (CARB, 1992)

Compound/Class	MIR Uncertainty	Compound/Class	MIR Uncertainty
CO	15 %	aromatics	30 %
C1-C8 alkanes	20 % or 0.5/#C[a,b]	styrene	50 %
C9 > alkanes	0.5/#C[b]	methanol	20 %
cycloalkanes	0.6/#C[b]	ethanol	20 %
ethene	20 %	formaldehyde	40 %
propene	25 %	acetaldehyde	40 %
C4 alkenes	30 %	propionaldehyde	40 %
C5 > alkenes	40 %	acetone	40 %
dialkenes	50 %	acrolein	50 %
cycloalkenes	50 %	methyl t-butyl ether	20 %
alkynes	50 %	ethyl t-butyl ether	40 %

[a] Greater of the two

[b] Absolute uncertainty in MIR. #C is the number of carbon atoms in the alkane

A second objective of the research was to understand how reactivity estimates developed using the single-cell model might differ from those developed using the CIT airshed model with the same chemical mechanism. To accomplish this objective, the SAPRC mechanism was implemented in the CIT airshed model, and the model was applied to a three-day episode in the

South Coast Air Basin. The CIT model was used to test the RAF adjustment used to equalize the impact of five alternative fuel exhaust reactivities. These five fuels, described previously, are M85, E85, LPG, CNG, and Phase 2 gasoline. The RAF adjustment was calculated with respect to the average gasoline. The fuel exhaust speciated composition data were obtained from speciated emissions Federal Test Procedures performed by CARB (1992, 1994) for M85, LPG, CNG, RF-A (base gasoline) and Phase 2 gasoline, and by NREL (1994) for E85. Data from the Auto/Oil AQIRP and Chevron Research and Technology Company (CRTC) were also used.

1.5 Scope of the Study

An important element of the design of this study was the coordinated use of a single-cell model and a three-dimensional, physically detailed airshed model. Each type of model has inherent limitations and advantages. Single-cell models are not computationally demanding, even when using relatively detailed chemical mechanisms. Also, they require fewer detailed input data, making them more widely accessible. Therefore, a single-cell model has been used to calculate reactivities for CARB (1992). Of relevance to the present study, single-cell models are well suited to conducting detailed sensitivity and uncertainty analysis of chemical mechanisms. This allows uncertainty analysis of a large number of parameters to be conducted using nonlinear, distributed-parameter techniques such as Monte Carlo analysis. In this regard, the use of a single-cell model was necessary. However, single-cell models have severe limitations in their formulation, which are especially pronounced in multiday applications. They do not supply spatial information or describe the corresponding nonlinear impacts, and they rely on highly parameterized descriptions of physical effects.

Airshed models do not share some major limitations of single-cell models because they are more detailed in their treatment of physical effects, but they are computationally intensive and require detailed input data. Their ability to provide spatial information has proven extremely important in past studies. For this reason, they are recommended for air quality analysis. Russell et al. (1991) have previously identified important differences in comparing the results of reactivity calculations performed with an airshed model and a single-cell model. In the previous AQIRP study, box model calculations were used to identify key uncertainties with respect to ozone formation in the parameters of the SAPRC chemical mechanism, and then the influence of these

uncertainties on reactivity calculations was tested in detailed airshed model simulations.

In the AQIRP study, the rate-parameter uncertainties treated in the analysis were compiled largely from panel reviews published by NASA and the International Union of Pure and Applied Chemistry (IUPAC). However, for this study, a more extensive investigation was necessary to assess the uncertainties in product yields in the mechanism. Therefore, the panel reviews were supplemented by analysis of the original studies and the SAPRC90 mechanism formulation. Chapter 2 contains further discussion of the uncertainty estimates used for this study.

1.6 Outline of the Report

Chapter 2 addresses the first issue in this report — how the chemical mechanism uncertainties affect the calculation of RAFs. It focuses on assessing the product speciation uncertainties in the SAPRC90 mechanism, using some rate-parameter uncertainties that were estimated in the previous study (Yang et al., 1994). The results of the two mechanism uncertainty assessments are combined in Chapter 3, and are used to quantify the uncertainty in VOC-reactivity estimation and RAFs by incorporating box modeling with sensitivity and uncertainty analysis performed using the Direct Decoupled Method (DDM) (Dunker, 1984) and Latin Hypercube Sampling (LHS) (Iman and Shortencarier, 1984). Chapter 4 presents the results of the three-dimensional CIT airshed model and its use to further investigate reactivity adjustment and assessment. Chapter 5 summarizes the results. A journal article that includes results from this work is included as Appendix A.

2. STOICHIOMETRIC PARAMETER UNCERTAINTY ESTIMATES FOR W.P.L. CARTER'S (1990a) DETAILED MECHANISM (SAPRC90)

2.1 Introduction

The purpose of this chapter is to describe correlations between reactions and to estimate the uncertainty associated with stoichiometric parameters for the parameters in W.P.L. Carter's (1990a) detailed mechanism. A listing of uncertain product yields and reactions in this mechanism at 298°K are provided in Appendixes B and C. The uncertainty in product yields is greatest for organic reactions in an atmospheric chemical mechanism, and results from both a lack of laboratory measurements and the condensation of a mechanism. Experimental measurements of the product yields for many secondary reactions are relatively limited, especially for higher molecular weight organic species. More and better measurements of product yields are needed for aromatic oxidation, ozonolysis of alkenes, biogenic hydrocarbons, RO_2 and RO reactions, nitrate radical-organic products, and organic nitrate yields and decomposition mechanisms. In addition to uncertainties in the chemical kinetics database, the choice of lumping procedure, the number of species, and the processes that are omitted all affect the uncertainties associated with a mechanism. Either highly condensed or highly detailed mechanisms may have the highest uncertainty levels. Highly condensed mechanisms may omit a number of relevant processes, and highly detailed mechanisms may have many estimated product yields and rate constants.

2.2 Estimation of Stoichiometric Parameter Uncertainties

It is possible to make uncertainty assignments to relatively well-known reactions such as:

$$HO + NO_2 \rightarrow HNO_3$$

One of the best and most recent studies of this reaction (Burkholder et al., 1987) could not account for almost 25% of the nitric acid yield. However, it is probably not reasonable to assign a ± 25% uncertainty to the yield because there does not appear to be a reasonable alternative nitrogen-containing product.

However, the possibility of surprise in atmospheric chemical kinetics should not be ruled out, especially when recent history is considered. Examples include the formation of nitric oxide from the NO_2-NO_3 reaction, the formation of HO from the HO_2-NO_3 reaction or the formation of HO_2 in the HO-SO_2 reaction. The formation of HO_2 from the HO-SO_2 reaction was especially surprising because it appeared to an endothermic process. It was later found that the thermodynamic data for the HO-SO_2 reaction were not correct.

It is not possible to predict the surprises that may remain in measurements of simple inorganic reactions. For most simple inorganic reactions that have been subjected to repeated studies, the products are probably completely known. There probably is only a small chance of an unknown and unexpected reaction channel for these reactions. In order to proceed it is necessary to place a limit on the number of product yields that are varied in a sensitivity calculation. The yields for the inorganic species were considered to be "certain," and we concentrated on the yields for the organic reactions. The only exception was the formation of sulfate from the reactions of Criegee intermediates. Because that reaction is highly uncertain, an uncertainty of 25% was assigned to the yield of H_2SO_4.

Our uncertainty estimates were based on an evaluation of the quality of experimental measurements of product yields for the organic and inorganic species produced by the organic reactions; they are shown in Table 2-1. In the laboratory, yields of inorganic species such as NO_2, HNO_3, CO, and CO_2 can typically be measured to an accuracy of ±10% (Finlayson-Pitts and Pitts, 1986).

Hydroxyl radicals and HO_2 radical yields are much more difficult to determine because their yields are often inferred through the measurement of their products. Figure 2-1 shows that the uncertainty increases as the product yield decreases. This was also assumed to be true for the peroxy radical yields. Because of this greater uncertainty, we assigned an additional ±10% uncertainty (total uncertainty ±20%) to the yield coefficient for HO_2 radicals with a yield coefficient of 0.7 or greater and an additional ±20% uncertainty (total uncertainty ±30%) if the

yield coefficient was less than 0.7. For hydroxyl radicals, which are produced through the photolysis of organic peroxides, we assigned uncertainty of ±30% to the yield.

For the organic radical yields, the lowest uncertainties were assigned to the yields for the products of the reaction of HO with acetaldehyde and higher aldehyde. Although there is some small amount of glycoaldehyde production, reaction of HO creates species that will most likely react as peroxy radicals. Therefore we assigned a value of ±10% to the products of these reactions. For surrogate radicals such as peroxy radicals (generated from reactions other than HO on aldehydes) and phenoxy radicals, we assigned the same yield uncertainty as was assigned to the yield for HO_2 radicals with yield greater than 0.7. Operator radical yields, such as total peroxy acyl radicals and extra NO-to-NO_2 conversions, are parameterizations of more complex chemistry, and therefore will have greater uncertainties. These were assigned an uncertainty level of ±30% regardless of the yield.

Table 2-1. Species Yield Uncertainty Factors for Carter (1990a) Mechanism

Inorganic Species	Species	σ	
Ozone	O3	10%	
Nitrogen Dioxide	NO2	10%	
Nitric Acid	HNO3	10%	
Carbon Monoxide	CO	10%	
Carbon Dioxide	CO2	10%	
Sulfuric Acid	H2SO4	25%	
Hydroxyl Radicals	HO	30%	
Hydroperoxy Radicals	HO2	20%	(Yield > 0.7)
	HO2	30%	(Yield < 0.7)
Stable Organic Species			
Formaldehyde	HCHO	15%	
Acetaldehyde	CCHO	15%	
Peroxyacetyl Nitrate	PAN	15%	
Propionaldehyde	RCHO	15%	
Peroxyperpionyl Nitrate	PPN	15%	
Acetone	ACET	15%	
Methylethyl Ketone	MEK	15%	
Organic Nitrates	RNO3	20%	
Glyoxal	GLY	20%	
PAN Analog from Glyoxal	GPAN	15%	
Methyl Glyoxal	MGLY	15%	
Phenol	PHEN	60%	
Cresol	CRES	30%	
Benzaldehyde	BALD	30%	
Peroxybenzoyl Nitrate	PBZN	30%	
Nitrophenols	NPHE	30%	

Table 2-1 (continued). Species Yield Uncertainty Factors for Carter (1990a) Mechanism

Unknown Aromatic Fragmentation Product #1	AFG1	30%
Unknown Aromatic Fragmentation Product #2	AFG2	30%
Acetaldehyde and Higher Aldehyde HO Reaction	RCO3	10%
Product Yields for:	CCO-O2	10%
	C2CO-O2	10%
<u>Organic Radical Species</u>		
Chemical Operator for -OOH Groups	-OOH	30%
Total Alkyl Peroxy Radicals	RO2	30%
Total Peroxyacyl Radicals	RCO3	30%
Intermediate Formed in the HCHO + HO2 Reaction	HOCOO	20%
Peroxyacetyl Radicals	CCO-O2	20%
Higher Peroxyacetyl Radicals	C2CO-O2	20%
Peroxyacyl Radical Formed from Glyoxal	HCOCO-O2	20%
Phenoxy Radicals	BZ-O	20%
Phenoxy Benzoyl Radicals	BZ-CO-O2	20%
Phenoxy Radicals with Nitro-Groups	BZ(NO2)-O	20%
Operator for SO2 Oxidation by O3-Alkene Products	O3OL-SB	30%
NO to NO2 Conversion Operator	RO2-R	30%
NO Consumption Operator	RO2-X	30%
NO Consumption with Nitrophenol Formation	RO2-NP	30%
NO Sink Reaction Operator	RO2-XN	30%
Operator for Extra NO to NO2 Conversions	R2O2	30%

Figure 2-1. Uncertainty Ratio as a Function of Product Yield for Aromatic Products (Adapted from Atkinson, 1990)

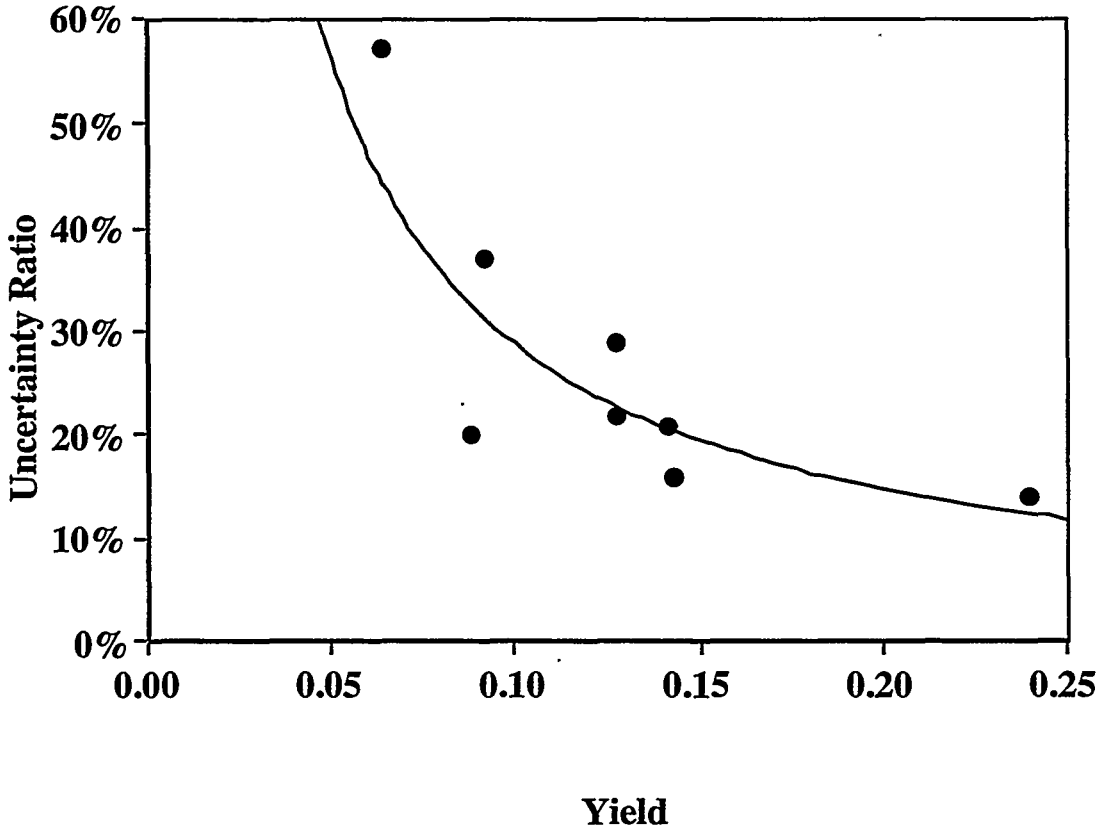

Stable organic product species, such as organic peroxides, organic nitrates, aldehydes, and ketones, are more difficult than stable inorganic species to identify and measure. Typical laboratory measurements are accurate to ±15% (Finlayson-Pitts and Pitts, 1986; Winegar and Keith, 1993). For this reason we assigned an uncertainty of ±15% to the stable species which are not produced through aromatic oxidation. These stable organic species include formaldehyde, acetaldehyde, peroxy acetyl nitrate and higher PAN analogs, propionaldehyde, acetone, methyl ethyl ketone, and methyl glyoxal.

The greatest level of uncertainty was assigned to the aromatic reactions. Atmospheric aromatic chemistry is both highly complex and uncertain. Detailed, explicit mechanisms may contain hundreds of reactions for toluene photooxidation (Calvert and Madronich, 1987). Known products of aromatic photooxidation include glyoxal, methylglyoxal, and unsaturated dicarbonyls. However, the yields and identities of many other products have not been identified through laboratory measurements. Large fractions (~ 40%) of the initial aromatic carbon mass are not accounted for in environmental chamber experiments, although a large fraction might be explained by the formation of organic aerosols (Calvert and Madronich, 1987; Gery et al., 1985; Tuazon et al., 1986).

Aromatic chemistry must be parameterized in air quality models because it is highly complex. Table 2-2 gives a listing of aromatic oxidation product yields determined by several different laboratories (Atkinson, 1990). The optimum values for the atmospheric parameters for aromatic reactions are not established; rather, they have been optimized to fit smog chamber data. Thus, the uncertainty range assigned to the parameters for aromatic reactions is relatively broad.

From a basic science viewpoint, the mechanisms for the atmospheric oxidation of aromatic chemicals are extremely uncertain because many products have not been identified experimentally. The rate constants for many of the primary aromatic reactions are reasonably well known, but the secondary chemistry requires much additional research. Measurement of many secondary organic reaction parameters is difficult because it may require examination of complex chemical mixtures. The analysis of complex mixtures can require the use of assumed

Table 2-2. Experimental Product Yield Uncertainties for Aromatics (Atkinson, 1990)

Toluene	Yield	Standard Deviation (σ)	Standard Deviation to Yield Ratio	Average
Benzaldehyde	0.0730	0.0220	30%	20%
	0.1100	0.0100	9%	
	0.1040	0.0290	28%	
	0.0645	0.0080	12%	
Cresol	0.1310	0.0720	55%	29%
	0.2040	0.0270	13%	
	0.0480	0.0090	19%	
Glyoxal	0.1500	0.0400	27%	22%
	0.1050	0.0190	18%	
Methyl glyoxal	0.1400	0.0400	29%	16%
	0.1460	0.0060	4%	
Xylene				
Tolualdehyde	0.0730	0.0360	49%	37%
	0.0500	0.0100	20%	
	0.1720	0.0700	41%	
	0.0400	0.0100	25%	
	0.1220	0.0590	48%	
Dimethyl phenol	0.0120	0.0060	50%	57%
	0.1020	0.0390	38%	
	0.0780	0.0650	83%	
Glyoxal	0.0800	0.0400	50%	21%
	0.0870	0.0120	14%	
	0.1300	0.0300	23%	
	0.0860	0.0110	13%	
	0.2400	0.0200	8%	
	0.2250	0.0390	17%	
Methyl glyoxal	0.2300	0.0300	13%	14%
	0.2460	0.0200	8%	
	0.4200	0.0500	12%	
	0.3190	0.0090	3%	
	0.1200	0.0200	17%	
	0.1050	0.0340	32%	

mechanisms with rate constants taken from the literature. Mechanism parameters derived from this type of analysis have a high degree of covariance.

Environmental chamber experiments represent a more practical approach for the development and testing of condensed aromatic photooxidation mechanisms than totally theoretical approaches or field measurements. Given the state of scientific knowledge, the pragmatic view is that the aromatic reactions in a condensed mechanism should be viewed as only a parameterization of chamber data. Chamber experiments are performed using mixtures of gases whose concentrations are measured as functions of time along with other experimental variables such as light distribution and intensity. If the measured chamber concentrations are well fit by the condensed mechanism, and if the predicted concentrations are sensitive to the choice of aromatic oxidation rate parameters, the concentrations predicted by the mechanism may be much less uncertain than would be expected from an uncertainty analysis of the basic kinetics of aromatic photooxidation. This is the approach we have taken in assessing the uncertainties in Carter's mechanism.

We determined the ratio of the measured yields to the reported uncertainty. Aromatic aldehyde yield is a measure of the direct HO_2 production from the reactions of HO with toluene and xylene. The average ratio for toluene and xylene together was 30%. This number was used as a typical HO_2 product yield uncertainty if the yield was less than 0.70 in agreement with our more general assignments given above. There is considerable uncertainty in the production of phenol and cresol from organic reactions. The most recent results (LACTOZ, 1994) suggest that phenolic compounds are not formed from aromatic oxidation under atmospheric conditions.

Table 2-2 shows that for cresol and dimethyl phenol, the uncertainties in the yields were ±29% and ±57%. We assigned uncertainties of ±30% to cresol and 60% to phenol. The uncertainties for the dicarbonyls were assigned lower values, the uncertainty for the glyoxal yield was assigned at ±20%, and the uncertainty for the methyl glyoxal yield was assigned at ±15%. We assumed that the yields for benzaldehyde, organic nitrates, nitrophenols, and the unknown products (AFG1 and AFG2) were among the more uncertain of the aromatic product yields, and they were assigned an uncertainty of ±30%.

We used the uncertainties assigned in Table 2-1 to determine the ranges of uncertainty for stoichiometric parameters. To report the uncertainties, we list the most uncertain reactions in Tables 2-3 through 2-7. Table 2-3 lists the reaction, reaction number, product species, yield, and uncertainty assignment. Tables 2-4, 2-5, and 2-6 give uncertainty assignments for the alkane, aromatic, and "other compounds" yields, respectively. The yields were assigned uncertainty values consistent with Table 2-1. Carter represents these reactions with a single generalized reaction having different yield factors for different compounds. These tables give our assignments to the uncertainty of the yields for the generalized reaction.

Table 2-7 is similar in principle to Tables 2-4 through 2-6, except that Carter presented a number of formulas to calculate the product yields for different alkenes. The formulas are based on the structure of each alkene. We assigned uncertainties to the yield formulas using Table 2-1. Table 2-7 also shows the assignments for ozone-alkene and NO_3-alkenes reactions. The products of the reaction of ozone and NO_3 with alkenes are not well characterized (Atkinson and Carter, 1984; Atkinson, 1990). Additional product measurements for these reactions should be performed. We assigned uncertainties to the yields of these reactions using the same approach as used for the HO-alkene reactions.

Stoichiometric parameters chosen for the reactions are subject to a number of constraints because of the need to conserve nitrogen and to prevent artificial radical generation. For some of the reactions, an upper limit on the allowable uncertainty range was set. As an example, Table 2-8, reaction B7, gives an upper limit for the total HO_2 + HO yield. A yield greater than 2.00 for total HO_x would not give a chemically realistic reaction. For some species, operator radicals should be equal to a "real" radical, which was taken as a constraint (for example reaction B7B).

Table 2-3. Assigned Uncertainty Factors for Carter (1990a) Mechanism

Carter's Label	Reaction		Species	Yield	σ	Species	Yield	σ	Species	Yield	σ	Species	Yield	σ	Species	Yield	σ	Species	Yield	σ
SR3	O3OL-SB + SO2	→	H2SO4	1.00	± 0.250															
B7	-OOH + hv	→	HO2	1.00	± 0.200	HO	1.00	± 0.300												
B7A	HO + -OOH	→	HO	1.00	± 0.300															
B7B	HO + -OOH	→	RO2-R	1.00	± 0.300	RO2	1.00	± 0.300												
B11	RO2-R + NO	→	NO2	1.00	---	HO2	1.00	± 0.200												
B13	RO2-R + RO2	→	RO2	1.00	---	HO2	0.50	± 0.150												
B14	RO2-R + RCO3	→	RCO3	1.00	---	HO2	0.50	± 0.150												
B20	RO2-N + HO2	→	-OOH	1.00	± 0.300	MEK	1.00	± 0.150	-C	1.50	---									
B21	RO2-N + RO2	→	RO2	1.00	---	HO2	0.50	± 0.150	MEK	1.00	± 0.150	-C	1.50	---						
B22	RO2-N + RCO3	→	RCO3	1.00	---	HO2	0.50	± 0.150	MEK	1.00	± 0.150	-C	1.50	---						
B25	RO2-XN + RO2	→	RO2	1.00	---	HO2	0.50	± 0.150												
B26	RO2-XN + RCO3	→	RCO3	1.00	---	HO2	1.00	± 0.200												
C10	CCHO + HO	→	CCO-O2	1.00	± 0.100	H2O	1.00		RCO3	1.00	± 0.100									
C15	CCO-O2 + HO2	→	-OOH	1.00	± 0.300	CO2	1.00	± 0.100	HCHO	1.00	± 0.150									
C16	CCO-O2 + RO2	→	RO2	1.00	---	HO2	0.50	± 0.150	CO	1.00	± 0.100	HCHO	1.00	± 0.150						
C17	CCO-O2 + RCO3	→	RCO3	1.00	---	HO2	1.00	± 0.200	CO2	1.00	± 0.100	HCHO	1.00	± 0.150						
C25	RCHO + HO	→	C2CO-O2	1.00	± 0.100	RCO3	1.00	± 0.100												
C28	C2CO-O2 + NO	→	CCHO	1.00	± 0.150	RO2-R	1.00	± 0.300	CO2	1.00	± 0.100	NO2	1.00	± 0.100	RO2	1.00	± 0.300			
C30	C2CO-O2 + HO2	→	-OOH	1.00	± 0.300	CCHO	1.00	± 0.150	CO2	1.00	± 0.100									
C31	C2CO-O2 + RO2	→	RO2	1.00	---	HO2	0.50	± 0.150	CCHO	1.00	± 0.150	CO2	1.00	± 0.100						
C32	C2CO-O2 + RCO3	→	RCO3	1.00	---	HO2	1.00	± 0.200	CCHO	1.00	± 0.150	CO2	1.00	± 0.100						
C38	ACET + HO	→	MGLY	0.80	± 0.120	RO2-R	1.00	± 0.300	R2O2	0.20	± 0.060	HCHO	1.00	± 0.150	CCO-O2	1.00	± 0.200	RCO3	1.00	± 0.300
C44	MEK + HO	→	CCHO	0.50	± 0.075	HCHO	1.00	± 0.150	CCO-O2	1.00	± 0.200	RCO3	1.00	± 0.300	R2O2	1.50	± 0.450	RO2	1.00	± 0.300
C57	MEK + hv	→	CCO-O2	1.00	± 0.200	CCHO	1.00	± 0.150	RO2-R	1.00	± 0.300	RCO3	1.00	± 0.300	RO2	1.00	± 0.300			
C58A	GLY + hv	→	HO2	0.80	± 0.160	HCHO	0.45	± 0.068	CO	1.55	± 0.155									
C58B	GLY + hv	→	HCHO	0.13	± 0.020	CO	1.87	± 0.187												
C59	GLY + HO	→	HO2	0.60	± 0.180	CO	1.20	± 0.120	HCOCO-O2	0.40	± 0.080	RCO3	1.00	± 0.300						
C60	GLY + NO3	→	HNO3	1.00	---	HO2	0.60	± 0.180	CO	1.20	± 0.120	HCOCO-O2	0.40	± 0.080	RCO3	1.00	± 0.300			
C62	HCOCO-O2 + NO	→	NO2	1.00	---	CO2	1.00	± 0.100	CO	1.00	± 0.100	HO2	1.00	± 0.200						
C63	HCOCO-O2 + NO2	→	GPAN	1.00	± 0.150															
C65	HCOCO-O2 + HO2	→	-OOH	1.00	± 0.300	CO2	1.00	± 0.100	CO	1.00	± 0.100									
C66	HCOCO-O2 + RO2	→	RO2	1.00	---	HO2	0.50	± 0.150	CO2	1.00	± 0.100	CO	1.00	± 0.100						
C67	HCOCO-O2 + RCO3	→	RCO3	1.00	---	HO2	1.00	± 0.200	CO2	1.00	± 0.100	CO	1.00	± 0.100						
C68A	MGLY + hv	→	HO2	1.00	± 0.200	CO	1.00	± 0.100	CCO-O2	1.00	± 0.200	RCO3	1.00	± 0.300						
C68B	MGLY + hv	→	HO2	1.00	± 0.200	CO	1.00	± 0.100	CCO-O2	1.00	± 0.200	RCO3	1.00	± 0.300						
C69	MGLY + HO	→	CO	1.00	± 0.100	CCO-O2	1.00	± 0.200	RCO3	1.00	± 0.300									
C70	MGLY + NO3	→	HNO3	1.00	---	CO	1.00	± 0.100	CCO-O2	1.00	± 0.200	RCO3	1.00	± 0.300						
C95	RNO3 + HO	→	MEK	0.16	± 0.023	RCHO	1.05	± 0.158	CCHO	0.48	± 0.072	HCHO	0.16	± 0.024	-C	0.11	---	R2O2	1.39	± 0.417
			RO2	1.00	± 0.300															
D1	ETHE + HO	→	CCHO	0.22	± 0.033	HCHO	1.56	± 0.234	RO2-R	1.00	± 0.300	RO2	1.00	± 0.300						
D6	ETHE + O3	→	HCHO	1.00	± 0.150	O3OL-SB	0.37	± 0.111	CO	0.44	± 0.044	-C	0.56	---	HO2	0.12	± 0.036			
D8	ETHE + O	→	HCHO	1.00	± 0.150	CO	1.00	± 0.100	HO2	1.00	± 0.200	RO2-R	1.00	± 0.300	RO2	1.00	± 0.300			
D9	ETHE + NO3	→	NO2	1.00	± 0.100	HCHO	2.00	± 0.300	R2O2	1.00	± 0.300	RO2	1.00	± 0.300						

Table 2-3 (continued). Assigned Uncertainty Factors for Carter (1990a) Mechanism

G2	RO2-NP + NO	→	NPHE	1.00	± 0.300												
G3	RO2-NP + HO2	→	-OOH	1.00	± 0.300	-C	6.00	---									
G4	RO2-NP + RO2	→	RO2	1.00	± 0.300	HO2	0.50	± 0.150	-C	6.00	---						
G5	RO2-NP + RCO3	→	RCO3	1.00	± 0.300	HO2	1.00	± 0.200	-C	6.00	---						
G7	AFG1	→	HCOCO-O2	1.00	± 0.200	RCO3	1.00	± 0.300									
G8	AFG1 + hv →	→	HO2	1.00	± 0.200	HCOCO-O2	1.00	± 0.200	RCO3	1.00	± 0.300						
G9	HO + AFG2	→	C2CO-O2	1.00	± 0.200	RCO3	1.00	± 0.300									
G10	AFG2 + hv →	→	HO2	1.00	± 0.200	CO	1.00	± 0.100	CCO-O2	1.00	± 0.200	RCO3	1.00	± 0.300			
G30	BALD + HO	→	BZ-CO-O2	1.00	± 0.200	RCO3	1.00	± 0.300									
G31	BALD + hv →	→	-C	7.00	---												
G32	BALD + NO3	→	HNO3	1.00	± 0.100	BZ-CO-O2	1.00	± 0.200	RCO3	1.00	± 0.300						
G33	BZ-CO-O2 + NO	→	BZ-O	1.00	± 0.200	CO2	1.00	± 0.100	NO2	1.00	± 0.100	R2O2	1.00	± 0.300	RO2	1.00	± 0.300
G34	BZ-CO-O2 + NO2	→	PBZN	1.00	± 0.300												
G35	PBZN	→	BZ-CO-O2	1.00	± 0.200	NO2	1.00	± 0.100	RCO3	1.00	± 0.300						
G36	BZ-CO-O2 + HO2	→	-OOH	1.00	± 0.300	CO2	1.00	± 0.100	PHEN	1.00	± 0.600						
G37	BZ-CO-O2 + RO2	→	RO2	1.00	± 0.300	HO2	0.50	± 0.150	CO2	1.00	± 0.100	PHEN	1.00	± 0.600			
G38	RCO3 + BZ-CO-O2	→	RCO3	1.00	± 0.300	HO2	1.00	± 0.200	CO2	1.00	± 0.100	PHEN	1.00	± 0.600			
G43	BZ-O + NO2	→	NPHE	1.00	± 0.300												
G44	BZ-O + HO2	→	PHEN	1.00	± 0.600												
G45	BZ-O + PHEN	→	PHEN	1.00	± 0.600												
G46	HO + PHEN	→	RO2-NP	0.15	± 0.045	RO2-R	0.85	± 0.255	GLY	0.20	± 0.040	RO2	1.00	± 0.300	-C	4.70	---
G51	NO3 + PHEN	→	HNO3	1.00	± 0.100	BZ-O	1.00	± 0.200									
G52	HO + CRES	→	RO2-NP	0.15	± 0.045	RO2-R	0.85	± 0.255	MGLY	0.20	± 0.030	-C	5.50	---	RO2	1.00	± 0.300
G57	NO3 + CRES	→	HNO3	1.00	± 0.100	BZ-O	1.00	± 0.200	-C	1.00	---						
G58	NPHE + NO3	→	HNO3	1.00	± 0.100	BZ(NO2)-O	1.00	± 0.200									
G59	BZ(NO2)-O + NO2	→	-N	2.00	---	-C	6.00	---									
G60	BZ(NO2)-O + HO2	→	NPHE	1.00	± 0.300												
G61	BZ(NO2)-O	→	NPHE	1.00	± 0.300												

Table 2-4. Alkane Yield Uncertainties

	RO2-R.		RO2-N		RO2-XN		R2O2		HCHO		CCHO	
	RR	σ= 30 %	NR	σ= 30 %	XN	σ= 30 %	R2	σ= 30 %	A1	σ= 15 %	A2	σ= 15 %
PROPANE	0.961	±0.288	0.000	±0.000	0.039	±0.012	0.000	±0.000	0.000	±0.000	0.000	±0.000
N-C4	0.924	±0.277	0.076	±0.023	0.000	±0.000	0.397	±0.119	0.001	±0.000	0.571	±0.086
N-C5	0.880	±0.264	0.120	±0.036	0.000	±0.000	0.544	±0.163	0.007	±0.001	0.080	±0.012
N-C6	0.815	±0.245	0.185	±0.056	0.000	±0.000	0.738	±0.221	0.000	±0.000	0.020	±0.003
N-C7	0.733	±0.220	0.267	±0.080	0.000	±0.000	0.727	±0.218	0.000	±0.000	0.000	±0.000
N-C8	0.667	±0.200	0.333	±0.100	0.000	±0.000	0.706	±0.212	0.000	±0.000	0.000	±0.000
N-C9	0.627	±0.188	0.373	±0.112	0.000	±0.000	0.673	±0.202	0.000	±0.000	0.000	±0.000
N-C10	0.603	±0.181	0.397	±0.119	0.000	±0.000	0.659	±0.198	0.000	±0.000	0.000	±0.000
N-C11	0.589	±0.177	0.411	±0.123	0.000	±0.000	0.654	±0.196	0.000	±0.000	0.000	±0.000
N-C12	0.580	±0.174	0.420	±0.126	0.000	±0.000	0.644	±0.193	0.000	±0.000	0.000	±0.000
N-C13	0.573	±0.172	0.427	±0.128	0.000	±0.000	0.638	±0.191	0.000	±0.000	0.000	±0.000
N-C14	0.569	±0.171	0.431	±0.129	0.000	±0.000	0.634	±0.190	0.000	±0.000	0.000	±0.000
N-C15	0.566	±0.170	0.434	±0.130	0.000	±0.000	0.631	±0.189	0.000	±0.000	0.000	±0.000
ISO-C4	0.973	±0.292	0.027	±0.008	0.000	±0.000	0.744	±0.223	0.744	±0.112	0.000	±0.000
ISO-C5	0.933	±0.280	0.064	±0.019	0.002	±0.001	0.734	±0.220	0.000	±0.000	0.614	±0.092
BR-C5	0.933	±0.280	0.064	±0.019	0.002	±0.001	0.734	±0.220	0.000	±0.000	0.614	±0.092
NEO-C5	0.949	±0.285	0.051	±0.015	0.000	±0.000	0.019	±0.006	0.019	±0.003	0.000	±0.000
2-ME-C5	0.873	±0.262	0.122	±0.037	0.005	±0.002	0.749	±0.225	0.006	±0.001	0.023	±0.003
3-ME-C5	0.888	±0.266	0.112	±0.034	0.000	±0.000	0.860	±0.258	0.005	±0.001	0.523	±0.078
22-DMB	0.847	±0.254	0.153	±0.046	0.000	±0.000	0.960	±0.288	0.295	±0.044	0.303	±0.045
23-DMB	0.901	±0.270	0.061	±0.018	0.039	±0.012	0.944	±0.283	0.000	±0.000	0.000	±0.000
4-ME-C6	0.815	±0.245	0.182	±0.055	0.002	±0.001	0.842	±0.253	0.000	±0.000	0.127	±0.019
24-DM-C5	0.867	±0.260	0.131	±0.039	0.002	±0.001	0.844	±0.253	0.000	±0.000	0.000	±0.000
23-DM-C5	0.860	±0.258	0.128	±0.038	0.011	±0.003	1.101	±0.330	0.036	±0.005	0.253	±0.038
ISO-C8	0.811	±0.243	0.188	±0.056	0.001	±0.000	0.942	±0.283	0.111	±0.017	0.000	±0.000
CYCC5	0.873	±0.262	0.127	±0.038	0.000	±0.000	1.745	±0.524	0.000	±0.000	0.000	±0.000
ME-CYCC5	0.856	±0.257	0.144	±0.043	0.000	±0.000	2.057	±0.617	0.321	±0.048	0.000	±0.000

	RCHO		ACET		MEK		CO		CO2	
	A3	σ= 15 %	K3	σ= 15 %	K4	σ= 15 %	CO	σ= 10 %	C2	σ= 10 %
PROPANE	0.303	±0.045	0.658	±0.099	0.000	±0.000	0.000	±0.000	0.000	±0.000
N-C4	0.140	±0.021	0.000	±0.000	0.533	±0.080	0.000	±0.000	0.000	±0.000
N-C5	0.172	±0.026	0.000	±0.000	0.929	±0.139	0.000	±0.000	0.000	±0.000
N-C6	0.105	±0.016	0.000	±0.000	1.134	±0.170	0.000	±0.000	0.000	±0.000
N-C7	0.056	±0.008	0.000	±0.000	1.241	±0.186	0.000	±0.000	0.000	±0.000
N-C8	0.002	±0.000	0.000	±0.000	1.333	±0.200	0.000	±0.000	0.000	±0.000
N-C9	0.001	±0.000	0.000	±0.000	1.299	±0.195	0.000	±0.000	0.000	±0.000
N-C10	0.001	±0.000	0.000	±0.000	1.261	±0.189	0.000	±0.000	0.000	±0.000
N-C11	0.001	±0.000	0.000	±0.000	1.241	±0.186	0.000	±0.000	0.000	±0.000
N-C12	0.001	±0.000	0.000	±0.000	1.223	±0.183	0.000	±0.000	0.000	±0.000
N-C13	0.001	±0.000	0.000	±0.000	1.211	±0.182	0.000	±0.000	0.000	±0.000
N-C14	0.001	±0.000	0.000	±0.000	1.202	±0.180	0.000	±0.000	0.000	±0.000
N-C15	0.001	±0.000	0.000	±0.000	1.196	±0.179	0.000	±0.000	0.000	±0.000
ISO-C4	0.229	±0.034	0.744	±0.112	0.000	±0.000	0.000	±0.000	0.000	±0.000
ISO-C5	0.133	±0.020	0.611	±0.092	0.303	±0.045	0.000	±0.000	0.000	±0.000
BR-C5	0.133	±0.020	0.611	±0.092	0.303	±0.045	0.000	±0.000	0.000	±0.000
NEO-C5	0.939	±0.141	0.010	±0.002	0.000	±0.000	0.000	±0.000	0.000	±0.000
2-ME-C5	0.545	±0.082	0.223	±0.033	0.724	±0.109	0.000	±0.000	0.000	±0.000
3-ME-C5	0.089	±0.013	0.000	±0.000	1.003	±0.150	0.000	±0.000	0.000	±0.000
22-DMB	0.372	±0.056	0.295	±0.044	0.542	±0.081	0.000	±0.000	0.000	±0.000
23-DMB	0.128	±0.019	1.584	±0.238	0.096	±0.014	0.000	±0.000	0.000	±0.000
4-ME-C6	0.329	±0.049	0.000	±0.000	1.119	±0.168	0.000	±0.000	0.000	±0.000
24-DM-C5	0.772	±0.116	0.257	±0.039	0.682	±0.102	0.000	±0.000	0.000	±0.000
23-DM-C5	0.185	±0.028	0.390	±0.059	0.960	±0.144	0.000	±0.000	0.000	±0.000
ISO-C8	0.747	±0.112	0.251	±0.038	0.643	±0.096	0.000	±0.000	0.000	±0.000
CYCC5	0.873	±0.131	0.000	±0.000	0.218	±0.033	0.873	±0.087	0.000	±0.000
ME-CYCC5	0.622	±0.093	0.000	±0.000	0.550	±0.083	0.535	±0.054	0.214	±0.021

Table 2-4 (continued). Alkane Yield Uncertainties

	RO2-R.		RO2-N		RO2-XN		R2O2		HCHO		CCHO	
	RR	σ= 30 %	NR	σ= 30 %	XN	σ= 30 %	R2	σ= 30 %	A1	σ= 15 %	A2	σ= 15 %
CYCC6	0.807	±0.242	0.193	±0.058	0.000	±0.000	0.352	±0.106	0.003	±0.000	0.000	±0.000
ME-CYCC6	0.784	±0.235	0.216	±0.065	0.000	±0.000	0.977	±0.293	0.100	±0.015	0.001	±0.000
ET-CYCC6	0.737	±0.221	0.263	±0.079	0.000	±0.000	1.464	±0.439	0.185	±0.028	0.310	±0.047
3-ME-C6	0.815	±0.245	0.182	±0.055	0.002	±0.001	0.842	±0.253	0.000	±0.000	0.127	±0.019
4-ME-C7	0.753	±0.226	0.244	±0.073	0.002	±0.001	0.803	±0.241	0.000	±0.000	0.000	±0.000
4-ET-C7	0.727	±0.218	0.271	±0.081	0.002	±0.001	0.804	±0.241	0.002	±0.000	0.059	±0.009
4-PR-C7	0.696	±0.209	0.301	±0.090	0.002	±0.001	0.775	±0.233	0.000	±0.000	0.004	±0.001
BR-C6	0.873	±0.262	0.122	±0.037	0.005	±0.002	0.749	±0.225	0.006	±0.001	0.023	±0.003
BR-C7	0.815	±0.245	0.182	±0.055	0.002	±0.001	0.842	±0.253	0.000	±0.000	0.127	±0.019
BR-C8	0.753	±0.226	0.244	±0.073	0.002	±0.001	0.803	±0.241	0.000	±0.000	0.000	±0.000
BR-C9	0.727	±0.218	0.271	±0.081	0.002	±0.001	0.804	±0.241	0.002	±0.000	0.059	±0.009
BR-C10	0.696	±0.209	0.301	±0.090	0.002	±0.001	0.775	±0.233	0.000	±0.000	0.004	±0.001
BR-C11	0.754	±0.226	0.246	±0.074	0.000	±0.000	1.273	±0.382	0.021	±0.003	0.054	±0.008
BR-C12	0.733	±0.220	0.267	±0.080	0.000	±0.000	1.350	±0.405	0.002	±0.000	0.422	±0.063
BR-C13	0.715	±0.215	0.285	±0.086	0.000	±0.000	1.226	±0.368	0.002	±0.000	0.008	±0.001
BR-C14	0.702	±0.211	0.298	±0.089	0.000	±0.000	1.122	±0.337	0.002	±0.000	0.000	±0.000
BR-C15	0.690	±0.207	0.310	±0.093	0.000	±0.000	1.103	±0.331	0.001	±0.000	0.000	±0.000
CYC-C6	0.807	±0.242	0.193	±0.058	0.000	±0.000	0.352	±0.106	0.003	±0.000	0.000	±0.000
CYC-C7	0.784	±0.235	0.216	±0.065	0.000	±0.000	0.977	±0.293	0.100	±0.015	0.001	±0.000
CYC-C8	0.737	±0.221	0.263	±0.079	0.000	±0.000	1.464	±0.439	0.185	±0.028	0.310	±0.047
CYC-C9	0.756	±0.227	0.244	±0.073	0.000	±0.000	1.970	±0.591	0.283	±0.042	0.264	±0.040
CYC-C10	0.739	±0.222	0.261	±0.078	0.000	±0.000	1.874	±0.562	0.208	±0.031	0.390	±0.059
CYC-C11	0.767	±0.230	0.233	±0.070	0.000	±0.000	1.855	±0.557	0.236	±0.035	0.376	±0.056
CYC-C12	0.757	±0.227	0.243	±0.073	0.000	±0.000	2.040	±0.612	0.202	±0.030	0.437	±0.066
CYC-C13	0.738	±0.221	0.261	±0.078	0.000	±0.000	1.638	±0.491	0.104	±0.016	0.243	±0.036
CYC-C14	0.725	±0.218	0.274	±0.082	0.001	±0.000	1.498	±0.449	0.069	±0.010	0.070	±0.011
CYC-C15	0.714	±0.214	0.283	±0.085	0.002	±0.001	1.611	±0.483	0.040	±0.006	0.027	±0.004
C4C5	0.927	±0.278	0.072	±0.022	0.001	±0.000	0.604	±0.181	0.188	±0.028	0.316	±0.047
C6PLUS	0.808	±0.242	0.184	±0.055	0.008	±0.002	0.844	±0.253	0.022	±0.003	0.042	±0.006

	RCHO		ACET		MEK		CO		CO2	
	A3	σ= 15 %	K3	σ= 15 %	K4	σ= 15 %	CO	σ= 10 %	C2	σ= 10 %
CYCC6	0.333	±0.050	0.000	±0.000	0.816	±0.122	0.000	±0.000	0.003	±0.000
ME-CYCC6	0.474	±0.071	0.000	±0.000	0.979	±0.147	0.003	±0.000	0.046	±0.005
ET-CYCC6	0.393	±0.059	0.000	±0.000	0.930	±0.140	0.010	±0.001	0.185	±0.019
3-ME-C6	0.329	±0.049	0.000	±0.000	1.119	±0.168	0.000	±0.000	0.000	±0.000
4-ME-C7	0.352	±0.053	0.000	±0.000	1.204	±0.181	0.000	±0.000	0.000	±0.000
4-ET-C7	0.303	±0.045	0.000	±0.000	1.167	±0.175	0.000	±0.000	0.000	±0.000
4-PR-C7	0.328	±0.049	0.000	±0.000	1.139	±0.171	0.000	±0.000	0.000	±0.000
BR-C6	0.545	±0.082	0.223	±0.033	0.724	±0.109	0.000	±0.000	0.000	±0.000
BR-C7	0.329	±0.049	0.000	±0.000	1.119	±0.168	0.000	±0.000	0.000	±0.000
BR-C8	0.352	±0.053	0.000	±0.000	1.204	±0.181	0.000	±0.000	0.000	±0.000
BR-C9	0.303	±0.045	0.000	±0.000	1.167	±0.175	0.000	±0.000	0.000	±0.000
BR-C10	0.328	±0.049	0.000	±0.000	1.139	±0.171	0.000	±0.000	0.000	±0.000
BR-C11	0.090	±0.014	0.000	±0.000	1.862	±0.279	0.000	±0.000	0.000	±0.000
BR-C12	0.012	±0.002	0.000	±0.000	1.647	±0.247	0.000	±0.000	0.000	±0.000
BR-C13	0.111	±0.017	0.000	±0.000	1.819	±0.273	0.000	±0.000	0.000	±0.000
BR-C14	0.003	±0.000	0.000	±0.000	1.820	±0.273	0.000	±0.000	0.000	±0.000
BR-C15	0.003	±0.000	0.000	±0.000	1.790	±0.269	0.000	±0.000	0.000	±0.000
CYC-C6	0.333	±0.050	0.000	±0.000	0.816	±0.122	0.000	±0.000	0.003	±0.000
CYC-C7	0.474	±0.071	0.000	±0.000	0.979	±0.147	0.003	±0.000	0.046	±0.005
CYC-C8	0.393	±0.059	0.000	±0.000	0.930	±0.140	0.010	±0.001	0.185	±0.019
CYC-C9	0.502	±0.075	0.000	±0.000	1.056	±0.158	0.000	±0.000	0.264	±0.026
CYC-C10	0.228	±0.034	0.000	±0.000	1.359	±0.204	0.011	±0.001	0.208	±0.021
CYC-C11	0.144	±0.022	0.000	±0.000	1.464	±0.220	0.001	±0.000	0.184	±0.018
CYC-C12	0.110	±0.017	0.000	±0.000	1.708	±0.256	0.001	±0.000	0.169	±0.017
CYC-C13	0.198	±0.030	0.000	±0.000	1.649	±0.247	0.002	±0.000	0.074	±0.007
CYC-C14	0.439	±0.066	0.000	±0.000	1.516	±0.227	0.002	±0.000	0.048	±0.005
CYC-C15	0.465	±0.070	0.000	±0.000	1.719	±0.258	0.002	±0.000	0.036	±0.004
C4C5	0.168	±0.025	0.339	±0.051	0.441	±0.066	0.000	±0.000	0.000	±0.000
C6PLUS	0.252	±0.038	0.350	±0.053	0.876	±0.131	0.000	±0.000	0.000	±0.000

Table 2-5. Aromatic Yield Uncertainties

	RO2-R		HO2		PHEN		CRES		BALD	
	RR	σ = 20 %	RH	σ = 20 %	PH	σ = 60 %	CR	σ = 30 %	BZ	σ = 30 %
Benzene	0.764	±0.153	0.236	0.047	0.236	±0.142	0.000	±0.000	0.000	±0.000
Toluene	0.740	±0.148	0.260	0.052	0.000	±0.000	0.260	±0.078	0.085	±0.026
C2-Benz	0.740	±0.148	0.260	0.052	0.000	±0.000	0.260	±0.078	0.085	±0.026
I-C3-Benz	0.740	±0.148	0.260	0.052	0.000	±0.000	0.260	±0.078	0.085	±0.026
N-C3-Benz	0.740	±0.148	0.260	0.052	0.000	±0.000	0.260	±0.078	0.085	±0.026
S-C4-Benz	0.740	±0.148	0.260	0.052	0.000	±0.000	0.260	±0.078	0.085	±0.026
m-Xylene	0.820	±0.164	0.180	0.036	0.000	±0.000	0.180	±0.054	0.040	±0.012
o-Xylene	0.820	±0.164	0.180	0.036	0.000	±0.000	0.180	±0.054	0.040	±0.012
p-Xylene	0.820	±0.164	0.180	0.036	0.000	±0.000	0.180	±0.054	0.040	±0.012
135-TMB	0.820	±0.164	0.180	0.036	0.000	±0.000	0.180	±0.054	0.030	±0.009
123-TMB	0.820	±0.164	0.180	0.036	0.000	±0.000	0.180	±0.054	0.030	±0.009
124-TMB	0.820	±0.164	0.180	0.036	0.000	±0.000	0.180	±0.054	0.030	±0.009
Naphthal	0.690	±0.138	0.170	0.034	0.170	±0.102	0.180	±0.054	0.000	±0.000
23-DMN	0.800	±0.160	0.040	0.008	0.000	±0.000	0.000	±0.000	0.000	±0.000
Me-Naph	0.745	±0.149	0.105	0.021	0.085	±0.051	0.020	±0.006	0.000	±0.000
Tetralin	0.790	±0.158	0.090	0.018	0.090	±0.054	0.000	±0.000	0.000	±0.000

	GLY		MGLY		AFG1		AFG2	
	GL	σ = 20 %	MG	σ = 15 %	U1	σ = 25 %	U2	σ = 25 %
Benzene	0.207	±0.041	0.000	±0.000	0.490	±0.123	0.000	±0.000
Toluene	0.118	±0.024	0.131	±0.020	0.000	±0.000	0.410	±0.103
C2-Benz	0.118	±0.024	0.131	±0.020	0.000	±0.000	0.410	±0.103
I-C3-Benz	0.118	±0.024	0.131	±0.020	0.000	±0.000	0.410	±0.103
N-C3-Benz	0.118	±0.024	0.131	±0.020	0.000	±0.000	0.410	±0.103
S-C4-Benz	0.118	±0.024	0.131	±0.020	0.000	±0.000	0.410	±0.103
m-Xylene	0.108	±0.022	0.370	±0.056	0.000	±0.000	0.666	±0.167
o-Xylene	0.108	±0.022	0.370	±0.056	0.000	±0.000	0.666	±0.167
p-Xylene	0.108	±0.022	0.370	±0.056	0.000	±0.000	0.666	±0.167
135-TMB	0.000	±0.000	0.620	±0.093	0.000	±0.000	0.600	±0.150
123-TMB	0.000	±0.000	0.620	±0.093	0.000	±0.000	0.600	±0.150
124-TMB	0.000	±0.000	0.620	±0.093	0.000	±0.000	0.600	±0.150
Naphthal	0.000	±0.000	0.000	±0.000	0.320	±0.080	0.000	±0.000
23-DMN	0.000	±0.000	0.490	±0.074	0.850	±0.213	0.000	±0.000
Me-Naph	0.000	±0.000	0.245	±0.037	0.585	±0.146	0.000	±0.000
Tetralin	0.000	±0.000	0.000	±0.000	0.164	±0.041	0.000	±0.000

Table 2-6. Alcohols, Ethers, and Acetylene Yield Uncertainties

	RO2-R		HO2		R2O2		HCHO		CCHO	
	RR	σ = 30 %	RH	σ = 20 %	R2	σ = 30 %	A1	σ = 15 %	A2	σ = 15 %
MEOH	0.000	±0.000	1.000	±0.200	0.000	±0.000	1.000	±0.150	0.000	±0.000
ETOH	0.000	±0.000	1.000	±0.200	0.000	±0.000	0.000	±0.000	1.000	±0.150
ME-O-ME	1.000	±0.300	0.000	±0.000	0.000	±0.000	0.000	±0.000	0.000	±0.000
I-C3-OH	0.000	±0.000	1.000	±0.200	0.000	±0.000	0.000	±0.000	0.000	±0.000
N-C3-OH	0.230	±0.069	0.770	±0.154	0.000	±0.000	0.230	±0.035	0.230	±0.035
N-C4-OH	0.400	±0.120	0.600	±0.120	0.060	±0.018	0.250	±0.038	0.120	±0.018
I-C4-OH	0.120	±0.036	0.840	±0.168	0.000	±0.000	0.000	±0.000	0.240	±0.036
T-C4-OH	1.000	±0.300	0.000	±0.000	0.000	±0.000	1.000	±0.150	0.000	±0.000
ET-GLYCL	0.000	±0.000	1.000	±0.200	0.000	±0.000	0.000	±0.000	1.000	±0.150
PR-GLYCL	0.000	±0.000	1.000	±0.200	0.000	±0.000	0.000	±0.000	0.000	±0.000
ACETYLEN	0.700	±0.210	0.300	±0.060	0.000	±0.000	0.000	±0.000	0.000	±0.000

Table 2-6 (continued). Alcohols, Ethers, and Acetylene Yield Uncertainties

	RCHO		ACET		MEK		GLY	
	A3	σ= 15 %	K3	σ= 15 %	K4	σ= 15 %	GL	σ= 20 %
MEOH	0.000	±0.000	0.000	±0.000	0.000	±0.000	0.000	±0.000
ETOH	0.000	±0.000	0.000	±0.000	0.000	±0.000	0.000	±0.000
ME-O-ME	1.000	±0.150	0.000	±0.000	0.000	±0.000	0.000	±0.000
I-C3-OH	0.000	±0.000	1.000	±0.150	0.000	±0.000	0.000	±0.000
N-C3-OH	0.770	±0.116	0.000	±0.000	0.000	±0.000	0.000	±0.000
N-C4-OH	0.850	±0.128	0.000	±0.000	0.090	±0.014	0.000	±0.000
I-C4-OH	0.000	±0.000	0.000	±0.000	0.840	±0.126	0.000	±0.000
T-C4-OH	0.000	±0.000	1.000	±0.150	0.000	±0.000	0.000	±0.000
ET-GLYCL	0.000	±0.000	0.000	±0.000	0.000	±0.000	0.000	±0.000
PR-GLYCL	0.314	±0.047	0.000	±0.000	0.686	±0.103	0.000	±0.000
ACETYLEN	0.000	±0.000	0.000	±0.000	0.000	±0.000	0.700	±0.140

Table 2-7. Alkene Yield Uncertainties

	Reaction	Product	Yield	σ
OnPR	HO	RO2-R	1-OnPN	± 0.30 (1-OnPN)
OnP1R		HCHO	OnPR * OnP1	± 0.15 (OnPR * OnP1)
OnP2R		CCHO	OnPR * OnP2	± 0.15 (OnPR * OnP2)
OnP3R		RCHO	OnPR * OnP3	± 0.15 (OnPR * OnP3)
OnP5R	HO	ACET	OnPR * OnP4	± 0.15 (OnPR * OnP4)
OnP4R		MEK	OnPR * OnP5	± 0.20 (OnPR * OnP5)
OnOHXC		Lost C	OnNC - OnP1R - OnP2R - OnP3R - OnP4R - OnP5R	± 0.30 (OnNC - OnP1R - OnP2R - OnP3R - OnP4R - OnP5R)
OnO3A1	O3	HCHO	0.5 (OnP1 + 0.3 OnP2 + 0.1 OnP5)	± 0.075 (OnP1 + 0.3 OnP2 + 0.1 OnP5)
OnO3A2		CCHO	0.5 (OnP2 + 0.3 OnP3 + 0.1 OnP5)	± 0.075 (OnP2 + 0.3 OnP3 + 0.1 OnP5)
OnO3A3		RCHO	0.5 OnP3	± 0.075 OnP3
OnO3K4		ACET	0.5 OnP4	± 0.075 OnP4
OnO3K3		MEK	0.5 (0.28 OnP2 + 0.42 OnP3 + 0.8 OnP4 + 0.8 OnP5)	± 0.075 (0.28 OnP2 + 0.42 OnP3 + 0.8 OnP4 + 0.8 OnP5)
OnO3K4		MGLY	0.1 OnP4	± 0.015 OnP4
OnO3MG		CO	0.5 (0.44 OnP1 + 0.15 OnP2 + 0.15 OnP3)	± 0.075 (0.44 OnP1 + 0.15 OnP2 + 0.15 OnP3)
OnO3CO	O3	O3OL-SB	0.5 (0.37 OnP1 + 0.20 OnP2 + 0.20 OnP3)	± 0.15 (0.37 OnP1 + 0.20 OnP2 + 0.20 OnP3)
OnO3P1		CCO-O2	0.05 OnP5	± 0.01 OnP5
OnO3P2		C2CO-O2	0.05 OnP5	± 0.01 OnP5
OnO3RH		HO2	0.5 (0.12 OnP1 + 0.21 OnP2 + 0.21 OnP3)	± 0.10 (0.12 OnP1 + 0.21 OnP2 + 0.21 OnP3)
OnO3OH		HO	0.5 (0.12 OnP2 + 0.12 OnP3 + 0.2 OnP4 + 0.2 OnP5)	± 0.10 (0.12 OnP2 + 0.12 OnP3 + 0.2 OnP4 + 0.2 OnP5)
OnO3RR		ROR-R	0.5 (0.27 OnP2 + 0.27 OnP3 + 0.2 OnP4)	± 0.15 (0.27 OnP2 + 0.27 OnP3 + 0.2 OnP4)
OnO3R2		R2O2	0.15 OnP5	± 0.045 OnP5
OnO3RO2		RO2	OnO3RR + OnO3R2	± 0.30 (OnO3RR + OnO3R2)
OnO3PS		RCO3	OnO3P1 + OnO3P2	±0.30 (OnO3P1 + OnO3P2)
OnO3XC		Lost C	OnNC - OnO3A1 - 2 OnO3A2 - 3 OnOA3 - 3 OnO3K3 - 4 OnO3K4 - 3 OnO3MG - OnO3CO -2 OnOP1 - 3 OnO3P2	± 0.30 (OnNC - OnO3A1 - 2 OnO3A2 - 3 OnOA3 - 3 OnO3K3 - 4 OnO3K4 - 3 OnO3MG - OnO3CO -2 OnOP1 - 3 OnO3P2

Table 2-7 (continued). Alkene Yield Uncertainties

OnOAXC	O	Lost C	OnNC - 3.5	± 0.30 (OnNC - 3.5)
OnN3XC	NO3	Lost C	OnNC - OnP1 - 2 OnP2 - 3 OnP3 - 4 OnP5	± 0.30 (OnNC - OnP1 - 2 OnP2 - 3 OnP3 - 4 OnP5

OnP1	Number of =CH2 Groups
OnP2	Number of =CH2CH3 Groups
OnP3	Number of =CHR Groups where R not H or CH3
OnP4	Number of =C(CH3)2 Groups
OnP5	Number of =C(CH3) (R) or =CH2 Groups
OnPN	Organic Nitrate in the HO reaction
OnNC	Number of carbon atoms in the alkene or average in mixture

An additional comment should be made regarding peroxy radical reactions. Thousands of peroxy radical-peroxy radical reactions could be included in a tropospheric gas-phase chemical mechanism because there are many possible cross reactions between the radicals. Carter uses an operator scheme that was developed as a parameterization for classes of peroxy radical reactions to retain the effects of the RO_2-RO_2 reactions while avoiding the addition of large numbers of reactions to a mechanism. These methods are valid only if the rate constants and product yields span a narrow range within each class. Recent laboratory measurements (LACTOZ, 1994) show that the rate constants for peroxy radical-peroxy radical reactions span a wide range of values and that there appears to be a trend in the measurements (Figure 2-2).

The range of values is wide even for peroxy radicals that operator methods would group into a single class. Operator schemes are likely to underestimate the rate of RO_2-RO_2 reactions. This should be the subject of future research.

2.3 Correlated Reactions

Because of the limitations in available laboratory measurement data, many chemical reactions and rates are determined by analogy with known reactions. Carter's (1990a) mechanism includes many of these reactions. These reaction groups are presented in Table 2-9. The parameters of these reactions are correlated because they are not the result of independent measurements. A limitation of our report is that the uncertainties within each set of reactions are assumed to be the same. In reality, the uncertainty of reaction parameters for which measurement data are not

Table 2-8. Constraints on Yield Variations for Carter (1990a) Mechanism

Carter's Label	Reaction		Yield	Species	Yield	Species	Yield	Species	Yield	Species	Yield	Species	Yield	Species	Constraint
SR3	O3OL-SB + SO2	→	1.00	H2SO4											None
B7	-OOH + hv →	→	1.00	HO2	1.00	HO									HO2 + HO ≤ 2
B7B	HO + -OOH	→	1.00	RO2-R	1.00	RO2									RO2-R = RO2
C10	CCHO + HO	→	1.00	CCO-O2	1.00	H2O	1.00	RCO3							CCO-O2 = RCO3
C25	RCHO + HO	→	1.00	C2CO-O2	1.00	RCO3									C2CO-O2 = RCO3
C28	C2CO-O2 + NO	→	1.00	CCHO	1.00	RO2-R	1.00	CO2	1.00	NO2	1.00	RO2			RO2-R = RO2
C38	ACET + HO	→	0.80	MGLY	1.00	RO2-R	0.20	R2O2	1.00	HCHO	1.00	CCO-O2	1.00	RCO3	CCO-O2 = RCO3
C44	MEK + HO	→	0.50	CCHO	1.00	HCHO	1.00	CCO-O2	1.00	RCO3	1.50	R2O2	1.00	RO2	CCO-O2 = RCO3
C57	MEK + hv →	→	1.00	CCO-O2	1.00	CCHO	1.00	RO2-R	1.00	RCO3	1.00	RO2			CCO-O2 = RCO3 and RO2-R = RO2
C58A	GLY + hv →	→	0.80	HO2	0.45	HCHO	1.55	CO							HCHO + 1.55 CO = 1
C58B	GLY + hv →	→	0.13	HCHO	1.87	CO									HCHO + 1.55 CO = 1
C68A	MGLY + hv →	→	1.00	HO2	1.00	CO	1.00	CCO-O2	1.00	RCO3					CCO-O2 = RCO3
C68B	MGLY + hv →	→	1.00	HO2	1.00	CO	1.00	CCO-O2	1.00	RCO3					CCO-O2 = RCO3
C69	MGLY + HO	→	1.00	CO	1.00	CCO-O2	1.00	RCO3							CCO-O2 = RCO3 and CO + 2 CCO-O2 ≤ 3
C70	MGLY + NO3	→	1.00	HNO3	1.00	CO	1.00	CCO-O2	1.00	RCO3					CCO-O2 = RCO3 and CO + 2 CCO-O2 ≤ 3
D1	ETHE + HO	→	0.22	CCHO	1.56	HCHO	1.00	RO2-R	1.00	RO2					RO2-R = RO2
D8	ETHE + O	→	1.00	HCHO	1.00	CO	1.00	HO2	1.00	RO2-R	1.00	RO2			RO2-R = RO2
D9	ETHE + NO3	→	1.00	NO2	2.00	HCHO	1.00	R2O2	1.00	RO2					R2O2 = RO2
G7	AFG1	→	1.00	HCOCO-O2	1.00	RCO3									HCOCO-O2 = RCO3
G8	AFG1 + hv →	→	1.00	HO2	1.00	HCOCO-O2	1.00	RCO3							HCOCO-O2 = RCO3
G9	HO + AFG2	→	1.00	C2CO-O2	1.00	RCO3									C2CO-O2 = RCO3
G10	AFG2 + hv →	→	1.00	HO2	1.00	CO	1.00	CCO-O2	1.00	RCO3					CCO-O2 = RCO3
G30	BALD + HO	→	1.00	BZ-CO-O2	1.00	RCO3									BZ-CO-O2 = RCO3
G32	BALD + NO3	→	1.00	HNO3	1.00	BZ-CO-O2	1.00	RCO3							BZ-CO-O2 = RCO3
G33	BZ-CO-O2 + NO	→	1.00	BZ-O	1.00	CO2	1.00	NO2	1.00	R2O2	1.00	RO2			R2O2 = RO2
G35	PBZN	→	1.00	BZ-CO-O2	1.00	NO2	1.00	RCO3							BZ-CO-O2 = RCO3
G46	HO + PHEN	→	0.15	RO2-NP	0.85	RO2-R	0.20	GLY	1.00	RO2	4.70	-C			RO2-NP + RO2-R ≤ 1.05
G52	HO + CRES	→	0.15	RO2-NP	0.85	RO2-R	0.20	MGLY	5.50	-C	1.00	RO2			RO2-NP + RO2-R ≤ 1.05

Table 2-8 (continued). Constraints on Yield Variations for Carter (1990a) Mechanism

Generalized Reactions

Label	Reaction		Yield	Species	Yield	Species	Yield	Species	Yield	Species	Yield	Species	Yield	Species	Constraint
AnOH	HO + AARn	→	AnRR	RO2-R	AnNR	RO2-N	AnXN	RO2-XN	AnNP	RO2-NP	ANRH	HO2		Alkanes	RR + NR + XN = 1
			AnR2	R2O2	AnRO2	RO2	AnA1	HCHO	AnA2	CCHO	AnA3	RCHO		Aromatics	RR + RH ≤ 1
			AnK3	ACET	AnK4	MEK	AnCO	CO	AnCO2	CO2	AnPH	PHEN		Alcohols, ect.	RR + RH = 1
			AnCR	CRES	AnBZ	BALD	AnGL	GLY	AnMG	MGLY	AnU1	AFG1		MEOH	A1 ≤ 1
			AnU2	AFG2	AnXC	-C								ETOH	A2 ≤ 1
OnOH	OLEn + HO	→												Alkenes	None
OnO3	OLEn + O3	→													
OnOA	OLEn + OA	→													
OnN3	OnN3 + NO3	→													

Figure 2-2. Trends in Peroxy Radical Self Reactions

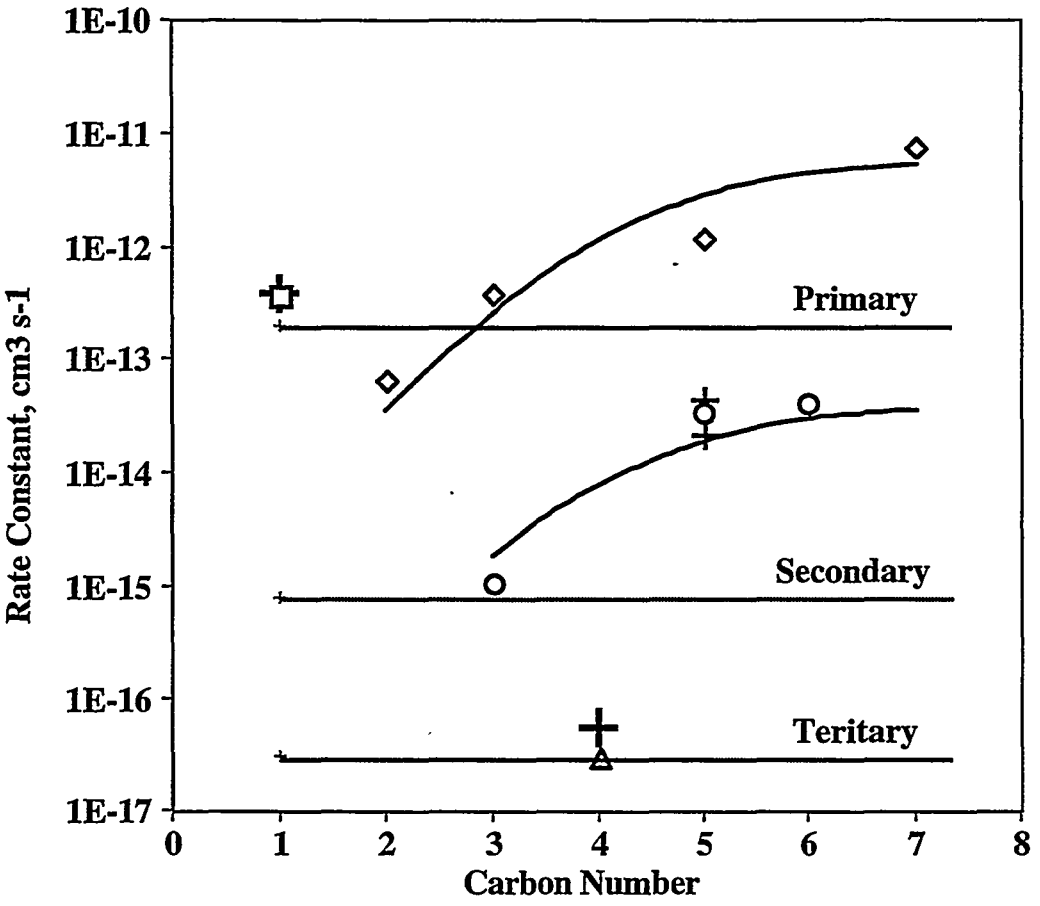

available will be greater than for those reactions for which measurement data are available. For the reaction parameters set by analogy, how much greater the uncertainty estimates should be is not clear and the difference between the measured reaction and the analog reaction will vary depending upon the reaction type. We therefore assumed that the uncertainties of the reaction parameters within a reaction group were all the same as those for the parameters of the base reaction.

Table 2-9. Reactions with Strongly Correlated Rate Constants

The rate constants for all of the reactions in the following groups are strongly correlated ($\rho = 1$).

HOx Group 1
A29A HO2 + HO2
A30A NO3 + HO2
A29B HO2 + HO2 + M
A30B NO3 + HO2 + M

HOx Group 2
A29C HO2 + HO2 + H2O
A30C NO3 + HO2 + H2O
A29D HO2 + HO2 + H2O
A30D NO3 + HO2 + H2O

B1 Group
B1 RO2 + NO → NO
B11 RO2R + NO → NO2 + HO2
B15 R2O2 + NO → NO2
B19 RO2N + NO → RNO3
B23 RO2XN + NO → -N
C4B HOCOO + NO → -C + NO2 + HO2
G2 RO2NP + NO → NPHE

B2 Group
B2 RCO3 + NO → NO
C13 CCOO2 + NO → CO2 + NO2 + HCHO + RO2R + RO2
C28 C2COO2 + NO → CCHO + RO2R + CO2 + NO2 + RO2
C62 HCOCOO2 + NO → NO2 + CO2 + CO + HO2
G33 BZCOO2 + NO → BZO + CO2 + NO2 + R2O2 + RO2

B4 Group (Also strongly correlated with C18 Group)
B4 RCO3 + NO2 → NO2
C14 CCOO2 + NO2 → PAN
C63 HCOCOO2 + NO2 → GPAN

B5 Group (Also strongly correlated with B6)
B5 RO2 + HO2 → HO2
B12 RO2R + HO2 → -OOH
B16 R2O2 + HO2 →

Table 2-9 (continued). Reactions with Strongly Correlated Rate Constants

B20 RO2N + HO2 → -OOH + MEK + #1.5-C
B24 RO2XN + HO2 → -OOH
G3 RO2NP + HO2 → -OOH + #6-C
G44 BZO + HO2 → PHEN
G60 BZ(NO2) + HO2 → NPHE

B6 Group (Also strongly Correlated with B5)
B6 RCO3 + HO2 → HO2
C15 CCOO2 + HO2 → -OOH + CO2 + HCHO
C30 C2COO2 + HO2 → -OOH + CCHO + CO2
G36 BZCOO2 + HO2 → -OOH + CO2 + PHEN
C65 HCOCOO2 + HO2 → HO2 → -OOH + CO2 + CO

B8 Group
B8 RO2 + RO2 →
B13 RO2R + RO2 → RO2 + #0.5 HO2
B17 R2O2 + RO2 → RO2
B21 RO2N + RO2 → RO2 + #0.5 HO2 + MEK + #1.5-C
B25 RO2XN + RO2 → RO2 + #0.5 HO2
G4 RO2-NP + RO2 → RO2 + #0.5 HO2 + #6-C

B9 Group
B9 RO2 + RCO3 →
B14 RO2R + RCO3 → RCO3 + #0.5 HO2
B18 R2O2 + RCO3 → RCO3
B22 RO2N + RCO3 → RCO3 + #0.5 HO2 + MEK + #1.5-C
B26 RO2XN + RCO3 → RCO3 + HO2
C16 CCOO2 + RO2 → RO2 + #0.5 HO2 + CO + HCHO
C31 C2COO2 + RO2 → RO2 + #0.5 HO2 + CCHO + CO2
C37 BZCOO2 + RO2 → RO2 + #0.5 HO2 + CO2 + PHEN
C66 HCOCOO2 + RO2 → RO2 + #0.5 HO2 + CO2 + CO
G5 RO2NP + RCO3 → RCO3 + HO2 + MEK + #6-C

B10 Group
B10 RCO3 + RCO3 →
C17 CCOO2 + RCO3 → RCO3 + HO2 + CO2 + HCHO
C32 C2COO2 + RCO3 → RCO3 + HO2 + CCHO + CO2
C67 HCOCOO2 + RCO3 → RCO3 + HO2 + CO2 + CO
G38 BZCOO2 + RCO3 → RCO3 + HO2 + CO2 + PHEN

C12 Group
C12 CCHO + NO3 → HNO3 + CCOO2 + RCO3
C60 GLY + NO3 → HNO3 + #0.6 HO2 + #1.2 CO + #0.4 HCOCOO2 + RCO3
C70 MGLY + NO3 → HNO3 + CO + CCOO2 + RCO3

C18 Group (Strongly Correlated with B4 Group)
C18 PAN → CCOO2 + NO2 + RCO3
C64 GPAN → HCOCOO2 + NO2 + RCO3

G43 Group
G43 BZO + NO2 → NPHE

Table 2-9 (continued). Reactions with Strongly Correlated Rate Constants

G59 $BZ(NO2)O + NO2 \rightarrow$ #2-N + #6-C

G45 Group
G45 $BZO \rightarrow PHEN$
G61 $BZ(NO2)O \rightarrow NPHE$

Photolysis Reactions
The photolysis rate constants for each pair are strongly correlated due to the use of the same absorption cross sections.

A12A $NO3 + h\nu \rightarrow NO + O2$
A12A $NO3 + h\nu \rightarrow NO2 + O3$

C1 $HCHO + h\nu \rightarrow$ #2 $HO2 + CO$
C2 $HCHO + h\nu \rightarrow H2 + CO$

C58A $GLY + h\nu \rightarrow$ #0.8 $HO2$ + #0.45 $HCHO$ + #1.55 CO
C58B $GLY + h\nu \rightarrow$ #0.13 $HCHO$ + #1.87 CO

The photolysis rate constants for AFG1 and AFG2 are strongly correlated and were arbitrarily chosen to fit environmental chamber tests.

G8 $AFG1 + h\nu \rightarrow HO2 + HCOCOO2 + RCO3$
G10 $AFG2 + h\nu \rightarrow HO2 + CO + CCOO2 + RCO3$

The products of reactions C68B and G10 are strongly correlated, but not the rates.

2.4 Recent Data Evaluations and their Uncertainties

Our original uncertainty assignments for the rate parameters (Stockwell et al., 1994) were based on the reviews of DeMore et al. (1990) (NASA 9) and Atkinson et al. (1989). There have been more recent versions of these data evaluations released: DeMore et al. (1992) (NASA 10) and Atkinson et al. (1992). Below, we compare the uncertainty estimates of Stockwell et al. (1994) to those of the newer evaluations for several key reactions.

$HO + NO_2 \rightarrow HNO_3$

The uncertainty estimates are unchanged between NASA 9 and NASA 10.

$NO_2 + h\nu \rightarrow NO + O$

NASA 9	1.3
NASA 10	1.2

$O_3 + h\nu \rightarrow O1D2$

NASA 9	1.4
NASA 10	1.2

The recommended quantum yields and absorption cross sections are the same in the NASA 9 and NASA 10 evaluations for both the NO_2 and O_3 photolysis reactions. The most important difference between the two evaluations for both reactions is the relative confidence of the reviewers in the recommended data. In NASA 10, for the O_3 reaction, the uncertainty estimates have been revised downward in spite of strong recommendations for additional measurements.

$HCHO + h\nu \rightarrow 2\,HO_2 + CO$

NASA 9	1.4
NASA 10	1.4

The uncertainty estimates are unchanged between the NASA 9 and NASA 10 evaluations.

$O_3 + NO \rightarrow NO_2 + O_2$

The uncertainty estimates are also unchanged between the NASA 9 and NASA 10 evaluations for this reaction.

CCO-O2 (CH_3CO_3) + $NO_2 \rightarrow$ PAN

This reaction is now included in the NASA 10 evaluations. The form of the rate constant is given as a termolecular reaction, described in DeMore et al. (1992) as:

$k_o = (8\pm4) \times 10^{-29}$	$n = 7.0 \pm 2.0$
$k_\infty = (12\pm2) \times 10^{-12}$	$m = 1.0\pm1.0$

There is relatively large uncertainty in the lower pressure limit, and the uncertainty assigned by Stockwell et al. (1994) is comparable with the more recent data. The main reduction in the uncertainty is that k_∞ appears to be better measured (1.2 compared to 2.0) and the temperature dependence uncertainty is now ± 1.0 compared to 4.0. Given the large sensitivity of PAN chemistry to these reactions, the uncertainty reductions do not greatly change the conclusions of the combined sensitivity/uncertainty analysis.

$$PAN \rightarrow CCO\text{-}O2\ (CH_3CO_3) + NO_2$$

According to Atkinson et al. (1992), the lower pressure limit for the $\Delta E/R$ is ±968, and the high pressure limit is ±136. Again, the major change was due to the high pressure limit.

$$CCO\text{-}O2\ (CH_3CO_3) + NO \rightarrow CO_2 + NO_2 + HCHO + RO2\text{-}R + RO_2$$

This reaction is now included in the NASA 10 evaluations. $k = 2.4 \times 10^{-11} \exp(-0/T)$ with $f(298) = 2$ and $\Delta E/R = \pm 200$. The f(298) is the same as assigned by Stockwell et al. (1994), but the $\Delta E/R$ has been revised downward slightly by 100.

$$O1D2 + H_2O \rightarrow 2\ HO$$

The uncertainty estimates are unchanged between the NASA 9 and NASA 10 evaluations for this reaction.

$$HO_2 + NO \rightarrow HO + NO_2$$

The uncertainty estimates are unchanged between the NASA 9 and NASA 10 evaluations for the reaction of HO_2 with NO.

2.5 Uncertainty Assignments for Specific Organic Species

Our comprehensive compilation of uncertainty estimates for Carter's detailed mechanism (Stockwell et al., 1994) was completed early in our study and used the most recent evaluations available at the time. We believe that our original assignments remain valid for most reactions. For the most influential rate constants, we have compared the assignments used in our study to the more recent evaluations. The only significant differences we found are for the estimated uncertainties in the action spectra for NO_2 and O_3 photolysis reactions, which have been revised downward (less uncertain). Given that in the combined sensitivity/uncertainty analysis we neglected the uncertainties in photolysis rates associated with actinic fluxes, we believe that the more conservative uncertainty estimates (Stockwell et al., 1994) are likely to be more realistic, and we have retained them for our analysis. For the reaction rate constants of organic-HO reactions, the only important uncertainty assignment that changes significantly based on Atkinson (1994) or NASA (1992) is that for methanol, for which Atkinson (1994) gives a lower uncertainty than assumed in the original sensitivity/uncertainty calculations. Because of the importance of this reaction, we have repeated our sensitivity/uncertainty analysis with the updated values.

We list the results of our most recent literature search. Atkinson (1994) gives revised rate parameters and their uncertainties for the reaction of HO with a number of specific organic species treated by Stockwell et al. (1994). In the rate expressions given by Atkinson (1994), the uncertainties represent 2.0 least squares standard deviations and are often nonsymmetric. He also estimated an overall uncertainty at 298°K, which is not as well defined.

Alkanes

The estimated overall uncertainty at 298°K for alkanes appears to differ little from previous assignments, except for cyclopropane.

Ethane

Atkinson (1994)

$(1.51, +0.16, -0.15) \times 10^{-17}\ T^2 \exp(-492 \pm 31) / T$

Estimated overall uncertainty at 298°K, ± 20%

n-Butane

Atkinson (1994)

$(1.55, +0.31, -0.26) \times 10^{-17}\ T^2 \exp(180 \pm 64) / T$

Estimated overall uncertainty at 298°K, ± 20%

2-Methylpropane

Atkinson (1994)

$(1.11, +0.14, -0.13) \times 10^{-17}\ T^2 \exp(256 \pm 47) / T$

Estimated overall uncertainty at 298°K, ± 25%

2,2,4-Trimethylpentane

Atkinson (1994)

$(2.06, +0.47, -0.39) \times 10^{-17}\ T^2 \exp(201 \pm 76) / T$

Estimated overall uncertainty at 298°K, ± 20%

Cyclopropane

Atkinson (1994)

8.4×10^{-14} at 298°K

f(298) = 1.5

Alkenes

Ethene

NASA 10 shows that HO + ethene should be treated as a termolecular reaction.

$k_0 = (1.0 \pm 0.6) \times 10^{-28}$ $\quad n = 0.08 \pm 2.0$

$k = (8.8 \pm 0.9) \times 10^{-12}$ $\quad m = 0, +0, -2$

Propene

The rate constant has been recently measured by Tsang (1991).

$k = 4.86 \times 10^{-12} \exp(+504 / T)$

Uncertainty factor = 1.15

2-Methyl-1-Butene

On the basis of the references consulted above, there does not appear to be much change for the other alkenes because these were assigned uncertainties similar to propene.

Aromatics

Toluene

Atkinson (1994) reports one new measurement at 299°K. The uncertainty of this measurement is a factor of 1.3, which is well within the estimates of Stockwell et al. (1994).

Oxygen-Containing Organics : Carbonyls

Formaldehyde

Atkinson (1994)

$$(1.2, +0.31, -0.26) \times 10^{-14}\ T \exp(287 \pm 74) / T$$

or

$$(8.24, +2.59, -1.98) \times 10^{-18}\ T^2 \exp(753 \pm 86) / T$$

Both have comparable values at 298°K with an estimated overall uncertainty of ± 25%.

Acetaldehyde

The uncertainty estimates are unchanged between the NASA 9 and NASA 10 evaluations for this reaction.

Oxygen-Containing Organics : Alcohols

Methanol

Atkinson (1994)

$(6.01, +0.58, -0.53) \times 10\text{-}18\ T^2 \exp(170 \pm 34) / T$

Estimated overall uncertainty at 298°K, ± 25%

The uncertainty estimates are unchanged between the NASA 9 and NASA 10 evaluations for this reaction.

Ethanol

The uncertainty estimates are unchanged between the NASA 9 and NASA 10 evaluations for this reaction.

Oxygen-Containing Organics : Ethers

Methyl tert-butyl ether

Atkinson (1994)

$(6.54, +2.13, -1.61) \times 10^{-18}\ T^2 \exp(483 \pm 88) / T$

Estimated overall uncertainty at 298°K, ± 40%

Ethene, Propene, and Higher Alkene Chemistry

The combined sensitivity/uncertainty analysis (shown in Chapter 3) identifies the product yields for the reactions of HO with alkenes as extremely important. Because of these concerns, the RO2 and RO2-R yields were examined more closely for ethene, propene, and higher alkenes.

For reactions of HO with ethene and propene, the RO2 and RO2-R yields should be regarded as certain. For the case of the formation of HCHO and CCHO from ethene, the yield of formaldehyde should be considered as uncertain by ±15% of the recommended yield coefficients, with the constraint that HCHO + 2 CCHO is constant.

Ethene Chemistry

Atkinson (1994) presents the most recent data on the reaction mechanism for HO with ethene. His mechanism is based on the experiments of Niki et al. (1981). The first step in the reaction is the addition of HO to the double bond.

$$H_2C{=}CH_2 + HO \rightarrow H_2C(HO)CH_2$$

The adduct reacts with oxygen to produce a peroxy radical that can react with nitric oxide.

$$H_2C(HO)CH_2 + O_2 \rightarrow H_2C(HO)CH_2O_2$$

$$H_2C(HO)CH_2O_2 + NO \rightarrow H_2C(HO)CH_2O + NO_2$$

A fraction of about 0.78 of the H2C(HO)CH_2O decomposes to yield two formaldehyde molecules.

$$H_2C(HO)CH_2O \rightarrow H_2C(HO) + HCHO$$
$$H_2C(HO) + O_2 \rightarrow HCHO + HO_2$$

The remaining fraction, about 0.22, reacts with O_2 directly to form glycolaldehyde.

$$H_2C(HO)CH_2O + O_2 \rightarrow H_2C(HO)CHO + HO_2$$

It appears that the most uncertain aspect is not the amount of RO2 and RO2-R which should be included in the mechanism, but rather the split between the HCHO and the glycolaldehyde forming steps. Because acetaldehyde, CCHO, is used to represent glycolaldehyde, the uncertainty in Carter's mechanism is in the relative yields for HCHO and CCHO production.

Propene

Atkinson (1994) presents results based on the work of Cvetanovic (1976). There are two possible addition sites for the HO radical. In the atmosphere, both reaction sites yield the same reaction products in the presence of NO. Either way, the products are HCHO, CCHO, and HO_2.

A fraction of about 0.35 HO reacts with the secondary carbon atom.

$$CH_3CH{=}CH_2 + HO \rightarrow CH_3(HO)CHCH_2$$
$$CH_3(HO)CHCH_2 + O_2 \rightarrow CH_3(HO)CHCH_2O_2$$
$$CH_3(HO)CHCH_2O_2 + NO \rightarrow CH_3(HO)CHCH_2O + NO_2$$
$$CH_3(HO)CHCH_2O + O_2 \rightarrow CH_3CHO + HCHO + HO_2$$

The remaining fraction of about 0.65 HO radicals react with the primary carbon attached to the double bond.

$CH_3CH{=}CH_2 + HO \rightarrow CH_3CHCH_2OH$

$CH_3CHCH_2OH + O_2 \rightarrow CH_3CHO_2CH_2OH$

$CH_3CHO_2CH_2OH + NO \rightarrow CH_3CHOCH_2OH + NO_2$

$CH_3CHOCH_2OH + O_2 \rightarrow CH_3CHO + HCHO + HO_2$

Higher Alkene Considerations

There are fewer data on product yields for alkenes C > 3 than for ethene and propene. Atkinson (1990), Grosjean and Seigneur (1991), and Atkinson (1994) discuss the current understanding of alkene chemistry. There are several sources of uncertainty for the yields of the reaction products for the reaction of higher alkenes with HO:

- Site of HO addition to the double bond
- Hydrogen atom abstraction reaction rates
- Isomerization of the β-hydroxyalkoxy radical
- Carbonyl product species and yields
- Yield of organic nitrates

The mechanisms for the reactions of higher alkenes with HO radicals are assumed to be analogous to the mechanisms for the ethene and propene reactions (Carter, 1990a). He gives the generalized reaction for higher alkenes as:

$$\text{alkene} + HO \rightarrow \quad (1\text{-}p_N)(\text{RO2-R} + p_1\,\text{HCHO} + p_2\,\text{CCHO} + p_3\,\text{RCHO} + p_4\,\text{ACET} + p_5\,\text{MEK}) + p_N\,\text{RO2-N}$$

where p_N = organic nitrate yield;

p_1, p_2, p_3, p_4, and p_5 = structural parameters of the reacting alkene;

RCHO = propionaldehyde and lumped higher aldehydes;

ACET = acetone;

MEK = methyl ethyl ketone and lumped higher ketones.

A number of assumptions have been made to create this generalized reaction. All introduce uncertainty into the product yields.

It is assumed that 65% of the HO radicals add to the terminal carbon for primary alkenes based on Cvetanovic's work (1976) with propene. This is a very uncertain assumption that has not been verified by any experimental work. Also, the work of Cvetanovic was not a published result. The site of the HO addition will affect the nature of the carbonyl products in many cases. The uncertainty in the nature of the products introduces uncertainty into the yield coefficients because the real products may require different yields of the model carbonyl species HCHO, CCHO, RCHO, ACET, or MEK, to be described properly. It is difficult to be precise on the magnitude of the uncertainty, but an estimate of 15% to 20% is a reasonable assignment for these yields. The uncertainty could be somewhat greater because the yields are related to the number of structural groups of the alkenes in the mixture. However, given the very limited extent of the data and that all the higher alkenes are assumed to react similarly to propene, it is difficult to be more precise than the uncertainty estimate of 15% to 20% given above.

Possible abstraction reactions are ignored in the generalized reaction. It is known that a fraction of HO radicals react with alkenes through abstraction (Atkinson 1994). For the smaller alkenes it is estimated to be less that 5% to 10%, but it may be as high as 15% for the larger alkenes (Grosjean and Seigneur, 1991). Measured fractions are less than 10% for 1-butene, 8.9 % for 1,3-cyclohexadiene, and 15.3% for 1,4-cyclohexadiene. For 1-hexene, the fraction of HO radicals that abstract a hydrogen has been estimated to be between 10% and 15% (Atkinson, 1990). Abstraction reactions have a significant effect on the uncertainty assignment for the RO2-R. The products of the HO-alkene abstraction reaction yield unsaturated compounds. The unsaturated compounds react again to produce additional peroxy radicals. An additional source of peroxy radicals is the possible isomerization of the β-hydroxyalkoxy radicals. Isomerization would lead to additional peroxy radicals (Atkinson and Lloyd, 1984) and additional NO to NO_2 conversions, which are not included in the mechanism. Finally, there is also the possibility of the production of methyl peroxy radicals through decomposition reactions of some of the hydroxyalkoxy radicals. All these effects taken together suggest that an uncertainty of ±30% is a reasonable assignment to the peroxy radical yields.

Another possible source of uncertainty derives from the uncertainty in the organic nitrate yield. This is assumed to be zero for many alkenes, but this could be a source of error for the higher alkenes. We fold this uncertainty into the estimates given above.

2.6 Summary

We estimated the uncertainty associated with stoichiometric parameters for the parameters in W.P.L. Carter's (1990a) detailed mechanism. The uncertainty in product yields is greatest for organic reactions. Experimental measurements of the product yields for many secondary reactions are limited for many species. Better measurements of product yields are needed for aromatic oxidation, ozonolysis of alkenes, biogenic hydrocarbons, RO_2 and RO reactions, nitrate radical-organic products, and organic nitrate yields and decomposition mechanisms. The choices of lumping procedure, the number of species, and the processes to omit all affect the uncertainties associated with a mechanism.

We made uncertainty estimates for the yield parameters of many reactions in Carter's detailed mechanism. Emphasis was placed on the products for the organic reactions because their uncertainties are the greatest. Uncertainty factors were assigned to the yield parameters for the secondary core chemistry and for the generalized reactions of alkane, aromatic, alkene, and other compounds. Because of conservation of radicals and nitrogen, we reported an uncertainty range for each uncertain stoichiometric parameter subject to constraints required.

The mechanism of aromatic oxidation is highly uncertain because a large fraction (20% to 40%) of the organic products has not been identified. The aromatic yield parameters have been optimized to fit smog chamber data. From a basic science point of view, the chemistry is relatively unknown. However, if the chemistry is viewed as a parameterization, it may be a reasonable approximation of the atmospheric oxidation of aromatic compounds.

More data on product yields for the reactions of alkenes $C > 3$ are needed. There are several sources of uncertainty for the reaction product yields in the reaction of higher alkenes with HO. These include: site of HO addition to the double bond, hydrogen atom abstraction reaction rates,

isomerization of the β-hydroxyalkoxy radical, carbonyl product species and yields, and the yield of organic nitrates.

3. UNCERTAINTIES IN INCREMENTAL REACTIVITIES AND REACTIVITY ADJUSTMENT FACTORS

3.1 Introduction

The results presented in this chapter extend those of a previous study (Yang et al., 1994, 1995, Bergin et al., 1995) in which rate parameters and exhaust emissions composition were the only sources of uncertainty considered. Here, a more comprehensive uncertainty analysis of reactivities of individual organic compounds and of motor vehicle exhaust emissions are provided, considering uncertainties associated with selected product yields in the SAPRC chemical mechanism in addition to uncertainties in rate parameters. We have incorporated correlations across parameters, rather than treating them independently. Exhaust emissions from recent tests of 11 fuels are used for the RAF uncertainty analysis, including eight fuels tested for CARB (1994) and three fuels tested for NREL (1994). For additional comparison, emissions data for three fuels included in our previous study are also incorporated into this analysis.

3.2 Method and Uncertainties in SAPRC Mechanism Parameters

This section documents the methods used for the uncertainty analysis, then describes the estimates of uncertainty made for SAPRC parameters and exhaust emissions composition. The uncertainty estimates for rate parameters have been described previously, but are summarized below. Next, the approaches used to develop estimates of uncertainties in product yields are described, along with the basis for selecting the product yields that would be treated as random variables in the Monte Carlo simulations. Estimates of correlations between parameters are discussed for rate parameters and product yields. The final subsection describes how the exhaust composition data were processed for this study.

3.2.1 Monte Carlo Analysis with Latin Hypercube Sampling

In order to evaluate the impacts of uncertainties in chemical parameters and exhaust composition on incremental reactivities (IRs) and RAFs, several steps have been performed. In the previous study (Yang et al., 1994), a first-order uncertainty analysis was performed to identify the most influential rate parameters. In this work, uncertain product yields and the set of influential rate parameters are treated as random variables in Monte Carlo simulations with Latin Hypercube Sampling (LHS) (Iman and Shortencarier, 1984) in order to estimate uncertainties in incremental

reactivities. Correlations across parameters are incorporated into the analysis where appropriate. The Monte Carlo results for IRs are then combined with uncertainties in exhaust emissions compositions to estimate uncertainties in RAFs for alternative fuels and reformulated gasolines.

As discussed in our previous report, California's regulations used average MIR (Maximum Incremental Reactivity) values from 39 simulations, representing high-ozone cases in cities across the United States (Carter, 1994). The simulations were conducted using a box model for a 10-hour simulation period. For each case, MIR conditions were defined by first adjusting the amount of NO_X input to the simulation to maximize the overall incremental reactivity of a base reactive organic gases (ROG) mixture. Maximum ozone incremental reactivity (MOIR) calculations were done in a similar manner, except that the amount of NO_X was adjusted to maximize the peak ozone concentration produced with the base ROG mixture. To make our calculations tractable, however, two approximations were made to the MIR and MOIR calculation procedures. First, IRs were estimated from a single set of simulation conditions (Carter, 1994) developed to yield results close to the average from the original 39 simulations. Second, IR values for all compounds were calculated from the same simulation, as the local sensitivity of the O_3 concentration to the initial concentration of each organic compound in a mixture. The local sensitivity coefficients were calculated using the Direct Decoupled Method (DDM) (Dunker, 1984; McCroskey and McRae, 1987). The MIR and MOIR simulation conditions used in the analysis are shown in Table 3-1. The input ROG:NO_X ratios for the MIR and MOIR simulations were 5.8:1 and 8.0:1, respectively. MIRs and MOIRs of 26 explicit organic compounds and five lumped organic classes are calculated in each simulation run. Yang et al. (1995) showed that the box-model results are not significantly affected by the approximation made in the way the alkanes and aromatics were lumped in this study.

In the previous study (Yang et al., 1994), first-order estimates were made of the contribution of uncertainty in the value of each rate parameter in the SAPRC mechanism to uncertainty in the predicted concentrations of selected product species. The DDM was used in that study to calculate sensitivities of key output species to rate parameters, which were then combined with uncertainty estimates (discussed below). Seventy-three of 201 rate parameters in the mechanism were identified as influential. Rate constants associated with the initial oxidation steps for all of the organic compounds of interest in the study were included in this set. For the MIR simulation

Table 3-1. Simulation Conditions for MIR and MOIR Cases

Latitude = 36.22° N	Temp. = 296 to 305° K
Declination = 16.5°	Total HC[a] = 15.38 mmol/m^2/day
Time = 8 a.m. to 6 p.m.	Total NO_x (for MIR)[a] = 3.84 mmol/m^2/day
Mixing height = 293 to 1823 m	Total NO_x (for MOIR)[a] = 2.57 mmol/m^2/day
Photolysis height = 640 m	

Initial and aloft concentrations (ppm) for the base mixture[g]

Species	initial	aloft	Species	initial	aloft
NO_2 (MIR)	3.62×10^{-2}	0	α-pinene	1.00×10^{-4}	0
NO (MIR)	1.09×10^{-1}	0	Ethene	1.01×10^{-2}	4.67×10^{-4}
HONO (MIR)	2.95×10^{-3}	0	HCHO	6.48×10^{-3}	2.25×10^{-3}
NO_2 (MOIR)	2.42×10^{-2}	0	CCHO[c]	3.90×10^{-3}	3.23×10^{-4}
NO (MOIR)	7.25×10^{-2}	0	RCHO[d]	2.30×10^{-3}	0
HONO (MOIR)	1.97×10^{-3}	0	Benzaldehyde	1.34×10^{-4}	0
O_3	0	7.04×10^{-2}	Unknown	1.00×10^{-4}	0
CO	2.03	2.03	AAR1[e]	4.10×10^{-2}	3.69×10^{-3}
CO_2[b]	$3.30\times10^{+2}$	$3.30\times10^{+2}$	AAR2[e]	4.33×10^{-2}	1.16×10^{-3}
H_2O	$1.99\times10^{+4}$	$1.99\times10^{+4}$	AAR3[e]	1.68×10^{-2}	1.08×10^{-4}
Methane[b]	1.79	1.79	OLE1[f]	8.85×10^{-3}	8.09×10^{-5}
Isoprene	1.00×10^{-4}	0	OLE2[f]	1.14×10^{-2}	1.09×10^{-4}

[a] Initial concentrations plus total emissions

[b] Constant-concentration species

[c] Acetaldehyde

[d] Propionaldehyde and higher aldehydes

[e] Lumped classes of alkanes and aromatics

[f] Lumped classes of alkenes

[g] For incremental reactivity calculations, initial concentrations equal to 4.76×10^{-5} ppm are added for each of 26 explicit organic compounds or classes

conditions, these 73 rate parameters accounted for more than 98% of the total variance of the output concentrations of O_3, PAN, HCHO, HO, and H_2O_2.

To reduce computational requirements in the Monte Carlo calculations, LHS was used to sample from the probability distributions of rate parameters. The optimal size of an LHS sample depends on balancing the cost of additional model runs against the accuracy required in the output distributions (Iman and Helton ,1985). Iman and Helton also recommended a sample size greater than the number of 4/3m, where m represents the number of randomly varying independent parameters. The results presented below are for a sample size of 400. For independent parameters, an option in the LHS code is used, which minimizes rank correlations between parameters, as is recommended for non-normally distributed random variables. For any

correlated parameter, however, an additional calculation is conducted to incorporate the correlation estimate with the corresponding random sample generated from the LHS.

In order to identify the rate constants that have the most influence on incremental reactivities, linear multivariate regression analysis is performed on the IR values generated in the Monte Carlo calculations. This approach is valid if the responses to parameter variations are approximately linear within the range of variation. The equation used is:

$$\frac{IR_{ij}}{IR_j} = B_{oj} + \sum_{l=1}^{w} B_{lj} \frac{p_{il}}{p_l} \qquad (3.1)$$

where IR_{ij} = IR value for compound j generated in simulation i;

IR_j = nominal IR value of compound j;

B_{oj} = constant coefficient;

B_{lj} = regression coefficient corresponding to lth uncertain rate constant;

p_{il} = value of lth parameter used in simulation i;

p_l = nominal value of lth parameter.

The equation is fit to the Monte Carlo results using a least squares criterion. Uncertainty contributions are estimated from the Monte Carlo results by combining normalized regression coefficients from Equation (3.1) with 1σ uncertainty estimates for the given parameter.

3.2.2 Estimates of Uncertainty in Rate Parameters

Rate parameter uncertainty estimates for the SAPRC mechanism were compiled by Stockwell et al. (1994) from panel reviews published by NASA (1990) and IUPAC (1989), supplemented with additional reviews and some original estimates. From this compilation, estimates were made of the standard deviations for each rate constant at the simulation conditions used in the IR calculations. In most cases, the published uncertainty factors represent the subjective judgment of the reviewers rather than statistical analysis of experimental results. The NASA and IUPAC panel estimates were interpreted as corresponding to $\pm 1\sigma$. However, in some independent reviews the definition of uncertainties was not clear, so our subjective judgment was added to that of the reviewers. Where different sources were in conflict or definitions unclear, we conservatively used the interpretation or assignment that would give the largest uncertainty.

For the photolysis rates in the SAPRC90 mechanism, only uncertainties in the action spectra were considered, with actinic fluxes viewed as given. For the action spectra, uncertainties given by NASA were adopted as multiplicative factors, which are assumed to apply uniformly across wavelengths. NASA panel uncertainty factors were available for most of the inorganic species, HCHO, and organic peroxide. For the more complex organic compounds, original assignments were made. Among all photolysis rates, the estimated uncertainties are lowest for O_3 and NO_2 and greatest for the unknown aromatic products (AFG1 and AFG2).

For rate constants of second-order reactions, the NASA panels give uncertainty factors at 298°K [f(298)] and estimates of uncertainty in the Arrhenius temperature coefficients (ΔE). From these values, the uncertainty of a second-order rate constant can be estimated as a function of temperature:

$$f(T) = f(298)\exp\left|\frac{\Delta E}{R}\left(\frac{1}{T} - \frac{1}{298}\right)\right| \tag{3.2}$$

where R is the ideal gas constant. The (1σ) uncertainty of a thermal rate constant is estimated as:

$$\sigma_k(T) \approx \frac{k(T) \times f(T) - k(T) / f(T)}{2} \tag{3.3}$$

If NASA and IUPAC uncertainty estimates were available, they were compared after converting the IUPAC estimates to the NASA format, and the larger uncertainty estimate was adopted. For parameters of several thermal reactions for which NASA and IUPAC have not reported uncertainty estimates, other reviews (Atkinson, 1986, 1990; Atkinson and Carter, 1984; and Atkinson and Lloyd, 1984) were used. For reactions determined by analogy, the uncertainty estimates of the root reactions were assigned.

For recombination (Troe) reactions, the NASA panel provides uncertainty estimates at 300°K for the lower pressure rate constant, k_o, and the high pressure rate constant, k_∞, and for the temperature dependence factors. Apparent second-order rate constants between the high and low pressure limits are estimated using the Troe expression:

$$k(T,M) = \frac{k_o(T)[M]}{1+\frac{k_o(T)[M]}{k_\infty}} 0.6\{1+\log_{10}[(k_o(T))[M]/k_\infty(T)]^2\}^{-1} \quad (3.4)$$

To estimate uncertainties for IR simulation conditions, uncertainties for $k_o(T)$ and $k_\infty(T)$ were estimated from the NASA formula, then Monte Carlo calculations were performed to propagate uncertainties through the Troe expression. Independent lognormal distributions were assumed for the random variables k_o^{300} and k_∞^{300} ,and normal distributions for n and m.

PAN and its analogs were all treated similarly. IUPAC evaluations were used to estimate the PAN formation and decomposition reaction uncertainties because they were not included in the 1990 NASA evaluation. A rather high uncertainty was assigned to the temperature dependence. Similar to the procedure for the inorganic Troe reactions, Monte Carlo calculations were performed to calculate the apparent second-order rate constant distribution for each k_o- k_∞ pair.

Finally, uncertainty estimates were compiled for rate parameters of the primary reactions of 26 organic compounds for which IRs were to be estimated. The compounds selected included alkanes, alkenes, aromatics, and oxygenated species. Uncertainties for the reactions of HO radicals with most of the selected organics were based on the review of Atkinson (1986), supplemented with original evaluations for several compounds. The ΔE assignments were chosen to be consistent with the uncertainties in similar reactions. Uncertainty assignments for O_3-alkene reactions were taken from Atkinson and Carter (1984). Original estimates of the uncertainty in ΔE values for these reactions were made for this study (Stockwell et al., 1994).

Based on the first-order uncertainty analysis for the rate parameters (Yang et al., 1994), the most influential rate constants were identified with respect to uncertainties in predicted O_3, PAN, HO, HO_2, and HNO_3 concentrations. Table 3-2 lists these influential rate parameters with their 1σ uncertainties, which were propagated as lognormally distributed variables through the Monte Carlo analysis.

Many rate constants in the SAPRC mechanism have been estimated by analogy, or share the same kinetic data or the same absorption cross sections. Consequently, strong correlations exist between some parameters, as listed in Table 2-9. The correlated parameters among the random variables in our analysis are indicated in Table 3-2. Because it is difficult to evaluate the degree of the correlations, a perfect correlation (i.e., correlation coefficient, $\rho = 1$) has been assumed in each case to simplify the correlation estimates. Results obtained with all random variables treated independently and results obtained using perfect correlations were used to bound the results that would be obtained for the intermediate correlations that might be more realistic than either extreme case.

3.2.3 Uncertainties in Product Yields

Products of reactions of atmospheric inorganic species are relatively well known. For many organic reactions in atmospheric chemical mechanisms, however, the product yields are relatively uncertain. Uncertainties in the products of organic reactions generally arise from a lack of chemical data, or from lumping procedures used to condense mechanisms. Detailed product information for many secondary reactions is relatively limited, especially for higher-molecular-weight organic species. More and better measurements of product yields are needed for aromatic oxidation, ozonolysis of alkenes, biogenic hydrocarbons, RO_2 and RO reactions, nitrate radical, organic products, and organic nitrate yields and decomposition mechanisms. In this study, uncertainty estimates were based on evaluation of the quality of experimental measurements of given products, with the published uncertainty values interpreted as lower and upper bounds. In addition to uncertainties in the available kinetics data, the lumping procedure, number of species, and reaction formulation all affect the uncertainties associated with a mechanism. However, tracing these uncertainties is beyond our present scope.

Uncertainty estimates of product yields are documented in Chapter 2. Because mechanisms include hundreds of product yields, it is not feasible to incorporate all of them into a comprehensive uncertainty analysis. Tables 2-3 through 2-7 list the most important product yields that are considered uncertain in the SAPRC mechanism, including most organic product species and radicals. It was necessary to further limit the number of product yields varied in the uncertainty calculations by focusing on the product yields associated with the reactions to which MIRs and MOIRs are most sensitive. The apportionment of uncertainty in IRs among rate

Table 3-2. Rate Constants Treated as Random Variables

Reactions	k(300° K)[a]	1σ	Reactions	k(300° K)[a]	1σ
Thermal reactions:			1,3-Butadiene + HO →	$9.67\times10^{+4}$	$1.79\times10^{+4}$
O3 + NO →	$2.76\times10^{+1}$	$5.18\times10^{+0}$	2-M^{-1}-butene + HO →	$8.80\times10^{+4}$	$1.62\times10^{+4}$
O1D + H2O →	$3.23\times10^{+5}$	$7.60\times10^{+4}$	2-M^{-2}-butene + HO →	$1.26\times10^{+5}$	$2.33\times10^{+4}$
O1D + M →	$4.29\times10^{+4}$	$1.01\times10^{+4}$	3-M-cyclopentene + HO →	$9.62\times10^{+4}$	$1.78\times10^{+4}$
HO + NO2 →	$1.66\times10^{+4}$	$4.53\times10^{+3}$	Isoprene + HO →	$1.46\times10^{+5}$	$2.72\times10^{+4}$
HO + CO →	$3.52\times10^{+2}$	$9.58\times10^{+1}$	Benzene + HO →	$1.89\times10^{+3}$	$5.08\times10^{+2}$
HO2 + NO →	$1.21\times10^{+4}$	$2.86\times10^{+3}$	Toluene + HO →	$8.67\times10^{+3}$	$1.62\times10^{+3}$
HO2 + HO2 →	$2.54\times10^{+3}$	$9.02\times10^{+2}$	Ethylbenzene + HO →	$1.04\times10^{+4}$	$3.22\times10^{+3}$
HO2 + HO2 + H2O →[b]	1.34×10^{-1}	4.74×10^{-2}	1,2,4-TMB + HO →	$4.77\times10^{+4}$	$1.47\times10^{+4}$
HO2 + HO2 + H2O →[b]	1.04×10^{-1}	3.64×10^{-2}	m,p-Xylene + HO →	$2.86\times10^{+4}$	$8.86\times10^{+3}$
RO2 + NO →	$1.13\times10^{+4}$	$8.55\times10^{+3}$	o-Xylene + HO →	$2.01\times10^{+4}$	$4.56\times10^{+3}$
RO2R + NO →[c]	$1.13\times10^{+4}$	$8.55\times10^{+3}$	MEK + HO →	$1.70\times10^{+3}$	$4.60\times10^{+2}$
RO2R + HO2 →	$7.19\times10^{+3}$	$5.48\times10^{+3}$	Methanol + HO →	$1.38\times10^{+3}$	$6.64\times10^{+2}$
NO2 + CRES →	$3.08\times10^{+4}$	$2.35\times10^{+4}$	Ethanol + HO →	$4.81\times10^{+3}$	$2.30\times10^{+3}$
CCHO + HO →	$2.30\times10^{+4}$	$8.15\times10^{+3}$	MTBE + HO →	$4.17\times10^{+3}$	$1.47\times10^{+3}$
RCHO + HO →	$2.89\times10^{+4}$	$1.02\times10^{+4}$	ETBE + HO →	$1.10\times10^{+4}$	$3.90\times10^{+3}$
CCO-O2 + NO →	$1.46\times10^{+4}$	$1.10\times10^{+4}$	**O3 reactions:**		
CCO-O2 + NO2 →	$1.07\times10^{+4}$	$7.22\times10^{+3}$	Ethene + O3 →	2.75×10^{-1}	4.25×10^{-2}
CCO-O2 + HO2 →[d]	$7.19\times10^{+3}$	$5.48\times10^{+3}$	Propene + O3 →	1.74×10^{-2}	6.03×10^{-3}
CCO-O2 + RO2 →	$1.60\times10^{+4}$	$1.21\times10^{+4}$	Isoprene + O3 →	2.20×10^{-2}	7.63×10^{-3}
C2CO-O2 + NO →[e]	$1.46\times10^{+4}$	$1.10\times10^{+4}$	1,3-Butadiene + O3 →	1.16×10^{-2}	4.89×10^{-3}
C2CO-O2 + NO2 →[f]	$1.23\times10^{+4}$	$9.52\times10^{+3}$	2-M-1-butene + O3 →	1.85×10^{-2}	6.40×10^{-3}
C2CO-O2 + HO2 →[d]	$7.19\times10^{+3}$	$5.55\times10^{+3}$	2-M-2-butene + O3 →	6.33×10^{-1}	2.65×10^{-1}
C2CO-O2 + RO2 →[g]	$1.60\times10^{+4}$	$1.21\times10^{+4}$	3-M-cyclopentene + O3 →	3.93×10^{-1}	1.65×10^{-1}
PPN →	$9.95\times10^{+11}$	$7.04\times10^{+11}$	**Troe reactions:**		
HCHO + HO →	$1.43\times10^{+4}$	$3.40\times10^{+3}$	CCO-O2 + NO2 →	$1.23\times10^{+4}$	$9.52\times10^{+3}$
AAR1 + HO →	$2.76\times10^{+3}$	$5.13\times10^{+2}$	PAN →	4.04×10^{-2}	2.76×10^{-2}
AAR2 + HO →	$8.80\times10^{+3}$	$3.04\times10^{+3}$			
AAR3 + HO →	$3.59\times10^{+4}$	$9.63\times10^{+3}$	**Photolysis reactions:**	Actn. Spectra.	Uncert. Fac.
OLE1 + HO →	$3.19\times10^{+5}$	$5.89\times10^{+4}$	NO2 + hν →		1.3
OLE2 + HO →	$9.69\times10^{+4}$	$1.79\times10^{+4}$	NO3 + hν → NO + O2		2.0
OLE1 + O2 →	1.72×10^{-2}	3.20×10^{-3}	NO3 + hν → NO2 + O[h]		2.0
OLE2 + O2 →	2.34×10^{-1}	4.35×10^{-2}	O3 + hν→ O1D + O2		1.4
HO reactions:			HCHO + hν→2HO2 + O2		1.4
Ethane + HO →	$4.02\times10^{+2}$	$7.42\times10^{+1}$	HCHO + hν →H2 + CO		1.4
Butane + HO →	$3.76\times10^{+3}$	$6.96\times10^{+2}$	CCHO + hν →		1.4
2-Methylpentane + HO →	$8.31\times10^{+3}$	$1.89\times10^{+3}$	RCHO +hν →		1.4
M-cyclopentane + HO →	$1.19\times10^{+4}$	$3.18\times10^{+3}$	MEK + hν →		1.5
2,2,4-TMB + HO →	$5.46\times10^{+3}$	$1.01\times10^{+3}$	MGLY + hν →		1.6
Ethene + HO →	$1.24\times10^{+4}$	$1.75\times10^{+3}$	AFG1 + hν →		3.0
Propene + HO →	$3.82\times10^{+4}$	$5.39\times10^{+3}$	AFG2 + hν →[i]		3.0

[a] nominal rate constants, ppm min units.

[b] correlated with HO2+HO2 + H2O → [c] correlated with RO2 + NO → [d] correlated with RO2R + HO2 →

[e] correlated with CCOO2 + NO → [f] correlated with CCOO2 + NO2 → [g] correlated with CCOO2 + RO2 →

[h] correlated with NO3 + hν → NO + O2 [i] correlated with AFG1 + hν →

constants completed earlier (Yang et al., 1994) was used as one guide for narrowing down the set of uncertain yields to be treated as random variables in the Monte Carlo simulations. A first-

order analysis of the sensitivity of O_3 and other key products to stoichiometric coefficients in the RADM2 mechanism (conducted by Gao et al. [1995]) was also used for qualitative guidance.

The previous study suggested that the rate constants of most primary oxidation reactions of explicit organic compounds are influential to MIR and MOIR uncertainties. For 30 representative organic compounds or classes in the mechanism, the uncertain product yields of reactions with HO and (where applicable) O_3 are included in the uncertainty analysis. Product yields of four photolysis reactions are also included: photolysis of carbonyl products from aromatics oxidation (AFG1 and AFG2), MEK, and methyl glyoxal. Product yields for HO reactions with methane and HCHO, and for HCHO photolysis, are excluded. The oxidation chemistry of methane and HCHO is relatively well known, so there is little probability of a significant product yield uncertainty for these reactions. The MIR scale used in RAF calculations has been defined at a low ROG:NO_X ratio (5.8:1) (Carter, 1994), so peroxy radical-peroxy radical reactions generally have little influence on the uncertainty of MIRs. Product yields of these reactions were also excluded from the analysis. The only peroxy radical reaction for which uncertainties in product yields are included is C2COO2 + HO2, because MIRs for alkenes and acetaldehyde were somewhat sensitive to the rate constant for this reaction. Finally, for products with relatively low nominal yields, such as acetone, glyoxal, methyl glyoxal, benzaldehyde, phenol, and cresol in most reactions, the product yields are treated as certain because the variation of their values would have a negligible effect on uncertainties of calculated reactivities.

To further reduce the number of parameters to be treated as random variables, a few additional simplifications were made. Uncertainties in yields of H_2O, CO_2, and C (to balance reactions) were assumed to be negligible. For many organics, uncertainties in the nominally small fractional yields of relatively unreactive species, such as acetone, methyl ethyl ketone, glyoxal, benzaldehyde, phenol, and cresol, were also assumed to be negligible. Similarly, we assumed that low fractional yields of peroxy radicals would be less important than higher yields of other peroxy radicals in the same reactions. In this case, only the peroxy radicals with higher yields were treated as uncertain. Finally, yields of some products of simple or well known reactions, such as the acetaldehyde yield in the reaction of ethene + HO and the HO_2 yield in the reaction

Table 3-3. Uncertainty Ranges Associated with Product Yields

Reaction			Uncertainties of product yields			
AFG1	hv	→	[0.8, 1.2] HO2	[0.8, 1.2] HCOCO	[0.8, 1.2] RCO3	
AFG2	hv	→	[0.8, 1.2] HO2	[0.8, 1.2] CCOO2	[0.8, 1.2] RCO3	
CCHO	HO	→	[0.9, 1.0] CCOO2	[0.9, 1.0] RCO3		
RCHO	HO	→	[0.9, 1.0] C2COO2	[0.9, 1.0] RCO3		
ACET	HO	→	[0.68, 0.92] MGLY	[0.17, 0.23] HCHO		
MEK	HO	→	[0.43, 0.58] HCHO	[0.43, 0.58] CCHO	[1.05, 1.95] R2O2	[1.05, 1.95] RO2
MEK	hv	→	[0.8, 1.2] CCOO2	[0.85, 1.0] CCHO	[0.7, 1.0] RO2R	[0.8, 1.2] RCO3
			[0.7, 1.0] RO2			
MGLY	hv	→	[0.8, 1.2] HO2	[0.8, 1.2] CCOO2	[0.8, 1.2] RCO3	
C2COO2	HO2	→	[0.7, 1.0] -OOH	[0.85, 1.15] CCHO		
ETHE	HO	→	[1.23, 1.56] HCHO	[0.7, 1.0] RO2R	[0.7, 1.0] RO2	
ETHE	O3	→	[0.85, 1.15] HCHO	[0.1, 1.4] HO2		
ETHANE	HO	→	[0.85, 1.0] CCHO			
BUTANE	HO	→	[0.28, 0.52] R2O2	[0.49, 0.66] CCHO	[0.45, 0.61] MEK	[1.28, 1.52] RO2
2MEC5	HO	→	[0.52, 0.97] R2O2	[0.46, 0.63] RCHO	[0.62, 0.83] MEK	[1.42, 2.08] RO2
BENZEN	HO	→	[0.34, 0.64] AFG1	[0.54, 0.76] RO2R	[0.54, 0.76] RO2	
TOLUEN	HO	→	[0.29, 0.53] AFG2	[0.52, 0.74] RO2R	[0.52, 0.74] RO2	
C2BENZ	HO	→	[0.29, 0.53] AFG2	[0.52, 0.74] RO2R	[0.52, 0.74] RO2	
OXYLEN	HO	→	[0.31, 0.43] MGLY	[0.47, 0.87] AFG2	[0.57, 0.82] RO2R	[0.57, 0.82] RO2
MPXYLE	HO	→	[0.31, 0.43] MGLY	[0.47, 0.87] AFG2	[0.57, 0.82] RO2R	[0.57, 0.82] RO2
124TMB	HO	→	[0.42, 0.78] AFG2	[0.57, 0.82] RO2R	[0.53, 0.71] MGLY	[0.57, 0.82] RO2
MEOH	HO	→	[0.8, 1.0] HCHO			
ETOH	HO	→	[0.78, 0.92] CCHO			
MTBE	HO	→	[0.33, 0.45] HCHO	[0.35, 0.47] MEK	[0.26, 0.48] R2O2	[1.26, 1.48] RO2
ETBE	HO	→	[0.99, 1.33] HCHO	[0.48, 0.66] MEK	[0.81, 1.27] R2O2	[1.81, 2.51] RO2
224TMC5	HO	→	[0.62, 1.14] R2O2	[0.63, 0.86] RCHO	[0.49, 0.66] MEK	[1.61, 2.14] RO2
MECYC5	HO	→	[0.24, 0.33] HCHO	[0.49, 0.91] RCHO	[1.39, 2.57] R2O2	[0.42, 0.56] MEK
			[2.39, 3.57] RO2			
PROPEN	HO	→	[0.7, 1.0] RO2R	[0.85, 0.93] CCHO	[0.85, 1.15] HCHO	[0.7, 1.0] RO2
PROPEN	O3	→	[0.55, 0.75] HCHO	[0.43, 0.58] CCHO		
13BUTD	HO	→	[0.7, 1.0] RO2R	[0.85, 1.15] HCHO	[0.85, 0.95] RCHO	[0.7, 1.0] RO2
13BUTD	O3	→	[0.43, 0.58] HCHO	[0.43, 0.58] RCHO		
2M1BUT	HO	→	[0.7, 1.0] RO2R	[0.85, 1.15] HCHO	[0.85, 0.96] MEK	[0.7, 1.0] RO2
2M1BUT	O3	→	[0.47, 0.63] HCHO	[0.77, 1.04] MEK		
2M2BUT	HO	→	[0.7, 1.0] RO2R	[0.85, 0.90] ACET	[0.85, 1.15] CCHO	[0.7, 1.0] RO2
2M2BUT	O3	→	[0.43, 0.58] CCHO	[0.46, 0.62] MEK	[0.43, 0.58] ACET	
3MCYCPNTE	HO	→	[0.66, 0.89] CCHO	[0.66, 0.89] RCHO	[0.54, 1.01] RO2R	
3MCYCPNTE	O3	→	[0.19, 0.35] RO2R	[0.55, 0.75] CCHO	[0.43, 0.58] RCHO	[0.30, 0.40] MEK
			[0.19, 0.35] RO2			
AAR1	HO	→	[0.12, 0.16] HCHO	[0.27, 0.36] CCHO	[0.14, 0.19] RCHO	[0.23, 0.43] R2O2
			[1.20, 1.40] RO2			
AAR2	HO	→	[0.44, 0.83] R2O2	[0.15, 0.20] CCHO	[0.17, 0.24] RCHO	[0.26, 0.35] MEK
			[1.38, 1.77] RO2			
AAR3	HO	→	[0.31, 0.41] MGLY	[0.34, 0.62] AFG2	[0.26, 0.35] MEK	
OLE1	HO	→	[0.61, 1.13] RO2R	[0.74, 1.00] HCHO	[0.22, 0.29] CCHO	[0.52, 0.71] RCHO
			[0.74, 1.26] RO2			
OLE1	O3	→	[0.46, 0.63] HCHO	[0.22, 0.29] CCHO	[0.30, 0.41] RCHO	
OLE2	HO	→	[0.65, 1.21] RO2R	[0.27, 0.37] HCHO	[0.55, 0.74] CCHO	[0.51, 0.70] RCHO
			[0.72, 1.28] RO2			
OLE2	O3	→	[0.24, 0.33] HCHO	[0.39, 0.52] CCHO	[0.28, 0.37] RCHO	[0.31, 0.42] MEK

of methanol + HO, were assumed to be certain. Table 3-3 lists the reactions for which product yields will be considered as random variables in the Monte Carlo analysis. Appendix B shows the corresponding constraints applied to these uncertain product yields and to the correlated peroxy radical products.

Correlations between product yields exist because of constraints on product formation. Constraints were applied to uncertain product yields based on the following three rules:

(1) Radical conservation: when the number of reactant radicals is equal to the number of product radicals, this balance should be maintained.

(2) Carbon mass balance: when possible, carbon mass balance should be maintained; however, in most cases of lumped species, carbon mass is lost and this constraint cannot be applied.

(3) Total peroxy radical operators: the total radical operators in the SAPRC mechanism, RO2 and RCO3, are usually equal to the sum of the organic peroxy or acyl peroxy radicals produced by the reaction. When this is true, it should be maintained.

Based on these constraints, a product yield could be correlated with two or more species in a reaction. For example, for peroxy radicals RCO3 is an operator for HCOCOO2, CCOO2, and C2COO2, so the yields of the explicit acyl peroxy radicals were treated as random variables, and the RCO3 yield was constrained to equal their sum, in each random sample. The constraints essentially assign a perfect correlation between the associated products.

Uniform distributions were used over the assigned range of error bounds for each uncertain stoichiometric coefficient. Combining both uncertain rate constants and product yields, a total of 171 independent random variables and 45 dependent variables were considered in the analysis.

3.2.4 Exhaust Emissions Compositions

Uncertainties in RAFs were calculated for exhaust emissions from fuels tested for CARB (1994) and NREL (1994). For calculating RAFs, 28 organic compounds are treated explicitly, with the remaining species identified in the emissions tests represented either by surrogate assignments, or by one of three lumped alkanes/aromatics classes or two lumped olefins classes. For those

alkanes and aromatics that were not treated explicitly, emissions were allocated to lumped classes according to the rate of reaction with hydroxyl radical, with:

$$c_k = \sum_{i=1}^{w} c_i \times \frac{1-\exp(-k_{OHi} \times INTOH)}{1-\exp(-k_{OHk} \times INTOH)} \tag{3.5}$$

where w = number of compounds assigned to lumped class;

c_k = total emissions rate for lumped class;

c_i = emissions rate for an explicit compound;

k_{OH} = rate constant for reaction with hydroxyl radicals;

INTOH = parameter representing typical hydroxyl radical concentrations integrated over duration of simulation.

Emissions of alkenes not treated explicitly are simply summed in their lumped classes without reactivity weighting.

After lumping the emissions into SAPRC species or classes, an estimate of uncertainty in exhaust composition for each fuel was calculated as the standard deviation in the emissions across vehicles tested on the fuel. If more than one test was conducted on a given vehicle, these results were first averaged, and the standard deviations calculated on the mean results for each vehicle. Correlations across species in the exhaust compositions were also calculated, and incorporated into the Monte Carlo simulations for RAFs as described in Yang et al. (1994). For fuels tested on only one or two vehicles, no standard deviations were calculated. Table 3-4 gives a list of the fuel/vehicle combinations used for the RAF calculations in this chapter. In order to compare results with and without product yield uncertainties and correlations, the calculations reported here also include three fuels from the Auto/Oil AQIRP (Burns et al., 1991; Hochhauser et al., 1992), which were considered in our previous study.

3.3 Effect of Uncertainties on MIRs and MOIRs

As stated above, 216 influential rate constants and product stoichiometric coefficients were treated as random variables in Monte Carlo simulations. Figure 3-1 shows the resulting uncertainties (1σ) in time-varying O_3 concentrations predicted for the MIR and MOIR

Table 3-4. Fuels Included in RAF Calculations

Source	Fuel Code	Description	No. of Vehicles Tested
CARB:	TLEV[a] RF-A	reformulated average gasoline	6
	TLEV[a] M85	%85 methanol, 15% gasoline (PH2) blend	2
	TLEV[a] E85	%85 ethanol, 15% gasoline (PH2) blend	2
	TLEV[a] CNG	compressed natural gas	1
	TLEV[a] LPG	liquefied petroleum gas	2
	TLEV[a] PH2	phase 2 gasoline	7
	LEV[b] RF-A	reformulated average gasoline	6
	LEV[b] PH2	phase 2 gasoline	8
NREL:	RFG	CA phase 2 reformulated gasoline	1
	E50	%50 ethanol, 50% gasoline (RFG) blend	1
	E85	%85 ethanol, 50% gasoline (RFG) blend	1
Auto/Oil:	AMOT A	industry average gasoline	8
	AMOT F	reformulated gasoline[c]	8
	METH Z	%85 methanol, 15% gasoline(AMOTA) blend	17

[a] transitional low-emission vehicle

[b] low-emission vehicle

[c] a test gasoline with a Reid Vapor Pressure of 8.8 psia and with reduced aromatics, olefins, and 90% distillation temperature

Figure 3-1. Predicted Ozone Concentrations with 1σ Uncertainties for MIR and MOIR Simulation Conditions

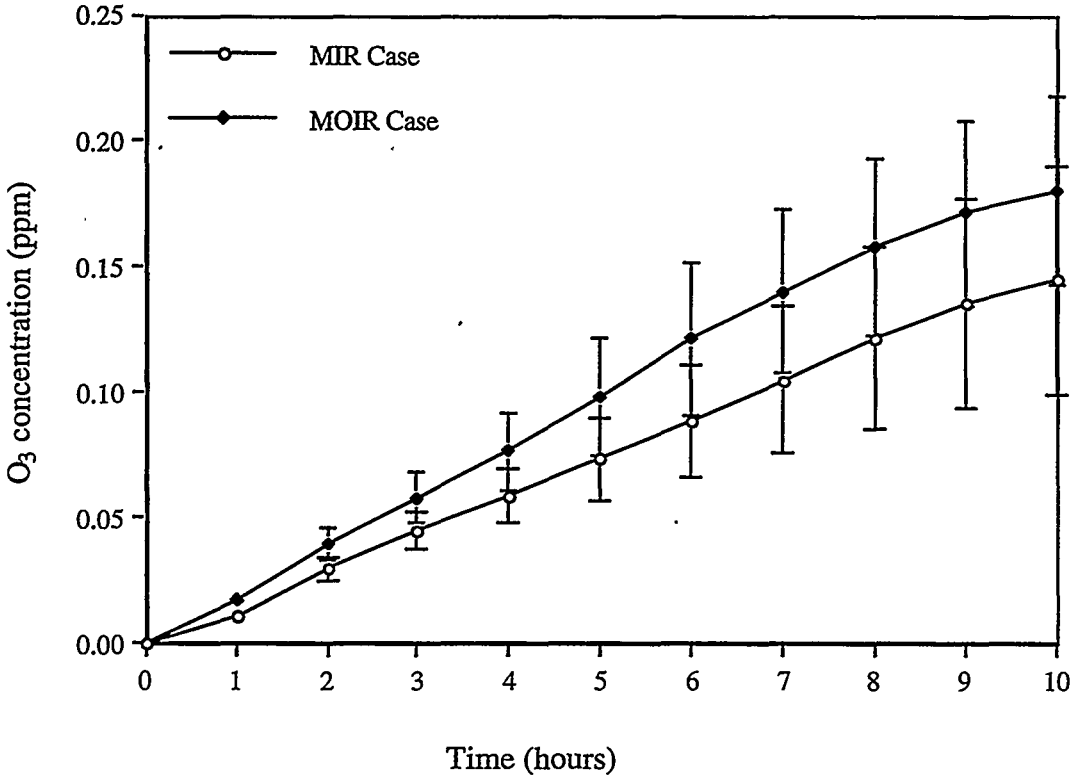

conditions. Somewhat higher uncertainty in predicted O_3 is seen for the MIR scenario than for the MOIR scenario, with respective uncertainties of 32% and 21% around the means from the two sets of simulations. Ozone exhibits higher sensitivity to the perturbation of most parameters at the lower ROG:NO_x ratio, as shown by the results of a regression analysis. The regression coefficients shown in Table 3-5 can be interpreted as the normalized sensitivities of O_3 the indicated parameters. Table 3-5 includes the parameters that contribute most to the uncertainty in the time-averaged O_3 concentrations. The dominant contribution to the uncertainty is associated with the rate constant for the HNO_3 formation reaction, which is a major sink for NO_x. Other parameters that strongly influence the uncertainty in predicted O_3 concentrations include rate constants for photolysis of O_3, NO_2, and AFG1/AFG2, for the chemistry of PAN and its analogs, and for the reactions O_3 + NO and AAR3 + HO.

Figure 3-2 shows estimated uncertainties (1σ) in the MIRs of 33 organic compounds or classes, calculated with Monte Carlo simulations, and accounting for potentially correlated uncertainties in product yields and rate constants. The uncertainties range from 25% of the mean estimate, for HCHO, to 66% of the mean, for ethanol. Of note, the inputs of NO_x for the MIR case were set specifically to maximize the IR of a base mixture, given nominal rate parameter values (Carter, 1994). This NO_x value was not adjusted from one Monte Carlo simulation to another. As a result, the system moves away from the condition of maximum reactivity as rate constants are assigned values different from their nominal values, and the average MIRs shown in Figure 3-2 are lower than the values calculated using nominal rate constants. This limitation of the study will also affect the regression results of the results for uncertainty apportionment that are presented below. To be precise, all results should be interpreted as uncertainties in incremental reactivities calculated for the simulation conditions shown in Table 3-1, as opposed to uncertainties in MIRs or MOIRs.

Figure 3-2 shows that relatively unreactive compounds tend to have somewhat higher uncertainties (as a percentage of the mean) than more reactive compounds. This is because the latter react completely over the 10-hour simulation period, so their impact on O_3 is not affected

Table 3-5. Uncertainty Apportionment for Average Ozone Concentrations by Regression Analysis

MIR case ($r^2 = 0.91$)			
Reactions or product yields	σ_k/k[a]	reg. coef.	UC%[b]
HO + NO2 →	0.27	-0.36	22.97
NO2 + hν →	0.26	0.31	16.99
O3 + NO →	0.19	-0.29	7.87
CCO-O2 + NO →[c]	0.75	0.07	7.61
CCO-O2 + NO2 →[d]	0.67	-0.08	6.92
O3 + hν →	0.34	0.13	4.82
HCHO + hν →[e]	0.34	0.10	3.14
AAR3 + HO →	0.27	0.11	2.17
O1D + M →	0.24	-0.12	2.09
AFG1 + hν →[f]	1.20	0.02	2.06
O1D + H2O →	0.24	0.11	1.61
PAN →	0.70	0.03	1.41
MOIR case ($r^2 = 0.90$)			
HO + NO2 →	0.27	-0.27	19.36
NO2 + hν →	0.26	0.26	16.61
CCO-O2 + NO →[c]	0.75	0.08	12.43
CCO-O2 + NO2 →[d]	0.67	-0.08	10.57
O3 + NO →	0.19	-0.24	7.39
AFG1 + hν →[f]	1.20	0.02	2.54
HCHO + hν →[e]	0.34	0.08	2.50
PAN →	0.70	0.04	2.40
O3 + hν →	0.34	0.07	2.29
AAR3 + HO →	0.27	0.08	1.92
HO + CO →	0.28	0.08	1.58
OLE2 + HO: RO2R,RO2	0.17	0.11	1.36

[a] Uncertainty of normalized rate constants or product yields

[b] Uncertainty contribution defined as $\{[(\sigma_k/k)(\text{reg. coef.})]^2/\sigma^2\}\times 100\%$

[c] Rate constant correlated with C2COO2 + NO →

[d] Rate constant correlated with C2COO2 + NO2 →

[e] Rate constant correlated with HCHO + hν → H2 + CO

[f] Rate constant correlated with AFG2 + hν →

by modest changes in their primary oxidation rates. In a previous analysis (Yang et al., 1994, 1995), we estimated uncertainties in relative reactivities resulting only from uncertainties in rate constants (i.e., product yield uncertainties were neglected) and assuming that the rate constants were independent. Comparing the results from the previous analysis with those shown in Figure 3-2 indicates that including correlations and product yield uncertainties generally leads to somewhat higher estimates of uncertainty in MIRs (about 10% for most compounds). The largest differences occurred for alkenes, where including product yield uncertainties increased

Figure 3-2. Uncertainties (1σ) in MIRs, Accounting for Uncertainties in Product Yields and Rate Constants of the SAPRC Mechanism

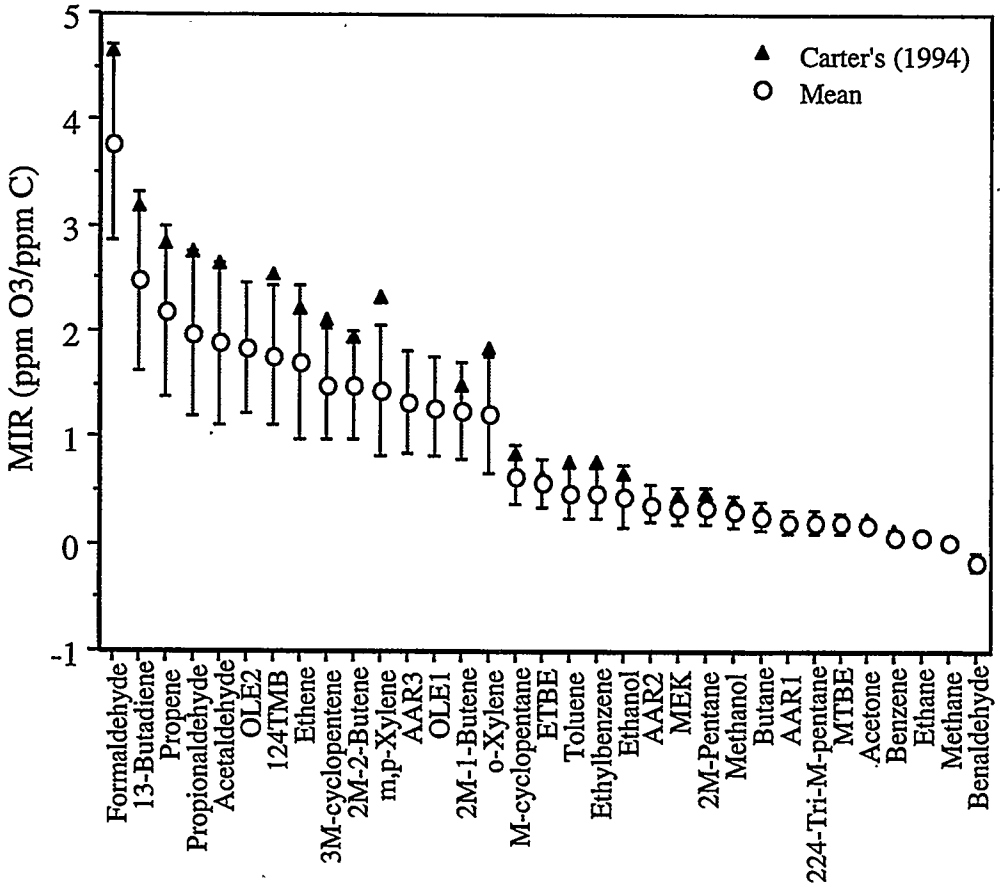

MIR uncertainty estimates by 10% to 35%. For example, the estimate of uncertainty in the MIR for propene increased from 33% to 37%, because of consideration of product yield uncertainties. In contrast to the other compounds, including product yield uncertainties and correlations reduced the estimated uncertainty in the MIR of HCHO from 32% to 25%. This reduction was due to the assumed correlation between the rates of the two HCHO photolysis reactions. The decrease represents an upper bound on the change, because a perfect correlation between the photolysis rates of the two HCHO reactions was assumed.

The rate constants and product stoichiometric coefficients that have the most influence on calculated MIRs were identified through regression analysis. Results for the MIRs of selected compounds are presented in Table 3-6. The uncertainty attribution results indicate that

parameters that are influential for predicting O_3 concentrations (rate parameters associated with PAN chemistry; HCHO, O_3, and NO_2 photolysis; HNO_3 formation; and O_3 + NO) are also influential for MIRs. In addition, the rate constant for its primary oxidation step is influential for most compounds, except for the alkenes. The alkenes react completely, so their reactivities are less sensitive to their primary oxidation rate constants. MIRs of relatively fast reacting compounds (alkenes and aldehydes) are especially sensitive to the peroxy radical yields in their reactions with HO. In a similar fashion, the aromatics are highly sensitive to the yields of AFG2 in their HO reactions. In addition to product yields, rate constants for the reactions of stable oxidation products are also influential for most compounds. For example, the MIRs of alcohols and olefins are sensitive to uncertainties in the associated aldehyde photolysis rates, and MIRs of aromatics are sensitive to uncertainties in AFG1 and AFG2 photolysis rates.

Table 3-6. Uncertainty Apportionment for MIRs by Regression Analysis

Formaldehyde (r^2 = 0.81)				Acetaldehyde (r^2 = 0.81)			
Reactions or product yields	σ_k/k[a]	reg. coef	UC%	Reactions or product yields	σ_k/k[a]	reg. coef.	UC%[b]
HCHO + hν →[c]	0.34	0.27	23.69	CCO-O2 + NO →[d]	0.75	0.18	22.48
CCO-O2 + NO →[d]	0.75	0.08	10.25	CCO-O2 + NO2 →[e]	0.67	-0.17	16.43
CCO-O2 + NO2 →[e]	0.67	-0.08	7.92	PAN →	0.70	0.13	11.15
HO + CO →	0.28	0.15	4.90	CCHO + HO →	0.36	0.19	5.84
PAN →	0.70	0.05	3.18	NO2 + hν →	0.26	0.25	5.54
NO2 + hν →	0.26	0.12	2.72	CCHO + hν →	0.34	0.19	5.10
O3 + hν →	0.34	0.09	2.66	O3 + NO →	0.19	-0.27	3.55
AAR3 + HO →	0.27	-0.11	2.57	HCHO + hν →	0.34	0.11	1.70
O3 + NO →	0.19	-0.14	2.05	CCHO + HO: CCOO2,RCO3	0.03	1.26	1.68
HCHO + HO →	0.24	-0.11	2.03	AFG2 + hν: HO2	0.12	-0.23	0.87
Propene (r^2 = 0.84)				1,3-Butadiene (r^2 = 0.83)			
PROPENE + HO: RO2R,RO2	0.17	0.69	19.48	13BUTD + HO: RO2R,RO2	0.17	0.67	20.25
CCO-O2 + NO →[d]	0.75	0.14	14.17	CCO-O2 + NO →[d]	0.75	0.15	18.52
CCO-O2 + NO2 →[e]	0.67	-0.13	10.41	CCO-O2 + NO2 →[e]	0.67	-0.15	15.45
NO2 + hν →	0.26	0.27	6.92	NO2 + hν →	0.26	0.21	4.49
PAN →	0.70	0.10	5.91	RCHO + hν →	0.34	0.15	3.76
HO + NO2 →	0.27	-0.23	5.31	PPN →	0.73	0.06	3.13
HCHO + hν →[c]	0.34	0.16	4.14	O3 + NO →	0.19	-0.22	2.67
O3 + NO →	0.19	-0.26	3.53	PAN →	0.70	0.05	2.16
PROPENE + HO →	0.14	0.26	1.77	HCHO + hν →[c]	0.34	0.09	1.28
CCHO + hν →	0.34	0.09	1.15	13BUTD + HO →	0.18	0.15	1.21

Table 3-6 (continued). Uncertainty Apportionment for MIRs by Regression Analysis

Toluene (r^2 = 0.76)				m,p-Xylene (r^2 = 0.80)			
CCO-O2 + NO →[d]	0.75	0.15	11.89	CCO-O2 + NO →[d]	0.75	0.14	15.90
HO + NO2 →	0.27	-0.35	8.89	MPXYL + HO →[e]	0.31	0.28	10.01
NO2 + hν →	0.26	0.35	8.22	CCO-O2 + NO2 →	0.67	-0.12	9.49
CCO-O2 + NO2 →[e]	0.67	-0.13	7.80	AFG1 + hν →[f]	1.20	0.06	7.43
TOL + HO →	0.19	0.47	7.58	NO2 + hν →	0.26	0.26	6.55
AFG1 + hν →[f]	1.20	0.07	6.55	MPXYL + HO: AFG2	0.17	0.37	5.60
TOL + HO: AFG2	0.17	0.42	5.11	HO + NO2 →	0.27	-0.22	4.81
PAN →	0.70	0.09	3.82	PAN →	0.70	0.08	4.05
O3 + NO →	0.19	-0.28	2.94	O3 + NO →	0.19	-0.24	3.08
TOL + HO: RO2R,RO2	0.09	0.44	1.44	MPXYL + HO: MGLY	0.09	0.38	1.53
MTBE (r^2 = 0.88)				MEK (r^2 = 0.83)			
MTBE + HO →	0.36	0.66	34.05	CCO-O2 + NO →[d]	0.75	0.22	19.20
HO + NO2 →	0.27	-0.59	15.41	CCO-O2 + NO2 →[e]	0.67	-0.20	13.08
O3 + hν →	0.34	0.31	6.80	MEK + hν →	0.42	0.29	10.26
NO2 + hν →	0.26	0.39	6.51	MEK + HO →	0.27	0.40	8.33
CCO-O2 + NO →[d]	0.75	0.12	4.97	NO2 + hν →	0.26	0.37	6.90
O1D + H2O →	0.24	0.30	3.17	PAN →	0.70	0.13	5.76
CCO-O2 + NO2 →[e]	0.67	-0.11	3.07	O3 + NO →	0.19	-0.35	3.37
O1D + M →	0.24	-0.29	2.91	HO + NO2 →	0.27	-0.25	3.27
O3 + NO →	0.19	-0.33	2.43	PPN →	0.73	0.05	1.04
HCHO + hν →	0.34	0.16	1.76	MEK + HO: R2O2,RO2	0.52	0.07	0.98
Butane (r^2 = 0.82)				Methanol (r^2 = 0.85)			
CCO-O2 + NO →[d]	0.75	0.23	16.13	HO + NO2 →	0.27	-0.59	21.04
HO + NO2 →	0.27	-0.56	12.67	MEOH + HO →	0.20	0.69	15.30
CCO-O2 + NO2 →[e]	0.67	-0.19	9.30	NO2 + hν →	0.26	0.39	8.60
NO2 + hν →	0.26	0.49	9.29	HCHO + hν →[c]	0.34	0.28	7.26
BUTANE + HO →	0.19	0.67	8.47	O3 + hν →	0.34	0.23	4.99
PAN →	0.70	0.13	4.46	CCO-O2 + NO →[d]	0.75	0.09	4.09
O3 + hν →	0.34	0.25	4.17	CCO-O2 + NO2 →[e]	0.67	-0.10	3.91
O3 + NO →	0.19	-0.42	3.69	O3 + NO →	0.19	-0.35	3.75
O1D + M →	0.24	-0.22	1.49	O1D + M →	0.24	-0.23	2.43
O1D + H2O →	0.24	0.22	1.47	O1D + H2O →	0.24	0.18	1.43

[a] Uncertainty of normalized rate constants or product yields

[b] Uncertainty contribution defined as $\{[(\sigma_k/k)(\text{reg. coef.})]^2/\sigma^2\}$x100%, where σ is 1σ uncertainty of the reactivity

[c] Rate constant correlated with HCHO + hν → H2 + CO

[d] Rate constant correlated with C2COO2 + NO →

[e] Rate constant correlated with C2COO2 + NO2 →

[f] Rate constant correlated with AFG2 + hν →

Uncertainties (1σ) of MOIRs calculated with Monte Carlo simulations are presented in Figure 3-3. Uncertainties in MOIRs range from 27% of the mean value for methane to 83% for toluene. For slowly reacting alkanes, alcohols, and ethers, the respective MOIR uncertainties are lower than the MIR uncertainties. The opposite is true for more rapidly reacting aromatics, alkenes,

and aldehydes. The inclusion of product yield uncertainties or correlations between parameters changed the uncertainties estimated for the MOIRs of most compounds by less than 15%. Exceptions included ethene, for which the uncertainty increased from 33% to 40%, and 2-methyl-1-butene, for which the uncertainty increased from 40% to 48%. In both cases the increased uncertainty resulted from high contributions from the product yields of their primary oxidation reactions. The uncertainty in the MOIR for HCHO decreased with the inclusion of correlations between the HCHO photolysis rates, from 58% to 55%.

Figure 3-3. Uncertainties (1σ) in MOIRs, Accounting for Uncertainties in Product Yields and Rate Constants of the SAPRC Mechanism

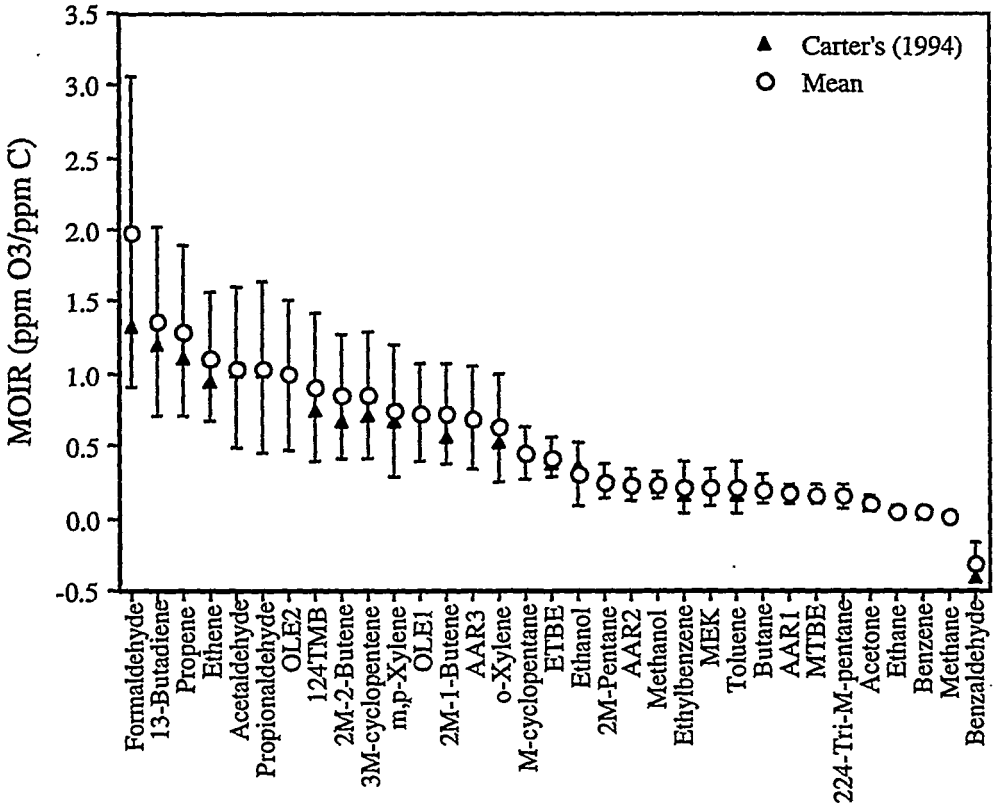

Table 3-7 shows the uncertainty apportionment results for MOIR values. Rate parameter uncertainties that were influential for MIRs, including those for O_3 and NO_2 photolysis, O^1D + H_2O, HNO_3 formation, and the chemistry of PAN and its analogs, are also important for MOIRs. However, for the rate constants that affect the supply of hydroxyl and peroxy radicals in the simulations, the response of MOIRs is opposite that of MIRs. Starting from nominal MOIR conditions, enhanced radical availability (e.g., through increased O_3 photolysis rates)

Table 3-7. Uncertainty Apportionment for MOIRs by Regression Analysis

Formaldehyde (r^2 = 0.86)				Acetaldehyde (r^2 = 0.86)			
Reactions or product yields	σ_k/k[a]	reg. coef.	UC%[b]	Reactions or product yields	σ_k/k[a]	reg. coef.	UC%[b]
O3 + hν →	0.34	-1.17	33.18	O3 + hν →	0.34	-0.61	16.82
O1D + H2O →	0.24	-1.02	12.26	PAN →	0.70	0.24	11.33
O1D + M →	0.24	1.01	11.98	CCO-O2 + NO2 →[e]	0.67	-0.24	10.45
HO + NO2 →	0.27	0.70	7.57	CCO-O2 + NO →[d]	0.75	0.18	7.53
AFG1 + hν →[c]	1.20	-0.09	2.59	O1D + H2O →	0.24	-0.56	7.12
RCHO + hν →	0.34	-0.30	2.15	O1D + M →	0.24	0.50	5.52
AAR3 + HO →	0.27	-0.35	1.92	NO2 + hν →	0.26	0.41	4.57
CCO-O2 + NO →[d]	0.75	-0.12	1.70	HO + NO2 →	0.27	0.34	3.42
OLE2 + O3 →	0.43	-0.17	1.13	CCHO + HO →	0.36	0.25	3.18
AAR3 + HO: MGLY	0.09	-0.84	1.11	O3 + NO →	0.19	-0.35	1.82
Propene (r^2 = 0.87)				1,3-Butadiene (r^2 = 0.88)			
O3 + hν →	0.34	-0.75	26.09	O3 + hν →	0.34	-0.78	25.83
PROPEN: RO2R,RO2	0.17	1.10	14.78	O1D + H2O →	0.24	-0.72	10.94
O1D + H2O →	0.24	-0.67	10.12	13BUTD: RO2R,RO2	0.17	0.94	9.85
O1D + M →	0.24	0.59	7.81	CCO-O2 + NO2 →[e]	0.67	-0.21	7.07
PAN →	0.70	0.15	4.54	O1D + M →	0.24	0.58	7.05
O2 + hν →	0.26	0.38	4.11	HO + NO2 →	0.27	0.44	5.42
CCO-O2 + NO2 →[e]	0.67	-0.13	3.17	CCO-O2 + NO →[d]	0.75	0.12	3.23
CCO-O2 + NO →[d]	0.75	0.10	2.33	NO2 + hν →	0.26	0.35	3.21
HO + NO2 →	0.27	0.24	1.69	PPN →	0.73	0.09	1.50
O3 + NO →	0.19	-0.31	1.49	AFG1 + hν →[c]	1.20	-0.05	1.27
Toluene (r^2 = 0.89)				m,p-Xylene (r^2 = 0.87)			
O3 + hν →	0.34	-1.49	30.73	O3 + hν →	0.34	-1.00	29.75
O1D + H2O →	0.24	-1.37	12.66	O1D + H2O →	0.24	-0.91	12.00
O1D + M →	0.24	1.19	9.53	O1D + M →	0.24	0.85	10.43
TOL + HO →	0.19	0.89	3.33	MPXYL + HO →	0.31	0.52	6.53
NO3 + CRES →	0.76	-0.21	3.01	HCHO + hν →[f]	0.34	-0.32	3.06
HCHO + hν →[f]	0.34	-0.45	2.83	HO + NO2 →	0.27	0.40	2.98
TOL + HO: RO2R,RO2	0.09	1.69	2.58	NO2 + hν →	0.26	0.40	2.90
HO + CO →	0.28	-0.51	2.45	MPXYL + HO: AFG2	0.17	0.58	2.62
NO2 + hν →	0.26	0.53	2.36	PAN →	0.70	0.13	2.18
HO + NO2 →	0.27	0.49	2.17	CCO-O2 + NO2 →[e]	0.67	-0.13	1.93
MTBE (r^2 = 0.92)				MEK (r^2 = 0.86)			
MTBE + HO →	0.36	0.73	56.11	CCO-O2 + NO2 →[e]	0.67	-0.39	15.97
NO2 + hν →	0.26	0.40	9.17	CCO-O2 + NO →[d]	0.75	0.33	14.77
HO + NO2 →	0.27	-0.28	4.60	O3 + hν →	0.34	-0.64	11.11
CCO-O2 + NO2 →[e]	0.67	-0.09	2.94	PAN →	0.70	0.27	8.62
O3 + NO →	0.19	-0.30	2.78	MEK + HO →	0.27	0.63	6.81
O3 + hν →	0.34	-0.17	2.76	NO2 + hν →	0.26	0.64	6.78
CCO-O2 + NO →[d]	0.75	0.06	1.93	O1D + M →	0.24	0.62	5.01
HO + CO →	0.28	-0.15	1.41	O1D + H2O →	0.24	-0.58	4.45
O1D + H2O →	0.24	-0.17	1.41	MEK + hν →	0.42	0.27	2.98
HO2 + NO →	0.24	0.17	1.37	O3 + NO →	0.19	-0.47	1.96

Table 3-7 (continued). Uncertainty Apportionment for MOIRs

Butane (r^2 = 0.84)				Methanol (r^2 = 0.90)			
CCO-O2 + NO →[d]	0.75	0.30	19.87	MEOH + HO →	0.20	0.99	25.93
CCO-O2 + NO2 →[e]	0.67	-0.31	17.27	O3 + hν →	0.34	-0.42	13.88
NO2 + hν →	0.26	0.60	10.17	NO2 + hν →	0.26	0.54	13.69
BUTANE + HO →	0.19	0.84	9.79	O1D + H2O →	0.24	-0.39	5.85
PAN →	0.70	0.22	9.66	O3 + NO →	0.19	-0.42	4.51
O3 + NO →	0.19	-0.46	3.24	HO + NO2 →	0.27	-0.29	4.06
HO + CO →	0.28	-0.27	2.31	O1D + M →	0.24	0.33	4.01
O3 + hν →	0.34	-0.21	2.03	HO2. + NO →	0.24	0.31	3.51
O1D + H2O →	0.24	-0.24	1.29	AAR2 + HO →	0.35	-0.14	1.54
HO + NO2 →	0.27	-0.20	1.17	HCHO + hν →[f]	0.34	0.13	1.28

[a] Uncertainty of normalized rate constants or product yields

[b] Uncertainty contribution defined as $\{[(\sigma_k/k)(\text{reg. coef.})]^2/\sigma^2\}$x100%, where σ is 1σ uncertainty of the reactivity

[c] Rate constant correlated with AFG2 + hν →

[d] Rate constant correlated with C2COO2 + NO →

[e] Rate constant correlated with C2COO2 + NO2 →

[f] Rate constant correlated with HCHO + hν → H2 + CO

leads to lower sensitivity of peak O_3 to added inputs of organic compounds. In contrast, under nominal MIR conditions, the main effect of increased radical availability on MIRs is positive in speeding up the rate of oxidation of the added organic compound or of its reaction intermediates, so that more NO to NO_2 conversions occur prior to the end of the simulations. As with MIRs, MOIRs for compounds that react relatively slowly with HO are sensitive to the value of that rate constant, whereas MOIRs for relatively fast-reacting compounds such as the alkenes are more sensitive to the associated peroxy radical yield.

3.4 Effect of Uncertainties on RAFs

To indicate which compounds are likely to have significant impacts on uncertainties in RAFs, Figure 3-4 shows their contributions to the composition of the exhaust emissions on a carbon basis, and Figure 3-5 shows contributions to the absolute reactivity of the exhaust emissions associated with selected test fuels, i.e., for compound j:

$$\frac{F_{Ai} IR_i}{\sum_{i=1}^{N} F_{Ai} IR_i} \qquad (3\text{-}6)$$

(Note that methane is included in the figures for completeness, but is excluded from RAF calculations.) For TLEV-RFA, TLEV-PH2, LEV-RFA, LEV-PH2, and AMOTA, the compounds or classes that contribute most to the total reactivity of exhaust emissions are fairly consistent across fuels. For these fuels, high reactivity contributions are spread across the AAR2, AAR3, OLE1, and OLE2 classes, together with ethene, propene, toluene, mp-xylene, and o-xylene, and 1,2,4-trimethylbenzene. As shown above in Figure 3-2, uncertainties relative to the mean in the MIRs of these compounds range from about 35% for the OLE2 and AAR3 classes to 52% for toluene, at the 1σ level. The absolute reactivity of M85 exhaust is dominated by HCHO and methanol. The uncertainty in the MIR for MEOH was estimated to be 47%; that for HCHO to be 25%. For E85, most of the reactivity comes from ethene (MIR uncertainty of 42%), acetaldehyde (41%), and ethanol (66%). The primary contributors to the reactivity of CNG are ethane (61%), methane (45%) and HCHO. For LPG, propane (AAR1, 49%), ethene, propene (37%), and HCHO are significant.

As discussed above, for some fuels we were able to incorporate uncertainties in emissions composition into our RAF uncertainty calculations, based on the variability of the emissions across vehicles tested on each fuel. Figure 3-6 shows uncertainties in the exhaust compositions for CARB's RF-A and Phase 2 fuels, in TLEVs and in LEVs, and for fuels AMOTF and METHZ, from the Auto/Oil study. For these fuels, organic compound emissions fractions were treated in the RAF Monte Carlo analysis as correlated, normally distributed random variables. CARB's M85, E85, CNG, and LPG data are from tests conducted on only one or two vehicles, and NREL's E85 and E50 data are from tests on only one vehicle. Thus, for the RAFs of these fuel/vehicle combinations, we neglected emissions composition uncertainties altogether. Our uncertainty estimates for these fuels reflect only uncertainty associated with parameters of the SAPRC chemical mechanism.

Figure 3-7 displays the uncertainties in the RAFs (mass basis) for the selected test fuels in the form of cumulative distribution functions. The mean and standard deviation for each RAF is printed above the figures. The median (50th percentile) values are displayed on the CDF plots.

Figure 3-4. Compositions of Exhaust Associated with Various Fuels

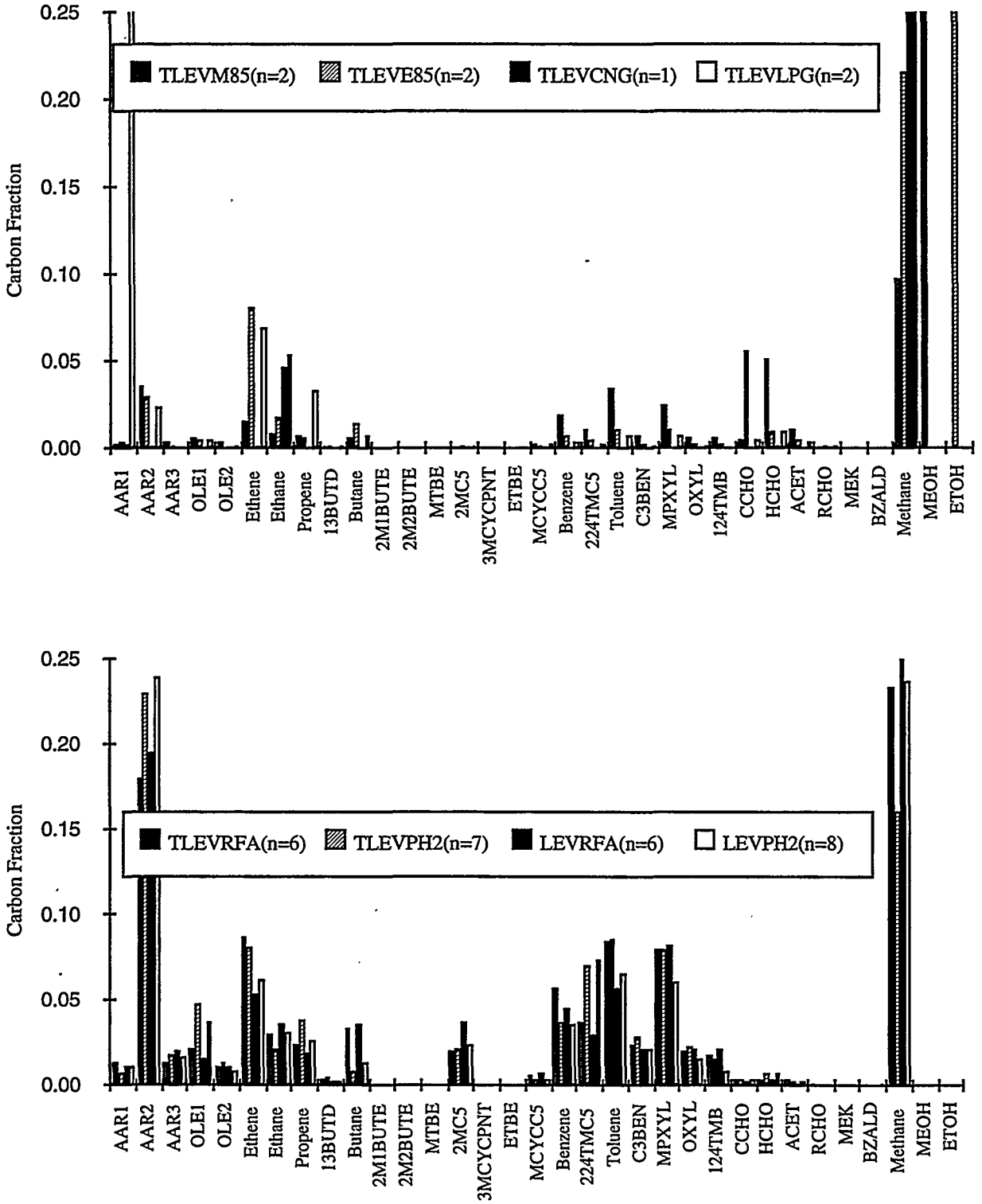

Figure 3-4 (continued). Compositions of Exhaust Associated with Various Fuels

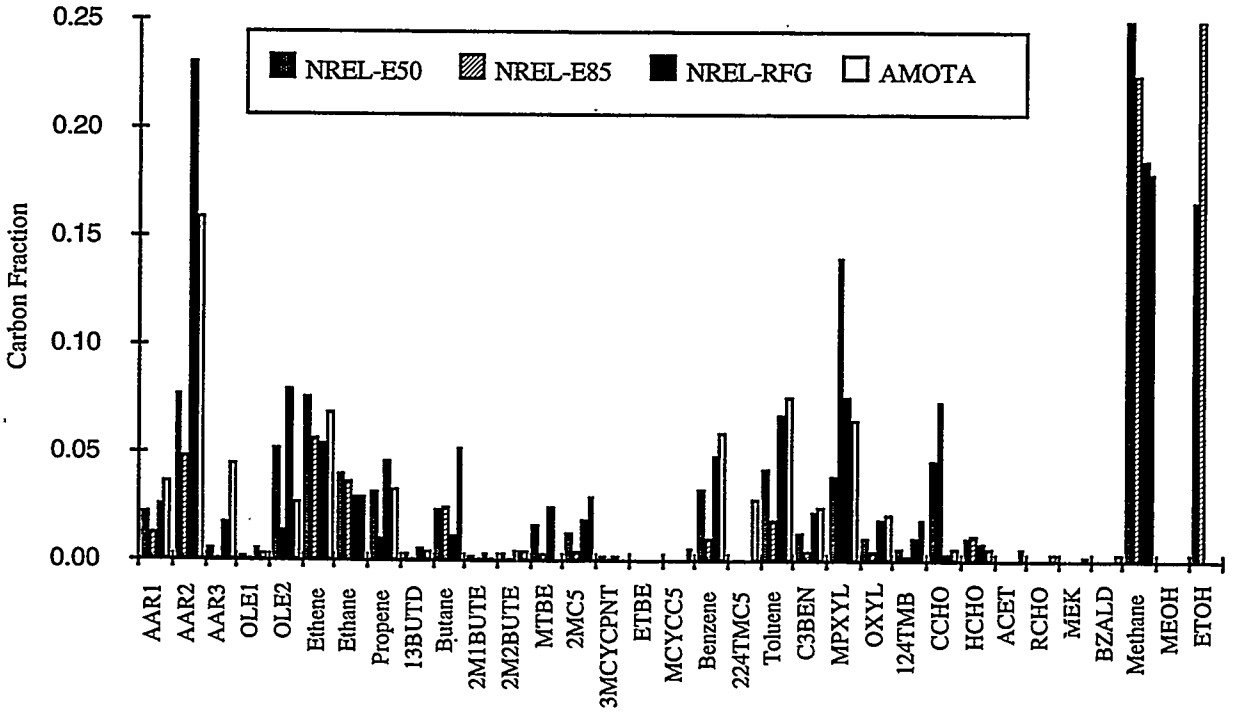

Figure 3-5. MIR-Weighted Exhaust Compositions Associated with Various Fuels

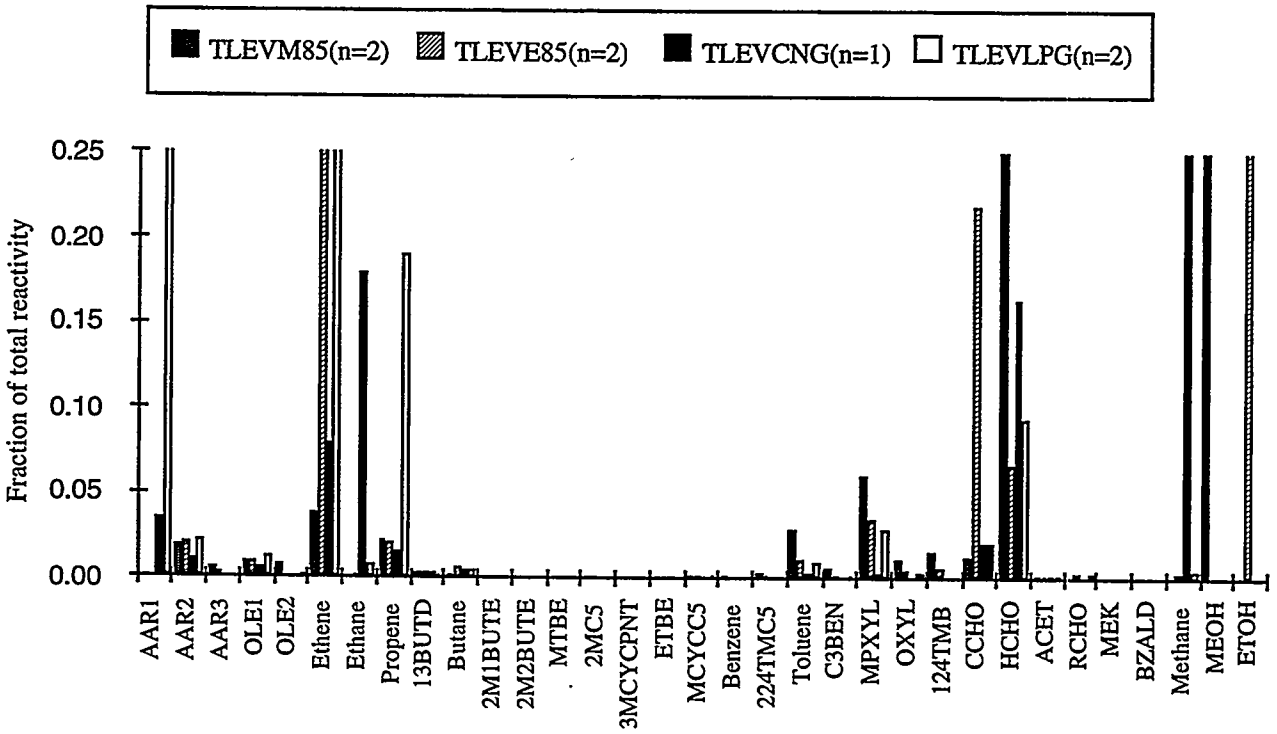

Figure 3-5 (continued). MIR-Weighted Exhaust Compositions

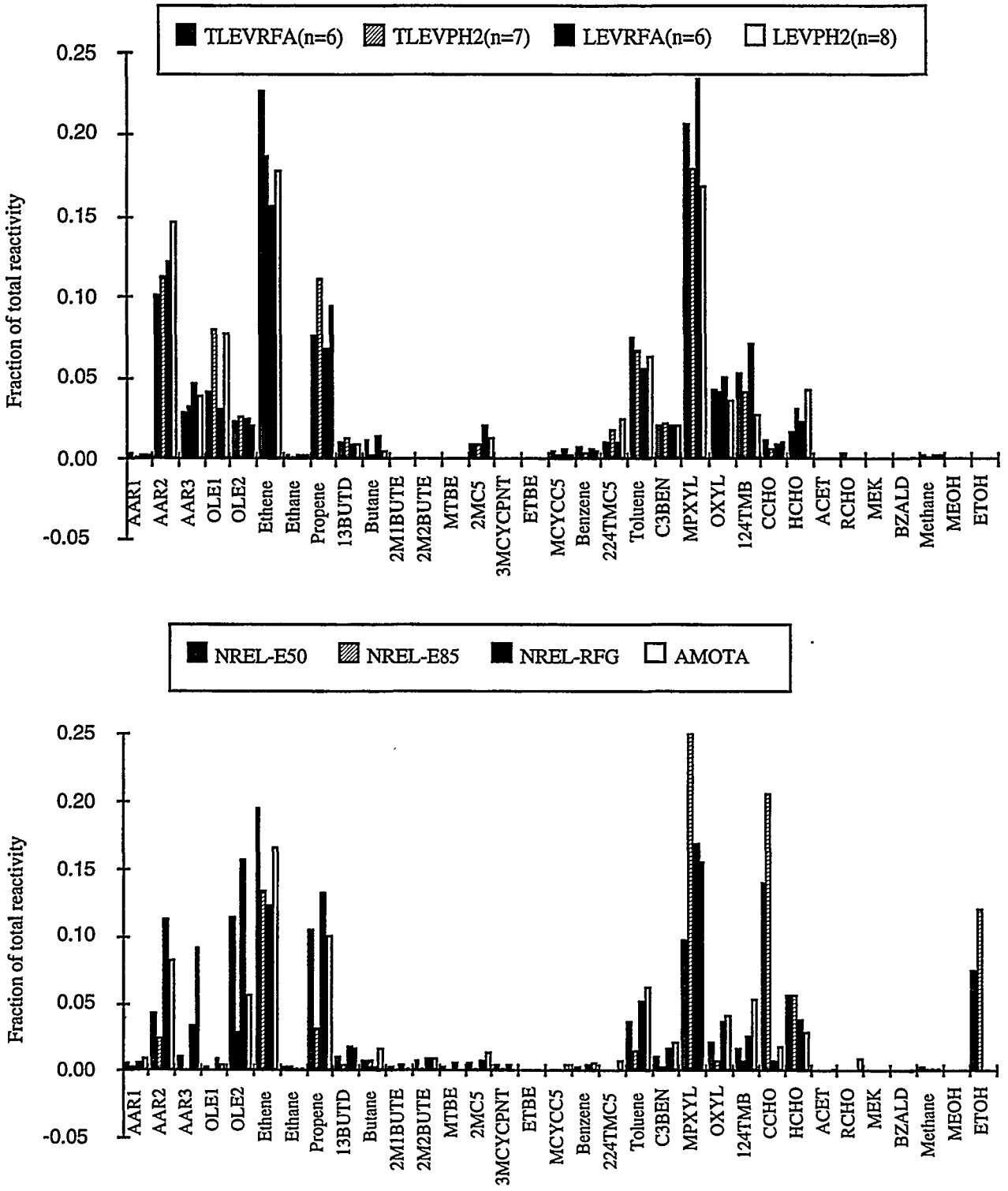

Figure 3-6. Variability of Exhaust Compositions Associated with TLEV RF-A, TLEV PH2, LEV RF-A and LEV PH2 Fuels

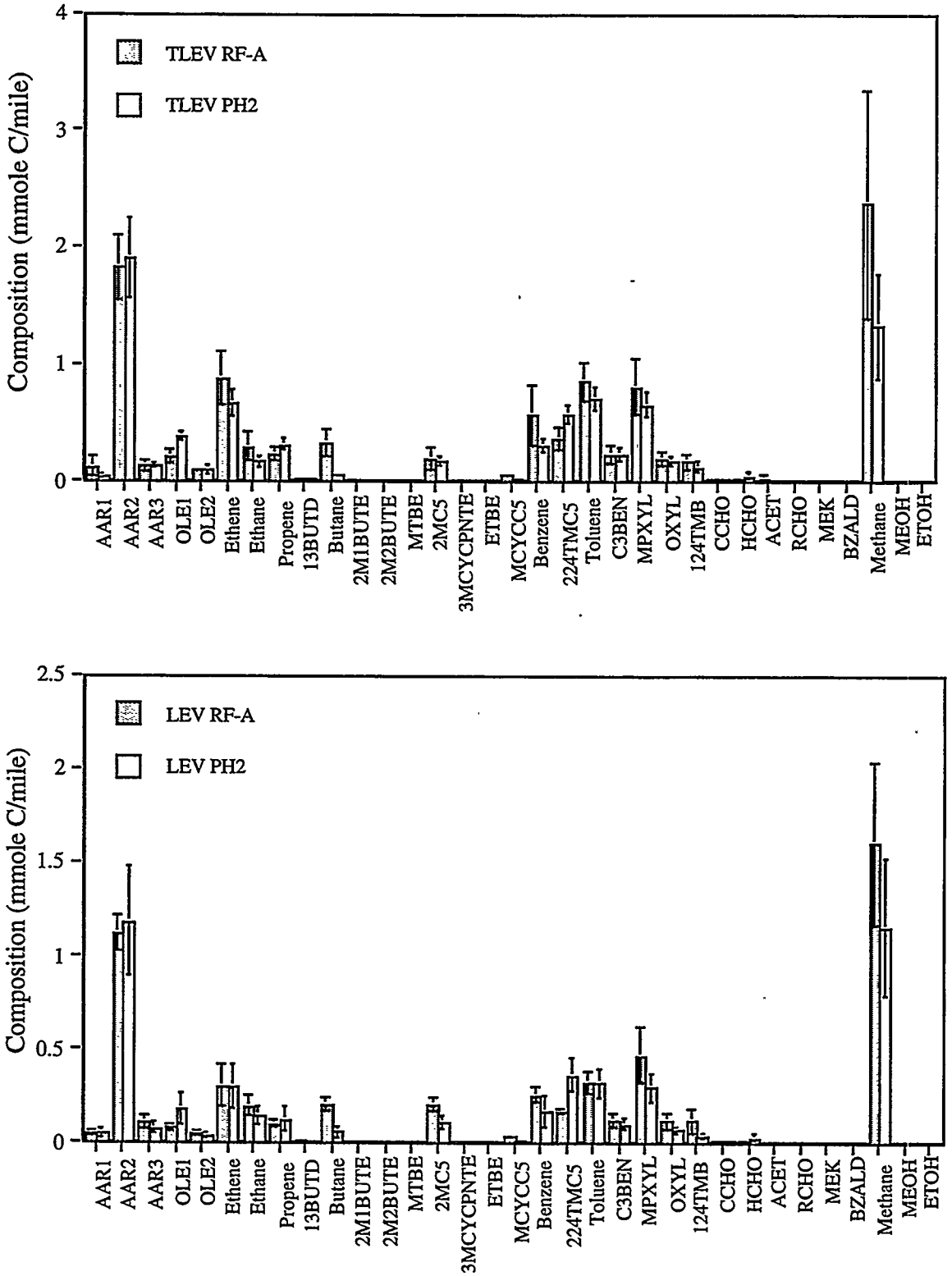

Figure 3-6 (continued). Variability of Exhaust Compositions Associated with AMOTA, AMOTF and METHZ Fuels

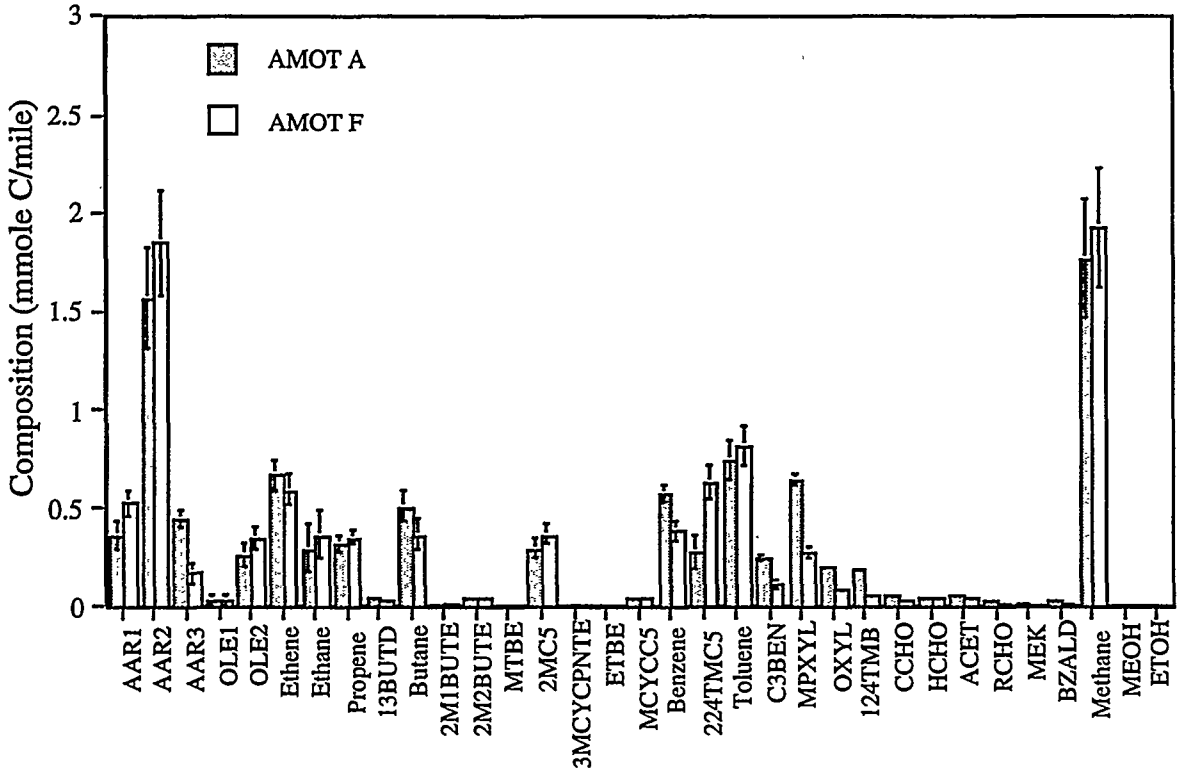

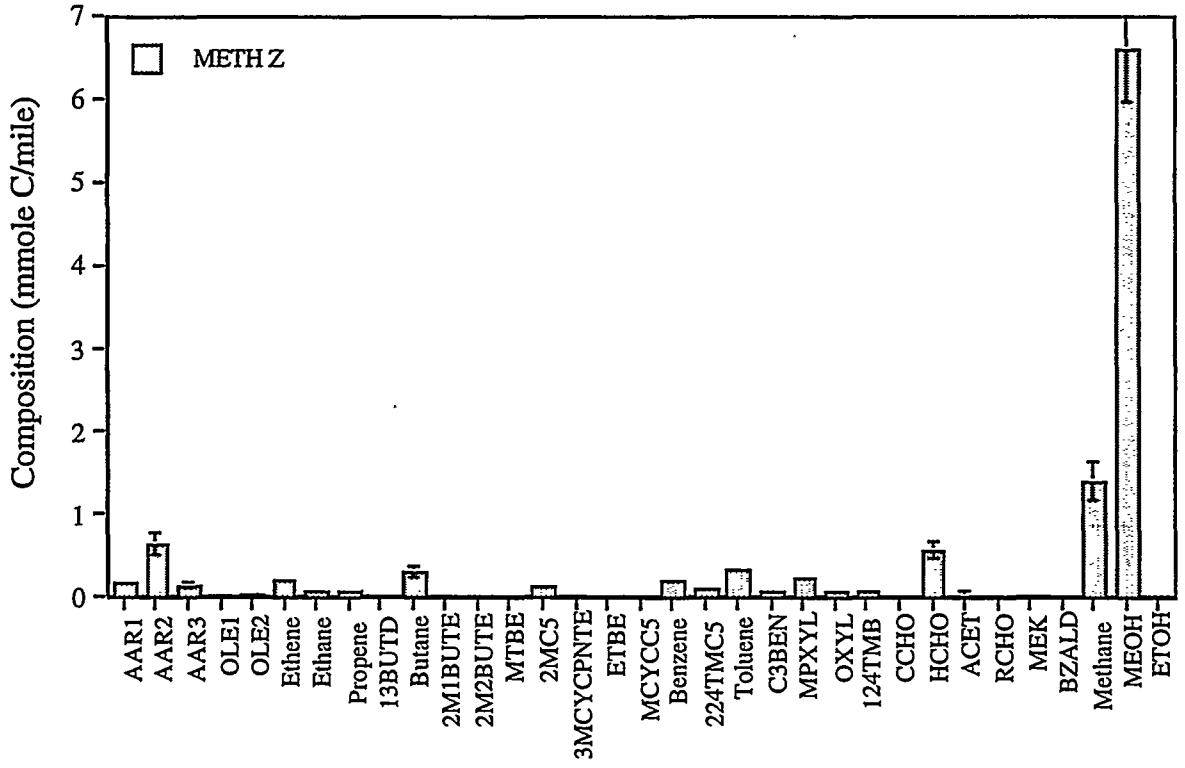

Figure 3-7. Mass-Based Cumulative Distribution Functions for the RAFs of Exhaust Emissions Associated with (a) TLEV M85/RF-A; (b) TLEV E85/RF-A; (c) TLEV CNG/RF-A; and (d) TLEV LPG/RF-A

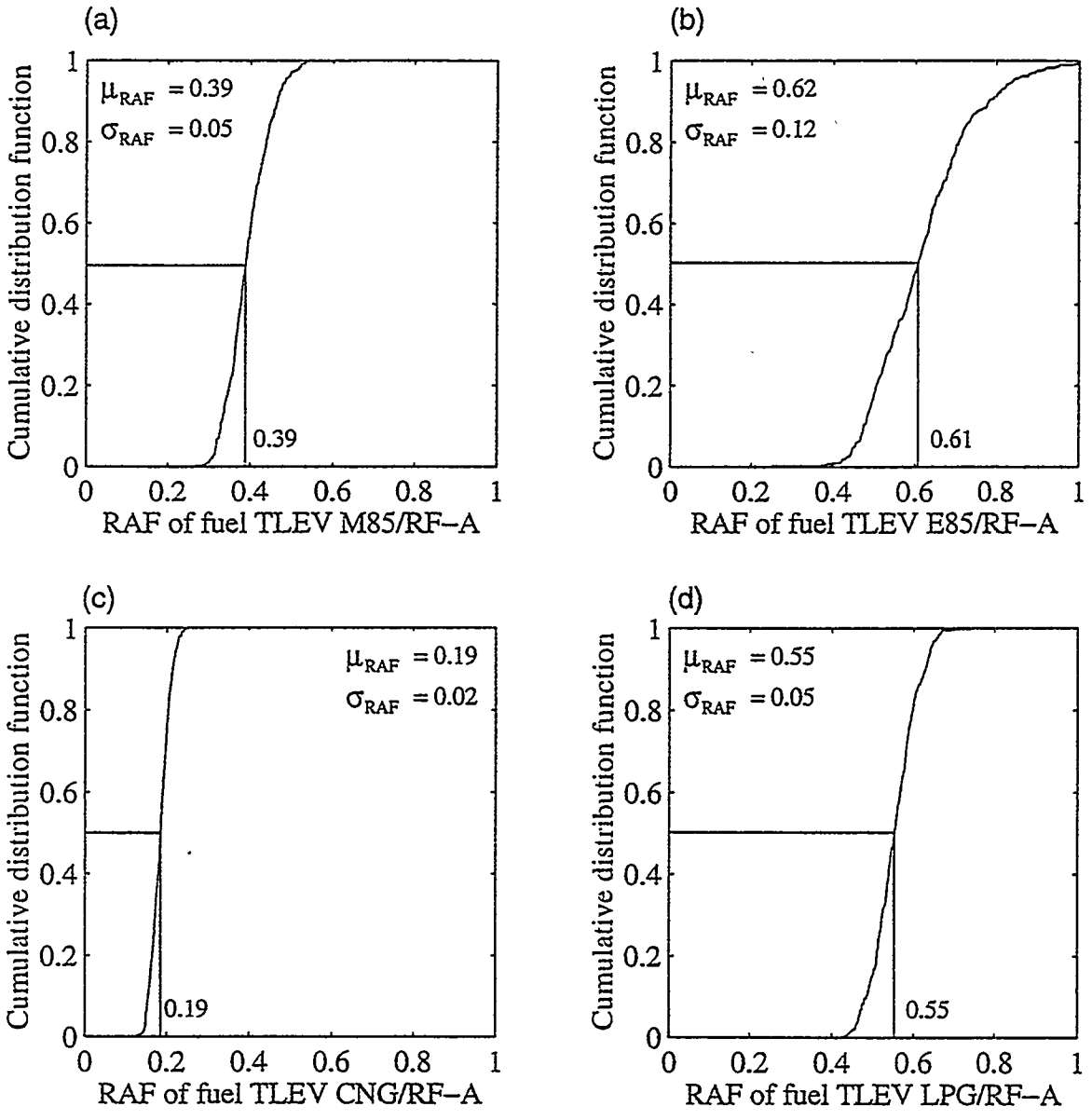

Figure 3-7 (continued). Mass-Based Cumulative Distribution Functions for the RAFs of Exhaust Emissions Associated with (e) TLEV PH2/RF-A; (f) LEV PH2/RF-A; (g) NREL E50/RFG; and (h) NREL E85/RFG

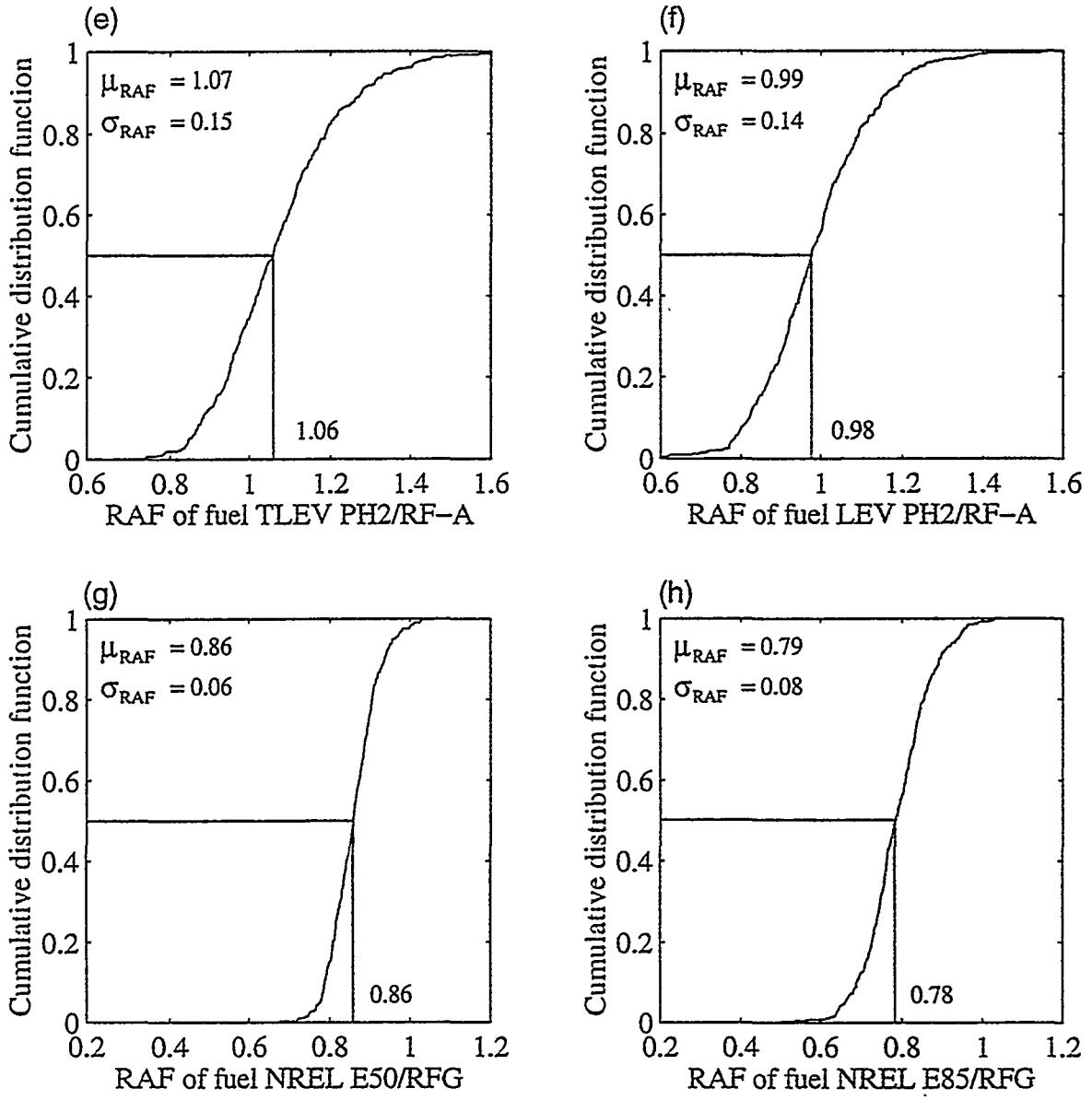

Figure 3-7 (continued). Mass-Based Cumulative Distribution Functions for the RAFs of Exhaust Emissions Associated with (i) TLEV RF-A/AMOTA; (j) NREL RFG/AMOTA; (k) AMOTF/AMOTA; and (l) METHZ/AMOTA

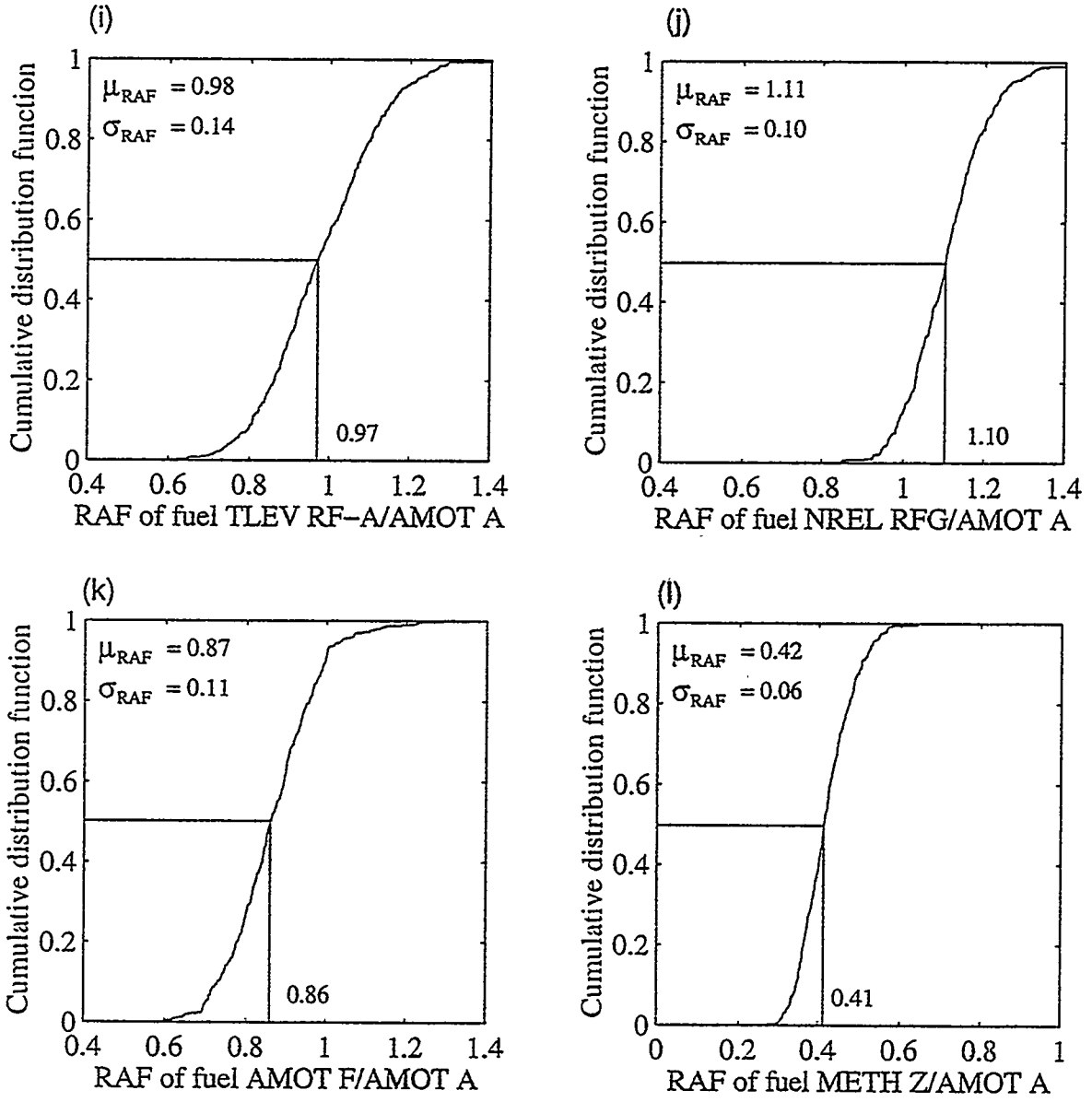

The mean (NMOG mass-based) RAF values calculated for the fuels considered in this analysis range from about 0.19 for exhaust from a CNG-fueled TLEV relative to RF-A, to 1.07 for a Phase 2-fueled TLEV relative to RF-A. There are small differences in the reactivities of the exhaust emissions associated with the various base fuels. This accounts for differences in the fuels and the vehicles. California's TLEV RF-A is slightly less reactive than the "industry average" gasoline (AMOTA) from the Auto/Oil research program, and NREL's RFG is more reactive than AMOTA. Accounting only for uncertainties in chemical parameters, the uncertainties (1σ) in the RAFs calculated for alternative fuel vehicle emissions data from CARB and NREL range from 7% to 19% of the mean values. The greatest uncertainty (19%) occurs for CARB's E85 fuel, corresponding to a high uncertainty in the MIR for ethanol, and moderately high uncertainties for ethene and acetaldehyde. In contrast, the lowest uncertainty (7%) occurs for NREL's E50 fuel, because, except for the ethanol contribution, its reactivity-weighted exhaust is similar in composition to that of the base fuel, RFG. With chemical and emissions uncertainties considered, the uncertainties in the RAFs for emissions associated with reformulated gasoline (CARB's Phase 2 and the Auto/Oil study's AMOTF) range from 13% to 14%.

Looking at Figure 3-7, it is interesting to compare the RAF values and associated uncertainties for E85 data from CARB versus those from NREL, and for M85 data from CARB versus those from the Auto/Oil study. Taking into account the differences in the reactivities of the base fuels used in each case, it is apparent that the M85 RAF values agree well across studies (0.39 from CARB's data, versus 0.42 from the Auto/Oil data), while the E85 RAF values differ to a greater degree (0.62 from CARB's data, versus 0.79 from NREL's data). The difference in the E85 RAF values calculated from CARB and NREL data appears to be due to a relatively high fraction of mp-xylene in the NREL data. The estimated uncertainty in the NREL E85 RAF is 10%, versus 19% for the RAF calculated for CARB's E85 data. Reactivities of both NREL's E85 and its base RFG fuel have significant contributions from mp-xylene and ethene, so the effects on the E85 RAF of uncertainties in the MIRs for these compounds are minimized. In contrast, the composition of exhaust and corresponding reactivity contributions for CARB's E85 versus its base RF-A fuel are substantially different, so uncertainties in MIRs have more influence on RAFs.

We also compared the results presented in Figure 3-7 for AMOTF and METHZ, with those of Yang et al. (1994) for the same emissions data but with MIR uncertainties due only to uncertainties in rate constants, instead of rate constants and product yields as considered here. The comparison shows that adding product yield uncertainties and correlations did not change the AMOTF RAF uncertainty significantly, and slightly reduced the uncertainty in the METHZ RAF, because of the reduced uncertainties in the MIRs for MEOH and HCHO.

Finally, for CARB's Phase 2 fuel relative to RF-A, in TLEVs and in LEVs, and for the Auto/Oil AMOTF and METHZ fuels, we also calculated uncertainties in RAFs associated with chemistry alone, and separately, those associated with emissions composition uncertainties alone. Results of these calculations are shown as scatter plots in Figure 3-8, along with scatter plots incorporating both sources of uncertainty together. These results indicate that the uncertainty in the Phase 2 RAFs is dominated by uncertainty in emissions composition, as is the uncertainty in the RAF for Auto/Oil AMOTF. Considering uncertainty in chemistry alone leads to 1σ uncertainties in these RAFs of only 2% to 3%, relative to the mean values. In contrast, for the Auto/Oil METHZ RAF, the uncertainty associated with chemical parameters alone is slightly larger than that associated with the emissions composition.

3.5 Discussion

Several limitations apply to the uncertainty analysis results presented in this chapter. First, at best only two sources of uncertainty in RAFs are considered: uncertainties in the parameters of the SAPRC mechanism, and variability in FTP exhaust profiles across vehicles tested on the same fuel. For several fuels, insufficient data are available to calculate variability in exhaust profiles, so this source of uncertainty is not incorporated into the calculations for their RAFs. Even where estimates of variability in laboratory tests are considered, this may underestimate the uncertainty in exhaust composition of vehicles on the road, because the vehicles tested do not represent the full range of models, model years, accumulated mileage, or maintenance conditions. In particular, how well the alternative-fueled vehicles used in the M85, E85, CNG, and LPG tests represent future mass-produced (and possibly dedicated) vehicles is a critical uncertainty that cannot be quantified at present. Moreover, in addition to uncertainties in product yields and rate constants, uncertainties in mechanism formulation and simulation conditions also affect the IR values used in the RAF calculations. The uncertainties in individual parameters that were propagated through the IR analyses were subjectively estimated, in most

Figure 3-8. Scatter Plots of Monte Carlo Results for Composite Reactivities (Mass Basis) of (a) TLEV PH2 Versus TLEV RF-A with Chemistry and Emissions Uncertainties; (b) TLEV PH2 Versus TLEV RF-A with Chemistry Uncertainties Alone; (c) TLEV PH2 Versus TLEV RF-A with Emissions Uncertainties Alone; and (d) LEV PH2 Versus LEV RF-A with Chemistry and Emissions Uncertainties

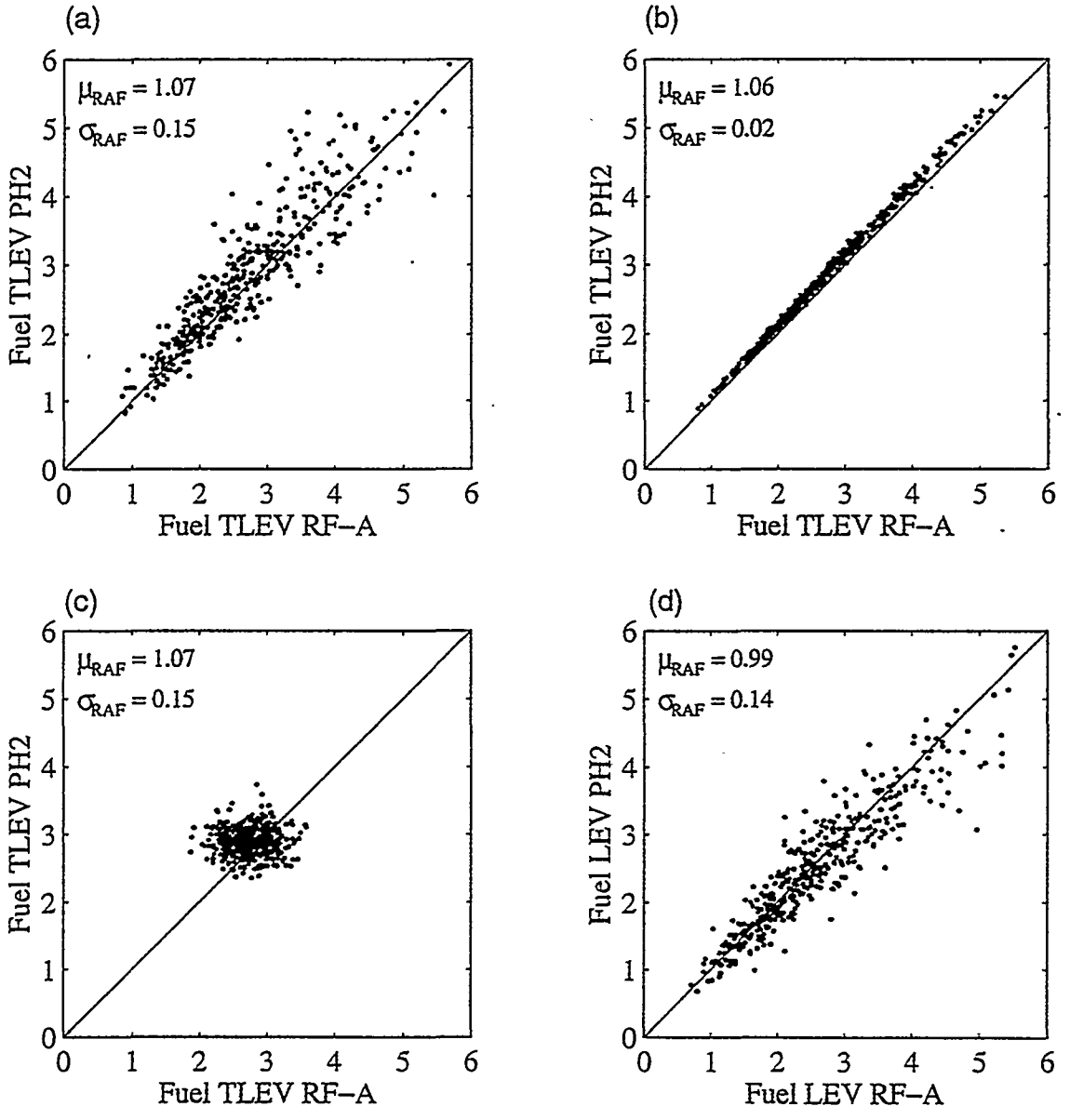

Figure 3-8 (continued). Scatter Plots of Monte Carlo Results for Composite Reactivities (Mass Basis) of (e) LEV PH2 Versus LEV RF-A with Chemistry Uncertainties Alone; (f) LEV PH2 Versus LEV RF-A with Emissions Uncertainties Alone; (g) AMOTF Versus AMOTA with Chemistry and Emissions Uncertainties; (h) AMOTF Versus AMOTA with Chemistry Uncertainties Alone

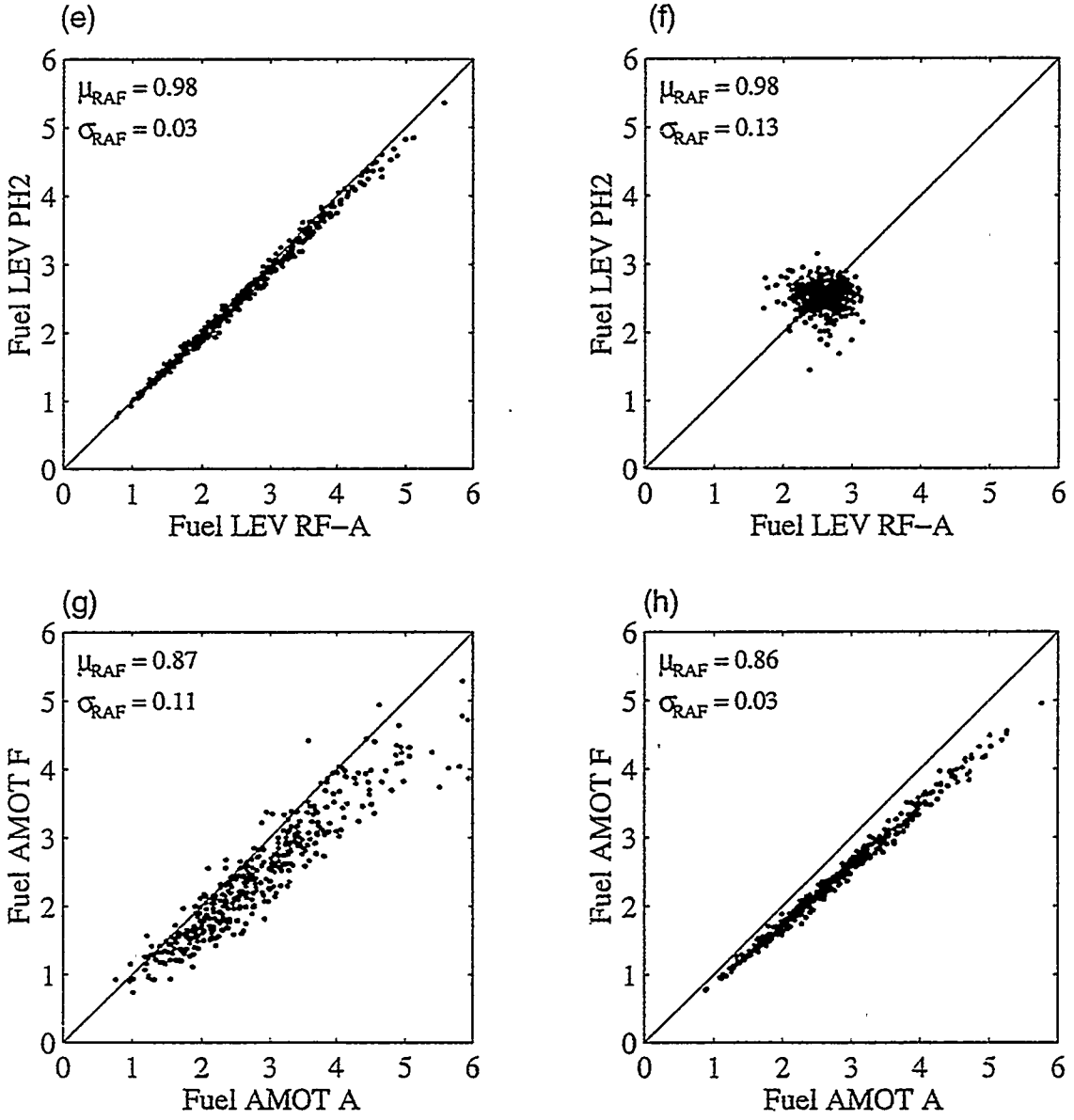

Figure 3-8 (continued). Scatter Plots of Monte Carlo Results for Composite Reactivities (Mass Basis) of (i) AMOTF Versus AMOTA with Emissions Uncertainties Alone; (j) METHZ Versus AMOTA with Chemistry and Emissions Uncertainties; (k) METHZ Versus AMOTA with Chemistry Uncertainties Alone; (l) METHZ Versus AMOTA with Emissions Uncertainties Alone

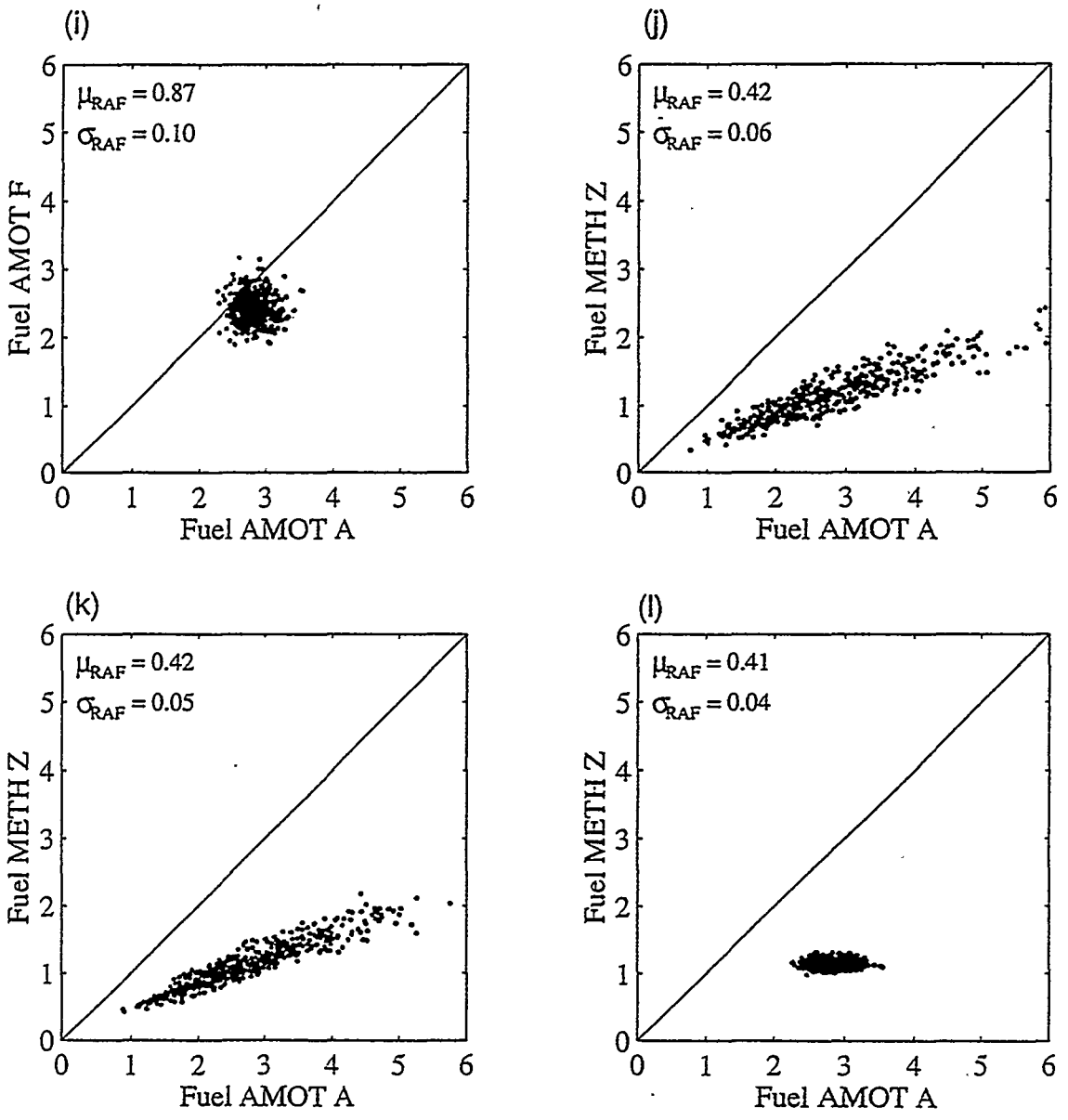

cases by NASA or IUPAC review panels. Finally, we took the SAPRC90 mechanism as published, despite the recognized need for some updates to the mechanism (Gery, 1991).

Compared to uncertainties in MIR values for individual organic compounds, uncertainties in calculated RAFs are relatively small because of strong correlations between MIR values of various compounds, and between the reactivities of the base and test fuels. The effect of uncertainties in chemistry on a relative measure of reactivity such as an RAF will be strongest when the compositions of the test and base emissions are radically different, as demonstrated here for M85, E85, CNG, and LPG. However, even for these cases, the uncertainties in the calculated RAFs were much lower than those in the MIRs for the dominant compounds in the exhaust emissions. This reduction in uncertainty occurs in the RAF calculations because rate-parameter uncertainties have directionally similar effects on MIRs of many compounds.

Referring back to Figure 3-5 and Table 3-6, reducing uncertainty in the MIRs for HCHO, acetaldehyde, methanol, ethanol, ethene, propene, and toluene and higher aromatics would apparently help to reduce the uncertainty in RAFs for alternative fuel vehicles. However, considering only chemical parameters as potential sources of uncertainty, opportunities for reducing uncertainty in predicted O_3 concentrations or in MIRs are relatively limited. Only a small number of reactions, some of which are already well studied, contribute significantly to uncertainty in predicted O_3 concentrations and incremental reactivities. Uncertainties in secondary aromatics chemistry, including the nature, yields, and reaction rates of product species such as AFG2, have been widely recognized as significant, but difficult to reduce. One step that should help reduce the uncertainty in predictions made with the SAPRC mechanism is revising it to incorporate new recommendations for parameters associated with PAN chemistry and HCHO photolysis. Additional measurements of HO rate constants and photolysis rates for oxygenated compounds, and of product yields for carbonyls and peroxy radicals in alkenes + HO reactions, would also be helpful. However, such modifications will probably have less effect on calculated RAFs than on MIRs for individual compounds.

3.6 Summary and Conclusions

This chapter has presented the results of a box-model analysis of uncertainties in IRs calculated for selected organic compounds, and in RAFs for selected test fuels. The sources of uncertainty considered were the parameters of the SAPRC mechanism used to calculate incremental reactivities, and where available, the composition of the exhaust emissions. Uncertainties in individual parameters propagated through the IR analyses were subjectively estimated. For rate parameters, these estimates were compiled primarily from NASA or IUPAC reviews. For selected product yields, uncertainty estimates were based primarily on assessments of errors in yield measurements made according to the type of product (organic peroxy radical, carbonyl, etc.). Correlations between parameters were introduced where values were estimated by analogy. Variances of exhaust concentrations across vehicles tested on the same fuel were taken as estimates of uncertainty in the emissions compositions, which were treated as normally distributed random variables. Correlations between emission rates for different species were also estimated from the test data and retained in the Monte Carlo analysis.

Uncertainties (1σ) in MIRs of the organic compounds and classes studied range from 25% of the mean estimate, for HCHO, to 66% of the mean, for ethanol. Uncertainties in MOIRs range from 27% for methane to 83% for toluene. Uncertainties (1σ) in the final ozone concentrations predicted for the MIR and MOIR simulation conditions were about 32% and 21%, respectively.

With respect to MIRs, the greatest potential for reducing uncertainties appears to exist for oxygenated compounds, for which additional measurements of HO rate constants and photolysis rates (where applicable) could substantially reduce uncertainty. Additional measurements of product yields for carbonyls and peroxy radicals in alkenes + HO reactions and elucidation of the secondary chemistry of aromatics oxidation would also be helpful.

Accounting for uncertainties in the rate parameters and product yields of the SAPRC mechanism, and for variability in exhaust composition across vehicles tested by CARB and by the AQIRP, uncertainties of about 15% (1σ) are indicated for the RAFs of exhaust emissions associated with reformulated gasolines. Uncertainties associated with chemical parameters alone

led to uncertainties in RAFs for M85, E85, CNG, and LPG of about 10% to 20%, based on CARB's data. Compared to the degree of uncertainty in IRs for influential compounds, the chemical uncertainties have only a modest impact on relative measures of reactivity such as RAFs. For alternative fuel vehicles, however, confidence in estimates of RAFs could still be improved by obtaining additional data on their emissions.

4. AIRSHED MODEL TESTING OF THE EFFECTS OF CHEMICAL UNCERTAINTIES ON FUEL REACTIVITIES

4.1 Introduction

One of the primary objectives of this project is to assess how the uncertainties in chemical parameters (rate constants and product yields) affect quantification of the reactivities of emissions from vehicles. In prior projects (e.g., McNair et al., 1992, 1994; Russell et al., 1995), RAFs, as calculated by using MIRs and the associated exhaust compositions, were tested for CNG, LPG, and M85 using the CIT airshed model applied to the Los Angeles area. While using a similar method, this project takes those studies further by including Phase 2 and E85 and by quantifying how the chemical uncertainties add to the uncertainty in the RAFs. This project also uses a newer, more detailed chemical mechanism. Information from the box-model uncertainty analysis described in the previous chapter, a previous study (Yang et al., 1994), and fuel emissions composition data (CARB, 1994; NREL, 1994) were used to assess which chemical mechanism parameter uncertainties would have the largest impact on fuel reactivities. The results are then used to judge the importance of the effects of chemical mechanism uncertainties in air quality modeling and the use of RAFs.

4.2 Model Application

The CIT airshed model was applied to the Los Angeles air basin for the simulation period of August 27-29, 1987. This was the period of the extensive data collection effort by the South Coast Air Quality Study (SCAQS) and has been the focus of a number of previous modeling studies, particularly those that look at reactivity issues (McNair et al., 1992, 1994; Yang et al., 1994; Bergin et al., 1995; Russell et al., 1995). Details of the modeling protocol can be found in those references. As part of the previous project that this study extends, a detailed chemical mechanism, SAPRC90, was installed and tested in the CIT model (Yang et al., 1994). That mechanism was further expanded for this study to include explicit propane chemistry, because propane is a dominant emitted species from a number of fuels, particularly LPG.

The added propane reaction (adapted from Atkinson et al., 1990) is:

$$PRPA + HO \xrightarrow{(k)} 0.972\ RO2R + 0.02\ R2O2 + 0.028\ RO2N + 0.02\ HCHO + 0.351\ CCHO + 0.248\ MEK + 1.02\ RO2$$

where the species are:

Abbreviation	Species
PRPA	propane
HO	hydroxyl radicals
RO2R	chemical operator used to represent NO to NO_2 conversion with generation of HO_2 radicals
R2O2	chemical operator used to represent extra NO to NO_2 conversion
RO2N	chemical operator used to represent NO consumption and nitrophenol formation
HCHO	formaldehyde
CCHO	acetaldehyde
MEK	methylethyl ketone and lumped higher ketones
RO2	total alkyl peroxy radicals

The rate constant, k, is:

$$k = 6.60 \times T \times \exp(-44/T)$$

where T is temperature in °K and the rate constant units are $ppm^{-1}min^{-1}$. This reaction is from an earlier version of the SAPRC mechanism, the LCC mechanism (Lurmann et al., 1987), but leads to a similar reactivity for propane. In the updated SAPRC mechanism, the reaction products are acetone (rather than methyl ethyl ketone) and propionaldehyde (rather than acetaldehyde). Because this reaction is important in the LPG scenarios, these model simulations are currently being performed with the updated propane reactions.

Seven base-case model scenarios were conducted by developing alternative mobile source emission inventories from the data of speciated exhaust emissions for six fuels and one null case, which has zero total organic gas (TOG) emissions from mobile sources. This null case is referred to as the NoTOG case. Only tailpipe exhaust emissions were considered because the current regulations apply only to these exhaust emissions. The seven emission inventories were developed to represent emissions from a base gasoline that represents the industry average (RFA), the null case (NoTOG), and five alternative fuels; CNG, LPG, California RFG (Phase 2), a blend of 85% methanol with 15% CA Phase 2 (M85), and a similar blend using ethanol (E85).

NO_x emissions were held constant. Because the Los Angeles air basin is VOC-limited, this method should not affect predicted ozone concentrations. The modeling methods are consistent with those used previously (e.g., McNair et al. 1992, 1994).

The emission inventories were developed by substituting an organic speciation profile for each fuel in the inventory preprocessor programs. The product splits and reaction rates in the SAPRC chemical mechanism are sensitive to the emission composition. In this study, the parameters were developed for a base mixture, which may have impacted results for the fuels with much different exhaust compositions. This issue is discussed further in section 4.4 (Results). The hot and cold start and hot stabilized mass emissions were adjusted to account for the fuel RAF and for the change in mode of emissions as found from vehicle testing. For example, CNG vehicles have significantly fewer cold start emissions than methanol vehicles, so the mass adjustment for cold start CNG is lower than that of M85. This method is further described in McNair et al., (1994). The total (exhaust and evaporative) mobile organic emissions were also doubled so that air quality impacts would become more apparent, and to account for the widely accepted belief that these emissions were underestimated by a factor of two to four in the Los Angeles air basin (Fujita et al., 1992).

If the RAFs are correct, the predicted ozone using these inventories should be approximately equal, except for the NoTOG case (which should have significantly lower levels.) The NoTOG case represents the air quality if there were no organic gas emissions from automobile exhaust. The predicted ozone should be equal because the RAF adjustment is intended to account for the differences in the reactivity of the combustion emissions associated with each fuel. However, the RAFs were calculated as an average over a range of meteorological conditions and emissions and assumed clear sky conditions, while this study was performed for the Los Angeles basin conditions and included cloud cover and significant variations in local concentrations of VOCs and NO_x. Therefore, identical ozone predictions should not be expected.

In addition to the seven base-case simulations, a series of additional simulations was conducted to quantify the effect of chemical mechanism uncertainties on the model and RAF agreement.

The 12 chemical mechanism parameters, which were examined for effect on relative reactivity predictions, are shown in Table 4-1. These were the parameters judged through the uncertainty and box-modeling work (presented in Chapters 2 and 3) to have, potentially, the largest effects on the RAFs.

Table 4-1. Reactions and their Associated Uncertainty in Normalized Rate Constants or Product Yields

Description	Reaction(s)	σ_k^a
NO2 photolysis	NO2+ hν → NO + O	0.27
HCHO photolysis	HCHO + hν → 2 HO2 + CO	0.34
AFGs photolysis	*AFG1 + hν → HO2 + HCOCOO + RCO3 AFG2 + hν → HO2 + CO + CCO-O2 + RCO3	1.26 1.26
MPXY + OH	MPXY + OH → 0.040 BALD + 0.180 CRES + 0.108 GLY + 0.370 MGLY + 0.666 AFG2 + 0.820 RO2R + 0.180 HO2 + 3.136 C + 0.820 RO2	0.31
MPXY yield	product yield of AFG2 (0.666) from MPXY + OH reaction above	0.17
OLE2 + OH	OLE2 + OH → 0.930 RO2R + 0.070 RO2N + RO2 + 0.321 HCHO + 0.647 CCHO + 0.605 RCHO + 0.111 ACET + 0.061 MEK + 0.056 BALD + 0.889 C	0.18
AAR2 + OH	AAR2 + OH → 0.0.828 RO2R + 0.109 RO2N + 0.002 RO2XN + 0.061 HO2 + 0.635 R2O2 + 1.574 RO2 + 0.013 HCHO + 0.173 CCHO + 0.205 RCHO + 0.179 ACET + 0.592 MEK + 0.032 CO + 0.007 CO2 + 0.061 CRES + 0.020 BALD + 0.028 GLY + 0.031 MGLY + 0.096 AFG2 + 0.973 C	0.19
ETOH + OH	ETOH + OH → 0.100 RO2R + 0.900 HO2 + 0.156 HCHO + 0.922 CCHO + 0.100 RO2	0.47
C2 rads + NO	CCO-O2 + NO → CO2 + NO2 + HCHO + RO2R + RO2 C2COO2 + NO → CCHO + RO2R + CO2 + NO2 + RO2	0.75 0.75
C2 rads + NO2	CCO-O2 + NO2 → PAN C2CO-O2 + NO2 → PPN	0.67 0.67
PAN decomp.	PAN → CCO-O2 + NO2 + RCO3	0.70
MEOH + OH	MEOH + OH → HO2 + HCHO	0.48

[a] Relative uncertainty in rate constant unless specified as product yield.
* Reaction sets are perfectly correlated pairs

The species names are defined in Appendix C, and the reaction descriptions are used throughout the rest of this document. The MEOH + OH uncertainty value (0.48) is more than double the value described in Chapter 3 and presented by Atkinson (1994) and Demore et al. (1992), and was chosen as the most conservative value given by the previous reviews (Yang et al., 1995).

As shown in Equation (4.1), each rate constant uncertainty estimate, σ, was doubled, added to one, then multiplied with the nominal rate constant value in the chemical mechanism (k), and the product yield uncertainty estimate was added to one and multiplied by the nominal product yield value (PY).

$$k = k_{nom}(2\sigma + 1) \qquad (4.1)$$

$$PY = PY_{nom}(\sigma + 1)$$

This process required 12 sensitivity runs for each of the seven fuel scenarios, resulting in 91 3-day model simulations.

4.3 Description of Analysis Metrics

One major advantage of the three-dimensional CIT model over zero-dimensional models is that a variety of air quality impacts can be defined to account for the temporal and spatial distribution of ozone, and can be combined with the human population distribution as a measure of potential exposures. Simulation results from the CIT model study were examined using various methods to quantify the effects of emissions increases on ozone formation. The reactivity quantification measures consider the impact on peak ozone and on population-weighted and spatial "exposure" to ozone levels over 0.12 and 0.09 ppm. An averaged exposure metric is also introduced.

Peak ozone is defined simply as the maximum ozone concentration (ppm) predicted in the modeling domain at any time using each emissions inventory. The predicted peak ozone forms significantly far downwind of Los Angeles, in an area of relatively low NO_X emissions, that is therefore less sensitive to VOC emissions than most of the urban basin. Peak ozone is either the "spatial peak" which is the maximum ozone concentration occurring in the entire model domain, or as the "populated peak" which is the maximum occurrence in any populated grid cell.

Population-weighted exposure (PE) is calculated as:

$$PE = \sum_{hour\ h} \sum_{cell\ g} \left(C_{g,h} \times P_g \times t \right) \qquad (4.2)$$

where, summed over each hour (h) and grid cell (g), the population (P) is multiplied by the

ozone concentration C and t, where $t = \begin{cases} 1\text{ hour} & \text{if } C_{g,h} > C_{th} \\ 0 & \text{if } C_{g,h} \leq C_{th} \end{cases}$, and Cth is a threshold ozone concentration. The units are ppm-person-hours, a potential exposure metric that does not account for personal activities, particularly time spent indoors. This metric may be sensitive to small concentration shifts in heavily populated grid cells.

Spatial exposure was defined in a similar manner to population exposure, only with a spatial rather than a population multiplier, leading to units of ppm-grid-hours, or ppm-km^2-hours (one model grid cell represents 25 km^2). Exposure metrics were calculated for two thresholds, 0.09 and 0.12 ppm O_3, representing the state and federal ozone standards, respectively.

The individual population metrics are susceptible to a threshold effect when the perturbation in emissions causes the ozone concentration in a cell to go from just under to just over the threshold. If that cell has a large population, the impact on the results will be large even though the actual change in concentration may have been small. For example, if two species have slightly different reactivities (or the spatial impacts are slightly different), and if for one species the ozone in a highly populated grid cell just breaks the threshold, the population weighted exposure above the threshold increases significantly. On the other hand, if the other species is just slightly less reactive, the ozone in that cell does not break the threshold. Also, ozone levels at or near one threshold value may respond differently than ozone levels at another location.

The concentration-shift effects and effects caused by changes in ozone behavior near the threshold concentrations are diminished by averaging the two different threshold metrics. This is shown by Equation (4.3) using population exposure as an example (it also applies to spatial exposure), resulting in the average threshold population exposure, $PE_{A.T.}$.

$$PE_{A.T.} = \frac{PE_{C_{th}=0.09} + PE_{C_{th}=0.12}}{2} \tag{4.3}$$

Further, averaging the threshold metrics takes into account both ozone standards and is a more compact measure. For these reasons, the averaged metric is used for the populated and spatial

exposure measures in this study rather than the individual threshold results, as was done previously (Yang et al., 1994; Bergin et al., 1995).

4.4 Results

Diurnal ozone plots at three stations located in different parts of the Los Angeles Basin are shown for the base-case of each fuel and the NoTOG case (Figure 4-1, a through f). Anaheim is in a southern region near the coast, Azusa is downwind of Los Angeles in the eastern valleys, and Banning is far downwind. Anaheim and Azusa are in regions that are relatively rich in NO_x, and Banning is in a more NO_x-limited region. The sites were chosen to show the fuel effects on a wide range of conditions. An analysis of the base-case model performance can be found in Bergin (1994). Each figure shows observed ozone levels and the model results using the base gasoline inventory (RFA) and for each alternative fuel or RFG simulation. If the simulations led to exactly the same ozone impacts, the alternative inventory results (solid lines) would lay identically on the base gasoline predictions (dashed line).

The NoTOG case (Figure 4-1a) shows the difference in predicted ozone formation when all the tested mobile source exhaust VOC emissions are removed. This is important, because the analysis concentrates on how the VOC emissions from each of the fuel simulations affect air quality with respect to not having any fuel VOC emissions. There are significant differences between the NoTOG and base-cases, particularly in areas such as Azusa. Because Banning is in a more NO_x-limited region, the impact of removing the mobile source exhaust VOC emissions is not so large (Figure 4-1a). The Phase 2 and M85 results are practically identical to the base-case. Larger differences are seen for the other fuels, particularly E85. This is also seen in the analysis of the more integrated metrics, as discussed below.

All model results for the base-cases and sensitivity runs are tabulated in Appendix D. An overall summary of these data is shown in Table 4-2. Some measures have been defined to examine these results in more detail, and were applied to the populated peak ozone and populated averaged exposure metrics. The predicted adjusted relative reactivity (ARR) of the five fuels with respect to RFA, shown in Figure 4-2, is calculated as:

$$ARR_{fuel} = (P_{fuel} - P_{NoTOG})/(P_{rfa} - P_{NoTOG}) \quad (4.4)$$

Here, P is the impact prediction parameter (either peak ozone or average potential population exposure), and the subscripts represent the inventory used to obtain the parameter (one of the five fuels, RFA, or NoTOG). In essence, the ARR is the relative reactivity of the exhaust with respect to RFA and the null case after the mass emissions have already been adjusted for the reactivity differences using the RAF. These base-case model results provide a representation of the agreement between the RAF value and the fuel reactivity predicted by the CIT model, because, ideally, the ARR for a fuel should be equal to one when the emissions are multiplied by the RAF.

Figure 4-2 shows that the reactivity corrections work very well for Phase 2 and M85, but CNG, E85, and LPG show significantly larger deviations. Both CNG and LPG show an ARR greater than one, and E85 shows an ARR value lower than one, indicating that the fuel is predicted to be less reactive than is calculated using the composite of the emitted species MIR values. The deviations found for CNG and LPG are surprising in that a previous study (McNair et al., 1994), which used the CIT model with an older chemical mechanism (LCC) (Lurmann et al., 1987), found much better agreement. E85 and Phase 2 were not included in that study. The CNG result found in that study had an ARR less than one, in contrast with this study. LPG had an ARR greater than one, consistent with the findings here; however, the LPG results here may be affected by the use of an early version of the propane + HO reaction. A brief comparison of these two studies is presented in Appendix E.

Still referring to Figure 4-2, the peak ozone and average exposure metrics show nearly equivalent relative reactivities when averaged across the fuels (an average ARR of 1.22 for peak ozone and 1.13 for averaged exposure over the five fuels); however, this does not hold for each fuel separately. Peak ozone is less sensitive to fuel changes because it occurs in a lower NO_x region than the exposure impacts, which means the region is less sensitive to changes in VOCs. For this reason, the peak ozone ARR is a ratio of small numbers. The largest metric difference is observed for CNG, with a 0.564 higher ARR predicted when considering the peak ozone impact of the fuel. Phase 2 shows a difference in sign between metrics; however, the ARRs are

Figure 4-1a. Ozone Time Series Plot For noTOG and RFA Model Simulations

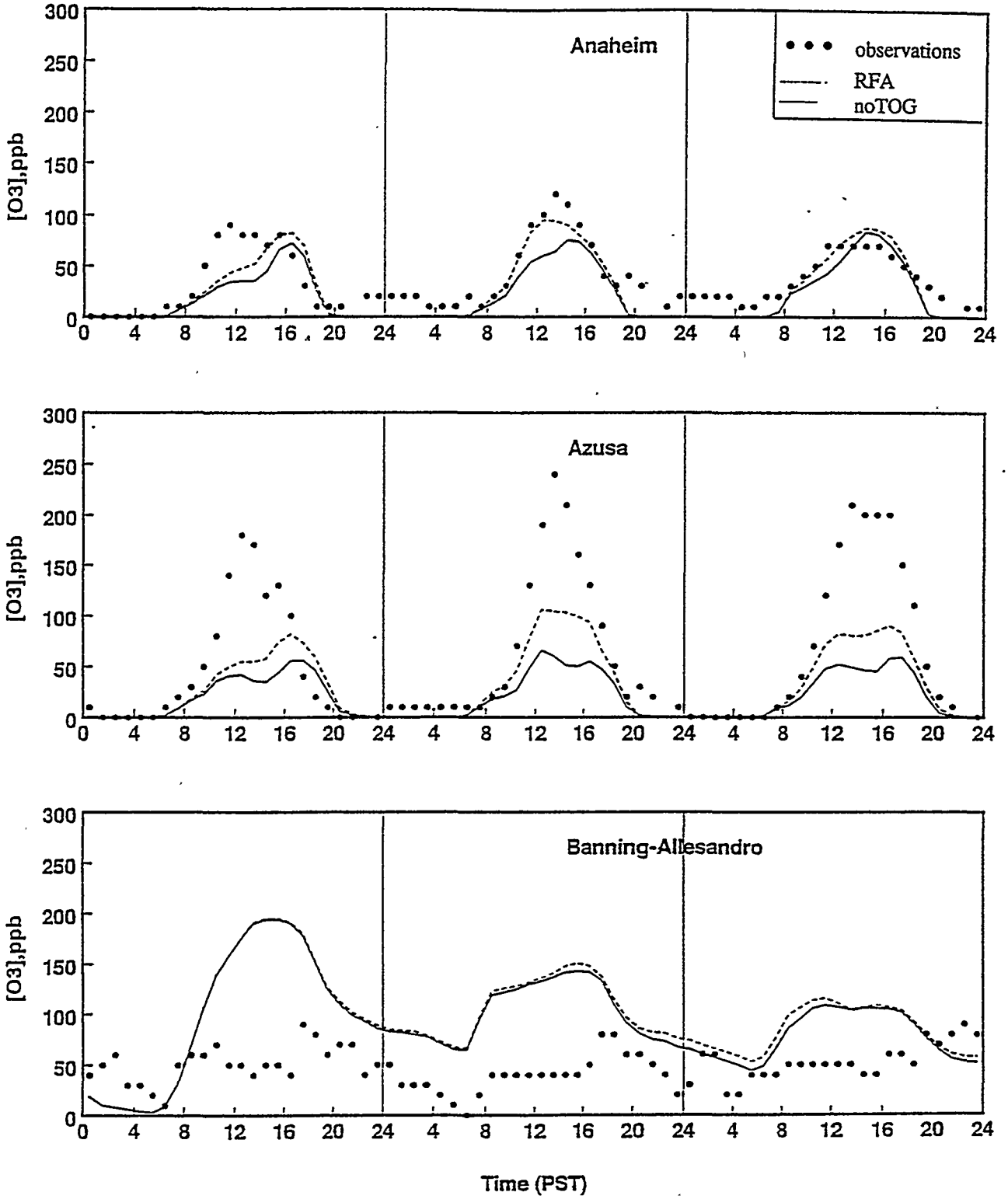

Figure 4-1b. Ozone Time Series Plot For CNG and RFA Model Simulations

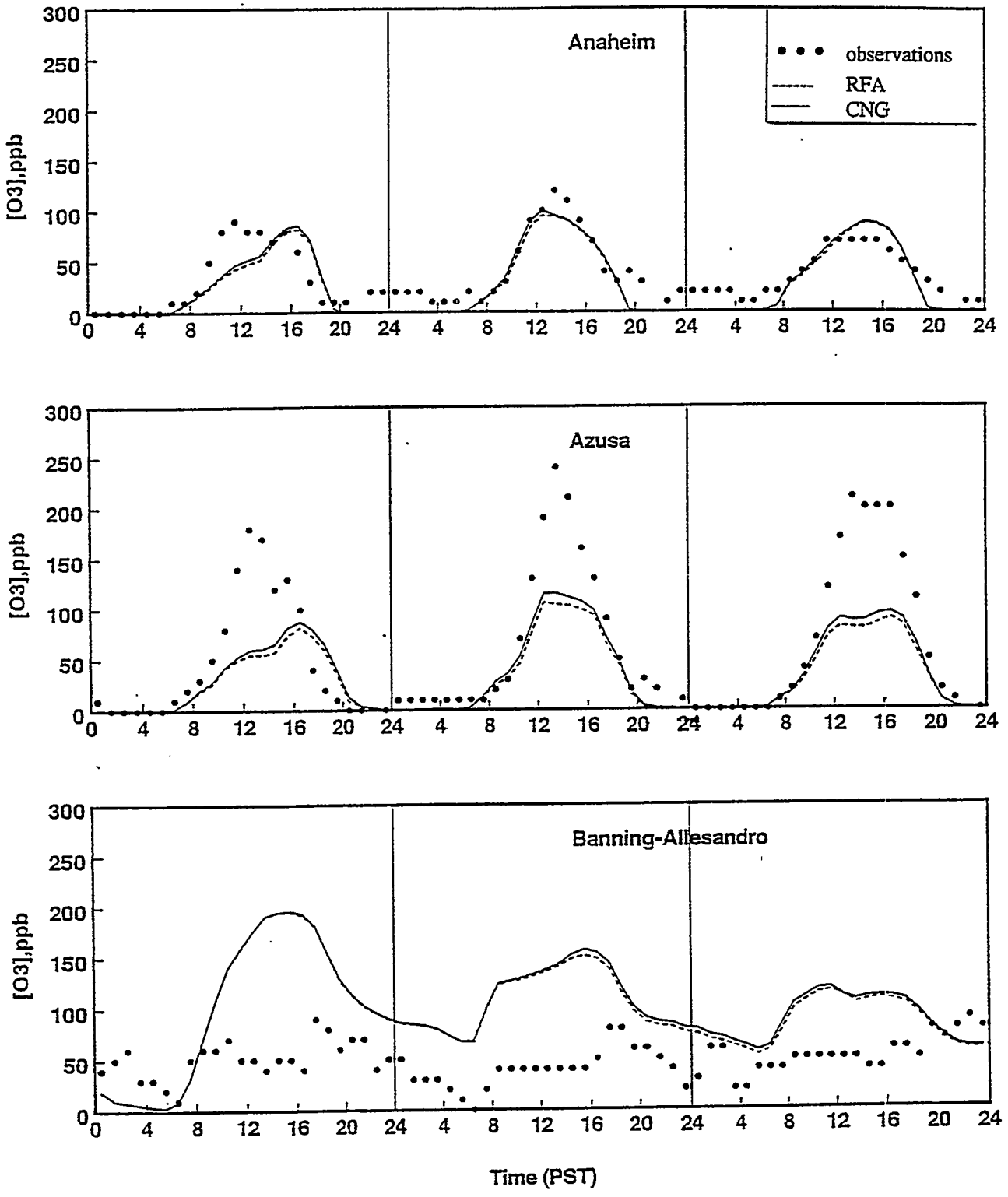

Figure 4-1c. Ozone Time Series Plot For LPG and RFA Model Simulations

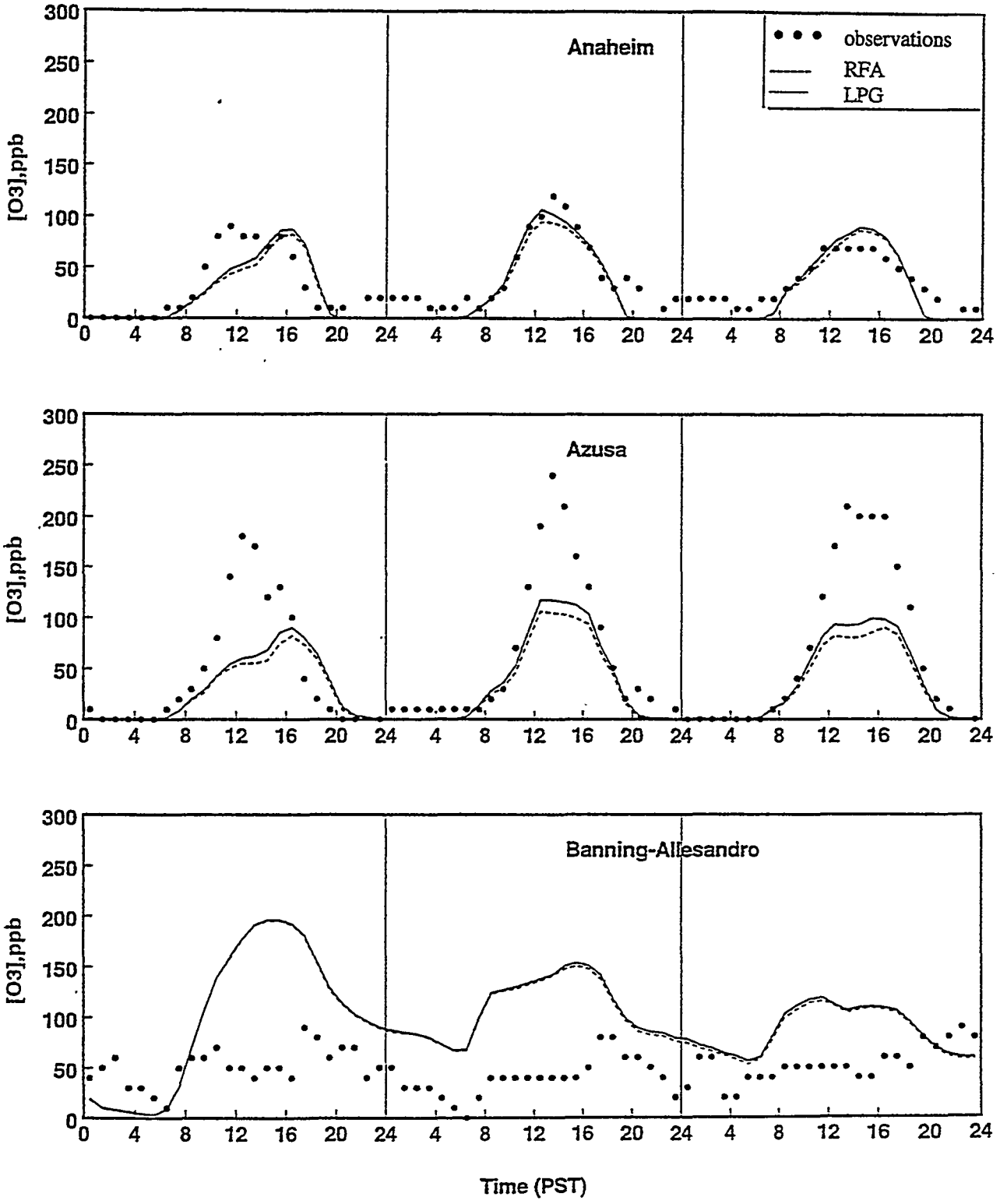

Figure 4-1d. Ozone Time Series Plot For M85 and RFA Model Simulations

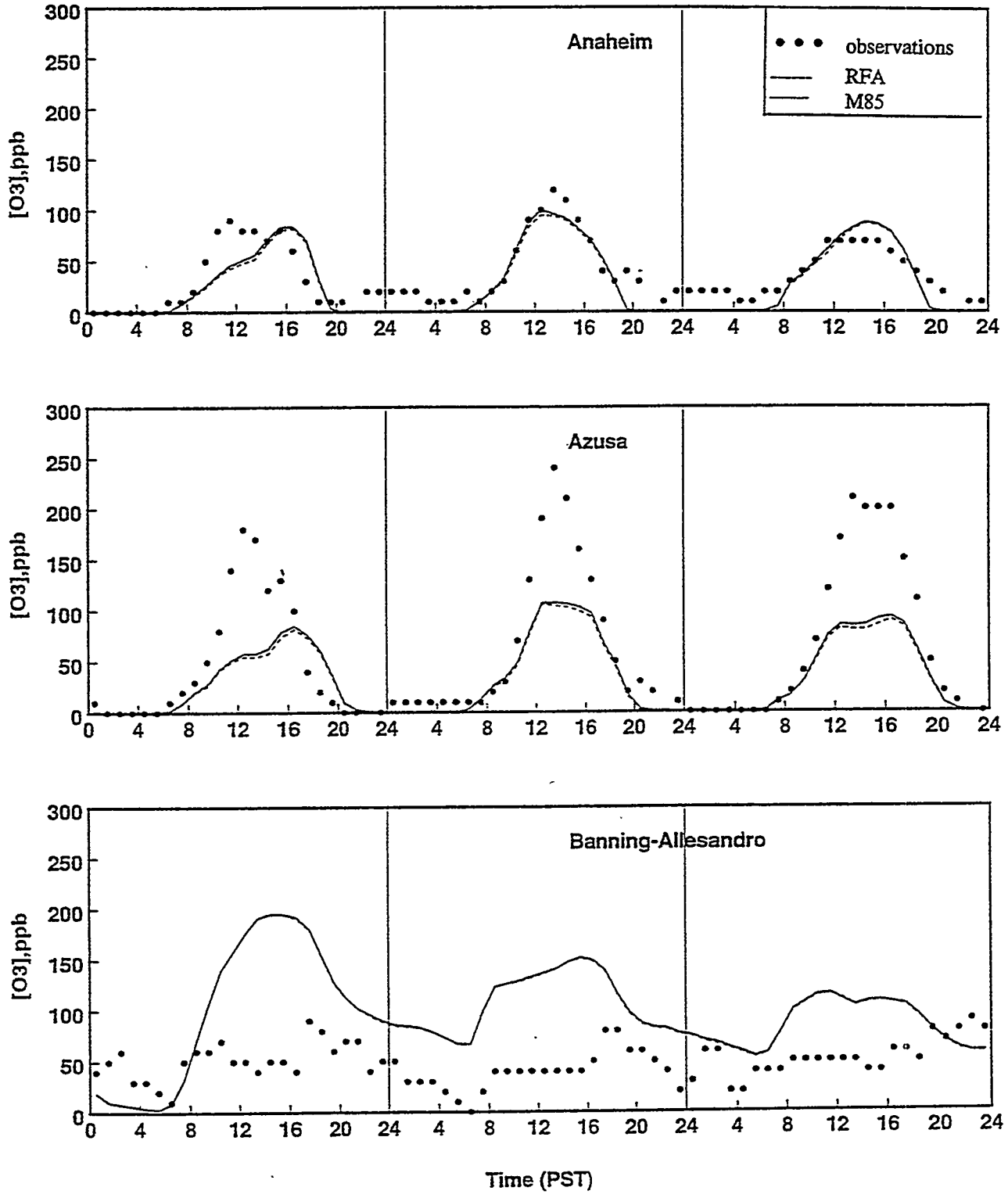

Figure 4-1e. Ozone Time Series Plot For E85 and RFA Model Simulations

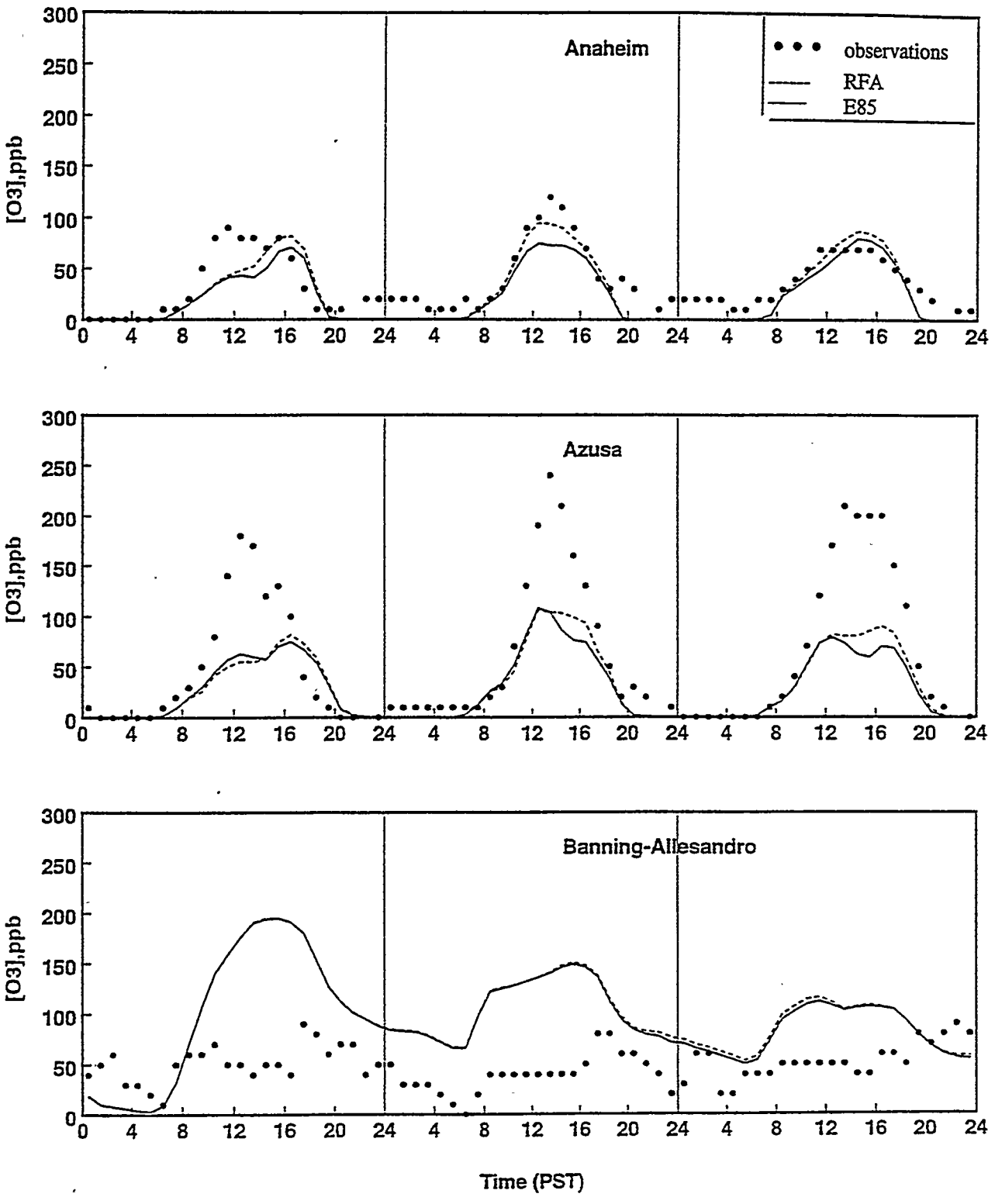

Figure 4-1f. Ozone Time Series Plot For Phase 2 and RFA Model Simulations

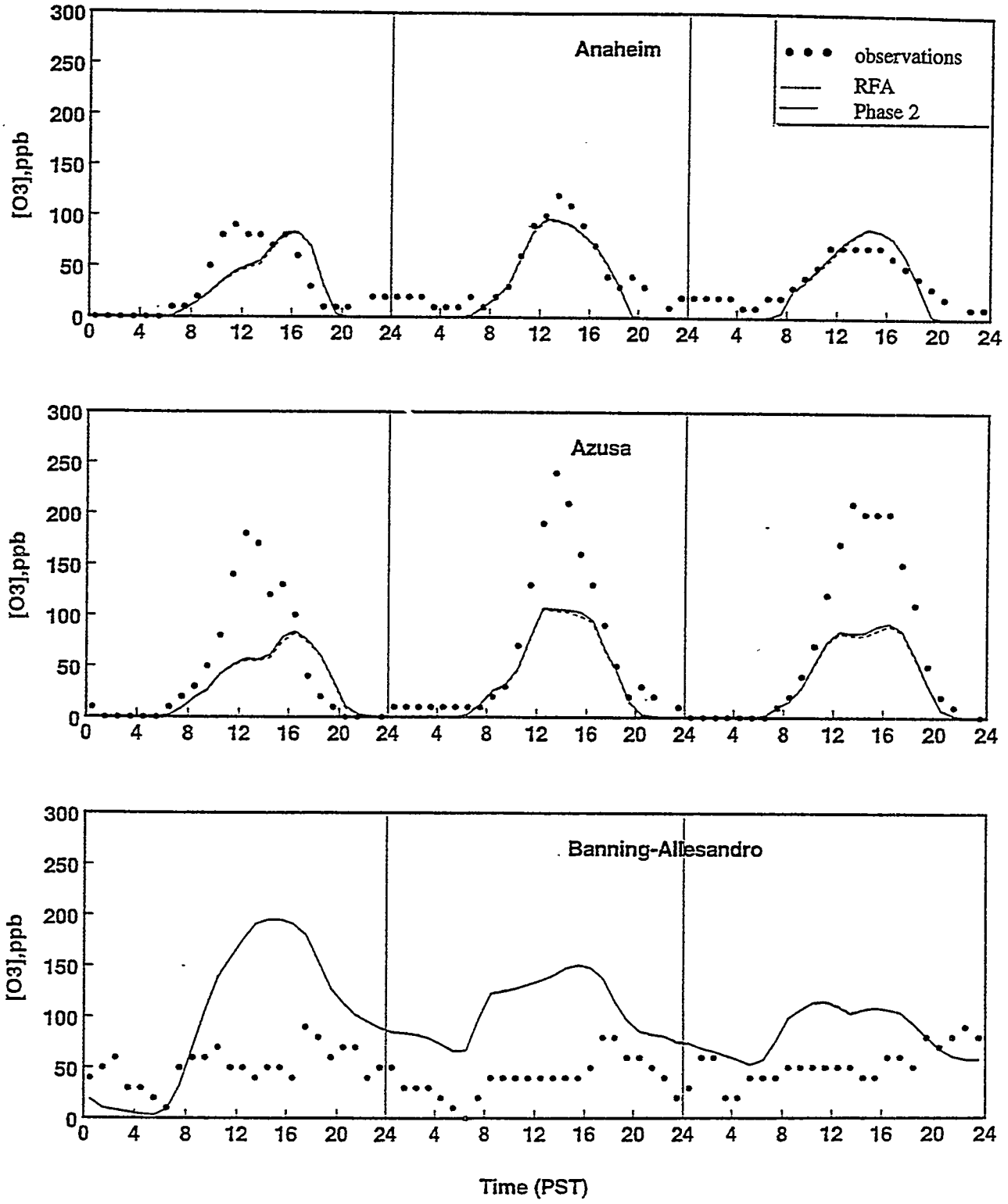

Table 4-2. Summary of Model Results for Each Fuel Over the 12 Uncertainty Runs

	Peak Ozone (ppm)					Average Populated (person-ppm-hours)					Average Spatial (km^2-ppm-hours)				
	Max.	Min.	Avg.	Std Dev.	Base	Max.	Min.	Avg.	Std Dev.	Base	Max.	Min.	Avg.	Std Dev.	Base
CNG	0.25	0.19	0.21	0.01	0.21	6587805	1266192	3726648	1523547	2496420	868	231	572	146	359
LPG	0.23	0.19	0.20	0.01	0.20	7085323	1456100	4120040	1582582	2788070	857	365	579	119	349
PHASE 2	0.22	0.18	0.19	0.01	0.19	6093610	1062387	3318984	1419092	2190685	775	312	513	111	312
M85	0.22	0.18	0.19	0.01	0.19	6299029	1239848	3604691	1422474	2422269	791	334	534	110	322
E85	0.23	0.17	0.19	0.01	0.19	4350551	592949	2194478	1030172	1393714	698	272	458	102	280
RFA	0.22	0.18	0.19	0.01	0.19	5913862	1036207	3170383	1389582	2103295	768	309	507	110	308
NoTOG	0.20	0.16	0.17	0.01	0.17	2374747	242827	967297	590486	605062	471	167	279	72	175

very close to one. The ARRs for M85 were also close to one, though biased slightly high. This is consistent with earlier work that considers the RAF adjustment (McNair et al., 1994) and looks at individual species (Yang et al., 1994; Bergin et al., 1995).

As seen in Figure 4-2, the ARRs for CNG and LPG are significantly different than 1. This was investigated. In the SAPRC mechanism, the product splits and reaction rates are sensitive to the emission composition. In this study, the parameters were developed for a base mixture and not adjusted afterward. In the case of LPG and CNG, the exhaust composition is very different from the base mixture. Future studies should account for this by extending the mechanism to have two sets of lumped organics, one for the base inventory that would be applied to the non-mobile source emissions and a second set for mobile source exhaust. The base lumped organics would not be changed between simulations, and the lumped parameters for the organics applied to the mobile source exhaust would be modified for each fuel. In this way, the increment from the exhaust emissions of each source can be correctly determined.

It was found in the latter set of studies that the least reactive individual VOC compounds (e.g., the alkanes and alcohols) had slightly higher relative reactivities when quantified using airshed modeling in comparison with the box-modeled MIR values. This can probably be traced back to the airshed model following the ozone dynamics over multiple days, allowing greater time for the individual species to react. Likely for this reason, both CNG and LPG, which have products with low reactivity values, are the most positively skewed.

Having quantified the degree to which the reactivity adjustment worked, the next issue was to investigate the degree to which chemical mechanism parameter uncertainties affect these results. To accomplish this task, sets of additional simulations were conducted to calculate the ARRs after perturbing individual parameters in the chemical mechanism. The parameters are shown in Table 4-1. In each case, the parameter was increased by 2σ, where σ is the assigned uncertainty. The sensitivity is then expressed through the calculated Normalized Uncertainty Response (NUR) from the base ARR:

Figure 4-2. Adjusted Relative Reactivity of Fuels with Respect to RFA

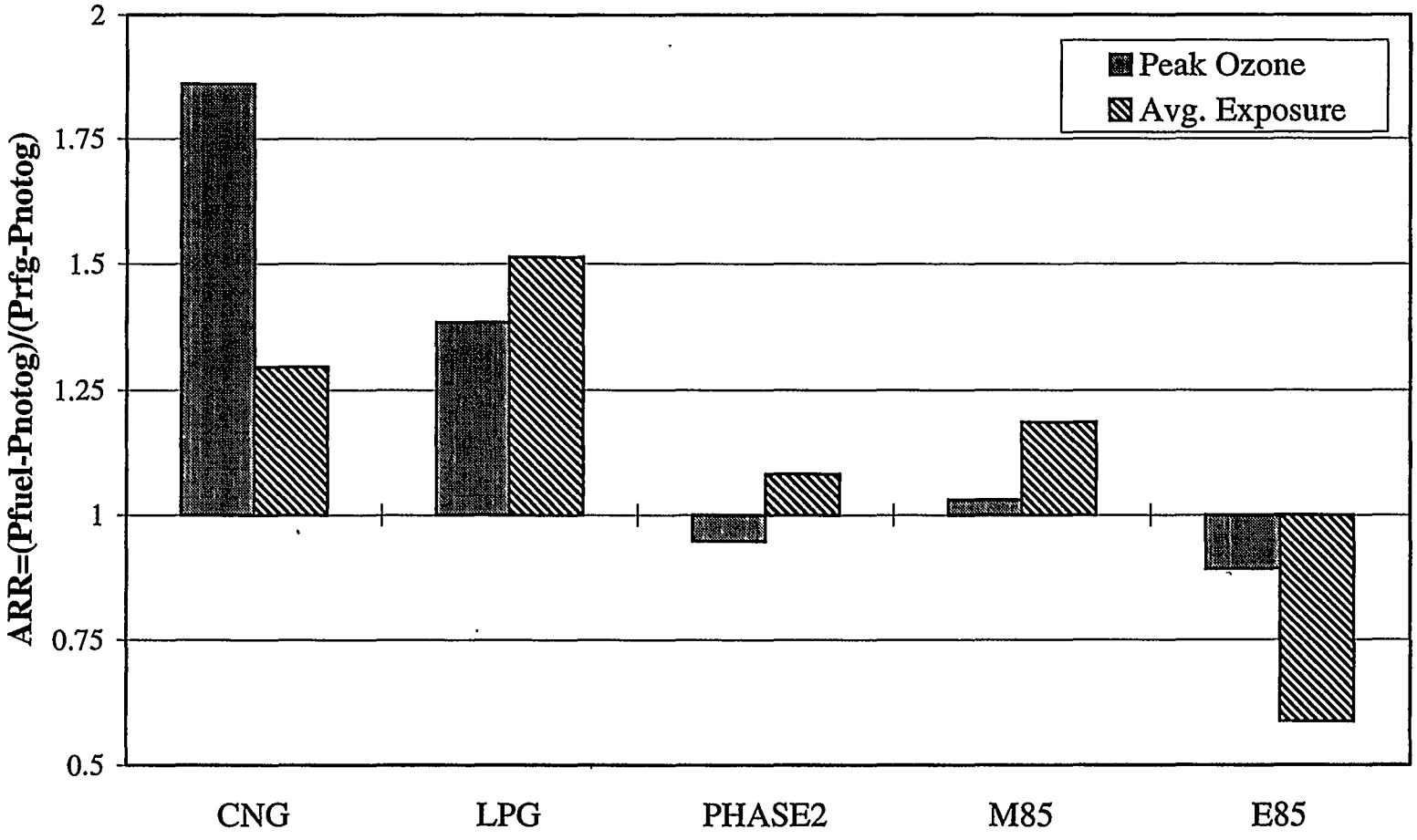

Table 4-3. Normalized Uncertainty Response of Fuels to Each Reaction(s)

	CNG		LPG		Phase 2		M85		E85	
	Peak Ozone	Avg. Expos.	Peak Ozone	Avg. Expos.	Peak Ozone	Avg. Expos.	Peak Ozone	Avg. Expos.	Peak Ozone	Avg. Expos.
NO2 photolysis	0.088	-0.085	0.026	-0.128	0.026	-0.028	0.028	-0.066	0.243	-0.051
C2 rads + NO	0.020	-0.098	-0.027	-0.154	0.029	-0.042	-0.069	-0.132	0.538	-0.015
C2 rads + NO2	-0.066	-0.004	0.134	0.011	0.037	-0.045	0.172	0.059	-0.213	-0.284
PAN decomp.	0.015	-0.036	-0.020	-0.116	0.023	-0.027	-0.021	-0.072	0.556	-0.119
HCHO photolysis	0.126	0.068	0.114	0.046	0.076	0.020	0.087	0.144	0.108	-0.139
MEOH + OH	-0.022	0.001	-0.028	0.005	0.061	-0.003	0.265	0.429	0.000	0.001
ETOH + OH	-0.016	0.004	-0.026	0.014	0.057	0.000	-0.009	0.005	0.199	0.156
MPXY yield	0.019	0.011	0.000	-0.001	0.035	-0.001	0.030	0.008	0.031	0.010
MPXY + OH	0.017	-0.026	0.003	-0.017	0.030	-0.003	-0.021	-0.013	0.017	-0.022
AAR2 + OH	0.033	-0.042	0.022	-0.048	0.088	0.005	0.045	-0.033	-0.003	-0.089
OLE2 + OH	0.029	0.003	0.033	0.005	0.103	-0.011	0.017	0.007	0.055	0.000
AFGs photolysis	-0.021	-0.146	-0.010	-0.154	0.044	-0.011	-0.021	-0.091	0.039	-0.213
Average	0.02	-0.03	0.02	-0.04	0.05	-0.01	0.04	0.02	0.13	-0.06
Standard Dev.	0.05	0.06	0.05	0.07	0.03	0.02	0.09	0.15	0.22	0.12

Figure 4-3. Normalized Uncertainty Response (NUR) of CNG to Mechanism Uncertainties

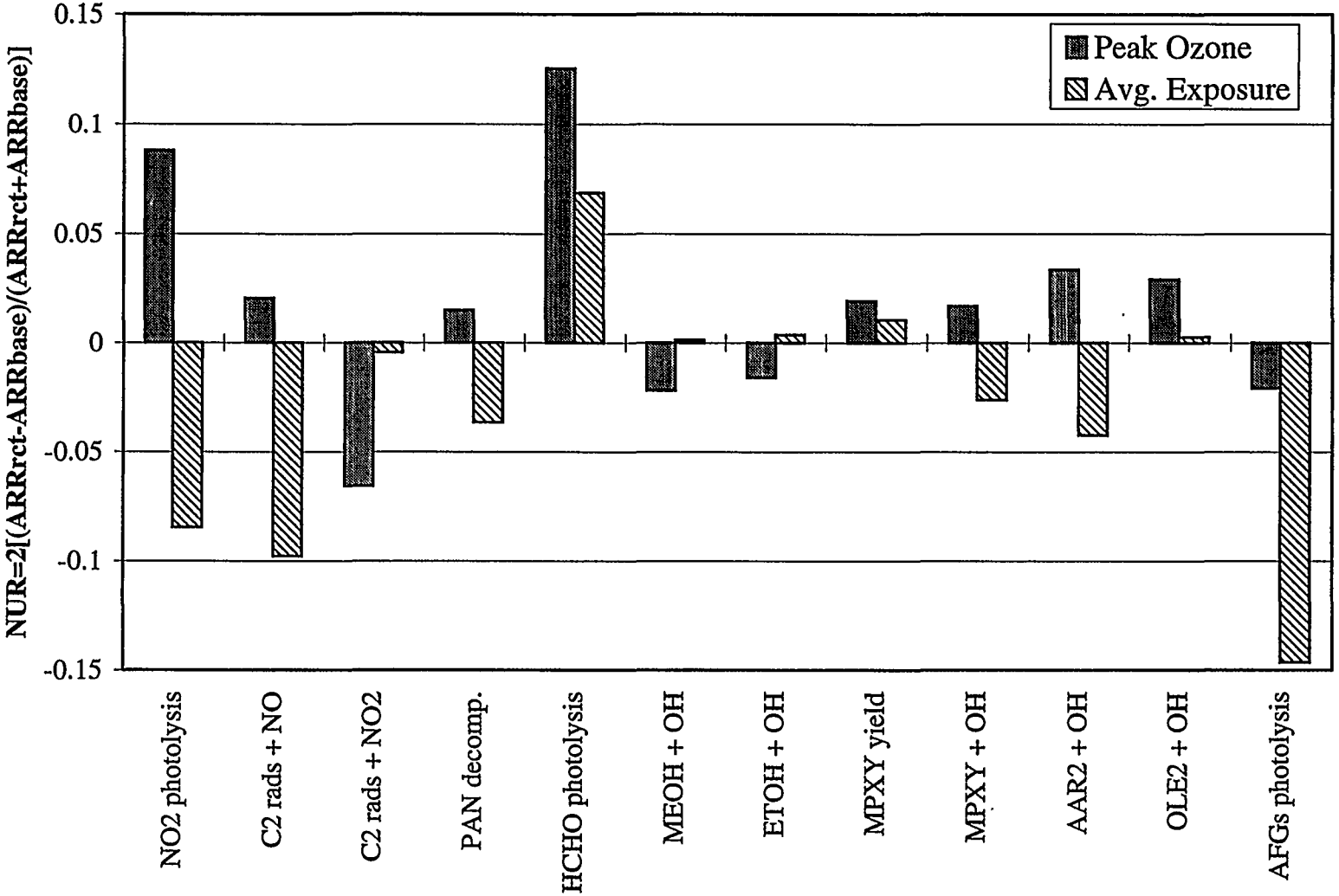

Figure 4-4. Normalized Uncertainty Response (NUR) of LPG to Mechanism Uncertainties

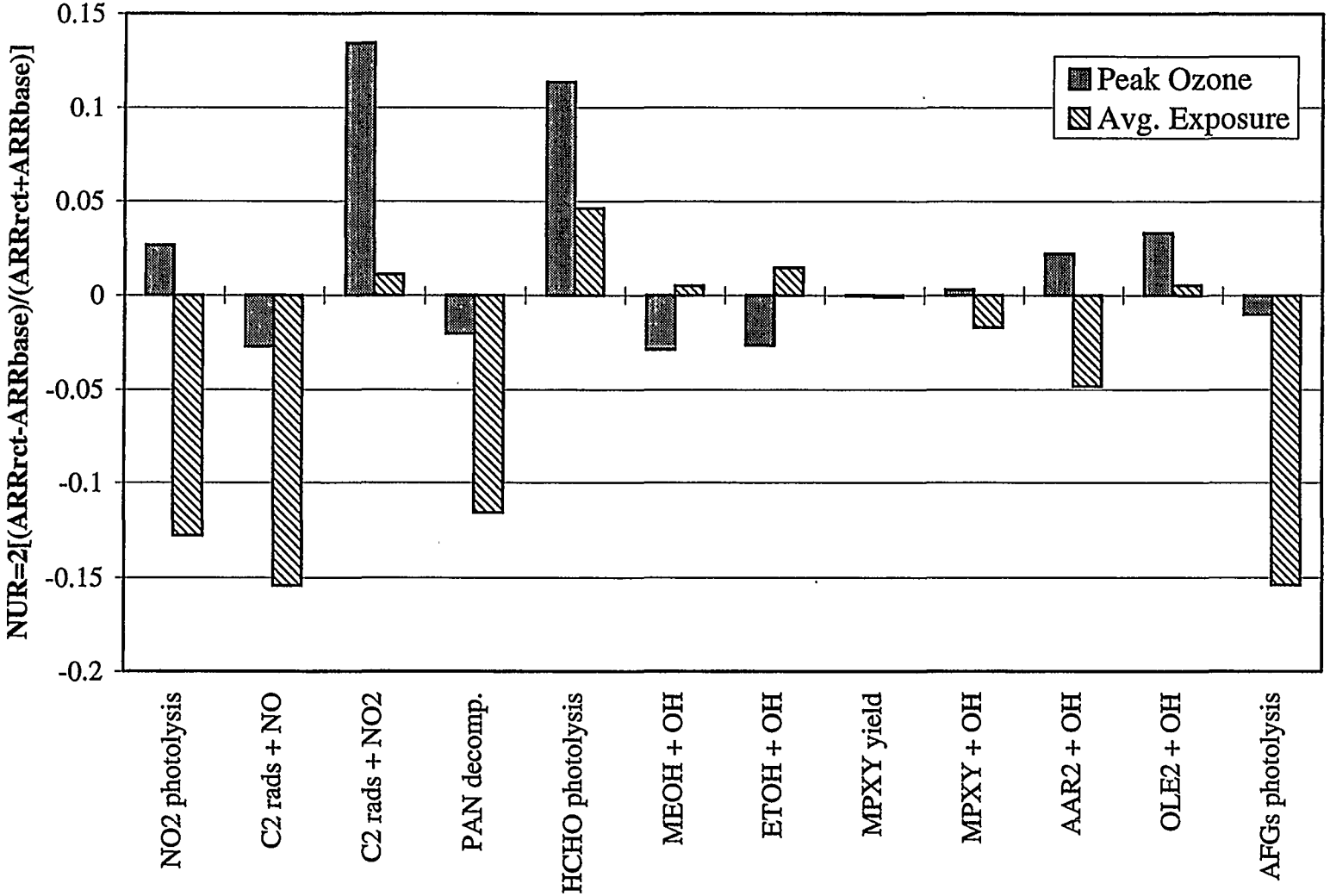

Figure 4-5. Normalized Uncertainty Response (NUR) of Phase 2 to Mechanism Uncertainties

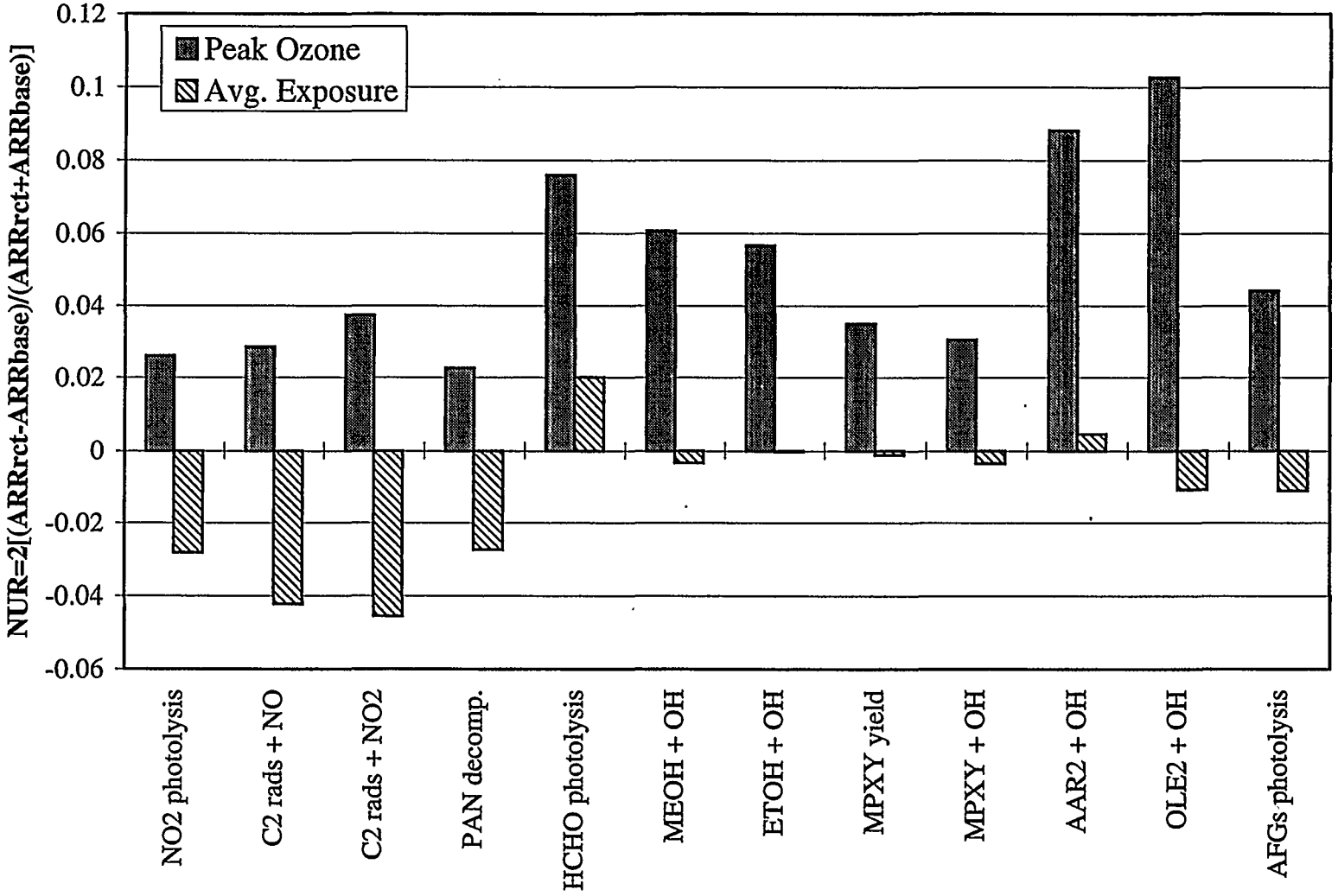

Figure 4-6. Normalized Uncertainty Response (NUR) of M85 to Mechanism Uncertainties

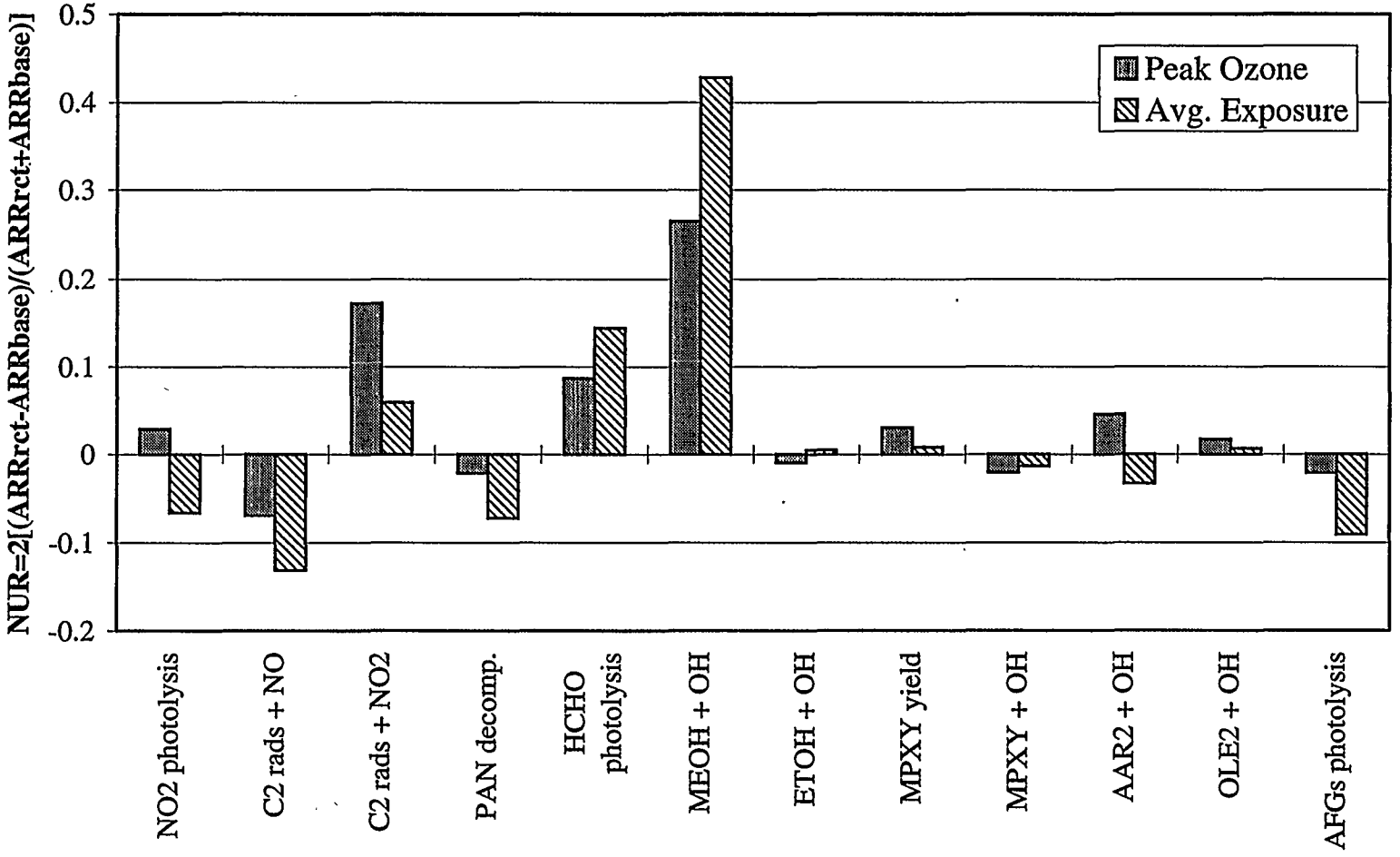

$$NUR_{rct} = 2[(ARR_{rct} - ARR_{base})/(ARR_{rct} + ARR_{base})] \quad (4.5)$$

where the ARR is calculated as shown in Equation (4.4) above, and the subscript $_{rct}$ denotes that the P values are from the model runs using the perturbed reaction (rate or speciation) parameters.

The NUR results are tabulated in Table 4-3, showing the results for each fuel to each reaction, with the average and standard deviation across reactions and across fuels. Figures 4-3 through 4-7 graphically show the NUR of each fuel to the 12 chemical mechanism uncertainties. The x-axis labels are defined in Table 4-1. By comparing the five figures showing the sensitivity results (Figures 4-3 through 4-7), or by examining Table 4-3, it becomes apparent that, except for the MEOH + OH reaction for M85 and a number of reactions in the E85 RAF tests (e.g. the ETOH + OH and the reactions involving PAN dynamics), the normalized bias (NUR) ranges are small to moderate, falling between 0.15 and -0.15. Also, comparing Figures 4-3 and 4-4, except for NO_2 photolysis, the acetyl peroxy radical + NO_2 reaction set (CCO-O_2 and C_2COO_2 + NO_2), and PAN decomposition, most of the sensitivities for CNG and LPG are very similar. This is not surprising, given the similarity of their emissions.

Which reaction dominates the normalized bias is not consistent between the two metrics, or between fuels. Looking at Figure 4-3 (CNG) for example, AFG photolysis shows the greatest uncertainty response for the average exposure measure, with the acetyl peroxy radical + NO being the next highest; the peak ozone measure shows the greatest sensitivity to HCHO photolysis with NO_2 photolysis second highest. It is interesting to note that the high peak measured sensitivities are positive, and the high exposure measured sensitivities are negative, for all fuels except M85. This can be explained, in part, by the location of the peak in a less NO_x-rich location, and the highest population density in a more NO_x-rich area, as is discussed below.

The NURs for CNG are generally less than 10%, except for the response to HCHO photolysis (the peak ozone response is about 12%) and AFG photolysis (the response is negative 14%). This is directly related to the CNG exhaust being somewhat richer in HCHO, and having

considerably less aromatic content (which is the precursor to AFG), as compared to the base gasoline.

Still referring to Figure 4-3 (CNG), the normalized bias calculated for NO_2 photolysis for the two metrics is approximately equal in magnitude, but opposite in sign. A peak ozone increase is predicted with the photolysis uncertainty, but a decrease is predicted when measured by average ozone exposure. These two metrics represent changes over various regions of the modeling domain, so the captured meteorological conditions and VOC:NO_X ratios are different (Bergin et. al, 1995). Ozone tends to peak downwind of Los Angeles, in a higher VOC:NO_X ratio area than most of the domain. The exposure metric is affected by the more NO_x-rich, highly populated downtown region. For this reason, the two metrics respond to NO_2 photolysis uncertainty with an opposite sign; however, they both predict a very similar magnitude of normalized bias. This behavior is noticeable for a few other reactions, particularly in the normalized uncertainty response calculated for Phase 2 fuel, which is shown in Figure 4-5.

The LPG NURs (Figure 4-4) show the importance of organic nitrate formation (e.g., PAN) by gasoline. Organic nitrates store NO_x, delaying it from photolyzing and forming ozone. Thus, in NO_x-limited regions, organic nitrate formation can lead to a local decrease in ozone. LPG is rich in propane, which reacts slowly. Gasoline has more reactive organics, such as olefins, that rapidly form organic nitrate precursors. Thus, increasing the rate of organic nitrate formation (e.g., organic peroxy radicals + NO_2) decreases peak ozone more in the base gasoline case than in the LPG case, leading to a positive peak ozone NUR. Alternatively, increasing the competing reactions (either peroxy radicals + NO or PAN decomposition), leads to a negative NUR for LPG. In both cases, the largest response is in the base gasoline case, as compared to the LPG case. As mentioned previously, these results may be affected by the use of an early version of the detailed propane + HO reaction.

ARRs for Phase 2 gasoline (Figure 4-5) showed very little response to mechanism uncertainties, generally having NURs less than 10% and most of the time less than 4%. This is not entirely surprising given that Phase 2 exhaust has a much more similar composition to RFA exhaust than

the other fuels. Thus, one would expect a very similar response between the RFA and Phase 2 results, leading to NURs of about 1.

For M85 (Figure 4-6), the NURs were generally small, except for the response to the MEOH + OH reaction. This is expected because MEOH is the dominant species in M85 exhaust, contributing to a large fraction of the net reactivity of the fuel, and because of the high rate-constant uncertainty estimate used in this study. Also, the HCHO photolysis result is important because HCHO is also a major component of M85 exhaust. Organic nitrate formation and decomposition still appear to be important for about 5% to 10% of the reduction in reactivity.

Overall, as shown in Table 4-3 (which includes the average normalized uncertainty response and the standard deviation for each fuel across all reactions), a clear trend appears of opposite responses to uncertainty between peak ozone average exposure, with the exception of the response of M85. However, the average for M85 is slightly skewed because of the large positive response calculated for the MEOH + OH reaction. This response is also outside the general range of normalized responses across the fuels and reactions.

Table 4-3 also shows the average normalized uncertainty response and the standard deviation for each reaction across all fuels, with no reaction showing a large deviance from the others. In general, the peak ozone measure has a slightly higher absolute NUR than the averaged response (0.052 versus -0.026 for average exposure).

The most notable deviations from showing no bias and having larger standard deviations are for reactions that involve NO_X and their effect on the peak ozone measure. Ozone exposure was generally less sensitive to these reactions. This can be explained by the location of the peak ozone concentrations in a region where the availability of NO_x has a high impact on the ozone levels. The effect on ozone exposure was less marked. The HCHO photolysis rate affects the reactivity of most fuels, because it is a constituent of the exhaust of all the fuels. Its effect is most pronounced for M85. Likewise, the MEOH + OH reaction has a large effect on the reactivity of methanol fuel, as does the ETOH + OH reaction on the ethanol fuel. The average bias in the peak ozone introduced by perturbing the reactions was 3%, and the bias for the

exposure metric was almost zero. The standard deviations ranged from almost zero to 25%, with an average of about 10% for both the peak and ozone exposure measures.

The highest average fuel NUR was found for E85, for both the peak and exposure metric. The highest average NUR for the reactions was for the peak ozone measure of PAN decomposition, which is dominated by the E85 results. For the exposure metric, the highest average NUR was found for AFG photolysis, to which most fuels showed some sensitivity.

4.5 Summary

A series of photochemical airshed model calculations was conducted to assess how uncertainties in the chemical mechanism parameters, both reaction rates and product speciation, would affect the ozone response for five alternative fuels. First, the SAPRC mechanism used in the CIT model was extended to include explicit propane chemistry. The change had virtually no effect on the base-case predictions, but is of interest because propane is a dominant emitted compound from many of the fuels examined; therefore, it may have an effect during the uncertainty experiments. Next, mobile source organic emissions inventories were constructed for each of the fuels: base gasoline, California Phase 2 gasoline, M85, CNG, LPG, and E85. The product splits and reaction rates in the SAPRC mechanism are sensitive to the emission composition, and in this study the parameters were developed for a base mixture. Some fuels have much different exhaust compositions from the base mixture, which may have effected the results. The inventories were constructed to account for the speciation and emissions timing (e.g., hot and cold start and hot stabilized), and the mass was adjusted by the fuel RAF and then doubled. The RAF adjustment is designed so the impact of the emissions on ozone should be nearly equivalent. In addition, a seventh inventory was constructed with no mobile source organic emissions.

These seven inventories were then used as inputs to the CIT airshed model. First, a base set of simulations were used to assess the RAF impact on predicted ozone concentrations for each fuel. The adjustment worked fairly well for most fuels, though the predicted impacts are not equivalent and vary depending on the measure considered. The closest agreement was found for Phase 2 and M85, and the largest differences were found with the peak ozone metric for CNG

and with the average exposure metric for LPG. There is also some discrepancy in the E85 average exposure results. Larger differences were observed in this study than in a similar previous study (McNair et. al, 1994) using the same air quality model with a less detailed chemical mechanism, particularly for CNG. These issues are being investigated further.

Next, some chemical mechanism parameters were adjusted to reflect the estimated uncertainties. The 12 reactions chosen for investigation were based on the results of the box modeling (Chapter 2 and 3 of this study) and on the previous study, which investigated individual species reactivities (Yang et. al, 1994). The impact of changing the reaction parameters was relatively small, leading to little increased bias or variation.

These results suggest that the RAFs are relatively insensitive to the chemical mechanism uncertainties, as was also suggested by the box modeling and previous results from Yang et al. (1994). The largest responses were found for E85 peak ozone measures to PAN decomposition and the C2 radicals + NO reaction set, and for M85, both measures, to the MEOH + OH reaction (which was assigned a very high estimate of uncertainty compared to various reviews). If one compares these uncertainties with the uncertainties in the emissions compositions and reactivity variability resulting from environmental conditions, they are seen to be relatively small (Russell et al., 1995). The results suggest that to decrease the impacts of chemical uncertainties on RAFs, the important reactions for further study are the OH-alcohol reactions (which has already been examined for MEOH + OH), the reactions involved in PAN formation and loss, and photolysis rates.

5. SUMMARY AND CONCLUSIONS

5.1 Overview

This project built on the results of an earlier study that investigated the sensitivity and uncertainty of individual VOC ozone-forming potentials to chemical rate parameters (Yang et al., 1994). In that study, box modeling and formal sensitivity and uncertainty analysis were combined with airshed modeling to assess how rate constant uncertainties affected the estimates of VOC reactivities. This project has further investigated uncertainties involved in quantification of VOC reactivity and in the development and use of RAFs. Here, similar techniques were used to extend that analysis to include selected uncertainties in the chemical mechanism product-yield parameters. Also, this project concentrated further on the application of species reactivities and uncertainty analysis to the calculation of Reactivity Adjustment Factors (RAFs). This is of direct interest because of the California Air Resources Board's requirement to use RAFs to account for differences in the reactivity of exhaust emissions from various fuel/vehicle combinations.

This final chapter first summarizes the major findings presented in Chapters 2 through 4, comparing and synthesizing the box-model results presented in Chapter 3 with the airshed-model results presented in Chapter 4. The final section of the report summarizes our conclusions, reiterates the limitations of our analysis, and presents recommendations for future research.

5.2 Summary and Synthesis of Box-model and Airshed Results

Chapter 2 presents the results of our analysis of the uncertainties in the selected product yield estimates of the SAPRC90 mechanism. This is important not only for the work here, which requires such information for conducting a quantitative uncertainty analysis, but also for a better understanding of the integrity of such chemical mechanisms in the future. This analysis, along with the analysis in Chapter 3, can guide future investigators to identify the most important unknowns. Such information is important to guiding future laboratory studies. Uncertainties in the product yields were found to be greatest for the reactions of aromatic compounds, because of the large fraction of products that have not been identified in past experiments. Product yields for reactions of higher alkenes were also found to be relatively uncertain.

Chapter 3 used the uncertainty estimates in the product yields, along with the results from the previous study on rate parameters, to identify the most important uncertainties. Formal sensitivity and uncertainty analysis was conducted using a box-model, applied for a relatively short simulation period (10 hours). For product yields, uncertainty estimates were based primarily on assessments of errors in yield measurements made according to the type of product (organic peroxy radical, carbonyl, etc.). Correlations between parameters were introduced where values were estimated by analogy. Variances of exhaust concentrations across vehicles tested on a given fuel were taken as estimates of uncertainty in the emissions compositions, which were treated as normally distributed random variables. Correlations between emission rates for various species were also estimated from the test data, and retained in the Monte Carlo analysis.

One of the more striking results here is that the most influential uncertainties in determining the species reactivities are the rate parameters, not the product yields. The most influential product yield uncertainties were for the products of aromatic (e.g., toluene and the xylenes) reactions with hydroxyl radicals. Inclusion of product yield uncertainties had an insignificant impact on calculation of MIRs of most species. Uncertainties (1σ) in MIRs of the organic compounds and classes we studied range from 25% of the mean estimate, for formaldehyde, to 66% of the mean, for ethanol. Uncertainties in MOIRs range from 27% for methane to 83% for toluene. Uncertainties (1σ) in the final ozone concentrations predicted for the MIR and MOIR simulation conditions were about 32% and 21%, respectively.

With respect to MIRs, the greatest potential for reducing uncertainties appears to exist for oxygenated compounds, for which additional measurements of HO rate constants and photolysis rates (where applicable) could substantially reduce uncertainty. Additional measurements of product yields for carbonyls and peroxy radicals in alkenes + HO reactions, and elucidation of the secondary chemistry of aromatics oxidation, would also be helpful.

Accounting for uncertainties in the rate parameters and product yields of the SAPRC mechanism, and for variability in exhaust composition across vehicles tested by CARB and by

the AQIRP, uncertainties of about 15% (1σ) are indicated for the RAFs of exhaust emissions associated with reformulated gasolines. Uncertainties associated with chemical parameters alone led to uncertainties in RAFs for M85, E85, CNG, and LPG of about 10% to 20%, based on CARB's data. Inclusion of product yield uncertainties had an insignificant effect on the uncertainties in the RAFs (as well as most species MIRs). For reformulated gasolines, the emissions variability accounts for more uncertainty than the chemical parameters. For alternative fuel vehicles, confidence in estimates of RAFs could be improved by obtaining additional data on their emissions and the rate parameters of key exhaust components.

In Chapter 4, the results of the box modeling were used to guide the airshed-model investigation of the way fuel RAFs are affected by parameter uncertainties. From the previous analysis, 12 parameters were identified that would most influence RAFs. Of these, one was a product yield uncertainty (the unknown dicarbonyl product yield from the mp-xylene + OH reaction), and the rest were rate parameters. A series of photochemical airshed-model calculations was conducted to assess the effects of uncertainties in the chemical mechanism parameters on ozone response for five alternative fuels whose emissions were adjusted using RAFs. First, the SAPRC mechanism used in the CIT model was extended to include explicit propane chemistry. The change had virtually no effect on the base-case predictions, but is of interest because propane is a major emitted product from many of the fuels examined. The reaction used was from an earlier chemical mechanism, and although this is not expected to significantly affect results, the impact is currently being examined.

Next, mobile source organic emissions inventories were constructed for each of the fuels investigated: base gasoline, California Phase 2 gasoline, M85, CNG, LPG, and E85. The inventories were constructed to account for the speciation and emissions timing (e.g., hot versus cold, starting versus running), and the mass was adjusted by their RAFs. The RAF is designed so the impact of the emissions on ozone should be nearly equivalent. The mobile organic emissions were also doubled to account for the widely accepted belief that these emissions are underpredicted by a factor of 2 to 4 in the Los Angeles air basin. In addition, a seventh inventory was constructed with no mobile source organic emissions.

These seven inventories were then used as inputs to the CIT airshed-model. First, a base set of simulations was used to assess the RAF impact on ozone concentrations for each fuel. The AAR results for M85 and Phase 2 gasoline were very near one, showing that for these fuels the adjustment worked well. However, some significant discrepancies were found for E85, CNG, and, to a lesser extent, LPG. These differences are being investigated further. The fuels also had varying impacts when considering the averaged ozone exposure or the peak ozone measures.

Next, the 12 chemical mechanism parameters were adjusted individually to reflect the estimated uncertainties. The parameters that had the largest effects were the reaction rates of methanol with OH on the reactivity of M85 fuel, and the reaction rate of ethanol and OH on the reactivity of E85 fuel. The reactions involving NO_x had a major impact on all fuels. The most important parameters in this case were the NO_2-photolysis rate, and the reaction rate parameters for peroxy acyl nitrate formation and decomposition (along with the competing reactions). An interesting result was that the response of the peak ozone was often opposite in direction from the response of the ozone exposure to changes in the reactions involving NO_x. This probably reflects that the modeled peak ozone is in a region of the Los Angeles basin that is somewhat NO_x limited, whereas the exposure is dominated by regions that are NO_x rich.

These results suggest that RAFs are relatively insensitive to the chemical mechanism uncertainties (except for the M85 and E85 cases being sensitive to the rate parameters for the reaction of the base alcohol with OH), as was also suggested by the box modeling and previous results from Yang et al. (1994). If one compares these uncertainties to the uncertainties in the emissions compositions and reactivity variability resulting from environmental conditions, they are seen to be relatively small (e.g., Russell et al., 1995). The results suggest that to decrease the chemical uncertainty impacts on uncertainties in RAFs, the important reactions for further study are the OH-alcohol reactions, photolysis reactions, and the reactions involved in PAN formation and loss.

5.3 Conclusions

This report has presented the results of an extensive uncertainty and sensitivity analysis of the ozone-forming potentials, or reactivities, of individual organic compounds and RAFs. The study, and its predecessor, are unique in several respects. One of the most important aspects of the studies was the integrated use of a variety of tools to study and quantify the reactivity of individual species and the sensitivities and uncertainties in those calculations. A box-model and a three-dimensional airshed-model were used in an integrated fashion, and the results synthesized to enhance the individual calculations. The simpler (or less computationally intensive) tools were used first to suggest which issues (or in this case, reaction-rate uncertainties) should be further studied. This made maximum use of the available resources. Even with such a strategy, however, the project was intensive, both computationally and in terms of the analysis and synthesis of the results.

A key limitation of the uncertainty analysis performed in the previous study was that it was confined to uncertainties in rate parameters in SAPRC90, neglecting uncertainties in product yields. These were considered here and found to have relatively little impact. This study quantified uncertainties in the SAPRC90 mechanism, but did not investigate broader issues in mechanism formulation (e.g., degree of explicitness or omission of important reactions or species). Beyond the chemical mechanism, the study did not attempt to treat uncertainties in the simulation conditions for which reactivities are calculated. Finally, the uncertainties in SAPRC parameters that were propagated through the analysis were subjectively estimated.

As in the previous study, the uncertainty analysis performed for RAFs was also incomplete in its treatment of uncertainties in emissions compositions. As a first step toward exploring the influence of uncertainties in emissions composition, the study considered the portion of the uncertainty that could be estimated statistically from vehicle-emissions tests. The variances of emissions across vehicles tested on the same fuel were taken as estimates of uncertainty in the emissions compositions, which were treated as correlated, normally distributed random variables. However, another source of uncertainty in emissions compositions is differences that occur between laboratory and in-use conditions. Developing the necessarily subjective estimates of this component of uncertainty was beyond the scope of this study.

One conclusion from this extension of our previous study is that product yield uncertainties generally add little to the uncertainty in the calculation of individual species reactivities. Taking this to the point of calculating fuel RAFs, very little uncertainty is a result of product yield uncertainties. Instead, the uncertainties are dominated by rate parameters and the emissions compositions.

The RAF uncertainties are significantly lower than uncertainties in the MIRs of individual organic compounds, which generally ranged from about 30% to 50%. Moreover, for the same box-model simulation conditions, the uncertainty in the predicted final ozone concentration was estimated to be about 30%. Compared to uncertainties in MIR values for individual compounds, uncertainties in calculated RAFs are small because of strong correlations between the MIR values of different compounds and between the reactivities of the base and test fuels. Chemical parameter uncertainties have directionally similar effects on MIRs of many organic compounds.

The variety of techniques used here provided a powerful analysis of the effects of chemical mechanism uncertainties on the assessment of vehicle exhaust reactivity. The primary conclusion is that chemical mechanism uncertainties have a relatively small effect on quantitative measures of vehicle exhaust impacts on ozone. More specifically, rate constant uncertainties appear to be more important than the product speciation uncertainties. Further studies could use a similar approach to develop a more quantitative understanding of the atmospheric chemical dynamics of vehicle exhaust emissions.

6. REFERENCES

Atkinson, R., Lloyd, A.C., Winges, L. (1982). "An Updated Chemical Mechanism for Hydrocarbon/NO_X/SO_2 Photooxidations Suitable for Inclusion in Atmospheric Simulation Models," *Atmos. Environ.*, **16**, 1341-1355.

Atkinson R., Carter, W.P.L. (1984). "Kinetics and Mechanisms of the Gas-Phase Reactions of Ozone with Organic Compounds under Atmospheric Conditions," *Chem Rev.*, **84**, 437-470.

Atkinson, R., Lloyd, A.C. (1984). "Evaluation of Kinetic and Mechanistic Data for Modeling of Photochemical Smog," *J. Phys. Chem. Ref. Data*, **13**, 315-444.

Atkinson, R. (1986). "Kinetics and Mechanisms of the Gas-Phase Reactions of the Hydroxyl Radical with Organic Compounds under Atmospheric Conditions," *Chem. Rev.*, **86**, 69-201.

Atkinson, R., Baulch, D.L., Cox, R.A., Hampson, R.F. Jr., Kerr, J.A., Troe, J. (1989). "Evaluated Kinetic and Photochemical Data for Atmospheric Chemistry: Supplement III. IUPAC Subcommittee on Gas Kinetic Data Evaluation for Atmospheric Chemistry," *J. Phys. Chem. Ref. Data*, **13**, 1259-1380.

Atkinson, R. (1990). "Gas-Phase Tropospheric Chemistry of Organic Compounds: A Review," *Atmos. Environ.*, **24A**, 1-41.

Atkinson, R., Baulch, D.L., Cox, R.A., Hampson, R.F., Kerr, J.A., Troe, J., (1992) "Evaluated Kinetic and Photochemical Data for Atmospheric Chemistry: Supplement IV," IUPAC Subcommittee on Gas Kinetic Data Evaluation for Atmospheric Chemistry, *J. Phys. Chem. Ref. Data,* **21**, 1125-1568.

Atkinson, R. (1994). "Gas-Phase Tropospheric Chemistry of Organic Compounds," *J. Phys. Chem. Ref. Data*, Monograph 2, 1-216.

Bergin, M.S. (1994) Ozone-Forming Potential of Reactive Organic Gases: Reactivity and Uncertainty Analayis, Master Thesis, Department of Mechanical Engineering, Carnegie Mellon University, Pittsburgh, PA, July.

Bergin, M.S., Russell, A.G., and Milford, J.B. (1995). "Quantification of Individual VOC Reactivity Using a Chemically Detailed, Three-Dimensional Photochemical Model." Submitted to *Environ. Sci. Technol.*, **29**, 3029-3027.

Bufalini, J.J., Dodge, M.C. (1983). "Ozone-Forming Potential of Light Saturated Hydrocarbons," *Environ. Sci. Technol.*, **17**, 308-311.

Burkholder, J. B., Hammer, P.D. and Howard, C.J. (1987). "Product Analysis of the OH + NO2 + M Reaction," *J. Phys. Chem.*, **91**, 2136-2144.

Burns, V.R., Benson, J.D., Hochhauser, A.M., Koehl, W.J., Kreucher, W.M., Reuter, R.M. (1991). "Description of the Auto/Oil Air Quality Improvement Research Program," SAE technical paper no. 912320, Society of Automotive Engineers, Warren, PA.

CARB (1990). *Proposed Regulations for Low-Emission Vehicles and Clean Fuels: Staff Report and Technical Support Document*, State of California Air Resources Board, Sacramento, CA, August.

CARB (1992). Research Division, *Development and Evaluation of Ozone Reactivity Scale for Low-Emission Vehicles and Clean Fuels Regulations*, State of California Air Resources Board, Sacramento, CA, April.

CARB (1994). Personal communication from B. Croes (State of California Air Resources Board, Sacramento, CA) to A.G. Russell (Carnegie Mellon University, Pittsburgh, PA).

Calvert, J. G., Madronich, S. (1987). "Theoretical Study of the Initial Products of the Atmospheric Oxidation of Hydrocarbons," *J. Geophys. Res.*, **92**, 2211-2220.

Carter, W.P.L., Atkinson, R. (1989). "A Computer Modeling Study of Incremental Hydrocarbon Reactivity," *Environ. Sci. Technol.*, **23**, 864-880.

Carter, W.P.L. (1990a). "A Detailed Mechanism for the Gas-Phase Atmospheric Reactions of Organic Compounds," *Atmos. Environ.*, **24A**, 481-518.

Carter, W.P.L. (1990b). *Development of Ozone Reactivity Scales for Volatile Organic Compounds*, Draft Final Report to the U.S. EPA, Contract # CR-814396-01-0, Statewide Air Pollution Research Center, University of California, Riverside, CA, November.

Carter, W.P.L. (1994). "Development of Ozone Reactivity Scales for Volatile Organic Compounds," *J. Air & Waste Manage. Assoc.*, **44**, 881-899.

Cvetanovic, R.J. (1976). "Chemical Kinetic Studies of Atmospheric Interest," 12th International Symposium on Free Radicals, Laguna Beach, CA, January 4-9.

DeMore, W.B., Sander, S.P., Golden, D.M., Molina, M.J., Hampson, R.F., Kurylo, M.J., Howard, C.J., Ravishankara, A.R. (1990). *Chemical Kinetics for Use in Stratospheric Modeling, Evaluation Number 9*, National Aeronautics and Space Administration, Jet Propulsion Laboratory, California Institute of Technology, Pasadena, CA.

DeMore, W.B., Sander, S.P., Golden, D.M., Hampson, R.F., Kurylo, M.J. , Howard, C.J., Ravishankara, A.R., Kolb, C.E., and Molina, M.J. (1992). *Chemical Kinetics and Photochemical Data for Use in Stratospheric Modeling, Evaluation Number 10*, National Aeronautics and Space Administration, Jet Propulsion Laboratory, California Institute of Technology, Pasadena, CA.

Dodge, M.C. (1984). "Combined Effects of Organic Reactivity and NMHC/NO_X Ratio on Photochemical Oxidant Formation — A Modeling Study," *Atmos. Environ.*, **18**, 1657-1665.

Dunker, A.M. (1984). "The Decoupled Direct Method for Calculating Sensitivity Coefficients in Chemical Kinetics," *J. Chem. Phys.*, **81**, 2385-2393.

Finlayson-Pitts, B.J., Pitts, J.N., Jr. (1986). *Atmospheric Chemistry: Fundamentals and Experimental Techniques*, John Wiley and Sons, New York, NY.

Fujita, E.M., Croes, B.E., Bennett, C.L., Lawson, D.R., Lurmann, F.W., Main, H.H. (1992). "Comparison of Emission Inventory and Ambient Concentration Ratios of CO, NMOG, and NO_x in California's South Coast Air Basin," *J. Air & Waste Manage. Assoc.*, **42**, 264.

Gao, D., Stockwell, W.R., Milford, J.B. (1995). "First Order Sensitivity and Uncertainty Analysis for a Regional-Scale Gas-Phase Chemical Mechanism," *J. Geophysical Res.*, **100**, 23153-23166.

Gery, M. W., Fox, D. L., Jeffries, J. E., Stockbuger, L., and Weathers, W.S. (1985). "A Continuous Stirred Tank Reactor Investigation of the Gas-Phase Reactions of Hydroxyl Radicals and Toluene," *Int. J. Chem. Kinet.*, **17**, 931-955.

Gery, M.W., Whitten, G.Z., Killus, J.P., Dodge, M.C. (1989). "A Photochemical Mechanism for Urban and Regional Scale Computer Modeling," *J. Geophys. Res.*, **94**, 12925-12956.

Gery, M.W. (1991). *Review of the SAPRC90 Chemical Mechanism*, California Air Resources Board, Contract No. A132-055, Sacramento, CA.

Grosjean, D. and Seigneur, C. (1991). *Needed Improvements in the Treatment of Chemistry in Grid-Based Photochemical Models*, Final Report prepared for South Coast Air Quality Management District, DGA, Ventura, CA.

Harley, R.A., Russell, A.G., McRae, G.J., McNair, L.A., Winner, D.A., Odman, M.T., Dabdub, D., Cass, G.R., Seinfeld, J.H. (1992). *Continued Development of a Photochemical Model and Application to the Southern California Air Quality Study (SCAQS) Intensive Monitoring Periods: Phase I*, Report to the Coordinating Research Council under project SCAQS-8, Carnegie Mellon University, Pittsburgh, PA, and California Institute of Technology, Pasadena, CA.

Hochhauser, A.M., Benson, J.D., Burns, V.R., Gorse, R.A. Jr., Koehl, W.J., Painter, L.J., Rueter, R.M., Rutherford, J.A. (1992). "Speciation and Calculated Reactivity of Automotive Exhaust Emissions and their Relation to Fuel Properties—Auto/Oil Air Quality Improvement Research Program," SAE technical paper no. 920325, Society of Automotive Engineers, Warren, PA.

Iman, R.L., Shortencarier, M.J. (1984). *A FORTRAN 77 Program and User's Guide for the Generation of Latin Hypercube and Random Samples for Use with Computer Models*, NUREG/CR-3624, Sandia National Laboratories, NM, March.

Iman, R.L., Helton, J.C. (1985). *A Comparison of Sensitivity Analysis Techniques for Computer Models*, NUREG/CR-3904, Sandia National Laboratories, NM, March.

IUPAC (1989). Same reference as Atkinson et al. (1989).

LACTOZ (1994). *EUROTRAC Annual Report 1993, Part 8, Laboratory Studies of Chemistry Related to Tropospheric Ozone*, EUROTRAC International Scientific Secretariat, Garmisch-Partenkirchen, Germany.

Lurmann, F.W., Lloyd, A.C., Atkinson, R. (1986). "A Chemical Mechanism for Use in Long-Range Transport/Acid Deposition Computer Modeling," *J. Geophys. Res.*, **91**, 10905-10936.

Lurmann, F.W., Carter, W.P.L., Coyner, L.A. (1987). *A Surrogate Species Chemical Reaction Mechanism for Urban-Scale Air Quality Simulation Models*, EPA/600/3-87-014, U.S. Environmental Protection Agency, Research Triangle Park, NC, June.

McCroskey, P.S., McRae, G.J. (1987). *Documentation for the Direct Decoupled Sensitivity Analysis Method—DDM*, report, Department of Chemical Engineering, Carnegie Mellon University, Pittsburgh, PA.

McNair, L.A, Russell, A.G., Odman, M.T. (1992). "Airshed Calculation of the Sensitivity of Pollutant Formation to Organic Compound Classes and Oxygenates Associated with Alternative Fuels," *J. Air & Waste Management Assoc.*, **42**, 174.

McNair, L.A., Russell, A.G., Croes, B., Kao, L. (1994). "Airshed Model Evaluation of Reactivity Adjustment Factors Calculated with the Maximum Incremental Reactivity Scale for Transitional-Low Emission Vehicles," *J. Air & Waste Management Assoc.*, **44**, 900.

NASA 9. Same reference as DeMore, et al. (1990).

NASA 10. Same reference as DeMore, et al. (1992).

NREL (1994). Personal communication from B. Bailey (National Renewable Energy Laboratory, Golden, CO) to M.S. Bergin (Carnegie Mellon University, Pittsburgh, PA).

Niki, H., Maker, P.D., Savage. C.M., Breitenbach, P.L. (1981). "An FT-IR Study of Mechanisms for the HO Radical Initiated Oxidation of C2H4 in the Presence of NO: Detection of Glycolaldehyde," *Chem. Phys. Lett.*, **80**, 499-503.

Russell, A.G., McNair, L.A., Odman, M.T., Kumar, N. (1991). *Organic Gas Reactivity and the Use of Alternative Fuels*, Final report to the California Air Resources Board, Sacramento, CA.

Russell, A.G., Milford, J.B., Bergin, M.S. McBride, S., McNair, L., Yang, Y-J., Stockwell, W.R., and Croes, B. (1995). "Urban Ozone Control and Atmospheric Reactivity of Organic Gases." *Science*, **269**, 491-495.

Stockwell, W.R., Yang, Y-J., Milford, J.B. (1994). *A Compilation of Estimated Uncertainty Factors for Rate Constants in W.P.L. Carter's Detailed Mechanism*, report prepared for the Auto/Oil Air Quality Improvement Research Program. Available from the Coordinating Research Council, Atlanta, GA.

Tsang, W. (1991). "Chemical Kinetic Data Base for Combustion Chemistry. Part V. Propene," *J. Phys. Chem. Ref. Data*, **20**, 221-274.

Tuazon, E. C., MacLeod, H., Atkinson, R. and Carter, W.P.L. (1986). "a-Dicarbonyl Yields from the NO_x-Air Photooxidations of a Series of Aromatic Hydrocarbons in Air," *Environ. Sci. Technol.*, **20**, 383-387 .

Winegar and Keith, ed. (1993). *Sampling and Analysis of Airborne Pollutants*, Lewis Publishers, Ann Arbor, MI.

Yang, Y-J., Das, M., Milford, J.B., Bergin, M.S., Russell, A.G., Stockwell, W.R. (1994). *Quantification of Organic Compound Reactivities and Effects of Uncertainties on Rate Parameters,* report prepared for the Auto/Oil Air Quality Improvement Research Program. Available from the Coordinating Research Council, Atlanta, GA.

Yang, Y-J., Stockwell, W.R., Milford, J.B. (1995). "Uncertainties in Incremental Reactivities of Volatile Organic Compounds," *Environ. Sci. Technol.*, **29**, 1336-1345.

reprint removed, ds

APPENDIX A

Urban Ozone Control and Atmospheric Reactivity of Organic Gases
Published in *Science*, July 1995

Urban Ozone Control and Atmospheric Reactivity of Organic Gases

A. Russell,* J. Milford, M. S. Bergin,† S. McBride, L. McNair, Y. Yang, W. R. Stockwell, B. Croes

Control strategies for urban ozone traditionally have been based on mass reductions in volatile organic compounds (VOCs). Studies show, however, that some organic gas species (such as alkanes and alcohols) form an order of magnitude less ozone than equal mass emissions of others (such as alkenes and aldehydes). Chemically detailed photochemical models are used to assess uncertainty and variability in reactivity quantification. VOC control strategies based on relative reactivity appear to be robust with respect to nationwide variations in environmental conditions and uncertainties in the atmospheric chemistry. Control of selective organic gas species on the basis of reactivity can offer cost savings over traditional strategies.

Tropospheric ozone, formed from nonlinear reactions between VOCs and nitrogen oxides (NO_x), is a primary constituent of urban smog (*1*). Estimates of VOC control costs needed to attain the National Ambient Air Quality Standard (NAAQS) for ozone of 0.12 parts per million are on the order of billions of dollars per year, and in the most severely impacted regions, the necessary control technologies have not been identified completely (*2, 3*). Despite considerable resource investment since the promulgation of the NAAQS, most large cities do not meet this standard. A variety of new directions are being explored to find more effective control strategies. One path, controlling NO_x emissions instead of VOC emissions, appears to be most effective for regional transport problems, in rural areas, and in urban areas with high biogenic VOC emissions. However, in the largest urban areas with the worst ozone problems, reducing VOC emissions also appears to be effective (*1, 2, 4*). Currently, control strategies and air quality regulations are based on reducing the total mass of VOCs emitted (excluding methane).

There are a number of reasons to consider incorporating specific information about the individual VOC species emitted in designing more effective control strategies. Of the hundreds of different VOC compounds emitted, each has a different impact on ozone levels. The relative ozone-forming potentials of individual VOCs, or "reactivity," can differ by more than an order of magnitude from one compound to another. For example, in a typical urban atmosphere, 1 kg of ethane will form about two orders of magnitude less ozone than 1 kg of formaldehyde. Ignoring the reactivity of emissions when regulations are developed may lead to ineffective, inefficient control strategies and possibly even lead to measures that worsen air quality. Consideration of reactivity focuses control efforts on those emissions with the greatest impacts on urban ozone. Other compelling reasons to consider reactivity-based strategies include providing strong incentives for accurate determination of emissions compositions, for pollution prevention through product redesign or reformulation, and the potential for large reductions in emissions control costs (*5*). We have examined the scientific basis for reactivity-based VOC regulations by quantifying the variability and uncertainties in reactivity estimates. We suggest that estimates of the relative impacts of individual VOCs on ozone can be incorporated into control strategies in order to refine control efforts nationwide.

Here we describe the analysis procedures used to quantify VOC reactivity, with particular attention to the reactivity scale used for automobile emission regulations in California (*6*). Although reactivity-based regulations are currently used in California, the potential environmental and economic advantages of this approach and the adoption of California vehicle regulations elsewhere (notably the Northeast) broaden the need to understand the scientific foundations, criticisms, benefits, and outstanding research issues associated with reactivity weighting (*7*). We examine the dependence of reactivity measures on (i) environmental conditions, particularly meteorology and precursor ratios; (ii) the level of chemical and physical detail and uncertainty in the models used for quantifying reactivity; and (iii) the uncertainties in emissions compositions. Our analysis shows that the relative reactivity of emissions mixtures, such as exhaust from alternatively fueled vehicles normalized to emissions from a base case fuel, is not very sensitive to any of these three factors. In conclusion, we present the results of an economic analysis which shows that strategies that use reactivity-based controls are not only more effective than those relying on mass-based controls but can also be less expensive.

We used photochemical air quality models and a variety of analysis methods. The two classes of photochemical models that have been used most extensively are chemically detailed but physically simplified zero-dimensional box models (*8–13*) and more comprehensive, physically detailed, three-dimensional (3D) airshed models (*10, 11, 14–17*). The method currently used for reactivity quantification in California was developed by Carter (*8*), who used a box model, and is based on the SAPRC90 chemical mechanism (*18*) to quantify how an incremental change in the emissions of a specific VOC would affect ozone. In addition to examining results from Carter's studies, we have also developed and applied both a box model (*10–12*) and a chemically detailed 3D model (*16, 17, 19*) for studying reactivity issues. For both models, atmospheric chemistry is treated using a version of SAPRC90 with 91 species (27 detailed organics) and 203 reactions. The box model is used for statistical analysis of reactivity quantification and uncertainty estimation over a wide range of variables. The more comprehensive 3D model is used to examine the dominant uncertainties identified through use of the box model while accounting for transport and multiday effects, and for estimation of pollutant exposure metrics. A linear optimization cost analysis model is developed to examine economic impacts of explicitly accounting for reactivity in control strategy design.

To illustrate the use of reactivity in the development of control strategies and regulations, we consider the reactivity scale used in California's Low Emission Vehicle (LEV) and Clean Fuels Regulations (*20*). Recently, Carter (*9*) used a chemically detailed, photochemical trajectory model to quantify the ozone formed from 180 differ-

A. Russell is in the Departments of Mechanical Engineering and Engineering and Public Policy, Carnegie Mellon University, Pittsburgh, PA 15213, USA. J. Milford is in the Department of Mechanical Engineering, University of Colorado, Boulder, CO 80309, USA. M. S. Bergin and L. McNair are in the Department of Mechanical Engineering, Carnegie Mellon University, Pittsburgh, PA 15213, USA. S. McBride is in the Department of Engineering and Public Policy, Carnegie Mellon University, Pittsburgh, PA 15213, USA. Y. Yang is in the Department of Civil Engineering, University of Connecticut, Storrs, CT 06269, USA. W. R. Stockwell is at the IFU–Fraunhöfer Institüt, Garmisch-Partenkirchen, Germany. B. Croes is at the California Air Resources Board, Sacramento, CA 95814, USA.

*To whom correspondence should be addressed.
†Present address: National Renewable Energy Laboratory, Golden, CO 80401, USA.

ent VOCs in 39 cities across the United States. Eighteen reactivity scales were developed from those model calculations. The scales differ in the assumptions about the levels of NO_x and the measure of ozone impact (such as impact on the peak ozone versus integrated impact over time). One scale, the maximum incremental reactivity (MIR) scale, has been chosen for regulatory application in California. MIRs for individual VOCs are calculated in 10-hour box model simulations and are defined as the maximum sensitivity of the peak ozone concentration ($[O_3]_p$) to a small increase in the initial conditions and emissions of the VOC (E_i). The MIRs are found for the input ratio of VOCs to NO_x that leads to the maximum sensitivity to VOCs:

$$MIR_i = \max\left(\frac{\partial[O_3]_p}{\partial E_i}\right) \text{ for all VOC/NO}_x \quad (1)$$

Examples of MIRs are given in Table 1, which shows both their averages and standard deviations across 39 sets of simulation conditions representing different cities. Typically, MIRs are observed at relatively low VOC/NO_x ratios (about 4 to 6 ppm C:1 ppm NO_x), as might be expected in dense source regions. This indicates that the MIR scale will be more applicable to urban core conditions, where VOC control is most effective, than to rural conditions where ratios are usually higher (and NO_x controls are more effective). Thus, the use of the MIR scale is meant to complement, not replace, NO_x controls. To determine the ozone formed per unit mass of emissions from a specific source [that is, the net reactivity (NR_j) for source j], the MIR of each compound is multiplied by the mass fraction of the compound in the emissions (f_{ji}), and the weighted emissions fractions are then summed:

$$NR_j = \sum_{i=1}^{n} f_{ji} MIR_i \quad (2)$$

For application in California, the MIR scale is used to quantify the reactivity of the exhaust emissions from alternatively fueled vehicles, scaled to the reactivity of exhaust emissions from a vehicle using standard gasoline (NR_j). The ratio of the reactivity of the alternative fuel to that of standard gasoline is called the reactivity adjustment factor (RAF) and is used to modify the allowable mass emissions rate from alternatively fueled vehicles:

$$RAF_j = \frac{\sum_{i=1}^{n} f_{ji} MIR_i}{\sum_{i=1}^{n} f_{bi} MIR_i} = \frac{NR_j}{NR_b} \quad (3)$$

RAFs calculated for exhaust emissions for five fuels, (i) standard gasoline (as the base, b), (ii) phase II reformulated gasoline, (iii) 85% methanol–15% gasoline blend (M85), (iv) liquefied petroleum gas (LPG), and (v) compressed natural gas (CNG), are given in Table 2. For example, the RAF for M85-fueled vehicle emissions indicates that on a mass-weighted basis, those emissions should produce about 37% as much ozone as the same mass emitted from a gasoline-fueled vehicle under urban conditions. Under the California regulations, M85-fueled vehicles could then emit 2.7 times as much mass, leading to an equivalent ozone impact.

One of the most widely noted criticisms of using VOC reactivity for developing control strategies is the possible large variation of individual compound reactivities between locations as a result of both the change in atmospheric conditions as well as the change in the relative abundance of VOC and NO_x (7). Although such variation might appear to complicate the use of a single reactivity weighting scheme across regions, box and airshed modeling results indicate that the variation in relative reactivities is not so severe. In the MIR scale, compound reactivities are an average of those quantified for conditions in 39 cities. The absolute MIRs of individual compounds vary significantly between locations (9), as demonstrated by the SDs of the reactivities across the cities (Table 1). On average, the SDs are about 22% of the mean reactivity values. However, the intercity variation is much lower for RAFs or when the MIR is normalized. Normalized MIRs are calculated by dividing each specie's city-specific MIR by the geometric mean reactivity of all the species reactivities for that city, and multiplying by the geometric mean reactivity of the 39-city average MIRs. As shown in Table 1, the SDs of the normalized reactivities are significantly less. The NRs of exhaust from vehicles operated on six fuels (6) are shown by box plots in Fig. 1A, indicating the variation in the calculated MIR values across the 39 cities. The variation in absolute ozone-forming potentials across cities is substantial. However, when the reactivities of exhaust from alternatively fueled vehicles are normalized by the reactivity of standard gasoline exhaust (that is, the RAF is calculated), variation among cities is sharply diminished (Fig. 1B). The important point here is not the absolute magnitude of the RAF, which will change as the composition is modified by control technology changes, but that the RAF is relatively invariant across the cities. This variation does not include the uncertainty due to the emissions composition, which is presented below.

Another issue of concern associated with environmental variability is that the relative abundance of VOCs and NO_x can differ markedly between locations, but the MIR scale was developed for conditions of relatively high NO_x that are most typical of urban areas. In California, the MIR scale was chosen intentionally to complement NO_x control. At lower NO_x levels, it is expected that the absolute level of ozone production of any individual VOC will be less than under MIR conditions (the level of NO_x, not VOCs, becomes the limiting factor). This effect is investigated in two

Table 1. Examples of MIRs and variations between locations (mean and SD).

Compound	Mean reactivities across cities (nonnormalized/normalized)	SD (nonnormalized/normalized)
HCHO	7.2/7.1	1.0/0.58
Methanol	0.56/0.55	0.11/0.064
Ethane	0.25/0.24	0.070/0.045
Toluene	2.7/2.7	0.52/0.28
Pentene	6.2/6.1	1.2/0.64

Table 2. Exhaust reactivity adjustment factors (6, 14).

Fuel	MIR-RAF	MOIR-RAF
Base	1.00	1.00
Phase II	0.94	0.97
M85	0.37	0.38
LPG	0.47	0.57
CNG	0.43	0.49

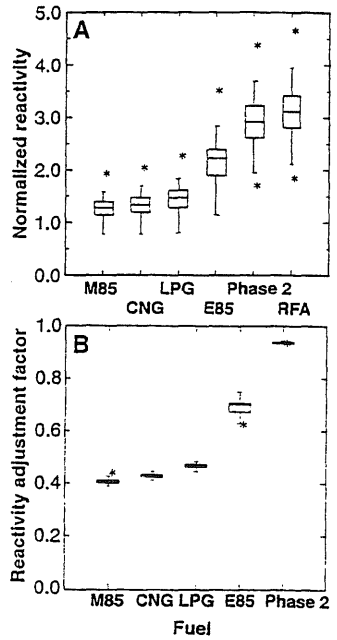

Fig. 1. Boxplots of the calculated (**A**) net reactivities (NRs) and (**B**) normalized reactivities (RAFs) across cities. The median is represented by a horizontal line. The edges of the boxes represent rough quantiles in the data. Horizontal lines represent the extremes of the data, and outliers are represented by stars.

ways. First, Carter developed an alternative scale, the maximum ozone incremental reactivity (MOIR) scale, which is similar to the MIR scale, except that the sensitivity is evaluated for initial VOC/NO_x conditions leading to the maximum ozone level (instead of conditions for which the sensitivity is greatest):

$$\mathrm{MOIR}_i = \frac{\partial \max([O_3]_p)}{\partial E_i} \quad (4)$$

Conditions leading to the MOIR are calculated to occur at higher VOC/NO_x levels (about 7 to 8:1) than those associated with the MIR scale. MOIR-based RAFs [Table 2 and (*6*, *14*)] are similar to those calculated with MIR values. Carter (*9*) also examined how using other measures of ozone sensitivity (such as the effect on time-integrated concentrations instead of peak concentrations) would affect RAF values, and found relatively little variation. In a second test of how changes in the relative abundance of VOC and NO_x affect reactivity weighting, two emissions inventories, differing in their VOC/NO_x ratios by about a factor of 2, were used in an airshed modeling study to test the efficacy of reactivity weighting of exhaust emissions (*15*). Reactivity weighting led to nearly equivalent ozone impacts when either inventory was used. That study also considered two ozone episodes with significantly different meteorological conditions. Reactivity weighting of emissions, again, led to similar ozone impacts for both episodes (within an uncertainty of about 10%).

A second concern frequently raised with the use of reactivity weighting is the effects of uncertainties and level of detail in the physical and chemical representation used for quantifying reactivity. A specific concern regarding the physical level of detail stems from the MIR scale being developed with the use of a zero-dimensional model. Such simplified models lack realistic treatment of pollutant transport and mixing, which could lead to poor characterization of reaction rates and consequently of reactivities. Moreover, MIRs have been developed on the basis of 10-hour simulations, whereas some organic compounds may remain in an urban airshed for 2 to 3 days. To investigate these issues, we applied an advanced, 3D photochemical model with the SAPRC90 mechanism to the Los Angeles basin (*16*, *17*). Detailed source emissions and meteorology for a 3-day period (27 to 29 August 1987) were used (*21*). This is one of the periods for which the model has been extensively evaluated. Ozone impacts, on a per carbon basis, of an incremental increase in the emissions of 28 VOCs were calculated relative to a base mixture representing gasoline vehicle exhaust. Use of the airshed model allows quantification of the impact of emission changes and reactivity on population-weighted ozone levels and spatial ozone impacts, as well as peak ozone levels (*22*).

Correspondence between two of the airshed metrics and the box model MIR (*9*) scales is shown in Fig. 2. The airshed model–derived spatial and population density–weighted results behave similarly to MIRs. The greatest differences are found for formaldehyde and other compounds whose reactivities are highly dependent on photolytic reactions. This is explained by the use of a reduced photolysis rate in the airshed modeling to account for the observed cloud cover. The box model used clear sky conditions. The reductions in the reactivities are consistent with the sensitivity to the rate constants for the photolytic reactions (*10*). In general, airshed model results for Los Angeles agree well with MIRs and further show that individual organics have very different ozone impacts. Similar studies should be considered for other regions (such as the Ozone Transport Region of the northeastern United States).

A third concern often raised is that the quantification of compound reactivities is limited by uncertainties in our knowledge of atmospheric chemistry and its representation through chemical mechanisms. Measurement errors in laboratory kinetic and product studies contribute to uncertainty in the chemical mechanisms used to calculate incremental reactivities. Moreover, the reactions of many of the organic compounds emitted into urban atmospheres have never been studied in controlled experiments. Their representation in chemical mechanisms is based on analogy to compounds of similar structure, creating added uncertainty. At issue is whether the uncertainties in the chemistry significantly impact the calculation of the reactivities for organic compounds. We used both the box model (*10*, *12*) and airshed model (*17*) to explore the extent to which uncertainties in chemical rate parameters impact the calculated reactivities.

Uncertainties in calculated reactivities are estimated from box model simulations through use of Monte Carlo analysis with Latin hypercube sampling. To reduce computational requirements, the simulations are conducted for a single set of trajectory conditions, which was designed by Carter (*9*) to give results close to the average MIRs from the 39 trajectories nationwide. Uncertainty estimates were compiled (*23*) for all of the rate parameters of the SAPRC90 mechanism, largely from concurrent reviews of kinetic data (*24*, *25*). Rate parameters are treated as lognormally distributed, independent random variables. Results are shown in Fig. 3.

Uncertainty estimates (1σ) range from 30 to 50% of the mean MIR values, for most compounds. The estimated uncertainty in the predicted peak ozone concentration for the average MIR simulation conditions was about 30%, relative to a mean prediction of ~0.15 ppm. For predicted O_3 and MIRs, the most influential uncertainties are those in rate parameters that control the availability of NO_x and radicals (*12*). For MIRs, uncertainties in the rate parameters of primary oxidation reactions, or reactions of stable intermediates, are also influential. Uncertainties in many rate parameters have similar effects on the reactivities of various compounds, so the resulting MIRs are strongly correlated. For example, an increase in the photolysis rate for NO_2 increases the reactivity of most species by about the same proportion. Thus, the relative reactivity of one species compared to

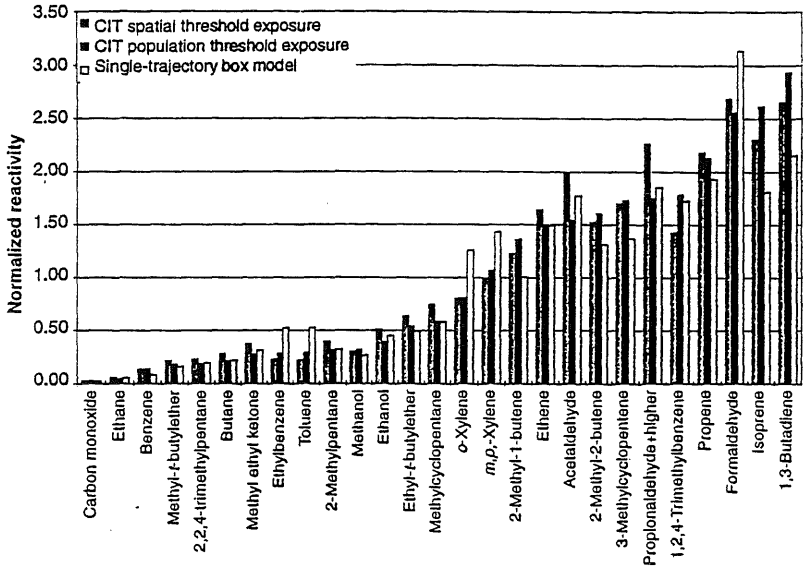

Fig. 2. Results and comparison of reactivity metrics for reactivity quantification.

another is not affected as much as the absolute MIRs by uncertainties in rate constants. After the most influential rate parameters are identified by Monte Carlo simulations, their values are varied, one at a time, in 3D airshed model simulations (*17*). This analysis confirmed the low sensitivity of relative reactivities to uncertainties in rate constants. The implication of this result is clearly shown by the following analysis of uncertainties in RAFs.

For exhaust emissions from selected fuel-vehicle combinations tested in the Auto/Oil Air Quality Improvement Research Program (AQIRP) (*26*), we calculated RAFs and associated uncertainties (*10*). Monte Carlo simulations with Latin hypercube sampling are used for this analysis, treating both chemical rate parameters and exhaust compositions as random variables. Uncertainties in the exhaust compositions were estimated from the variance and covariance of emissions of each compound across the vehicles that the AQIRP study tested on a given fuel. Emissions of each compound were then treated as correlated, normally distributed random variables. No attempt was made for this analysis to estimate uncertainties associated with whether the test vehicles were representative of vehicles on the road.

Results of RAF uncertainty calculations are shown in Fig. 4 for exhaust emissions from prototype flexible- and variable-fueled vehicles operated on M85 compared to exhaust emissions from passenger cars operated on industry average gasoline. The mass-based RAF for the AQIRP M85 exhaust composition has a mean value of 0.49 with an uncertainty of 17% (1σ relative to the mean). Compared to the degree of uncertainty in the MIRs for HCHO (32%) and MeOH (48%), the RAF uncertainty is significantly reduced as a result of interspecies correlation. This reduction in uncertainty is even more pronounced for RAFs of fuels such as reformulated gasoline that have exhaust compositions closer to that associated with conventional gasoline.

Further treatment of uncertainties should account for product yields and correlation among some rate parameters for the chemical mechanism used to calculate MIRs. Preliminary results have indicated that uncertainties in product yields also have a small effect on relative reactivities (*27*), but this question is being examined further with the airshed model for specific application to alternative fuels (*19*).

Uncertainties in emissions composition have been cited as confounding factors in the use of reactivity weighting for ozone control. We have previously addressed this issue through the combined reactivity-composition uncertainty estimate for M85 fuel discussed above. To examine the role of variation in emissions composition across fuels, variances of RAFs were calculated with the use of exhaust composition data (*6*) for four alternative fuels and standard gasoline. The data consisted of mass fractions of VOC exhaust from transitional low-emission vehicles (TLEVs) for each exhaust type and the SD associated with that fraction. Variances of the RAFs for each fuel are calculated by the Delta Method (*28*). Each fuel's RAF was calculated as the ratio of two normally distributed random variables, the MIR of the alternative fuel divided by the MIR of standard gasoline. MIR values were calculated on the basis of the average MIR scale. The results are shown in Fig. 5, which displays the 5th, mean, and 95th percentiles of each fuel's RAF value. Comparison of Fig. 5, which has only one degree of uncertainty, with Fig. 4 suggests that much of the uncertainty results from the composition. Exhaust emission compositions are derived from a small number of tests on a small number of vehicles, particularly for the alternatively fueled vehicles (*6*). Further, there is relatively little information on the effect of deterioration on the species emitted. More tests across a wide range of vehicles are required to better characterize the impact of uncertainty in fuel composition on calculation of RAFs.

Source emissions are usually not as well characterized as those from automobiles. Although lack of detailed knowledge on the emissions compositions of different sources, automotive and others, does add uncertainty to control strategy design, regulations that explicitly credit industry for using less-reactive compounds could add a valuable economic incentive to more completely characterize source emissions, particularly for the largest emitters. This has already been the case for automotive emissions. This information would be useful for better identifying the efficacy of controls and for other studies that depend on an accurate knowledge of emissions compositions (such as a basis for receptor modeling studies to help determine emissions inventories).

Although the results presented above suggest that relative reactivity scales are robust with respect to uncertainties in chemistry, environmental conditions, and emissions, and hence support accounting for VOC reactivity in developing strategies to control ozone, the economic consequences of doing so also warrant consideration. A mixed-integer programming approach to optimization of ozone control strategies across cost, tons of VOC emissions, and reactivities of VOCs indicates that there is potential for cost savings with the adoption of reactivity-based regulations (*5*). Using emission compositions and costs for the Los Angeles air basin, economically optimized VOC-based control strategies are determined on the basis of two approaches, one neglecting and one accounting for the reactivity differences of the emissions. In the first case, an optimized mass-based strategy is simulated such that the total VOC mass reductions are maximized at each cost level. Second, a reactivity-based scheme is assumed in which the reactivity of each source's emissions is calculated and the ozone reductions are maximized at each cost level. Results from the two approaches

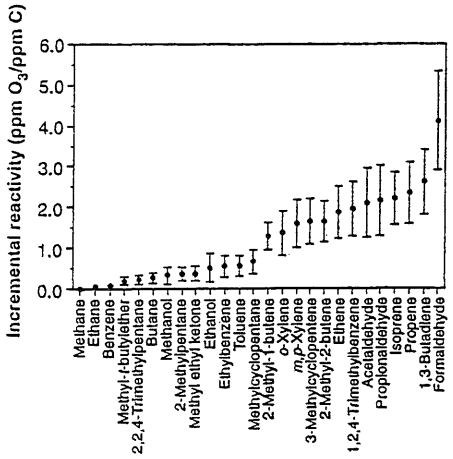

Fig. 3. Mean values and 1σ uncertainties of MIRs for selected organic compounds, as calculated from uncertainties in kinetic parameters.

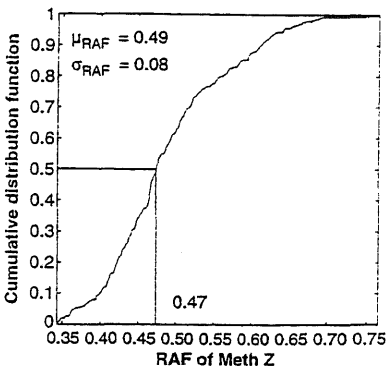

Fig. 4. Cumulative distribution function of the uncertainty in the RAF of prototype flexible-fueled M85 vehicles.

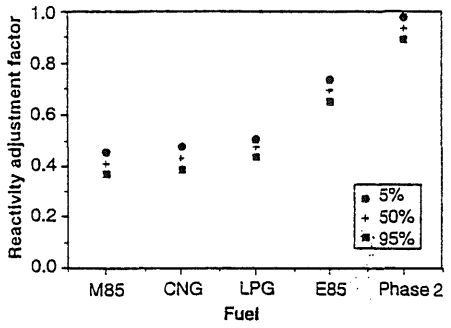

Fig. 5. Variation in RAFs due to exhaust composition for four alternative fuels (5th, 50th, 95th percentiles shown).

are compared in Fig. 6 for ozone reduction at a given expenditure level.

Figure 6 depicts the results for the optimization model across different levels of total cost. Optimal reductions for mass- and reactivity-based systems are scaled according to source reactivities. From this graph, it is clear that on an annual basis the reactivity-based system achieves the same ozone reductions at a lower total cost than the mass-based system. For example, at control costs of $15 million per year, the ozone reduction achieved with a reactivity-based scheme is about two times that achieved under the mass-based scheme. As control costs escalate, the two methods converge, because a greater proportion of all sources will be controlled in both cases. Up to control levels of about 25% of the total controllable emissions, the reactivity-based scheme gives greater ozone reductions for the same cost. The graph does not converge at zero because of the inclusion of a category with a negative cost-effectiveness. A negative value of cost-effectiveness is estimated in this case because of anticipated savings from the reformulation of a particular coatings process. Further economic benefits beyond those found below can accrue over time as control technologies are developed specifically for reactivity adjustment. Cities that can best utilize such strategies include those areas where ozone formation is VOC-limited, as is suggested for the coastal California cities, Phoenix and Chicago. Another application of reactivity quantification to lower total control costs is as a basis for VOC emissions trading between sources. Without a sound foundation for quantifying the impact of one source's emissions compared to another, it is difficult to ensure that a VOC trade would not adversely impact air quality. This issue was of primary concern in the RECLAIM trading program in southern California where VOCs are not included in the program (*2*).

The use of reactivity adjustments in control strategy design allows a new avenue for air quality improvement. Reactivity-based control strategies include economic incentives which would ensure that reformulation would lower reactive VOCs and improve air quality. Present mass-based regulations credit industry for reducing tons of all VOCs, rather than for reducing the most reactive compounds. A hidden problem in reformulation regulations, familiar to the surface coating and consumer products industries, is that while the reformulated product may emit a smaller mass of VOCs, the composition of the emissions may lead to greater ozone formation. Thus, the cost of reformulating may not necessarily yield improved air quality. By creating a regulatory structure that would promote selective control of VOCs with higher reactivity, reformulation and other control technologies can be evaluated and developed with respect to trade-offs between reactivity and mass of emissions, leading to pollution prevention through a more cost-effective process and product design.

Although there are still some uncertainties, this analysis suggests that both scientific understanding and potential economic benefits support the consideration of VOC reactivity weighting in ozone control strategies. Many of the uncertainties and criticisms previously raised about quantification of reactivities are found to be less pronounced when relative reactivity is used, as would be the case in regulatory practice. There are significant differences between individual compound impacts even when the uncertainties are considered. Additional benefits of accounting for reactivity include increased incentives for industry to fully characterize its emissions and for pollution prevention through product reformulation.

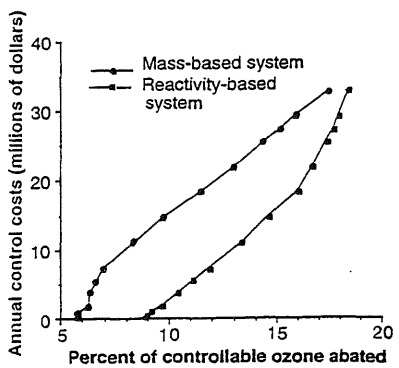

Fig. 6. Percent of controllable ozone abated at different levels of total control cost.

REFERENCES AND NOTES

1. National Research Council, *Rethinking the Ozone Problem in Urban and Regional Air Pollution* (National Academy Press, Washington, DC, 1991).
2. "1994 Air quality management plan" (South Coast Air Quality Management District, Diamond Bar, CA, 1994).
3. K. Chess and A. G. Russell, unpublished results.
4. "Regional oxidant modeling of northeastern transport: ROMNET" (U.S. Environmental Protection Agency, Research Triangle Park, NC, 1992).
5. S. McBride and A. G. Russell, in preparation.
6. "Preliminary reactivity adjustment factors" (State of California Environmental Protection Agency, 1995); "Proposed reactivity adjustment factors for transitional low emission vehicles—technical support document" (California Air Resources Board, Sacramento, CA, September 1991); "Public hearing to consider amendments to certification requirements and procedures for low-emission passenger cars, light duty trucks and medium duty vehicles—supporting documents and information" (California Air Resources Board, Sacramento, CA, March 1993). Data are from CARB testing, the Auto/Oil Air Quality Improvement Research Program, and Chevron Research and Technology Company. The statistical model accounts both for variation among vehicles and repeated tests on the same vehicles, although most of the variation is due to differences in vehicles. For the base fuel, there were 36 tests performed on 9 vehicles; for phase II, 41/12 (tests/vehicles); M85, 14/6; LPG, 23/7; E85, 8/2; and CNG, 29/7.
7. B. Croes, J. Holmes, A. Lloyd, *J. Air Waste Manage. Assoc.* **42**, 657 (1992); *Western States Petroleum Association versus Air Resources Board, Los Angeles County Superior Court No. BC067159* (filed 26 October 1992).
8. W. P. L. Carter and R. Atkinson, *Environ. Sci. Technol.* **23**, 864 (1989).
9. W. P. L. Carter, *J. Air Waste Manage. Assoc.* **44**, 881 (1994).
10. Y. Yang *et al.*, "Quantification of organic compound reactivities and effects of uncertainties in rate parameters," report prepared for the Auto/Oil Air Quality Improvement Research Program (available from the Coordinating Research Council, Atlanta, GA, Contract No. AQIRP-19-92, August 1994). This report combines the information presented in (*11*), (*12*), (*16*), and (*17*).
11. M. Bergin *et al.*, "Effects of uncertainty in SAPRC rate constants and product yields on reactivity adjustment factors for alternatively fueled vehicle emissions," draft report to the National Renewable Energy Laboratory, Golden, CO (1995). Also see (*10*).
12. Y. Yang, J. Milford, W. Stockwell, *Environ. Sci. Technol.* **29**, 1336 (1995). Also see (*10*).
13. F. M. Bowman and J. H. Seinfeld, *J. Geophys. Res.* **99(D3)**, 5309 (1994); R. G. Derwent and M. E. Jenkins, *Atmos. Environ.* **25A**, 1661 (1991).
14. L. A. McNair, A. G. Russell, M. T. Odman, *J. Air Waste Manage. Assoc.* **42**, 174 (1992).
15. ———, B. E. Croes, L. Kao, *ibid.* **44**, 900 (1994).
16. M. S. Bergin *et al.*, *Environ. Sci. Technol.*, in press. Also see (*10*).
17. M. S. Bergin, thesis, Carnegie Mellon University, Pittsburgh, PA (1994). Also see (*10*).
18. W. P. L. Carter, *Atmos. Environ.* **24A(3)**, 481 (1990).
19. M. S. Bergin and A. G. Russell, in preparation. See also (*11*).
20. "Proposed regulations for low-emission vehicles and clean fuels" (California Air Resources Board, Sacramento, CA, 1990).
21. R. Harley *et al.*, *Environ. Sci. Technol.* **27**, 378 (1993).
22. Spatial and population-weighted exposures are calculated with the use of cutoff thresholds of 0.09 and 0.12 ppm, the California and national standards. For spatial exposure, the total time the ozone concentration exceeds the threshold is multiplied by the concentration and spatial area and is summed over all modeling cells and hours. The two values (one for each threshold) are then averaged. Population-weighted exposure is similarly calculated, replacing the spatial area with the local population density.
23. W. Stockwell, Y. Yang, J. Milford, *A Compilation of Estimated Uncertainty Factors for Rate Constants is W. P. L. Carter's Detailed Mechanism*, report prepared for the Auto/Oil Air Quality Improvement Research Program (available from the Coordinating Research Council, Atlanta, GA, 1994).
24. W. B. DeMore *et al.*, *Chemical Kinetics for Use in Stratospheric Modeling, Evaluation Number 9* (NASA, Jet Propulsion Laboratory, California Institute of Technology, Pasadena, CA, 1990).
25. R. Atkinson *et al.*, *J. Phys. Chem. Ref. Data* **13**, 1259 (1989).
26. V. R. Burns *et al.*, *Description of the Auto/Oil Air Quality Improvement Research Program*, SAE technical paper no. 912320, Society of Automotive Engineers, Warren, PA (1991).
27. Y. Yang and J. Milford, in preparation.
28. Y. M. M. Bishop, S. E. Fienberg, P. W. Holland, *Discrete Multivariate Analysis: Theory and Practice* (MIT Press, Cambridge, MA, 1975).

29. We thank W. P. L. Carter and S. Johnson for assistance in providing key information, and U. Diwekar and H. Dowlatabadi for helpful discussions. Financial support for this project was provided, in part, by the California Air Resources Board, the Auto/Oil Air Quality Improvement Research Program, the National Science Foundation, the U.S. Department of Energy National Renewable Energy Laboratory, and the National Aerosol Association. Computational facilities were made available in part by support from the National Science Foundation, the Pittsburgh Supercomputer Center, and Digital Equipment Corporation.

Appendix B. Uncertain Product Yields and Associated Constraints

Reactants			Products of uncertain yields				Constraints	Dependent yields
AFG1	+ *hν*	→	HO2	, HCOCOO2	, RCO3			RCO3=HCOCOO2
AFG2	+ *hν*	→	HO2	, CCOO2	, RCO3			RCO3=CCOO2
CCHO	+ HO	→	CCOO2	, RCO3			CCOO2≤1	RCO3=CCOO2
RCHO	+ HO	→	C2COO2	, RCO3			C2COO2≤1	RCO3=C2COO2
ACET	+ HO	→	MGLY	, HCHO			3MGLY+HCHO≤2.6	
MEK	+ HO	→	HCHO	, CCHO	, R2O2	, RO2	2CCHO+HCHO≤1.5	RO2=R2O2
MEK	+ *hν*	→	CCOO2	, CCHO	, RO2R	, RCO3	CCHO≤1	RCO3=CCOO2, RO2=RO2R
			RO2					
MGLY	+ *hν*	→	HO2	, CCOO2	, RCO3			RCO3=CCOO2
C2COO2	+ HO2	→	-OOH	, CCHO				
ETHE	+ HO	→	HCHO	, RO2R	, RO2		HCHO≤1.56	RO2=RO2R
ETHE	+ O3	→	HCHO	, HO2				
ETHANE	+ HO	→	CCHO				CCHO≤1, RO2R=1	RO2=RO2R
BUTANE	+ HO	→	R2O2	, CCHO	, MEK	, RO2		RO2=RO2N+RO2R+R2O2
2MEC5	+ HO	→	R2O2	, RCHO	, MEK	, RO2		RO2=RO2XN+RO2N
								+RO2XN+R2O2
BENZEN	+ HO	→	AFG1	, RO2R	, RO2		RO2R≤0.764	RO2=RO2R
TOLUEN	+ HO	→	AFG2	, RO2R	, RO2		RO2R≤0.74	RO2=RO2R
C2BENZ	+ HO	→	AFG2	, RO2R	, RO2		RO2R≤0.74	RO2=RO2R
OXYLEN	+ HO	→	MGLY	, AFG2	, RO2R	, RO2	RO2R≤0.82	RO2=RO2R
MPXYLE	+ HO	→	MGLY	, AFG2	, RO2R	, RO2	RO2R≤0.82	RO2=RO2R
124TMB	+ HO	→	AFG2	, RO2R	, MGLY	, RO2	RO2R≤0.82	RO2=RO2R
MEOH	+ HO	→	HCHO				HCHO≤1	
ETOH	+ HO	→	CCHO				CCHO≤0.922	RO2=RO2R
MTBE	+ HO	→	HCHO	, MEK	, R2O2	, RO2		RO2=RO2N+R2OR+R2O2
ETBE	+ HO	→	HCHO	, MEK	, R2O2	, RO2		RO2=RO2N+R2OR+R2O2
224TMC5	+ HO	→	R2O2	, RCHO	, MEK	, RO2		RO2=RO2N+R2OR+R2O2
MECYC5	+ HO	→	HCHO	, RCHO	, R2O2	, MEK		RO2=RO2N+R2OR+R2O2
		→	RO2					
PROPEN	+ HO	→	RO2R	, CCHO	, HCHO	, RO2	HCHO+2CCHO≤3	RO2=RO2R
PROPEN	+ O3	→	HCHO	, CCHO		,		RO2=RO2R
13BUTD	+ HO	→	RO2R	, HCHO	, RCHO	, RO2	HCHO+3RCHO≤4	RO2=RO2R
13BUTD	+ O3	→	HCHO	, RCHO				RO2=RO2R
2M1BUT	+ HO	→	RO2R	, HCHO	, MEK	, RO2	HCHO+4MEK≤5	RO2=RO2R
2M1BUT	+ O3	→	HCHO	, MEK				RO2=RO2R
2M2BUT	+ HO	→	RO2R	, ACET	, CCHO	, RO2	2CCHO+3ACET≤5	RO2=RO2R
2M2BUT	+ O3	→	CCHO	, MEK	, ACET			RO2=RO2R
3MCYCPN	+ HO	→	CCHO	, RCHO	, RO2R		RO2R+RO2N=1	RO2=RO2R
3MCYCPN	+ O3	→	RO2R	, CCHO	, RCHO	, MEK		RO2=RO2R
			RO2					
AAR1	+ HO	→	HCHO	, CCHO	, RCHO	, R2O2	RO2R+RO2XN+RO2N=1	RO2=RO2R+RO2N
			RO2					
AAR2	+ HO	→	R2O2	, CCHO	, RCHO	, MEK	RO2R+RO2XN+RO2N=1	RO2=RO2R+RO2N
			RO2					+RO2XN+R2O2
AAR3	+ HO	→	MGLY	, AFG2	, MEK		RO2N+RO2R=1	RO2=RO2R+RO2N+R2O2
OLE1	+ HO	→	RO2R	, HCHO	, CCHO	, RCHO		RO2=RO2R+RO2N
			RO2					
OLE1	+ O3	→	HCHO	, CCHO	, RCHO			
OLE2	+ HO	→	RO2R	, HCHO	, CCHO	, RCHO		RO2=RO2R+RO2N
			RO2					
OLE2	+ O3	→	HCHO	, CCHO	, RCHO	, MEK		RO2=RO2R+R2O2

Appendix C. The SAPRC90 Chemical Mechanism (Carter, 1990a)

C1. List of Species Names

C2. List of Mechanism Reactions Used in Box and CIT Model Study (reported at a fixed temperature of 298°K)

Table C1. List of Species Names

No.	Name	Description
Active inorganic species*		
1	O3	Ozone
2	NO	Nitric oxide
3	NO2	Nitrogen dioxide
4	NO3	NO_3 radicals
5	N2O5	N_2O_5
6	HNO3	Nitric acid
7	HONO	Nitrous acid
8	HNO4	Peroxynitric acid
9	HO2.	HO_2 radicals
12	CO	Carbon monoxide
10	HO2H	Hydrogen peroxide
11	SO2	Sulphur dioxide
Active organic product species		
13	HCHO	Formaldehyde
14	CCHO	Acetaldehyde
15	PAN	Peroxy acetyl nitrate
16	RCHO	Propionaldehyde and lumped higher aldehydes
17	PPN	Peroxy propionyl nitrate and higher PAN analogues
18	ACET	Acetone
19	MEK	Methylethyl ketone and lumped higher ketones
20	RNO3	Lumped organic nitrates
21	GLY	Glyoxal
22	GPAN	PAN analogue formed from glyoxal
23	MGLY	Methyl glyoxal
24	PHEN	Phenol
25	CRES	Cresols and other alkyl phenols
26	BALD	Benzaldehyde and other aromatic aldehydes
27	PBZN	Peroxy benzoyl nitrate
28	NPHE	Nitrophenols and other aromatic nitro-compounds
29	AFG1	Unknown aromatic fragmentation product #1. (Formed from benzene, tetralin. and naphthalenes.)
30	AFG2	Unknown aromatic fragmentation product #2. (Formed from aromatics containing alkyl groups.)
31	-OOH	Chemical operator used to represent reactions at hydroperoxy groups
Active primary emitted species		
32	ETHE	Ethene
33+	AARn	*n*'th lumped group used to represent lumped alkanes and/or aromatics. (In general, there will be more than one such species.)
34+	OLEn	*n*'th lumped group used to represent lumped higher alkenes. (In general, there will be more than one such species.)
Active total peroxy radical species		
35	RO2.	Total alkyl peroxy radicals
36	RCO3.	Total peroxyacyl radicals
Product only species		
36	CO2	Carbon dioxide
37	H2SO4	Sulphuric acid
38	H2	Hydrogen
39	-C	"Lost carbon." Used to account for carbon balance.
40	-N	"Lost nitrogen." Used to account for nitrogen balance. (Primarily represents C_1–C_3 organic nitrates and dinitrophenols, whose reactions are neglected.)

Table C1 (continued). List of Species Names

No.	Name	Description
Steady state† inorganic species		
41	HO.	Hydroxyl radicals
42	O	Ground state oxygen atoms
43	O*1D2	Excited oxygen atoms
Steady state organic radical species		
44	HOCOO.	Intermediate formed in the $HCHO+HO_2$ reaction
45	CCO–O2.	Peroxy acetyl radicals
46	C2CO–O2.	Higher peroxyacyl radicals
47	BZ–CO–O2.	Peroxy benzoyl radicals
48	HCOCO–O2.	Peroxyacyl radical formed from glyoxal
49	BZ–O.	Phenoxy radicals
50	BZ(NO2)–O.	Phenoxy–type radicals containing nitro-groups
Steady state chemical "operators"		
51	O3OL–SB	Chemical operator used to account for the oxidation of SO_2 by ozone–alkene reaction intermediates (This is a product–only species if reactions of SO_2 are removed from the mechanism.)
52	RO2–R.	Chemical operator used to represent NO to NO_2 Conversion with generation of HO_2 radicals
53	RO2–X.	Chemical operator used to represent NO consumption and alkyl nitrate formation
54	RO2–NP.	Chemical operator used to represent NO consumption and nitrophenol formation
55	RO2–XN.	Chemical operator used to represent NO sink reactions
56	R2O2.	Chemical operator used to represent extra NO to NO_2 conversions
Constant species		
57	O2	Oxygen
58	M	Air
59	HV	Light factor (1.0 = normal intensity)
60	H2O	Water

*"Active" species are those which undergo chemical reaction and for which the steady state approximation is not applied.

†"Steady state" species are those where the steady state approximation can be employed.

Table C2. SAPRC Mechanism (Carter, 1990a) Used in Box and CIT Model Study

	Reaction	k(298) ppm min^{-1}	sigma k(298) ppm min^{-1}
1	NO2 ---> 1.000 NO + 1.000 O	--------photolytic--------	
2	O + O2 + M ---> 1.000 O3 + 1.000 M	2.22E-05	1.85E-06
3	O + NO2 ---> 1.000 NO + 1.000 O2	1.44E+04	2.02E+03
4	O + NO2 ---> 1.000 NO3 + 1.000 M	2.33E+03	2.12E+02
5	O3 + NO ---> 1.000 NO2 + 1.000 O2	2.69E+01	4.95E+00
6	O3 + NO2 ---> 1.000 O2 + 1.000 NO3	4.70E-02	6.61E-03
7	NO + NO3 ---> 2.000 NO2	4.16E+04	1.17E+04
8	NO + NO + O2 ---> 2.000 NO2	7.07E-10	1.65E-10
9	NO2 + NO3 ---> 1.000 N2O5	1.87E+03	9.08E+02
10	N2O5 ---> 1.000 NO2 + 1.000 NO3	3.26E+00	2.09E+00
11	N2O5 + H2O ---> 2.000 HNO3	1.48E-06	3.00E-07
12	NO2 + NO3 ---> 1.000 NO + 1.000 NO2 + 1.000 O2	6.00E-01	2.50E-01
13	NO3 ---> 1.000 NO + 1.000 O2	--------photolytic--------	
14	NO3 ---> 1.000 NO2 + 1.000 O	--------photolytic--------	
15	O3 ---> 1.000 O + 1.000 O2	--------photolytic--------	
16	O3 ---> 1.000 O1D2 + 1.000 O2	--------photolytic--------	
17	O1D2 + H2O ---> 2.000 HO	3.25E+05	7.59E+04
18	O1D2 + M ---> 1.000 O + 1.000 M	4.33E+04	1.01E+04
19	HO + NO ---> 1.000 HONO	7.20E+03	2.25E+03
20	HONO ---> 1.000 HO + 1.000 NO	--------photolytic--------	
21	HO + NO2 ---> 1.000 HNO3	1.70E+04	4.65E+03
22	HO + HNO3 ---> 1.000 H2O + 1.000 NO3	1.55E+02	4.02E+01
23	HO + CO ---> 1.000 HO2 + 1.000 CO2	3.55E+02	9.43E+01
24	HO + O3 ---> 1.000 HO2 + 1.000 O2	1.01E+02	3.53E+01
25	HO2 + NO ---> 1.000 HO + 1.000 NO2	1.23E+04	2.87E+03
26	HO2 + NO2 ---> 1.000 HNO4	2.05E+03	2.70E+02
27	HNO4 ---> 1.000 HO2 + 1.000 NO2	5.18E+00	1.24E+01
28	HNO4 + HO ---> 1.000 H2O + 1.000 NO2 + 1.000 O2	6.87E+03	2.87E+03
29	HO2 + O3 ---> 1.000 HO + 2.000 O2	3.03E+00	1.44E+00
30	HO2 + HO2 ---> 1.000 HO2H + 1.000 O2	2.59E+03	9.10E+02
31	HO2 + HO2 + M ---> 1.000 HO2H + 1.000 O2	1.86E-03	6.54E-04
32	HO2 + HO2 + H2O ---> 1.000 HO2H + 1.000 O2 + 1.000 H2O	1.44E-01	5.06E-02
33	HO2 + HO2 + H2O ---> 1.000 HO2H + 1.000 O2 + 1.000 H2O	1.04E-01	3.64E-02
34	NO3 + HO2 ---> 1.000 HNO3 + 1.000 O2	2.59E+03	1.95E+03
35	NO3 + HO2 + M ---> 1.000 HNO3 + 1.000 O2	1.86E-03	1.40E-03
36	NO3 + HO2 + H2O ---> 1.000 HNO3 + 1.000 O2 + 1.000 H2O	1.44E-01	1.08E-01
37	NO3 + HO2 + H2O ---> 1.000 HNO3 + 1.000 O2 + 1.000 H2O	1.04E-01	7.78E-02
38	HO2H ---> 2.000 HO	--------photolytic--------	
39	HO2H + HO ---> 1.000 HO2 + 1.000 H2O	2.49E+03	5.82E+02
40	HO + HO2 ---> 1.000 H2O + 1.000 O2	1.47E+05	3.91E+04
41	RO2 + NO ---> 1.000 NO	1.14E+04	8.56E+03
42	RCO3 + NO ---> 1.000 NO	1.47E+04	1.11E+04
43	RCO3 + NO2 ---> 1.000 NO2	1.07E+04	7.22E+03
44	RO2 + HO2 ---> 1.000 HO2 + 1.000 RO2HO2	7.36E+03	5.53E+03
45	RCO3 + HO2 ---> 1.000 HO2 + 1.000 RO2HO2	7.36E+03	5.53E+03
46	RO2 + RO2 ---> 1.000 RO2RO2	1.48E+00	1.11E+00
47	RO2 + RCO3 ---> 1.000 RO2RO2	1.63E+04	1.22E+04

Table C2 (continued).

	Reaction	k(298) ppm min⁻¹	sigma k(298) ppm min⁻¹
48	RCO3 + RCO3 ---> 1.000 RO2RO2	2.45E+04	1.84E+04
49	RO2R + NO ---> 1.000 NO2 + 1.000 HO2	1.14E+04	8.56E+03
50	RO2R + HO2 ---> 1.000 OOH	7.36E+03	5.53E+03
51	RO2R + RO2 ---> 1.000 RO2 + 0.500 HO2	1.48E+00	1.11E+00
52	RO2R + RCO3 ---> 1.000 RCO3 + 0.500 HO2	1.63E+04	1.22E+04
53	RO2N + NO ---> 1.000 RNO3	1.14E+04	8.56E+03
54	RO2N + HO2 ---> 1.000 OOH + 1.000 MEK + 1.500 C	7.36E+03	5.53E+03
55	RO2N + RO2 ---> 1.000 RO2 + 0.500 HO2 + 1.000 MEK + 1.500 C	1.48E+00	1.11E+00
56	RO2N + RCO3 ---> 1.000 RCO3 + 0.500 HO2 + 1.000 MEK + 1.500 C	1.63E+04	1.22E+04
57	R2O2 + NO ---> 1.000 NO2	1.14E+04	8.56E+03
58	R2O2 + HO2 --->	7.36E+03	5.53E+03
59	R2O2 + RO2 ---> 1.000 RO2	1.48E+00	1.11E+00
60	R2O2 + RCO3 ---> 1.000 RCO3	1.63E+04	1.22E+04
61	RO2XN + NO ---> 1.000 N	1.14E+04	8.56E+03
62	RO2XN + HO2 ---> 1.000 OOH	7.36E+03	5.53E+03
63	RO2XN + RO2 ---> 1.000 RO2 + 0.500 HO2	1.48E+00	1.11E+00
64	RO2XN + RCO3 ---> 1.000 RCO3 + 1.000 HO2	1.63E+04	1.22E+04
65	OOH ---> 1.000 HO2 + 1.000 HO	--------photolytic--------	
66	HO + OOH ---> 1.000 HO	2.68E+03	1.12E+03
67	HO + OOH ---> 1.000 RO2R + 1.000 RO2	5.51E+03	2.30E+03
68	GLY ---> 0.800 HO2 + 0.450 HCHO + 1.550 CO	--------photolytic--------	
69	GLY ---> 0.130 HCHO + 1.870 CO	--------photolytic--------	
70	GLY + HO ---> 0.600 HO2 + 1.200 CO + 0.400 HCOCOO + 0.400 RCO3	1.68E+04	1.26E+04
71	GLY + NO3 ---> 1.000 HNO3 + 0.600 HO2 + 1.200 CO + 0.400 HCOCOO + 0.400 RCO3	4.03E+00	3.03E+00
72	HCOCOO + NO ---> 1.000 NO2 + 1.000 CO2 + 1.000 CO + 1.000 HO2	1.47E+04	1.11E+04
73	HCOCOO + NO2 ---> 1.000 GPAN	1.07E+04	7.22E+03
74	GPAN ---> 1.000 HCOCOO + 1.000 NO2 + 1.000 RCO3	2.99E-02	2.02E-02
75	HCOCOO + HO2 ---> 1.000 OOH + 1.000 CO2 + 1.000 CO	7.36E+03	5.53E+03
76	HCOCOO + RO2 ---> 1.000 RO2 + 0.500 HO2 + 1.000 CO2 + 1.000 CO	1.63E+04	1.22E+04
77	HCOCOO + RCO3 ---> 1.000 RCO3 + 1.000 HO2 + 1.000 CO2 + 1.000 CO	2.45E+04	1.84E+04
78	HO + PHEN ---> 0.150 RO2NP + 0.850 RO2R + 0.200 GLY + 4.700 C + 1.000 RO2	3.89E+04	8.75E+03
79	NO3 + PHEN ---> 1.000 HNO3 + 1.000 BZO	5.32E+03	4.00E+03
80	HO + CRES ---> 0.150 RO2NP + 0.850 RO2R + 0.200 MGLY + 5.500 C + 1.000 RO2	6.21E+04	1.40E+04
81	NO3 + CRES ---> 1.000 HNO3 + 1.000 BZO + 1.000 C	3.10E+04	2.33E+04
82	BALD + HO ---> 1.000 BZCOO2 + 1.000 RCO3	1.91E+04	6.69E+03
83	BALD ---> 7.000 C	--------photolytic--------	
84	BALD + NO3 ---> 1.000 HNO3 + 1.000 BZCOO2	3.70E+00	1.75E+00
85	BZCOO2 + NO ---> 1.000 BZO + 1.000 CO2 + 1.000 NO2 + 1.000 R2O2 + 1.000 RO2	1.47E+04	1.11E+04
86	BZCOO2 + NO2 ---> 1.000 PBZN	1.24E+04	9.33E+03

Table C2 (continued).

	Reaction	k(298) ppm min*	sigma k(298) ppm min*
87	BZCOO2 + HO2 ---> 1.000 OOH + 1.000 CO2 + 1.000 PHEN	7.36E+03	5.53E+03
88	BZCOO2 + RO2 ---> 1.000 RO2 + 0.500 HO2 + 1.000 CO2 + 1.000 PHEN	1.63E+04	1.22E+04
89	BZCOO2 + RCO3 ---> 1.000 RCO3 + 1.000 HO2 + 1.000 CO2 + 1.000 PHEN	2.45E+04	1.84E+04
90	PBZN ---> 1.000 BZCOO2 + 1.000 NO2 + 1.000 RCO3	9.72E-03	6.70E-03
91	BZO + NO2 ---> 1.000 NPHE	5.26E+04	3.95E+04
92	BZO + HO2 ---> 1.000 PHEN	7.36E+03	5.53E+03
93	BZO ---> 1.000 PHEN	6.00E-02	1.35E-02
94	NPHE + NO3 ---> 1.000 HNO3 + 1.000 BZNO2O	5.32E+03	2.52E+03
95	BZNO2O + NO2 ---> 2.000 N + 6.000 C	5.26E+04	3.95E+04
96	BZNO2O + HO2 ---> 1.000 NPHE	7.36E+03	5.53E+03
97	BZNO2O ---> 1.000 NPHE	6.00E-02	4.13E-02
98	HO + AFG1 ---> 1.000 HCOCOO + 1.000 RCO3	1.68E+04	1.26E+04
99	AFG1 ---> 1.000 HO2 + 1.000 HCOCOO + 1.000 RCO3	-------photolytic-------	
100	HO + AFG2 ---> 1.000 C2COO2 + 1.000 RCO3	2.54E+04	1.91E+04
101	AFG2 ---> 1.000 HO2 + 1.000 CO + 1.000 CCOO2 + 1.000 RCO3	-------photolytic-------	
102	RO2NP + NO ---> 1.000 NPHE	1.14E+04	8.56E+03
103	RO2NP + HO2 ---> 1.000 OOH + 6.000 C -	7.36E+03	5.53E+03
104	RO2NP + RO2 ---> 1.000 RO2 + 0.500 HO2 + 6.000 C	1.48E+00	1.11E+00
105	RO2NP + RCO3 ---> 1.000 RCO3 + 1.000 HO2 + 6.000 C	1.63E+04	1.22E+04
106	CCHO + HO ---> 1.000 CCOO2 + 1.000 H2O + 1.000 RCO3	2.33E+04	8.17E+03
107	CCHO ---> 1.000 CO + 1.000 HO2 + 1.000 HCHO + 1.000 RO2R + 1.000 RO2	-------photolytic-------	
108	CCHO + NO3 ---> 1.000 HNO3 + 1.000 CCOO2 + 1.000 RCO3	4.03E+00	1.91E+00
109	RCHO + HO ---> 1.000 C2COO2 + 1.000 RCO3	2.92E+04	1.03E+04
110	RCHO ---> 1.000 CCHO + 1.000 RO2R + 1.000 RO2 + 1.000 CO + 1.000 HO2	7.29E-04	2.50E-04
111	NO3 + RCHO ---> 1.000 HNO3 + 1.000 C2COO2 + 1.000 RCO3	4.03E+00	1.91E+00
112	ACET + HO ---> 0.800 MGLY + 0.800 RO2R + 0.200 R2O2 + 0.200 HCHO + 0.200 CCOO2 + 0.200 RCO3 + 1.000 RO2	-------photolytic-------	
113	ACET ---> 1.000 CCOO2 + 1.000 HCHO + 1.000 RO2R + 1.000 RCO3 + 1.000 RO2	-------photolytic-------	
114	MEK + HO ---> 1.000 H2O + 0.500 CCHO + 0.500 HCHO + 0.500 CCOO2 + 0.500 C2COO2 + 1.000 RCO3 + 1.500 R2O2 + 1.500 RO2	1.71E+03	4.54E+02
115	MEK ---> 1.000 CCOO2 + 1.000 CCHO + 1.000 RO2R + 1.000 RCO3 + 1.000 RO2	-------photolytic-------	
116	RNO3 + HO ---> 1.000 NO2 + 0.155 MEK + 1.050 RCHO + 0.480 CCHO + 0.160 HCHO + 0.110 C + 1.390 R2O2 + 1.390 RO2	3.00E+03	5.51E+02
117	MGLY ---> 1.000 HO2 + 1.000 CO + 1.000 CCOO2 + 1.000 RCO3	-------photolytic-------	
118	MGLY + HO ---> 1.000 CO + 1.000 CCOO2 + 1.000 RCO3	2.54E+04	1.91E+04
119	MGLY + NO3 ---> 1.000 HNO3 + 1.000 CO + 1.000 CCOO2 + 1.000 RCO3	4.03E+00	3.03E+00
120	CCOO2 + NO ---> 1.000 CO2 + 1.000 NO2 + 1.000 HCHO	1.47E+04	1.11E+04

Table C2 (continued).

	Reaction	k(298) ppm min*	sigma k(298) ppm min*
	+ 1.000 RO2R + 1.000 RO2		
121	CCOO2 + NO2 —> 1.000 PAN	1.07E+04	7.22E+03
122	CCOO2 + HO2 —> 1.000 OOH + 1.000 CO2 + 1.000 HCHO	7.36E+03	5.53E+03
123	CCOO2 + RO2 —> 1.000 RO2 + 0.500 HO2 + 1.000 CO2 + 1.000 HCHO	1.63E+04	1.22E+04
124	CCOO2 + RCO3 —> 1.000 RCO3 + 1.000 HO2 + 1.000 CO2 + 1.000 HCHO	2.45E+04	1.84E+04
125	PAN —> 1.000 CCOO2 + 1.000 NO2 + 1.000 RCO3	2.99E-02	2.02E-02
126	C2COO2 + NO —> 1.000 CCHO + 1.000 RO2R + 1.000 CO2 + 1.000 NO2 + 1.000 RO2	1.47E+04	1.11E+04
127	C2COO2 + NO2 —> 1.000 PPN	1.24E+04	9.33E+03
128	C2COO2 + HO2 —> 1.000 OOH + 1.000 CCHO + 1.000 CO2	7.36E+03	5.53E+03
129	C2COO2 + RO2 —> 1.000 RO2 + 0.500 HO2 + 1.000 CCHO + 1.000 CO2	1.63E+04	1.22E+04
130	C2COO2 + RCO3 —> 1.000 RCO3 + 1.000 HO2 + 1.000 CCHO + 1.000 CO2	2.45E+04	1.84E+04
131	PPN —> 1.000 C2COO2 + 1.000 NO2 + 1.000 RCO3	2.97E-02	2.04E-02
132	ETHE + HO —> 0.220 CCHO + 1.560 HCHO + 1.000 RO2R + 1.000 RO2	1.26E+04	1.77E+03
133	ETHE + O3 —> 1.000 HCHO + 0.440 CO + 0.560 C + 0.120 HO2	2.61E-03	5.87E-04
134	ETHE + O —> 1.000 HCHO + 1.000 CO + 1.000 HO2 + 1.000 RO2R + 1.000 RO2	1.08E+03	1.98E+02
135	ETHE + NO3 —> 1.000 NO2 + 2.000 HCHO + 1.000 R2O2 + 1.000 RO2	2.97E-01	2.23E-01
136	HCHO —> 2.000 HO2 + 1.000 CO	--------photolytic--------	
137	HCHO —> 1.000 H2 + 1.000 CO	--------photolytic--------	
138	HCHO + HO —> 1.000 HO2 + 1.000 CO + 1.000 H2O	1.44E+04	3.37E+03
139	HCHO + HO2 —> 1.000 HOCOO	1.17E+02	2.80E+02
140	HOCOO —> 1.000 HO2 + 1.000 HCHO	9.06E+03	4.32E+03
141	HOCOO + NO —> 1.000 C + 1.000 NO2 + 1.000 HO2	1.14E+04	8.56E+03
142	HCHO + NO3 —> 1.000 HNO3 + 1.000 HO2 + 1.000 CO	8.91E-01	6.69E-01
143	CH4 + HO —> 1.000 RO2R + 1.000 HCHO + 1.000 RO2	1.23E+01	2.26E+00
144	ISOPRE + HO —> 1.000 RO2R + 1.000 RO2 + 1.000 HCHO + 1.000 RCHO + 1.000 C	1.49E+05	2.73E+04
145	ISOPRE + O3 —> 0.135 RO2R + 0.165 HO2 + 0.135 RO2 + 0.500 HCHO + 0.150 CCHO + 0.500 RCHO + 0.210 MEK + 0.295 CO + 1.565 C + 0.060 HO	2.12E-02	7.27E-03
146	ISOPRE + NO3 —> 1.000 R2O2 + 1.000 RO2 + 1.000 HCHO + 1.000 RCHO + 1.000 C + 1.000 NO2	1.00E+03	7.53E+02
147	ISOPRE + O —> 0.400 HO2 + 0.500 RCHO + 0.500 MEK + 1.500 C	8.87E+04	2.36E+04
148	APINEN + HO —> 1.000 RO2R + 1.000 RO2 + 1.000 RCHO + 7.000 C	7.93E+04	1.45E+04
149	APINEN + O3 —> 0.135 RO2R + 0.105 HO2 + 0.150 R2O2 + 0.285 RO2 + 0.050 CCOO2 + 0.050 C2COO2 + 0.100 RCO3 + 0.050 HCHO + 0.200 CCHO + 0.500 RCHO + 0.610 MEK + 0.075 CO	1.46E-01	5.00E-02

Table C2 (continued).

	Reaction	k(298) ppm min⁻¹	sigma k(298) ppm min⁻¹
	+ 5.285 C + 0.160 HO		
150	APINEN + NO3 ---> 1.000 R2O2 + 1.000 RO2 + 1.000 RCHO + 7.000 C + 1.000 NO2	9.11E+03	6.84E+03
151	APINEN + O ---> 0.400 HO2 + 0.500 RCHO + 0.500 MEK + 6.500 C	4.43E+04	1.18E+04
152	UNKN + HO ---> 1.000 RO2R + 1.000 RO2 + 0.500 HCHO + 6.500 C	9.70E+04	1.78E+04
153	UNKN + O3 ---> 0.135 RO2R + 0.135 HO2 + 0.075 R2O2 + 0.210 RO2 + 0.025 CCOO2 + 0.025 C2COO2 + 0.050 RCO3 + 0.275 HCHO + 0.175 CCHO + 0.500 RCHO + 0.410 MEK + 0.185 CO + 5.925 C + 0.110 HO	8.65E-02	2.97E-02
154	UNKN + NO3 ---> 1.000 R2O2 + 1.000 RO2 + 0.500 HCHO + 1.000 RCHO + 6.500 C + 1.000 NO2	6.35E+03	4.77E+03
155	UNKN + O ---> 0.400 HO2 + 0.500 RCHO + 0.500 MEK + 6.500 C	4.29E+04	1.14E+04
156	ETHANE + HO ---> 1.000 RO2R + 1.000 CCHO + 1.000 RO2	3.95E+02	7.25E+01
157	BUTANE + HO ---> 0.076 RO2N + 0.924 RO2R + 0.397 R2O2 + 0.001 HCHO + 0.571 CCHO + 0.140 RCHO + 0.533 MEK + -0.076 C + 1.397 RO2	3.75E+03	6.88E+02
158	Z2MEC5 + HO ---> 0.122 RO2N + 0.005 RO2XN + 0.873 RO2R + 0.749 R2O2 + 0.006 HCHO + 0.023 CCHO + 0.223 ACET + 0.545 RCHO + 0.724 MEK + 0.137 C + 1.749 RO2	8.34E+03	1.88E+03
159	BENZEN + HO ---> 0.236 PHEN + 0.207 GLY + 0.490 AFG1 + 0.764 RO2R + 0.236 HO2 + 3.190 C + 0.764 RO2	1.89E+03	5.02E+02
160	TOLUEN + HO ---> 0.085 BALD + 0.260 CRES + 0.118 GLY + 0.131 MGLY + 0.410 AFG2 + 0.740 RO2R + 0.260 HO2 + 2.726 C + 0.740 RO2	8.80E+03	1.61E+03
161	C2BENZ + HO ---> 0.085 BALD + 0.260 CRES + 0.118 GLY + 0.131 MGLY + 0.410 AFG2 + 0.740 RO2R + 0.260 HO2 + 3.726 C + 0.740 RO2	1.05E+04	3.20E+03
162	OXYLEN + HO ---> 0.040 BALD + 0.180 CRES + 0.108 GLY + 0.370 MGLY + 0.666 AFG2 + 0.820 RO2R + 0.180 HO2 + 3.136 C + 0.820 RO2	2.02E+04	4.56E+03
163	MPXYLE + HO ---> 0.040 BALD + 0.180 CRES + 0.108 GLY + 0.370 MGLY + 0.666 AFG2 + 0.820 RO2R + 0.180 HO2 + 3.136 C + 0.820 RO2	2.88E+04	8.78E+03
164	Z124MB + HO ---> 0.030 BALD + 0.180 CRES + 0.620 MGLY + 0.600 AFG2 + 0.820 RO2R + 0.180 HO2 + 3.870 C + 0.820 RO2	4.80E+04	1.46E+04
165	MEOH + HO ---> 1.000 HO2 + 1.000 HCHO	1.38E+03	6.53E+02
166	ETOH + HO ---> 0.100 RO2R + 0.900 HO2 + 0.156 HCHO + 0.922 CCHO + 0.100 RO2	4.83E+03	2.29E+03
167	MTBE + HO ---> 0.020 RO2N + 0.980 RO2R + 0.370 R2O2 + 0.390 HCHO + 0.410 MEK + 2.870 C + 1.370 RO2	4.18E+03	1.44E+03
168	ETBE + HO ---> 0.030 RO2N + 0.970 RO2R + 1.160 R2O2	1.11E+04	3.80E+03

Table C2 (continued).

	Reaction	k(298) ppm min*	sigma k(298) ppm min*
	+ 1.160 HCHO + 0.570 MEK + 2.410 C + 2.160 RO2		
169	Z224C5 + HO ---> 0.188 RO2N + 0.001 RO2XN + 0.811 RO2R + 0.878 R2O2 + 0.115 HCHO + 0.001 CCHO + 0.254 ACET + 0.745 RCHO + 0.573 MEK + 1.650 C + 1.878 RO2	5.44E+03	9.97E+02
170	MECYC5 + HO ---> 0.153 RO2N + 0.847 RO2R + 1.978 R2O2 + 0.283 HCHO + 0.697 RCHO + 0.490 MEK + 0.564 CO + 0.189 CO2 + 0.153 C + 2.978 RO2	1.19E+04	3.17E+03
171	PROPEN + HO ---> 1.000 RO2R + 1.000 RO2 + 1.000 HCHO + 1.000 CCHO	3.89E+04	5.45E+03
172	PROPEN + O3 ---> 0.135 RO2R + 0.165 HO2 + 0.135 RO2 + 0.650 HCHO + 0.500 CCHO + 0.140 MEK + 0.295 CO + 0.495 C + 0.060 HO	1.67E-02	5.74E-03
173	PROPEN + NO3 ---> 1.000 R2O2 + 1.000 RO2 + 1.000 HCHO + 1.000 CCHO + 1.000 NO2	1.39E+01	1.04E+01
174	PROPEN + O ---> 0.400 HO2 + 0.500 RCHO + 0.500 MEK + -0.500 C	5.88E+03	1.08E+03
175	Z13BUD + HO ---> 1.000 RO2R + 1.000 RO2 + 1.000 HCHO + 1.000 RCHO	9.83E+04	1.80E+04
176	Z13BUD + O3 ---> 0.135 RO2R + 0.165 HO2 + 0.135 RO2 + 0.500 HCHO + 0.150 CCHO + 0.500 RCHO + 0.210 MEK + 0.295 CO + 0.565 C + 0.060 HO	1.11E-02	4.62E-03
177	Z13BUD + NO3 ---> 1.000 R2O2 + 1.000 RO2 + 1.000 HCHO + 1.000 RCHO + 1.000 NO2	1.48E+02	1.11E+02
178	Z13BUD + O ---> 0.400 HO2 + 0.500 RCHO + 0.500 MEK + 0.500 C	3.10E+04	8.25E+03
179	Z2M1BU + HO ---> 1.000 RO2R + 1.000 RO2 + 1.000 HCHO + 1.000 MEK	8.96E+04	1.64E+04
180	Z2M1BU + O3 ---> 0.060 HO2 + 0.150 R2O2 + 0.150 RO2 + 0.050 CCOO2 + 0.050 C2COO2 + 0.100 RCO3 + 0.550 HCHO + 0.050 CCHO + 0.900 MEK + 0.220 CO + 0.280 C + 0.100 HO	1.79E-02	6.14E-03
181	Z2M1BU + NO3 ---> 1.000 R2O2 + 1.000 RO2 + 1.000 HCHO + 1.000 MEK + 1.000 NO2	4.91E+02	3.68E+02
182	Z2M1BU + O ---> 0.400 HO2 + 0.500 RCHO + 0.500 MEK + 1.500 C	2.25E+04	5.99E+03
183	Z2M2BU + HO ---> 1.000 RO2R + 1.000 RO2 + 1.000 CCHO + 1.000 ACET	1.28E+05	2.35E+04
184	Z2M2BU + O3 ---> 0.235 RO2R + 0.105 HO2 + 0.235 RO2 + 0.150 HCHO + 0.500 CCHO + 0.500 ACET + 0.540 MEK + 0.075 CO + 0.100 MGLY + -0.185 C + 0.160 HO	6.26E-01	2.61E-01
185	Z2M2BU + NO3 ---> 1.000 R2O2 + 1.000 RO2 + 1.000 CCHO + 1.000 ACET + 1.000 NO2	1.38E+04	1.04E+04
186	Z2M2BU + O ---> 0.400 HO2 + 0.500 RCHO + 0.500 MEK + 1.500 C	7.02E+04	1.87E+04

Table C2 (continued).

	Reaction	k(298) ppm min^{-1}	sigma k(298) ppm min^{-1}
187	Z3MCYP + HO ---> 0.775 RO2R + 0.225 RO2N + 1.000 RO2 + 0.775 CCHO + 0.775 RCHO + 1.000 C	9.80E+04	1.80E+04
188	Z3MCYP + O3 ---> 0.270 RO2R + 0.210 HO2 + 0.270 RO2 + 0.150 HCHO + 0.650 CCHO + 0.500 RCHO + 0.350 MEK + 0.150 CO + 1.500 C + 0.120 HO	3.87E-01	1.61E-01
189	Z3MCYP + NO3 ---> 1.000 R2O2 + 1.000 RO2 + 1.000 CCHO + 1.000 RCHO + 1.000 C + 1.000 NO2	5.77E+02	4.33E+02
190	Z3MCYP + O ---> 0.400 HO2 + 0.500 RCHO + 0.500 MEK + 2.500 C	4.43E+04	1.18E+04
191	AAR1 + HO ---> 0.917 RO2R + 0.042 RO2N + 0.007 RO2XN + 0.034 HO2 + 0.330 R2O2 + 1.295 RO2 + 0.141 HCHO + 0.315 CCHO + 0.163 RCHO + 0.254 ACET + 0.250 MEK + 0.024 CO + 0.010 PHEN + 0.065 GLY + 0.021 AFG1 + 0.188 C	2.90E+03	5.32E+02
192	AAR2 + HO ---> 0.828 RO2R + 0.109 RO2N + 0.002 RO2XN + 0.061 HO2 + 0.635 R2O2 + 1.574 RO2 + 0.013 HCHO + 0.173 CCHO + 0.205 RCHO + 0.179 ACET + 0.592 MEK + 0.032 CO + 0.007 CO2 + 0.061 CRES + 0.020 BALD + 0.028 GLY + 0.031 MGLY + 0.096 AFG2 + 0.973 C	8.88E+03	1.63E+03
193	AAR3 + HO ---> 0.785 RO2R + 0.079 RO2N + 0.136 HO2 + 0.198 R2O2 + 1.063 RO2 + 0.003 HCHO + 0.010 CCHO + 0.046 RCHO + 0.300 MEK + 0.002 CO2 + 0.136 CRES + 0.027 BALD + 0.046 GLY + 0.360 MGLY + 0.480 AFG2 + 3.630 C	4.37E+04	8.02E+03
194	OLE1 + HO ---> 0.871 RO2R + 0.129 RO2N + 1.000 RO2 + 0.871 HCHO + 0.256 CCHO + 0.615 RCHO + 1.284 C	4.85E+04	8.89E+03
195	OLE1 + O3 ---> 0.135 RO2R + 0.165 HO2 + 0.135 RO2 + 0.544 HCHO + 0.253 CCHO + 0.353 RCHO + 0.189 MEK + 0.295 CO + 1.995 C + 0.060 HO	1.68E-02	3.07E-03
196	OLE1 + NO3 ---> 1.000 R2O2 + 1.000 RO2 + 1.000 HCHO + 0.294 CCHO + 0.706 RCHO + 1.451 C + 1.000 NO2	1.70E+01	3.13E+00
197	OLE1 + O ---> 0.400 HO2 + 0.500 RCHO + 0.500 MEK + 1.657 C	6.07E+03	1.11E+03
198	OLE2 + HO ---> 0.930 RO2R + 0.070 RO2N + 1.000 RO2 + 0.321 HCHO + 0.647 CCHO + 0.605 RCHO + 0.111 ACET + 0.061 MEK + 0.056 BALD + 0.889 C	9.95E+04	1.83E+04
199	OLE2 + O3 ---> 0.195 RO2R + 0.163 HO2 + 0.032 R2O2 + 0.228 RO2 + 0.006 CCOO2 + 0.006 C2COO2 + 0.012 RCO3 + 0.283 HCHO + 0.453 CCHO + 0.325 RCHO + 0.060 ACET + 0.364 MEK	2.32E-01	4.25E-02

Table C2 (continued).

	Reaction	k(298) ppm min*	sigma k(298) ppm min*
	+ 0.193 CO + 0.030 BALD + 0.012 MGLY		
	+ 1.282 C + 0.120 HO + 0.015 BZO		
200	OLE2 + NO3 ----> 1.000 R2O2 + 1.000 RO2 + 0.346 HCHO	1.54E+03	2.83E+02
	+ 0.696 CCHO + 0.651 RCHO + 0.119 ACET		
	+ 0.066 MEK + 0.060 BALD + 0.908 C		
	+ 1.000 NO2		
201	OLE2 + O ----> 0.400 HO2 + 0.500 RCHO + 0.500 MEK	4.24E+04	7.78E+03
	+ 2.140 C		

* ppm min units as appropriate for the order of each reaction

Appendix D. CIT Model Results Used to Calculate Chapter 4 Figures

Reaction Set	Fuel	Population weighted results				Spatial results			
		Peak Ozone	O3ppm-person-hrs			Peak Ozone	O3ppm-km^2-hrs		
			>0.12	>0.09	Avg.		>0.12	>0.09	Avg.
Base	CNG	0.21	1743885	4110767	2927326	0.22	387	671	529
	LPG	0.20	1966508	4642219	3304364	0.21	384	674	529
	Phase2	0.19	1476437	3632973	2554705	0.20	325	606	465
	M85	0.19	1577651	3892627	2735139	0.20	335	622	479
	E85	0.19	910556	2486549	1698552	0.20	291	537	414
	RFA	0.19	1434342	3394366	2414354	0.20	320	598	459
	NoTOG	0.17	108981	1248644	678813	0.17	125	374	249
NO2	CNG	0.25	3982444	9193167	6587805	0.26	713	1023	868
	LPG	0.23	4508989	9661657	7085323	0.24	702	1011	857
	Phase2	0.22	3538465	8648754	6093610	0.23	617	933	775
	M85	0.22	3709991	8888066	6299029	0.23	633	950	791
	E85	0.23	2539084	6162019	4350551	0.24	553	844	698
	RFA	0.22	3451577	8376147	5913862	0.23	610	925	768
	NoTOG	0.20	962150	3787344	2374747	0.20	340	603	471
C2r+NO	CNG	0.22	3611253	8873621	6242437	0.23	575	909	742
	LPG	0.21	4052053	9311200	6681627	0.22	558	893	725
	Phase2	0.20	3205879	8278583	5742231	0.21	484	827	655
	M85	0.20	3205954	8294191	5750072	0.20	477	823	650
	E85	0.21	2257957	5919363	4088660	0.22	432	749	590
	RFA	0.20	3128080	8093830	5610955	0.21	476	821	648
	NoTOG	0.17	495876	3498669	1997273	0.18	200	510	355
C2r+NO2	CNG	0.19	710898	1821487	1266192	0.20	463		231
	LPG	0.19	822163	2090036	1456100	0.19	255	476	365
	Phase2	0.18	522936	1601838	1062387	0.18	205	418	312
	M85	0.18	661311	1818385	1239848	0.19	226	441	334
	E85	0.17	138944	1046954	592949	0.18	171	373	272
	RFA	0.18	524574	1547839	1036207	0.18	205	413	309
	NoTOG	0.16	32840	452814	242827	0.16	76	258	167
PAN	CNG	0.21	2742331	7118115	4930223	0.22	462	797	629
	LPG	0.20	2971821	7477192	5224506	0.21	451	785	618
	Phase2	0.19	2224532	6449014	4336773	0.20	378	715	547
	M85	0.19	2356727	6619708	4488217	0.20	383	721	552
	E85	0.20	1528147	3962808	2745477	0.21	351	640	495
	RFA	0.19	2136714	6227399	4182056	0.20	373	707	540
	NoTOG	0.17	161541	2199872	1180707	0.17	137	428	282
HCHO	CNG	0.22	3081684	7070065	5075874	0.23	517	822	670
	LPG	0.21	3683749	7593120	5638434	0.21	519	822	670
	Phase2	0.20	2442341	6082140	4262240	0.20	421	724	573
	M85	0.20	3021390	7023359	5022374	0.21	470	778	624
	E85	0.19	1617038	3525540	2571289	0.21	373	641	507
	RFA	0.19	2280579	5655968	3968274	0.20	411	711	561
	NoTOG	0.17	387726	1829930	1108828	0.18	183	437	310

Appendix D (continued). CIT Model Results Used to Calculate Chapter 4 Figures

MEOH	CNG	0.21	1745229	4127160	2936194	0.22	388	672	530
	LPG	0.20	1969997	4677592	3323794	0.21	385	675	530
	Phase2	0.19	1487995	3619039	2553517	0.20	325	607	466
	M85	0.20	2372681	5355088	3863884	0.21	418	713	565
	E85	0.19	912582	2493680	1703131	0.20	292	537	414
	RFA	0.19	1435385	3402988	2419186	0.20	320	598	459
	NoTOG	0.17	110847	1250459	680653	0.17	126	374	250
ETOH	CNG	0.21	1744481	4136159	2940320	0.22	389	673	531
	LPG	0.20	1984389	4709456	3346922	0.21	386	676	531
	Phase2	0.19	1490972	3627658	2559315	0.20	326	608	467
	M85	0.19	1589877	3910360	2750118	0.20	338	625	481
	E85	0.19	1046981	2707457	1877219	0.20	319	567	443
	RFA	0.19	1448628	3390541	2419584	0.20	322	600	461
	NoTOG	0.17	113628	1258142	685885	0.17	127	376	251
MPXY (product)	CNG	0.21	1733469	4131368	2932418	0.22	388	672	530
	LPG	0.20	1953803	4606623	3280213	0.21	384	673	528
	Phase2	0.19	1477774	3596439	2537107	0.20	324	606	465
	M85	0.19	1586896	3882576	2734736	0.20	336	622	479
	E85	0.19	912441	2487487	1699964	0.20	292	537	414
	RFA	0.19	1434737	3365290	2400013	0.20	320	597	458
	NoTOG	0.17	108981	1248644	678813	0.17	125	374	249
MPXY (rate const.)	CNG	0.21	1744745	4123914	2934330	0.22	388	671	530
	LPG	0.20	1986127	4687943	3337035	0.21	385	676	531
	Phase2	0.19	1500849	3705997	2603423	0.20	328	611	470
	M85	0.19	1594122	3941839	2767980	0.20	337	624	481
	E85	0.19	914313	2496577	1705445	0.20	292	537	415
	RFA	0.19	1461204	3470093	2465648	0.20	324	604	464
	NoTOG	0.17	108981	1248644	678813	0.17	125	374	249
AAR2	CNG	0.21	1939276	4605994	3272635	0.22	408	698	553
	LPG	0.20	2120563	5224478	3672520	0.21	407	702	554
	Phase2	0.19	1703729	4215795	2959762	0.20	351	640	495
	M85	0.19	1787641	4374600	3081120	0.20	359	650	504
	E85	0.19	1030447	2692684	1861565	0.20	310	559	434
	RFA	0.19	1622393	3953270	2787832	0.20	345	631	488
	NoTOG	0.17	157226	1411213	784220	0.17	147	394	271
OLE2	CNG	0.21	1750427	4169992	2960209	0.22	389	675	532
	LPG	0.20	1989598	4706975	3348287	0.21	387	676	532
	Phase2	0.19	1495516	3622227	2558871	0.20	326	609	468
	M85	0.19	1587002	3962992	2774997	0.20	338	625	482
	E85	0.19	919124	2514133	1716629	0.20	293	540	416
	RFA	0.19	1446607	3428282	2437444	0.20	322	601	462
	NoTOG	0.17	111560	1266772	689166	0.17	128	377	252
AFGS	CNG	0.21	2033112	4847816	3440464	0.22	413	705	559
	LPG	0.20	2259030	5463753	3861391	0.21	414	711	563
	Phase2	0.19	1904369	4741330	3322850	0.20	366	661	513
	M85	0.19	1924901	4782023	3353462	0.20	368	664	516
	E85	0.19	1071440	2762135	1916788	0.20	312	564	438
	RFA	0.19	1858758	4460375	3159566	0.20	363	654	508
	NoTOG	0.17	152973	1435274	794124	0.17	142	393	267

Appendix E. A Brief Comparison of CIT Modeling of RAF Effects Using Two Different Chemical Mechanisms.

This is a brief comparison of two air quality studies that examined RAF-adjusted fuel impacts using the CIT airshed model. One study (1) used the LCC chemical mechanism (2), and the other study (presented in this report) used the SAPRC90 chemical mechanism (3). Details of the modeling protocol can be found in either of the study reports.

Both studies used the CIT model applied to the August 27, 28, and 29, 1987 South Coast Air Quality Study (SCAQS) pollution episode in the Los Angeles air basin. Both increased the mobile organic emissions by the amount allowed by the fuel-specific RAF, accounting for differences in mass emissions during hot and cold start and hot stabilized driving modes. The emissions were also doubled to account for the commonly recognized underprediction of mobile organic emissions in this area.

The main difference between these two studies is the chemical mechanism version used in the model. SAPRC90 is an extensive update of LCC. Table E1 shows an overview of the two mechanisms. Both mechanisms are based on the same lumping method and smog chamber data (excluding updates).

Table E1. Overview of the LCC and SAPRC90 Mechanisms

	LCC	SAPRC90
Chemical Species:		
Transported	35	71
Reactive Organic Gases	16	33
Steady-state	9	15
Constant	5	5
Total	47	91
Reactions:		
Photolytic	13	20
Total	106	203

The chemical mechanism is a primary component of an air quality model, and is important in the development of reactivity measures. Many uncertainty analysis studies are focusing on this model component (4,5,6,7, and this report). Changing the chemical mechanism in an air quality model such as the CIT is a major alteration, affecting the emissions inventories and the Ordinary Differential Equation (ODE) solver performance, as well as the reaction mechanism routines. The implementation and testing of SAPRC90 with the CIT model is described in a previous report (4).

Another difference between these studies is the number of fuels considered. The LCC study examined CNG, M85, and LPG, with respect to an industry average gasoline (RFA) and a scenario with no mobile source organic emissions (NoTOG). The SAPRC90 study also

examined these scenarios, as well as California Phase 2 and E85. Only the fuels examined in both studies are presented here.

The following four plots illustrate the results of these two studies. Figure E1 shows the Adjusted Relative Reactivity (ARR) for CNG, LPG, and M85, calculated as shown in equation E1 (and in Chapter 4 of this report).

$$ARR_{fuel} = \frac{P_{fuel} - P_{NoTOG}}{P_{rfa} - P_{NoTOG}} \qquad \text{(E1)}$$

Here, P is the impact prediction parameter, either peak ozone or exposure to greater than 0.12 or 0.09 ppm of ozone, either on a spatial or population-weighted basis. The subscripts represent the inventory used to obtain the parameter (one of the three fuels, RFA, or NoTOG). In essence, the ARR is the relative reactivity of the exhaust with respect to RFA and the null case after the mass emissions have already been adjusted for the reactivity differences using the RAF. These basecase model results provide a representation of the agreement between the RAF value and the fuel reactivity predicted by the CIT model, because, ideally, the ARR for a fuel should be equal to one when the emissions are multiplied by the RAF.

As can be seen in Figure E1, there is variation in both magnitude and direction of the fuels predicted deviation from one, depending on the mechanism used. No variation exceeds 2 (or 0.5). The largest differences in magnitude are observed for LPG by the exposure metrics, and a directional discrepancy is observed for CNG, again with the exposure metrics.

The absolute predictions for each fuel/scenario are shown in Figures E2 through E4. These are the unadjusted model predictions. These plots show a wider variation in predictions when using SAPRC90, particularly for the populated-exposure measure. The RAFs were calculated using a zero-dimensional model with the SAPRC90 mechanism, and the more explicit mechanism may have magnified the effects of local meteorological and ambient conditions, or of mechanism and inventory uncertainties, but this is unlikely. These issues are being examined further.

Figure E1. Adjusted Relative Reactivity (ARR) Calculated Using LCC and SAPRC90

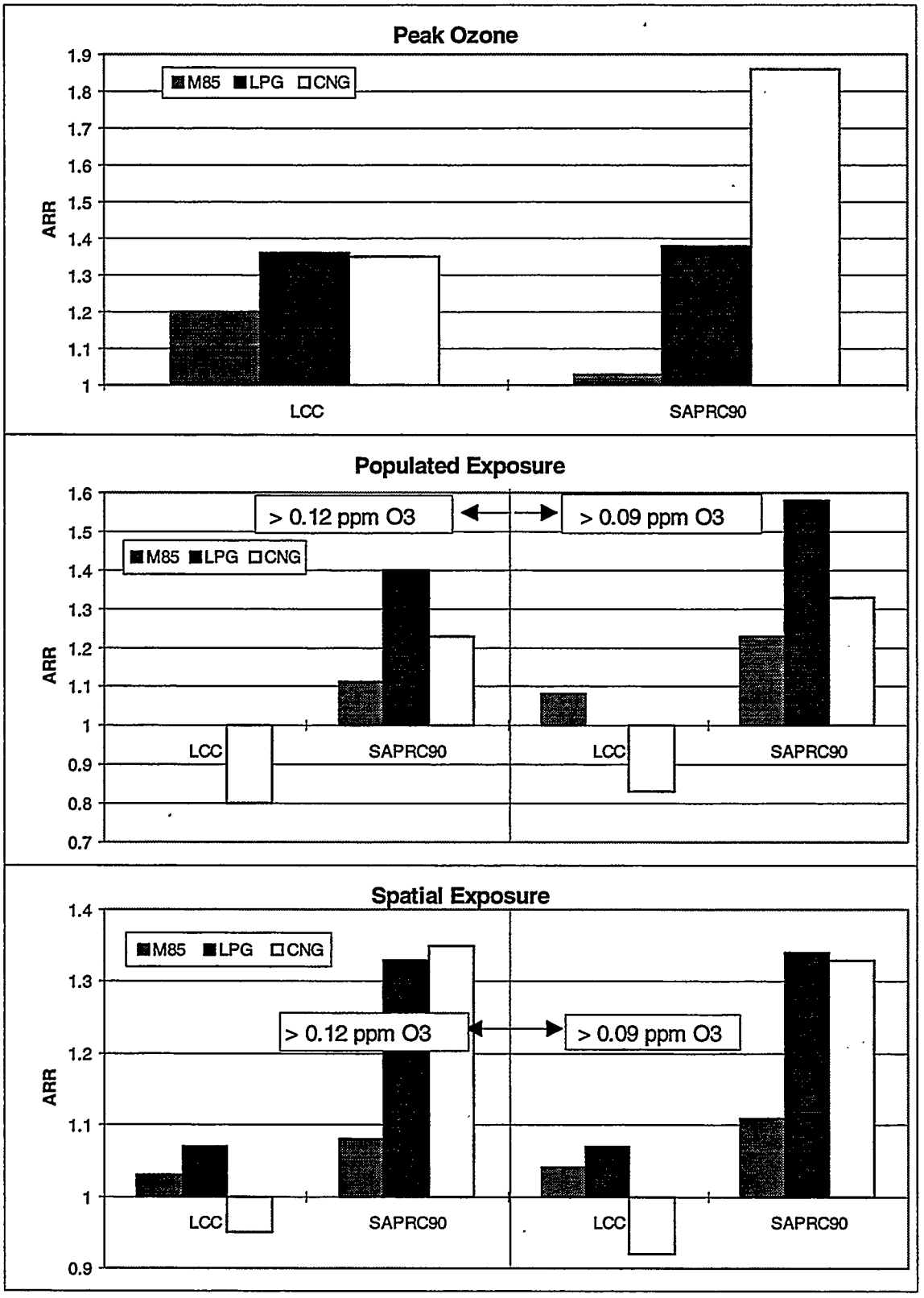

Figure E2. Peak Ozone (absolute)

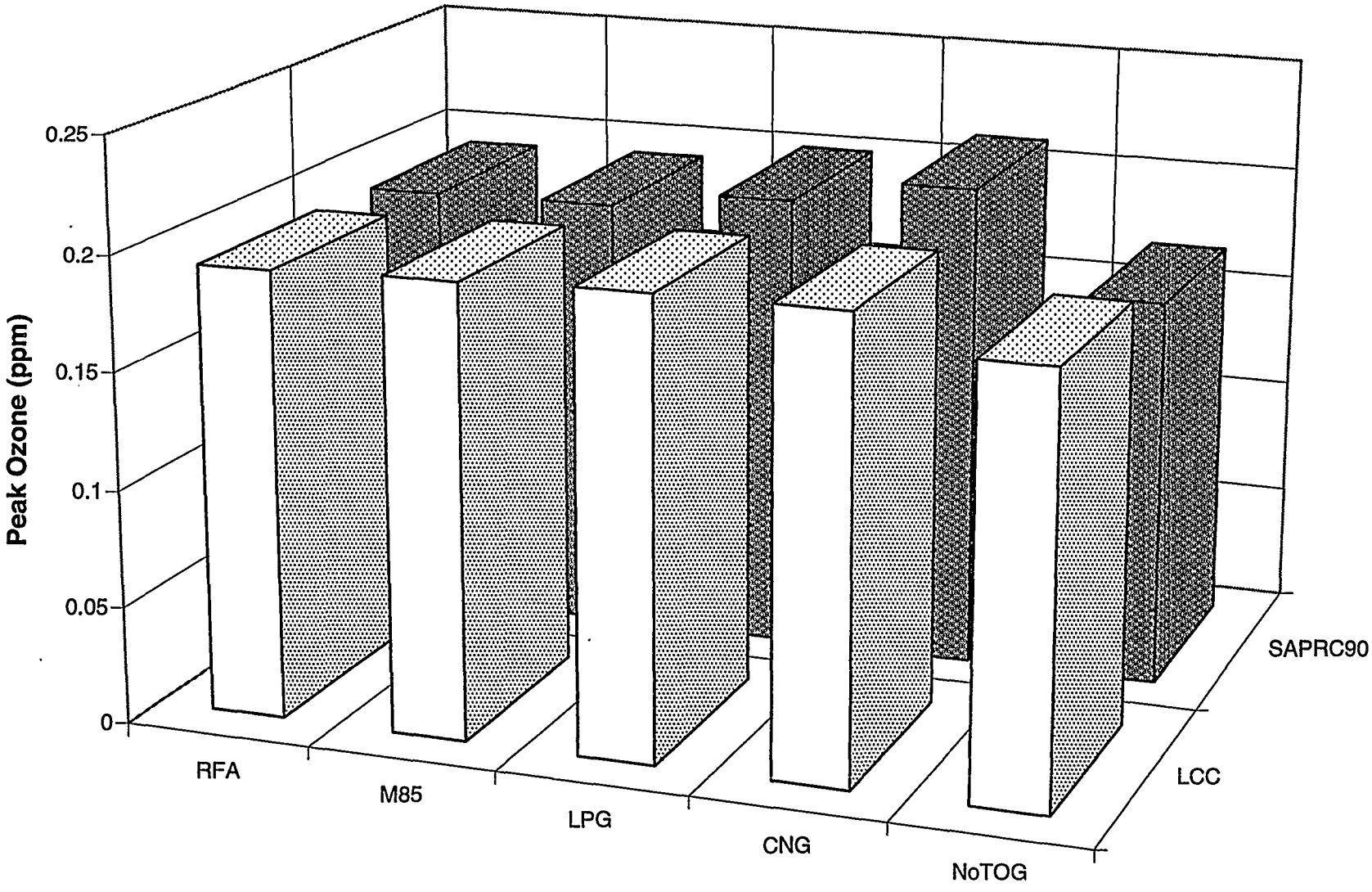

Figure E3. Spatial Exposure (absolute)

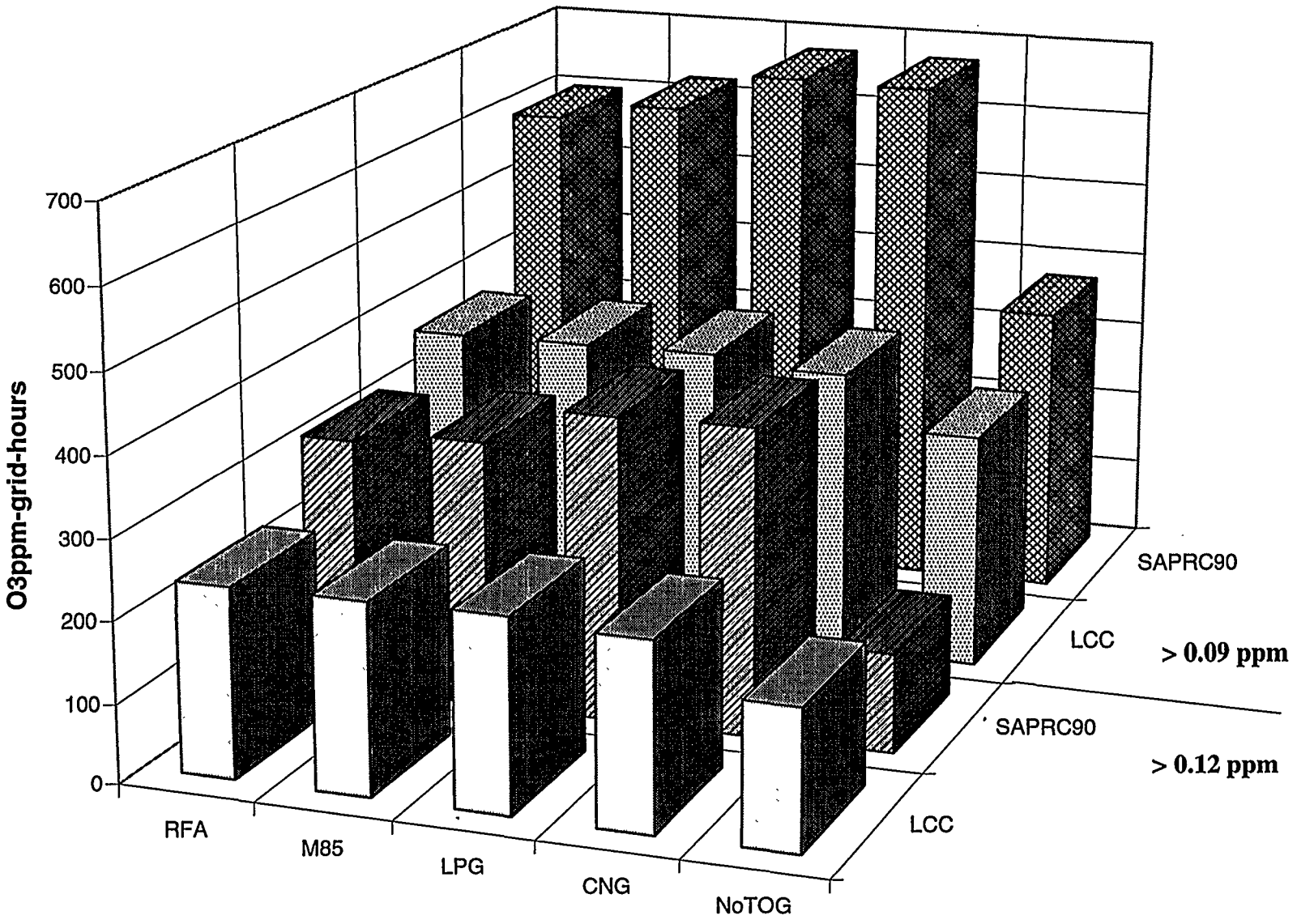

Figure E4. Population Exposure (absolute)

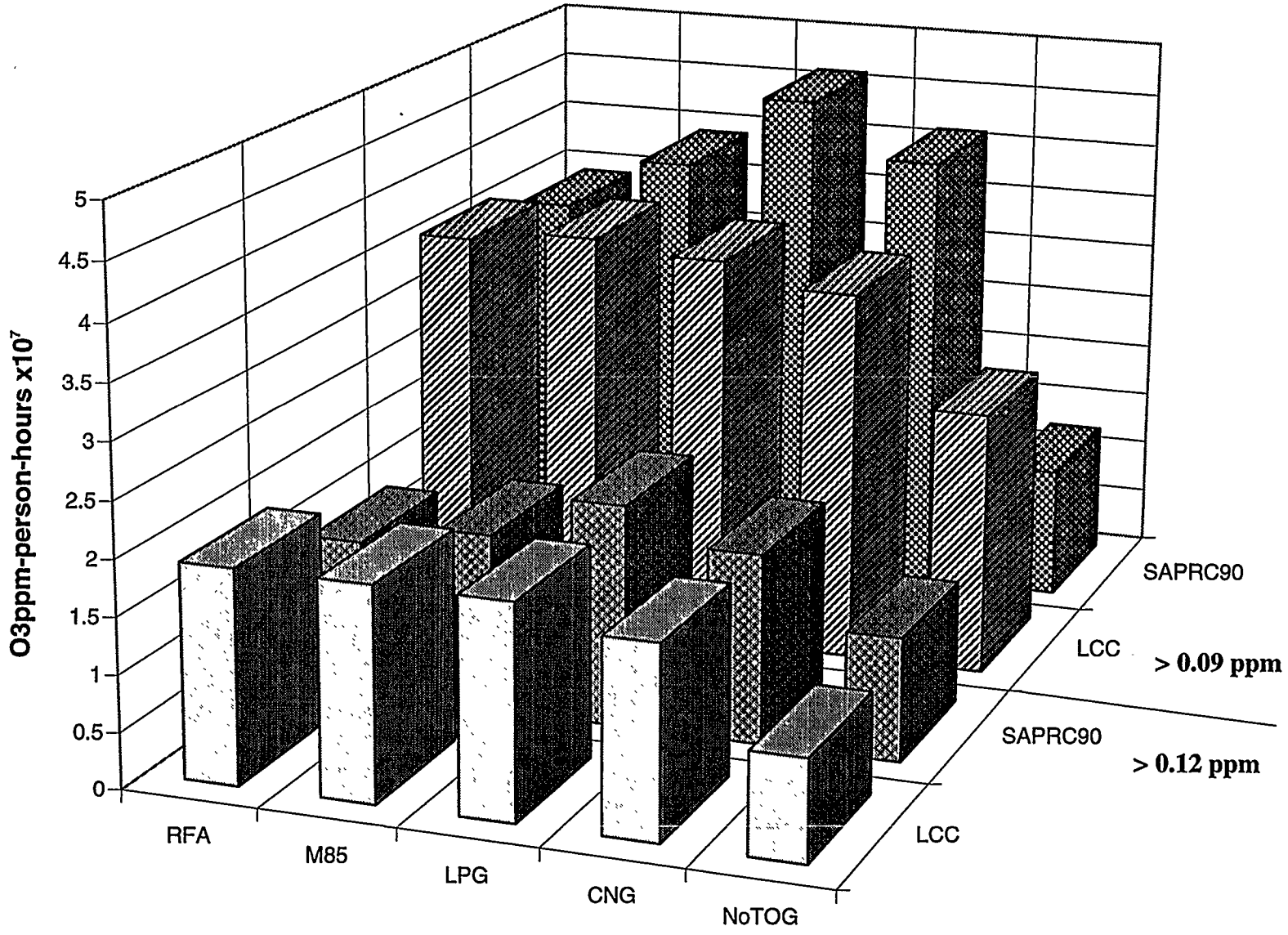

References for Appendix E

(1) McNair, L.A., Russell, A.G., Croes, B., Kao, L. (1994). "Airshed Model Evaluation of Reactivity Adjustment Factors Calculated with the Maximum Incremental Reactivity Scale for Transitional-Low Emission Vehicles," *J. Air & Waste Management Assoc.*, **44**, 900.

(2) Lurmann, F.W., Carter, W.P.L., Coyner, L.A. (1987). *A Surrogate Species Chemical Reaction Mechanism for Urban-Scale Air Quality Simulation Models*, EPA/600/3-87-014, U.S. Environmental Protection Agency, Research Triangle Park, NC, June.

(3) Carter, W.P.L. (1990). "A Detailed Mechanism for the Gas-Phase Atmospheric Reactions of Organic Compounds," *Atmos. Environ.*, **24A**, 481-518.

(4) Yang, Y-J., Das, M., Milford, J.B., Bergin, M.S., Russell, A.G., Stockwell, W.R. (1994). *Quantification of Organic Compound Reactivities and Effects of Uncertainties on Rate Parameters,* report prepared for the Auto/Oil Air Quality Improvement Research Program. Available from the Coordinating Research Council, Atlanta, GA.

(5) Russell, A.G., Milford, J.B., Bergin, M.S. McBride, S., McNair, L., Yang, Y-J., Stockwell, W.R., Croes, B. (1995). "Urban Ozone Control and Atmospheric Reactivity of Organic Gases," *Science*, **269**, 491-495.

(6) Bergin, M.S., Russell, A.G., Milford, J.B. (1995). "Quantification of Individual VOC Reactivity Using a Chemically Detailed, Three-Dimensional Photochemical Model," *Environ. Sci. Technol*, **29**, 3029-3037.

(7) Stockwell, W.R., Yang, Y-J., Milford, J.B. (1994). *A Compilation of Estimated Uncertainty Factors for Rate Constants in W.P.L. Carter's Detailed Mechanism*, report prepared for the Auto/Oil Air Quality Improvement Research Program. Available from the Coordinating Research Council, Atlanta, GA.

(8) Yang, Y-J., Stockwell, W.R., Milford, J.B. (1995). "Uncertainties in Incremental Reactivities of Volatile Organic Compounds," *Environ. Sci. Technol.*, **29**, 1336-1345.

REPORT DOCUMENTATION PAGE

Form Approved
OMB NO. 0704-0188

1. AGENCY USE ONLY (Leave blank)	2. REPORT DATE	3. REPORT TYPE AND DATES COVERED
	July 1996	NREL Subcontractor Report

4. TITLE AND SUBTITLE

Effects of Uncertainty in SAPRC90 Rate Constants and Product Yields on Reactivity Adjustment Factors for Alternative Fuel Vehicle Emissions

5. FUNDING NUMBERS

FU622010

6. AUTHOR(S)

M. Bergin, A. Russell, Y.-J. Yang, J. Milford, F. Kirchner, W. Stockwell

7. PERFORMING ORGANIZATION NAME(S) AND ADDRESS(ES)

Carnegie Mellon University
Pittsburgh, PA 15213

University of Connecticut
Storrs, CT 06269

University of Colorado
Boulder, CO 80309

Fraunhofer Institute for Atmospheric Environmental Research
Kreuzeckbahnstrasse 19
82467 Garmisch-Partenkirchen
Germany

8. PERFORMING ORGANIZATION REPORT NUMBER

DE96007953

9. SPONSORING/MONITORING AGENCY NAME(S) AND ADDRESS(ES)

National Renewable Energy Laboratory
1617 Cole Boulevard
Golden, CO 80401-3393

10. SPONSORING/MONITORING AGENCY REPORT NUMBER

NREL/TP-473-7636

11. SUPPLEMENTARY NOTES

12a. DISTRIBUTION/AVAILABILITY STATEMENT

National Technical Information Service
U.S. Department of Commerce
5285 Port Royal Road
Springfield, VA 22161

12b. DISTRIBUTION CODE

UC-1500

13. ABSTRACT *(Maximum 200 words)*

Tropospheric ozone is formed in the atmosphere by a series of reactions that involve volatile organic compounds (VOCs) and nitrogen oxides (NOx). NOx emissions are composed primarily of NO and NO_2, but hundreds of VOCs are being emitted. Generally, VOCs promote ozone formation; however, the rate and extent of ozone produced by VOCs vary considerably.

14. SUBJECT TERMS

volatile organic compounds, tropospheric ozone, nitrogen oxides

15. NUMBER OF PAGES

154

16. PRICE CODE

17. SECURITY CLASSIFICATION OF REPORT	18. SECURITY CLASSIFICATION OF THIS PAGE	19. SECURITY CLASSIFICATION OF ABSTRACT	20. LIMITATION OF ABSTRACT